UNIVERSITÀ DI PARMA

UNIVERSITA' DEGLI STUDI DI PARMA

DOTTORATO DI RICERCA IN
"SCIENZA E TECNOLOGIA DEI MATERIALI"

CICLO XXXV

in CO-TUTELA con

Sabic Technology Center, Geleen (Netherlands)

Non-covalent polymeric networks *via* hydrogen bonds and electrostatic interactions.

Coordinatore:

Prof. Enrico Dalcanale

Tutore:

Prof. Enrico Dalcanale

Dr. Jerome Vachon

Dottorando: Silvia D'Auria

Anni Accademici 2019/2020-2022/2023

The financial support from SABIC is gratefully acknowledged.

List of abbreviations

^{1}H NMR proton nuclear magnetic resonance

^{13}C NMR carbon nuclear magnetic resonance

2PM two-photon microscopy

A acceptor

ADMET acyclic diene metathesis

AFM atomic force microscopy

ATR attenuated total reflectance

ATRP atom transfer radical polymerization

CED cohesive energy density

$CDCl_3$ deuterated chloroform

$CHCl_3$ chloroform

CLS classical least-squares

C_p heat capacity

CTA chain transfer agent

D donor

DBTDL dibutyltin dilaurate

DC direct current

DCP dicumyl peroxide

DMSO dimethyl sulfoxide

DMTA dynamical mechanical thermal analysis

DPI polydispersity index

DSC differential scanning calorimetry

E' storage modulus (tension)

EA elemental analysis

EHM Eisenburg-Hird-Moore

EU European Union

EVOH ethylene vinyl alcohol

FFV free volume

FT-IR Fourier transformed infrared spectroscopy

FRP free radical polymerization

G' storage modulus (shear)

G" loss modulus (shear)

GPC gel permeation chromatography

H-bond Hydrogen bond

HCl hydrochloric acid

HDI hexamethylene diisocyanate

HDPE high density polyethylene

HEMA hydroxyethyl methacrylate

H_f enthalpy of fusion

HVDC High voltage direct current

IPC ion pair comonomers

K_a association constant

l_c lamellar thickness

LDPE low density polyethylene

$LDPE_A$ low density polyethylene made in the autoclave

$LDPE_C$ low density polyethylene commercial

MAH maleic anhydride

M_c molecular weight between crosslinks

MeOH methanol

MFI melt flow index

MFR melt flow rate

M_{IPC} IPC molecular weight

M_n number average molecular weight

mol% molar percentage

M_w weight average molecular weight

NaCl sodium chloride

NaOH sodium hydroxide

N_c number of crosslinks

NMR Nuclear magnetic resonance

ODIN 1-(7-oxo-7,8-dihydro-1,8-naphtiridin-2-yl)urea

PE polyethylene

PE-HEMA poly (ethylene-co-(2-hydroxethyl methacrylate)

PET polyethylene terephthalate

PP polypropylene

ppm parts per million

PVOH polyvinyl acetate

RAFT reversible addition fragmentation chain transfer

RH relative humidity

RT room temperature

ODCB o-dichlorobenzene

SANS small angle neutron scattering

SAXS small angle X-ray scattering

SEC size exclusion chromatography

T temperature

tan δ tangent of delta

TC thermal conductivity

T_c crystallization temperature

TCE tetrachloroethane

T_c crystallization temperature

TEM transmission electron microscopy

T_g glass transition

TGA thermogravimetric analysis

T_m melting temperature

TPEF two-photon excited fluorescence

T_β β transition temperature

UPy 2-(6-isocyanatohexylaminocarbonyl amino)-6-methyl- 4[1H]pyrimidinone

UV ultraviolet

WAXS wide-angle X-ray scattering

wt% weight percentage

X_c degree of crystallinity

XLPE crosslinked polyethylene

α thermal diffusivity

σ_{DC} direct current conductivity

σ_e surface energy

ρ density

κ thermal conductivity

ν Poisson's ratio

τ_d relaxation time

Abstract

"Supramolecular chemistry has been defined as *chemistry beyond the molecule*, as it aims at designing and implementing functional chemical systems based on molecular components held together by noncovalent intermolecular forces". This definition provided by the Nobel Price, Jean-Marie Lehn, lays the foundation of a new branch of chemistry based on the non-covalent interactions and the effect of such bonds on a system. Even though these noncovalent interactions are generally weak, they have a significant impact on the behavior of self-assemble complex structures. Supramolecular interactions include electrostatic interactions, hydrogen bonds, ion-dipole and dipole-dipole interactions, metal coordination, hydrophobic forces, and van der Waals forces. This thesis describes the use of electrostatic interactions and hydrogen bonds as tools for the formation of polymeric networks in polyolefins, featuring new thermal, mechanical, and electric properties. Polyethylene (PE) is the most widely used thermoplastic polymer and the leader in most applications in the global plastic industry. It exhibits strong resistance to solvents, exceptional flexibility, low cost, lightness, and simplicity of processing. However, its use is limited by its low strength and stiffness, low upper service temperature, stress cracking, and poor UV resistance. Additionally, its apolar nature makes it unsuitable for any coating and adhesive application unless a surface treatment is applied (like flame and corona treatment). To overcome those issues, and drastically improve its properties, crosslinking of polyethylene is performed.

Chapters 1 and 2, report the synthesis of a new type of polyethylene-based ionomer, where a few mole percent of positively and negatively charged groups, are covalently bound to the polymer backbone. Amino-terminated methacrylates and methacrylic acid, present in the form of ion pairs, are used as comonomers (ion pair comonomer, IPC) together with ethylene, in a high-temperature/high-pressure process. Specifically, Chapter 1 will present a study of the polymerization reaction of a polyethylene-based ionomer using different reaction conditions, such as temperature, IPC content, in the presence/absence of a chain transfer agent (CTA). The introduction of ionic groups into the PE matrix is an effective way to increase its hydrophilicity and thus its adherence properties to aluminum. In Chapter 2 polyethylene-based ionomers are demonstrated to feature a thermo-mechanical and dielectric property portfolio that is comparable to crosslinked polyethylene (XLPE), which may enable the design of more sustainable high-voltage direct-current (HVDC) power cables, a crucial component of future electricity grids that seamlessly integrate renewable sources of energy. Chapters 3 and 4, present the use of multiple hydrogen bonding as a tool to compatibilize immiscible polymers. Chapter 3 introduces two-photon microscopy (2PM) as an original technique to investigate the compatibilization between PE-HEMA and EVOH at the sub-micrometer level, both on the surface

and in the bulk. 2PM allows to visualize polymer blending through 3D images of the obtained films. Compatibilization was performed in solution, upon functionalization of PE-HEMA with 1.4% molar of ODIN, a fluorescent molecule able to form multiple hydrogen bonding with EVOH and to act as fluorescent probe. Different blends were synthesized, and the obtained films analyzed by 2PM. For all compositions, it was demonstrated that ODIN is evenly distributed both on the surface and in the bulk. 2PM analysis of the thermally reprocessed specimen revealed that repeated reprocessing allows the reformation of ODIN dimers as the most stable H-bonding array in the solid state, partially reversing the compatibilization.

Chapter 4 discusses the possibility to create polymer blends acting as oxygen barrier, to evaluate the applicability of a monolayer instead of a multilayer as a solution to produce monolayer packaging films to substitute triple-layer films.. Ethylene-co-vinyl alcohol (EVOH) which is already used in the food and pharmaceutical industry for its oxygen barrier property, and polyethylene-co-hydroxyethyl methacrylate (PE-HEMA), which acts as a water barrier, have been utilized. The study involved the permeability characterization of the blends produced in Chapter 3 as well as the production of new binary mixtures produced by functionalizing PE-HEMA with phenyl-urea and combining it with EVOH. The following assessment of the blends, paying special attention to the oxygen permeability tests, shows an unequal distribution of the two polymers within the blends. The PE-HEMA fraction is mainly present at the surface, while EVOH is concentrated in the inner bulk. This self-segregation in the films leads to improved oxygen barrier properties.

Table of content

Two-photon Microscopy as visual tool for polymer compatibilization monitoring: The PE-EVOH case

Synthesis and characterization of EVOH and PE blends for oxygen barrier monolayer films

Fundamentals

Supramolecular polymer networks

Polymer networks are categorized as “covalent” or “physical” networks. The first consists of chains joined together by covalent bonds, instead, the physical ones are obtained by non-covalent interconnections. Networks that are physical or chemical both have advantages and disadvantages. Chemical networks' stability is beneficial for applications that require tough polymer materials, but it is disadvantageous in terms of processing and recycling. It also reduces the usefulness of these networks for applications requiring controlled release and encapsulation. Crosslinking in physical networks, on the other hand, is reversible, which considerably simplifies processing and recycling, but is more complex to design.

Supramolecular polymer networks are a promising new class of materials that have recently emerged in the polymer sciences. The interest in this class of material is growing thanks to their unique characteristics, like flexibility and their adaptable nature. As seen in Figure 1, these networks are created by non-covalent contacts with a wide range of strengths, such as hydrogen bonds,[1],[2] π-π interactions,[3],[4] metal complexation,[5] hydrophobic interaction,[6] and ionic attraction.[7] As a result, by tailoring these interactions for polymer cross-linking, supramolecular polymer materials can exhibit diverse mechanical properties.

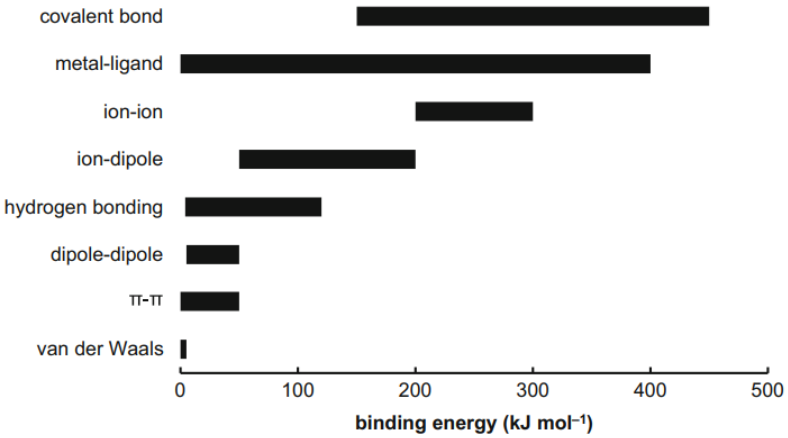

Figure 1. typical range of binding strength of the most important non-covalent interactions and covalent bonds.[8]

Two main approaches can be used to construct such supramolecular networks. Supramolecular bonds are inserted to either form network chains from non-covalently associating monomers (Figure 2a) or to associate polymer chains together by functionalizing them with complementary supramolecular motifs (Figure 2b). In both cases, the resulting supramolecular polymer networks combine the properties of chemical and physical networks: they are tailor-made and can be designed to meet specific requirements, they can be designed to meet particular needs, and they can form strong materials, but they can also be easily disassembled or de-crosslinked under specific conditions (Figure 2c and d).[9]

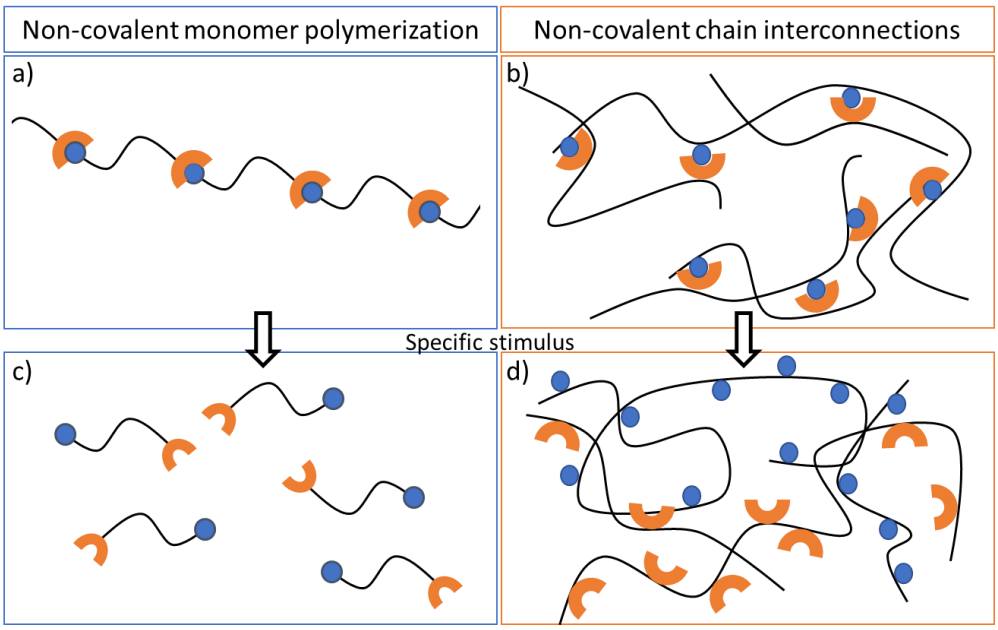

Figure 2. Schematic representation of two types of polymer networks. Upper row: a) non-covalent association of bifunctional monomers, b) non-covalent chain interconnection of two polymers grafted with complementary functionalities, lower row: c) and d) rupture of the non-covalent interactions after a specific stimulus.

Polymer networks can be formed by (co-)polymerization of multifunctional monomers or by post-crosslinking a polymeric precursor. In the first instance, a chain extension process results in the simultaneous development and interconnection of chains, but in the second instance, linear or branched chains already exist and are crosslinked in a later stage. This second approach is also used to blend immiscible polymers by functionalizing the polymer chains with complementary functionalities. A supramolecular approach based on host-guest interactions has been used to obtain a homogenous mixture of polystyrene and poly(butyl methacrylate), two immiscible polymers (Figure 3).[10] As illustrated in the figure below, the polystyrene has been functionalized with a tetra-phosphonate cavitand as the host, while the poly(butyl methacrylate) with a methyl pyridinium works as guest. The host-guest interactions, overcome the repulsive interfacial energy between the two polymers allowing their compatibilization possible, as confirmed by AFM measurements.

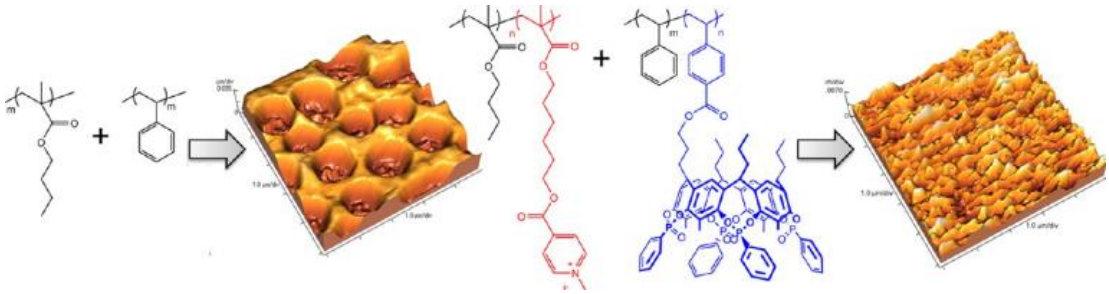

Figure 3. Compatibilization of polystyrene and poly(butyl methacrylate) via host-guest interactions.[10]

Supramolecular polymer networks due to their reversible cross-linking are susceptible to external stimuli such as temperature,[11] solvent polarity,[12] pH,[13] competitive ligation,[14] and redox reactions.[15] Because of this, they can be used for a wide range of applications. They can serve as tissue engineering matrix materials[16] and drug delivery systems.[17] Additionally, supramolecular polymer networks frequently exhibit self-healing capabilities: when a supramolecular connection breaks, it can reassociate when the functionalities come into contact, repairing the material.[18],[19] Furthermore, shape-memory materials are created by combining supramolecular and covalent crosslinking.[20]

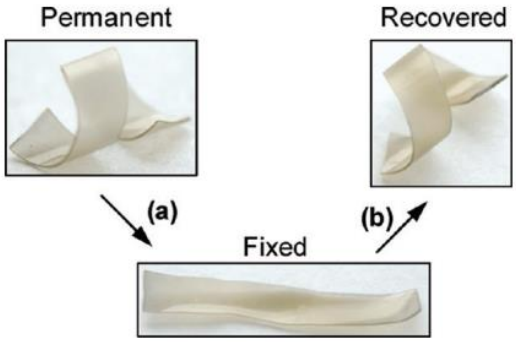

Figure 4. Photographs demonstrating the shape-memory behavior: (a) sample irradiated with 320-390 nm UV light to fix the temporary shape, (b) recovery of the permanent shape.[20]

If a sample contains both supramolecular and permanent covalent crosslinks, the supramolecular one can be broken under certain stimuli and the material can be deformed. A subsequent stimulus can cause the re-association of the supramolecular crosslinks restoring the original shape of the material (Figure 4).

Hydrogen bonds

Because of their directionality and adaptability, hydrogen bonds are one of the most used weak interactions in supramolecular chemistry. It consists of a non-covalent interaction between a

partially charged donor (D) (partially negative) and a partially charged acceptor (A) (partially positive). A single hydrogen bond's strength (1-40 kcal/mol)[21] is typically insufficient to build a supramolecular architecture, but arrays of many hydrogen bonds can be used instead.[22] Multiple hydrogen bonding molecules are characterized by more than one hydrogen bond placed in an array that works together to generate an assembled species with complementary molecule (hetero-dimerization) or by dimerizing (homo-dimerization). The crucial characteristic of linear multiple hydrogen bonding motifs is that their association constant varies on both the quantity and the arrangement of hydrogen bonds. Three ADA-DAD, AAD-DDA, and AAA-DDD (A-acceptor, D-donor) arrays can be found in literature when considering triple hydrogen bonding motifs (Figure 5).[23] Figure 5 shows how the presence of both attractive and repulsive interactions consistently influences the association constant of the final motif.

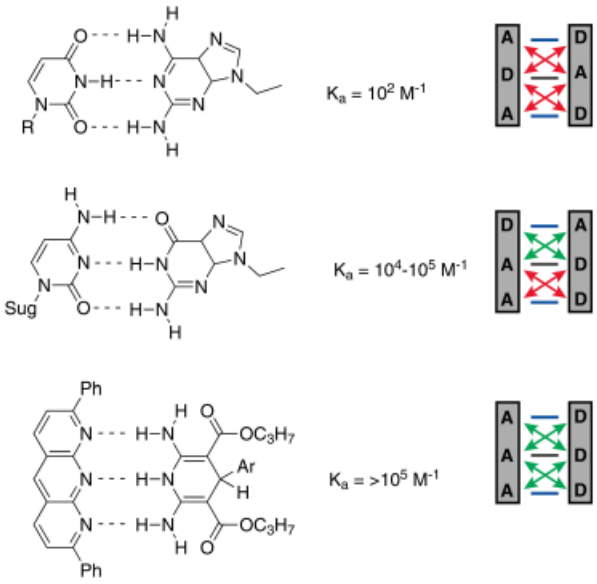

Figure 5. attractive and repulsive secondary interactions affect the association constant of triple hydrogen bonding motifs.[23]

Meijer and Sijbesma's invention of the quadruple hydrogen bonding unit UPy (ureidopyrimidinone) marked a major advancement in supramolecular polymer chemistry.[24] This hydrogen bonding system displays several advantages, among which is simple to synthesize and to introduce onto polymeric backbones and has a high dimerization constant of 6 10^7 M^{-1} thanks to its planar DDAA motif and the low amount of repulsive interactions.[25] The Upy motif exhibits a tautomeric equilibrium consisting of a self-complementary pyrimidin-4-ol with a DADA array. Because of the emergence of a secondary repulsive interaction, the dimerization constant is lowered to 9 10^5 M^{-1} in this form (Figure 6).

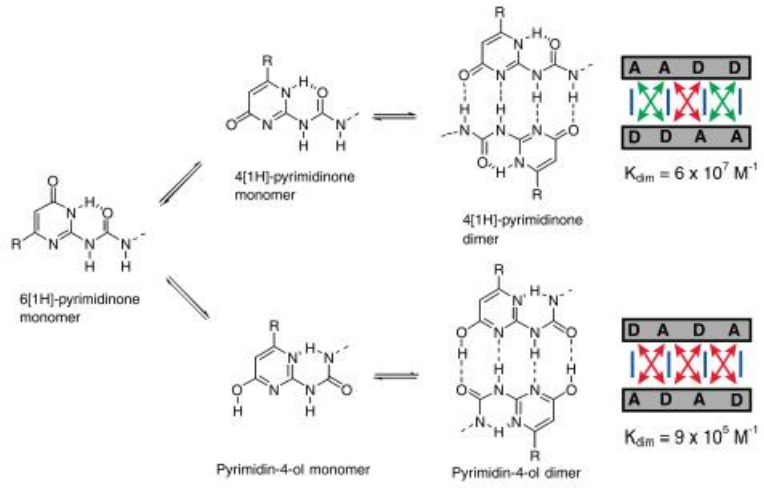

Figure 6. Tautomeric equilibrium of Upy motif.[23]

UPy can be synthesized in a single step from commercially available methyl isocytosine and hexamethylene diisocyanate and integrated into polymers by a variety of synthetic methods.[24] The isocyanate linker can easily react with polymers containing hydroxy or amino groups.[26],[27] Amino-terminated UPy has also been produced as an alternative method to react with polyurethane.[28]

However, due to concerns about thermal stability of the urea bond into UPy at high temperatures,[29],[30] and a degradation temperature of UPy moieties in polymers given at 150 °C,[31] this research group designed an alternative.[32] While maintaining the benefits of UPy, such as simplicity of synthesis, self-dimerization, high reactivity, and strong directionality of the motif afforded by numerous hydrogen bonds, this alternative has to be more temperature stable. Six hydrogen bond motif, (1-(7-oxo-7,8-dihydro-1,8- naphtiridin-2-yl)urea (ODIN), has been obtained by reacting a di-isocyanate with the free amine group of naphthyridine (Scheme 1).

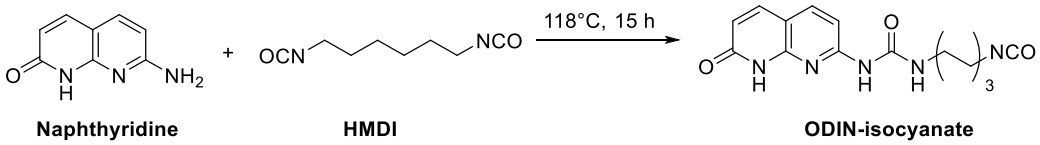

Scheme 1. Synthesis of ODIN-isocyanate.

The resultant urea group supplies an additional hydrogen bonding donor that can interact with one of the lone pairs of the lactam, resulting in two more hydrogen bonds than naphthyridine provided.[33] Additionally, the free isocyanate groups provide an easy entry of ODIN into polymers with proper functionalities. The ODIN assembly mechanism was clarified by generating single crystals of the compound in Figure 7a, which shows a higher solubility in organic solvents necessary

for the formation of crystals. The obtained product has a DDADA arrangement that involves two regular and two bifurcated hydrogen bonds, resulting in a Ka of 4 10^4 M^{-1} (Figure 7b).[32]

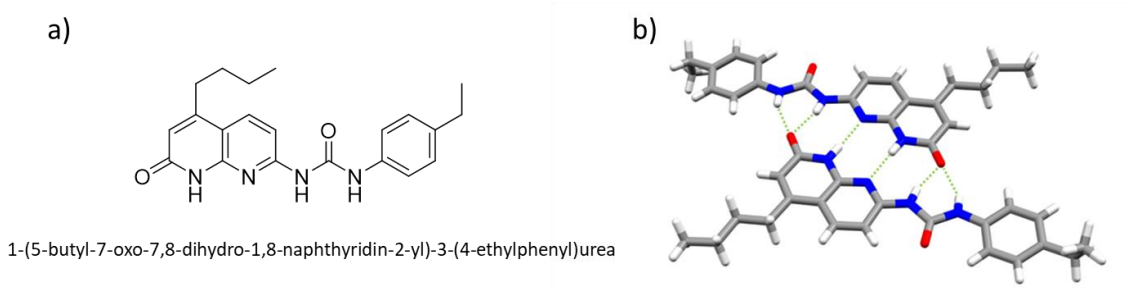

Figure 7. a) chemical structure of a chloroform soluble ODIN motif *1-(5-butyl-7-oxo-7,8-dihydro-1,8-naphthyridin-2-yl)-3-(4-ethylphenyl)urea*, b) its dimeric structure obtained *via* single crystal X-ray diffraction, the six hydrogen bonds are highlighted in green.[32]

References

[1] W. Binder, *Hydrogen Bonded Polymers*, Springer, Berlin New York, **2007**.
[2] G. A. Jeffrey, W. Saenger, in *Hydrogen Bonding in Biological Structures*, Springer Berlin Heidelberg, Berlin, Heidelberg, **1994**, 3.
[3] H. Shao, J. R. Parquette, *Chem. Commun.* **2010**, *46*, 4285.
[4] S. Burattini, H. M. Colquhoun, J. D. Fox, D. Friedmann, B. W. Greenland, P. J. F. Harris, W. Hayes, M. E. Mackay, S. J. Rowan, *Chem. Commun.* **2009**, 6717.
[5] G. R. Whittell, M. D. Hager, U. S. Schubert, I. Manners, *Nat. Mater* **2011**, *10*, 176.
[6] D. C. Tuncaboylu, M. Sari, W. Oppermann, O. Okay, *Macromolecules* **2011**, *44*, 4997.
[7] T. Aida, E. W. Meijer, S. I. Stupp, *Science* **2012**, *335*, 813.
[8] D. B. Varshey, J. R. G. Sander, T. Friščić, L. R. MacGillivray, in *Supramolecular Chemistry* (Eds.: P. A. Gale, J. W. Steed), John Wiley & Sons, Ltd, Chichester, UK, **2012**.
[9] T. Rossow, S. Seiffert, in *Supramolecular Polymer Networks and Gels* (Ed.: S. Seiffert), Springer International Publishing, Cham, **2015**.
[10] M. Dionisio, L. Ricci, G. Pecchini, D. Masseroni, G. Ruggeri, L. Cristofolini, E. Rampazzo, E. Dalcanale, *Macromolecules* **2014**, *47*, 632.
[11] G. Grassi, R. Farra, P. Caliceti, G. Guarnieri, S. Salmaso, M. Carenza, M. Grassi, *Am. J. Drug Delivery* **2005**, *3*, 239.
[12] T. Rossow, S. Hackelbusch, P. van Assenbergh, S. Seiffert, *Polym. Chem.* **2013**, *4*, 2515.
[13] M. Lemmers, J. Sprakel, I. K. Voets, J. van der Gucht, M. A. Cohen Stuart, *Angew Chem Int. Ed.* **2010**, *49*, 708.
[14] Y. Zhang, W. Zhang, J. Li, J. Dang, T. Wei, *Materials Lett.* **2012**, *82*, 227.
[15] T.-A. Asoh, H. Yoshitake, Y. Takano, A. Kikuchi, *Macromol. Chem. Phys.* **2013**, *214*, 2534.
[16] P. Y. W. Dankers, E. W. Meijer, *BCSJ* **2007**, *80*, 2047.
[17] Y. Qiu, K. Park, *Adv. Drug Deliv. Rev.* **2001**, *53*, 321.
[18] E. B. Murphy, F. Wudl, *Progress Polym. Sci.* **2010**, *35*, 223.
[19] P. Cordier, F. Tournilhac, C. Soulié-Ziakovic, L. Leibler, *Nature* **2008**, *451*, 977.
[20] J. R. Kumpfer, S. J. Rowan, *J. Am. Chem. Soc.* **2011**, *133*, 12866.
[21] S. J. Grabowski, *J. Phys. Chem. A* **2001**, *105*, 10739.
[22] R. P. Sijbesma, E. W. Meijer, *Chem. Commun.* **2003**, 5.
[23] W. P. J. Appel, M. M. L. Nieuwenhuizen, E. W. Meijer, in *Supramolecular Polymer Chemistry* (Ed.: A. Harada), Wiley, **2011**.
[24] R. P. Sijbesma, F. H. Beijer, L. Brunsveld, B. J. B. Folmer, J. H. K. K. Hirschberg, R. F. M. Lange, J. K. L. Lowe, E. W. Meijer, *Science* **1997**, *278*, 1601.
[25] F. H. Beijer, R. P. Sijbesma, H. Kooijman, A. L. Spek, E. W. Meijer, *J. Am. Chem. Soc.* **1998**, *120*, 6761.
[26] W. J. Blank, Z. A. He, E. T. Hessell, *Progress Org. Coatings* **1999**, *35*, 19.
[27] M. C. Pannone, C. W. Macosko, *J. Appl. Polym. Sci.* **1987**, *34*, 2409.
[28] B. Zhu, Z. Feng, Z. Zheng, X. Wang, *J. Appl. Polym. Sci.* **2012**, *123*, 1755.
[29] G. Armstrong, M. Buggy, *Materials Sci. Eng: C* **2001**, *18*, 45.
[30] G. Armstrong, M. Buggy, *Polym. Int.* **2002**, *51*, 1219.
[31] D. J. M. van Beek, A. J. H. Spiering, G. W. M. Peters, K. te Nijenhuis, R. P. Sijbesma, *Macromolecules* **2007**, *40*, 8464.
[32] J. Tellers, S. Canossa, R. Pinalli, M. Soliman, J. Vachon, E. Dalcanale, *Macromolecules* **2018**, *51*, 7680.
[33] S. Goswami, S. Dey, J. F. Gallagher, A. J. Lough, S. García-Granda, L. Torre-Fernández, I. Alkorta, J. Elguero, *J. Mol. Struct.* **2007**, *846*, 97.

Chapter 1

PE-based ionomers, novel method to both crosslink and enhance adhesive properties of polyethylene

1. Introduction

1.1 Polyethylene-Crosslinking methods

Polyethylene (PE) is the most widely used thermoplastic polymer and the leader in most applications in the global plastic industry. It exhibits strong resistance to solvents, exceptional flexibility, low cost, lightness, and simplicity of processing. It finds application in many common objects, ranging from single use plastics like plastic bags and packaging, to durable goods in automotive, electronics, medicine, fiber, and textiles.[1],[2] However, its use is limited by its low strength and stiffness, low upper service temperature, stress cracking, poor UV resistance. Additionally, its apolar nature makes it unsuitable for any coating and adhesive application unless a surface treatment is applied (like flame and corona treatment). To overcome those issues, and drastically improve its properties, crosslinking of polyethylene is performed. There are different methods to crosslink polyethylene, which can be physical, or chemical (Figure 1).

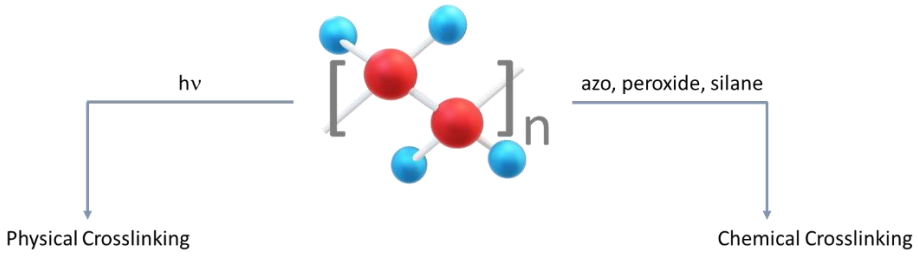

Figure 1. Polyethylene crosslinking methods.

Physical methods involve the use of high-energy radiation to generate free radicals. The radiation is provided by different sources like electron beams, gamma rays, or ultraviolet radiation.[3] These kinds of methods are usually carried out in the solid state and in an inert atmosphere to prevent oxidative degradation. The physical method allows for obtaining a high crosslinking rate, without residual peroxide or unwanted byproducts. However, the crosslinking, performed in the solid state, results to be uneven and has limitations related to the thickness of the sample used.

Chemical methods consist of the use of initiators like peroxide or azo and coupling agents like silane. High-temperature peroxide crosslinking of polyethylene is known to produce cable insulation, foams, and high-performance piping.[4],[5] This method involves the addition of peroxide (dicumyl peroxide is the most common) to polyethylene in the molten state, at a temperature lower than the activation temperature of the peroxide to prevent premature

crosslinking. The crosslinking reaction takes place during the extrusion process, where further heating promotes the decomposition of the peroxide and thus the initiation of the reaction. The same procedure is used for the crosslinking reaction catalyzed by azo compounds. The main difference is that azo compounds are generally more stable than peroxides, which makes them more suitable for the crosslinking of high molecular weight polyethylene. [6] However, the low activity of the primary radicals leads to a low crosslinking efficiency and leads to the formation of several byproducts, among which carbon monoxide. For this reason, this method is mostly used to produce expanded crosslinked polyethylene products. The cross-linking method through silane consists of two consecutive stages.[7] As illustrated in Figure 2, first there is the grafting reaction catalyzed by peroxide, of vinyl silane onto the polyethylene, followed by the hydrolysis and condensation reactions to obtain the silane crosslinked polyethylene.

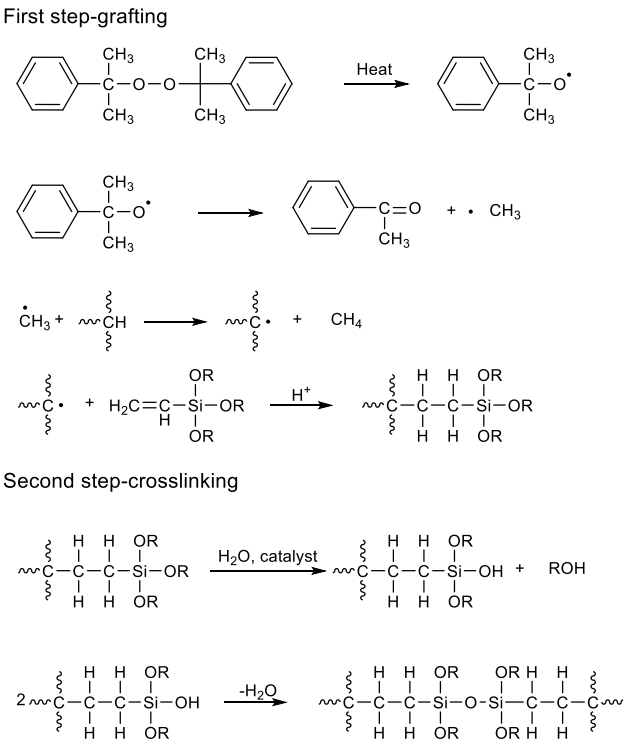

Figure 2. Reaction mechanism of silane crosslinking of polyethylene.

Vinyl alkoxy silanes are the most common silane used for these kinds of reactions due to their double bonds and ability to rapid crosslinks.[8] This technique is the most popular because it not only allows for crosslinking but also adds polar groups, which increases the potential applications of non-polar polyethylene.[9]

All these methods have drawbacks, the main one is the formation of byproducts that lead to several defects in the PE structure, so innovative methods are required to functionalize PE and crosslink it.

1.2 Ionomers

1.2.1 Definition of ionomers

Polymers with a few mole percent of ionic groups into the chains are known as ionomers, a term first coined by R. W. Rees from E. I. Dupont deNemours & Co. Inc. in the ’60s. In particular, ionomers are polymers whose bulk properties are governed by ionic interactions in discrete regions of the material, specifically materials with an ionic group content of 15 mol%.[10],[11] This definition emphasizes the importance of the behavior of these materials rather than their composition. The covalent introduction of bonded ionic groups along a hydrophobic backbone, like the polyolefin one, deeply changes the physical and chemical behavior of the resulting material. The incorporation of even a small amount of ionic groups causes a dramatic improvement in some polymer properties, such as impact and tensile strength as well as tear and abrasion resistance.[12] Additionally, improving the polarity of the polymer can greatly amplify the application window of polyolefin, paving the way to adhesives, dying, and printing ink uses.

1.2.2 Ionomers morphology and rheological behavior

Ionomers are usually deemed as multiphase material, due to the formation of ion-rich nanometer-size aggregates into a polymer matrix.[13] Techniques such as Small-angle-X-ray scattering,[14] electron microscopy,[15] and dielectric measurement[15] have been used to investigate the morphology of these ion clusters. In 1990 Eisenburg, Hird, and Moore described the clustering behavior in the Eisenburg-Hird-Moore (EHM) model (see Figure 3a*)*, which relates ionomer morphology to their mechanical properties. The ion pairs, according to the model, bind their connected polymer chains bringing to the formation of ionic domains in the amorphous phase of the semicrystalline polymer. This results in a region of restricted mobility compared to the bulk polymer thanks to the physical crosslinking in the vicinity of ionic domains. The increasing number and size of restricted mobility regions can eventually overlap and further restrict movement (Figure 3b).[16]

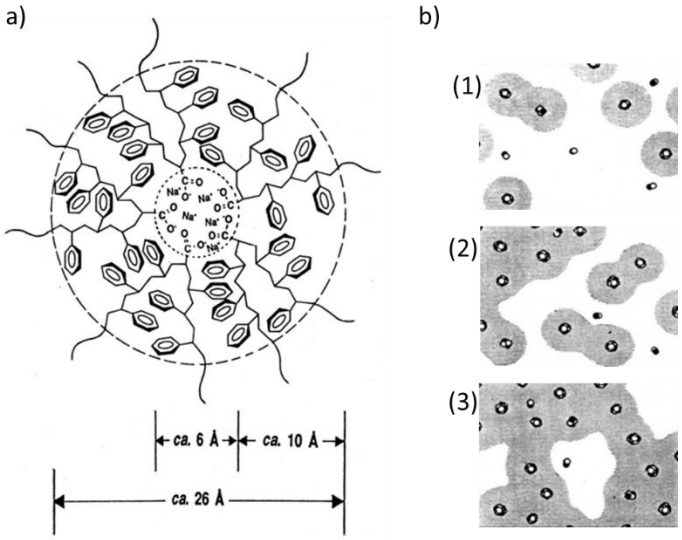

Figure 3. a) Schematic diagram of the region of restricted mobility of the EHM model; b) representation of the morphologies of ionomers with low content (1) intermediate content (2) and with higher content (3) of ionic aggregates.[16]

Tadano et al. through calorimetric and thermal expansion investigations studied the morphological changes that take place during heating.[17] The model was divided into three stages (see Figure 4). Phase one was referred to as the state of order, made up of an amorphous area, polyethylene crystallites, and organized ionic clusters. The ionic cluster crystal arrangement became disorganized as the temperature goes up (T_i), and when it rose even higher (T_m), the crystals began to melt while still holding the disordered ionic clusters. Re-crystallization occurs quickly during cooling (T_c), whereas the relaxation process takes longer to reorganize the ionic clusters.

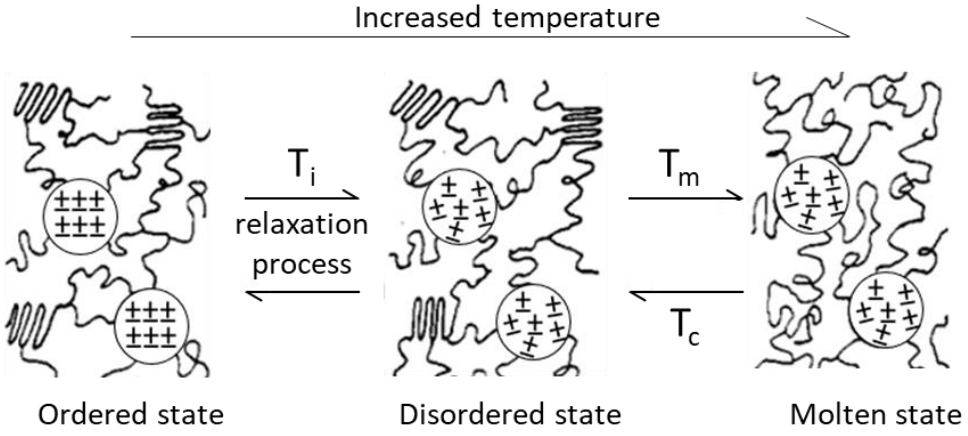

Figure 4. Order-disorder transition driven by the temperature of the ionic cluster.[17]

These nano-domains, acting as a crosslinker for the polymer chains, cause an increase in viscosity and therefore a decrease in the mobility of polymer chains in the molten state and consequently a long relaxation time. Ionomers offer a wide range of potential applications, but their use has been limited by the materials' incapacity to melt during typical production procedures. The rheology behavior of ionomers and the dynamic nature of their bonds is thus a very interesting area to investigate since the physical crosslinks generated by the ionic domains persist to elevated temperatures up to 300 °C.[18] Cooper proposed the ion-hopping mechanism to clarify how the flow of ionomers proceeds in 1958.[19] This mechanism consists of the diffusion of an ionic pair from one aggregate into another in a finite lifetime τ. The slow dynamic of ion-hopping results in long relaxation times of the ionic associations and consequently in very low melt flow properties of the ionomer. This results in a characteristic behavior when tested with a small amplitude oscillatory rheometer: at low frequencies, the ionomer will show a solid-like behavior rather than a typical liquid-like one.[20] Furthermore, the flow is dependent on the temperature, the ion pair, and their concentration.

1.2.3 Synthesis

The synthesis of ionomers can be achieved through the copolymerization of an ionic monomer with a non-ionic one or by the post-functionalization of a polymer (for example by sulfonation, grafting, or quaternarization reactions). Post-functionalization is usually the most used, despite the problems associated with it, like the formation of byproducts, incomplete functionalization, and aggressive reaction conditions. The most well-known ionic polymer, namely, Surlyn® introduced by DuPont is made by copolymerization of ethylene with acrylic acid followed by a partial neutralization step with a metal salt (typically Na or Zn based, see Scheme 1). [21]

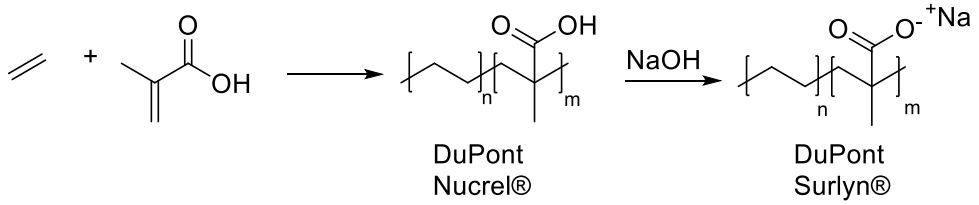

Scheme 1. Synthetic pathway of Dupont Nucrel® and Surlyn® by DuPont.

The neutralization step is typically performed in the melt by adding the metal hydroxide, which requires manufacturing equipment highly resistant to corrosive chemicals. The process can be performed also in solution, but in both cases, it is difficult to control and determine the

final neutralization degree of the polymer. Another commercial success is a PP-based ionomer obtained by reactive extrusion grafting of a Zn methacrylate salt (Dymalink® from Total) on a PP backbone (Scheme 2).[22] This method is typically constrained by the incomplete grafting reaction, the potential for polymer backbone degradation or breaking, and the laborious process required to remove the unreacted ionic component.

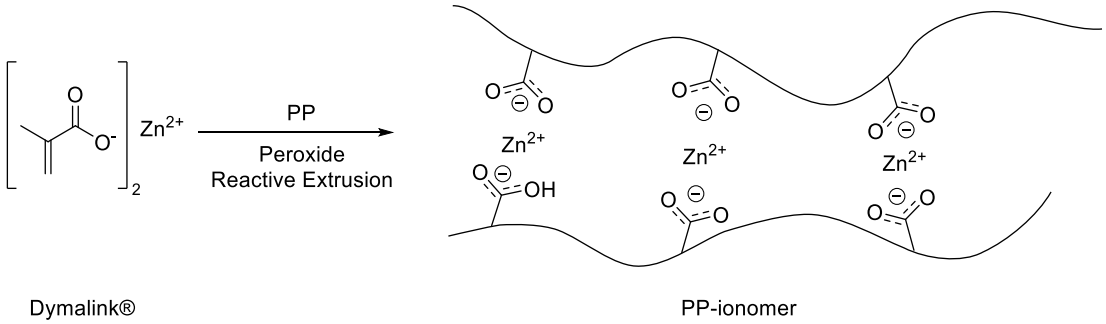

Scheme 2. Use of Dymalink® (Total) to create PP-ionomer.

The direct copolymerization between a non-ionic monomer with an ionic one overcomes the issues of a multistep process, even if some difficulties can also arise related to the solubility of the two components or the choice of the polymerization technique. Reactions like free radical polymerization (FRP),[23] reversible addition-fragmentation chain transfer (RAFT),[24] or acyclic diene metathesis (ADMET)[25] polymerization, are mostly used to achieve the final polymer without the need for an extra step. Co-polymerization reactions frequently experience catalyst poisoning and low molecular weight product. Moreover, all these methods are not suitable for monomers like ethylene since there are no functional groups able to promote this kind of mechanism.

Here we report the synthesis of a new type of polyethylene-based ionomer, where a few mole percent of positively and negatively charged groups are covalently bound to the polymer backbone.[26] Amino-terminated methacrylates and methacrylic acid, present in the form of ion pairs, are used as comonomers together with ethylene, in a high-temperature / high-pressure process.[27] The concept of having a direct copolymerization of ion-pair comonomers (IPC) with non-charged monomers was first reported by Salomone et al.[28],[29] and later extended to other charged monomers and types of polymerization, including atom transfer and free radical polymerization (ATRP, FRP) as well as reversible addition fragmentation chain transfer (RAFT).[30],[31]However, these synthetic schemes are not suitable for ethylene, particularly when polymerized using metal-based catalysts that can be poisoned by charged molecules. We

thus extend the IPC concept to polyethylene copolymers, which were obtained *via* high-pressure free radical copolymerization in the presence of ethylene and a suitable initiator.

The formation of ion pairs comprising an ammonium and carboxyl group, which are both embedded within the polyethylene backbone, removes the need for labile counterions such as Na^+ or Zn^{2+} that are present in other types of ionomers such as ethylene-acrylate and ethylene-methacrylate copolymers.[32],[10] This approach not only removes the need for an additional neutralization step after the synthesis but also the need avoids the use of corrosion-resistant processing equipment. Instead, IPC-based materials do not require specialized equipment since the acid is fully neutralized by the amine counterpart.

Herein, a study of the polymerization reaction of a polyethylene-based ionomer using different reaction conditions, such as temperature, IPC content, and the use of a chain transfer agent (CTA) was carried out. In particular, dimethyl-amino terminated methacrylate and methacrylic acid were chosen for the formation of the ion pair comonomer, since they are cheap, commercially available at industrial scale, and they both are approved in European Union (EU) for food contact application plastics.

1.3 Result and discussion

1.3.1 Synthesis study of fully organic polyethylene-based ionomer

The one-step synthesis of polyethylene-based ionomers where both the cationic and anionic groups are covalently bound to the backbone is performed by directly reacting the ion-pair comonomer (IPC) with ethylene through a high-pressure/high-temperature free radical copolymerization.[27] This approach allows for avoiding the presence of mobile inorganic cations, which is the case for commercially available ionomers such as Surlyn® (Dupont),[21] and Dymalink (Total Cray Valley), where zinc diacrylate is used as crosslinker between two acidic groups.[33] High-pressure/high-temperature free radical polymerization of ethylene leads to a branched chain configuration comparable to that of low-density polyethylene (LDPE). The synthesis is compatible with a large range of comonomers with various functionalities, that would not be feasible when using typical industrial Ziegler-Natta or metallocene catalysts, where any “polar” moieties such as hydroxyl or amino groups would poison the catalyst.[34] Instead, by using free radical polymerization, it is possible to introduce randomly such polar groups directly without any protecting group (Figure 5).

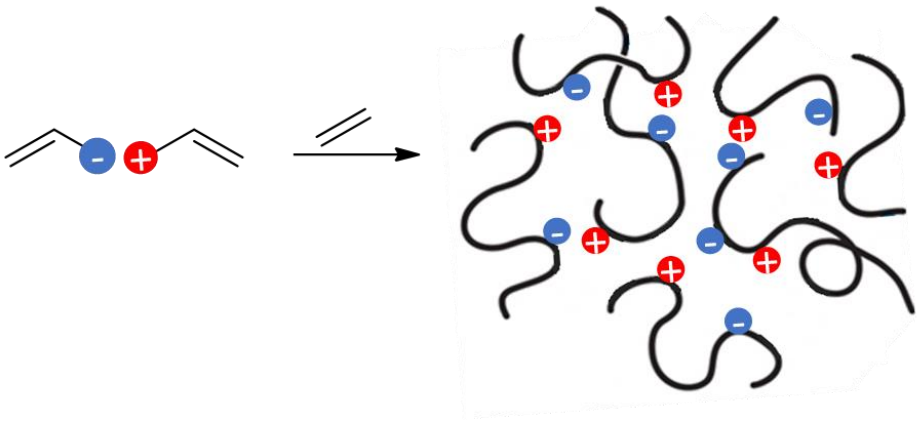

Figure 5. Schematic illustration of the ion-pair comonomer (IPC) concept.

A study on high-pressure/high-temperature free radical polymerization has been carried out using high-pressure autoclave equipment, by testing different reaction conditions (temperature, IPC, and chain transfer agent (CTA) content).

1.3.2 Synthesis of ion pair comonomer

The IPC was synthesized *via* an acid-base reaction by mixing the two starting reagents without the use of solvents (Scheme 3). Due to the exothermicity of the reaction, this is typically performed by adding dropwise the acid into the amine being careful to use an ice bath to cool the reaction.

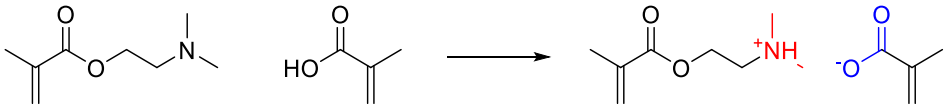

Scheme 3. Synthesis of the IPC.

^{1}H-NMR spectroscopy was used to confirm the formation of the ion pair by monitoring the chemical shift of the protons before and after the formation of the salt (Figure 6).

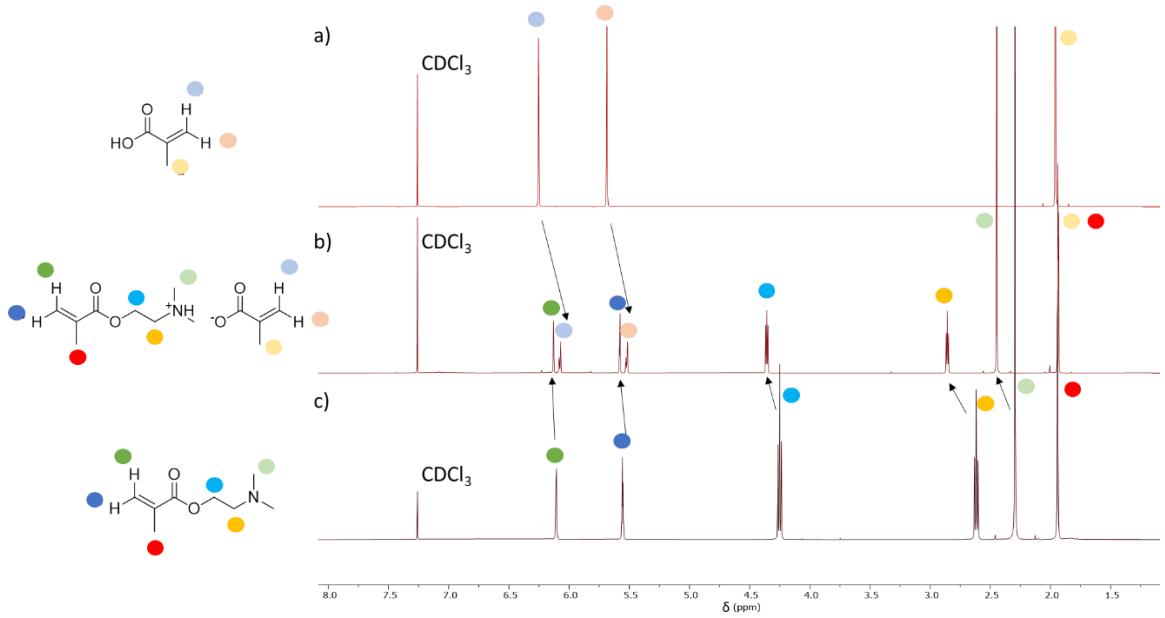

Figure 6. Comparison between ^{1}H-NMR (400 MHz, r.t.) of a) Methacrylic acid, b) IPC, c) and 2-(dimethylamino)ethyl methacrylate in $CDCl_3$.

As pointed out in the figure above, the vinyl protons of the methacrylate are shifted to a higher field, while a downfield shift of the ethane and the methyl protons connected to the amino group is observed. Several aspects were considered to copolymerize IPC with ethylene to create different polymers and to investigate how and how many modifications in the polymerization reaction affect the properties of the final polymer.

1.3.3 General procedure of the polymerization reaction

IPC (0.05, 0.1, or 0.2 mol%) was dissolved in methanol (50 wt%) and mixed with high-pressure ethylene through a static mixer. Consequently, the peroxide initiator, Luperox®11M75 (1.5 g/L), and propanal as charge transfer agent CTA (0 or 0.07 mol%) are added to the mixture and heated at 60 °C before being injected in the reactor set at a fixed temperature (from 180 °C to 270 °C).

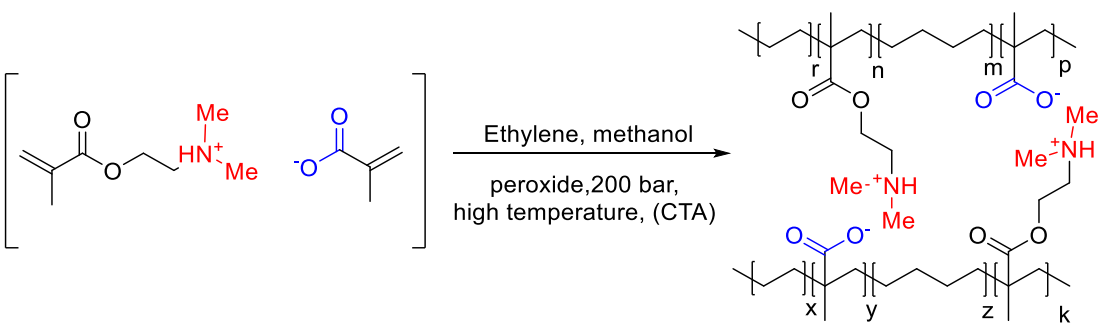

Scheme 4. Copolymerization reaction of IPC and ethylene.

Methanol was chosen as a solvent since it does not have a large effect on polymerization thanks to its very low chain transfer constant.[35],[36] During the reaction, the pressure and the temperature are maintained constant, and the final polymer is recovered in the recuperation vessel (see the schematic illustration in the figure below).

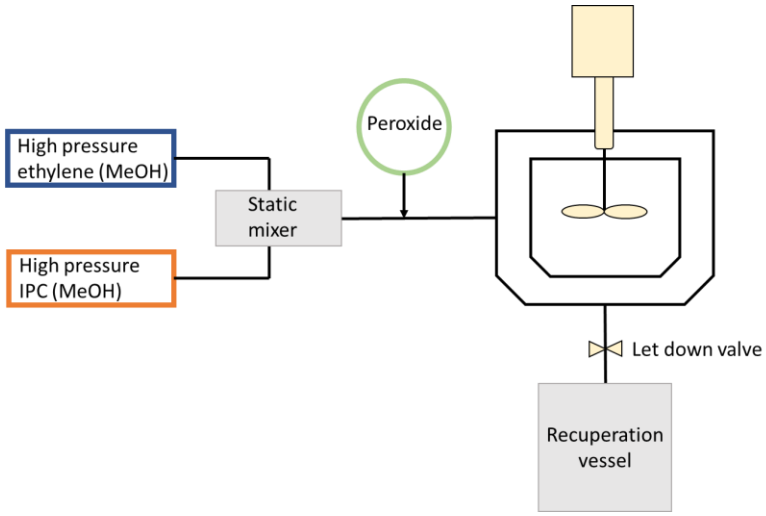

Figure 7. Autoclave setup for high-pressure/high-temperature polymerization.

Table 1 illustrates the reaction conditions used to obtain each polymer and the melting flow index measured at the reactor exit.

Table 1. Reaction conditions used during the polymerization reaction and MFI measured.

Name	*Pressure (bar)*	*IPC content (mol%)*	*CTA (mol%)*	*Temperature (°C)*	*MFI (g/10 min)*
P1	2000	0.05	0.07	180	0.1
P2	2000	0.05	None	180	n.d.
P3	2000	0.05	0.07	200	1
P4	2000	0.05	None	200	n.d.
P5	2000	0.05	0.07	220	0.6
P6	2000	0.05	None	220	n.d.
P7	2000	0.05	0.07	240	5.5
P8	2000	0.05	0.07	250	12.2
P9	2000	0.05	0.07	270	64.1
P10	2000	0.1	None	180	0.4
P11	2000	0.1	None	200	1.6
P12	2000	0.1	0.07	220	13
P13	2000	0.1	0.07	240	66
P14	2000	0.1	0.07	250	25.3
P15	2000	0.1	0.07	270	143.4
P16	2000	0.2	None	180	3
P17	2000	0.2	None	200	8.3
P18	2000	0.2	0.07	220	25
P19	2000	0.2	0.07	240	138
P20	2000	0.2	0.07	250	52.5
P21	2000	0.2	0.07	270	196

A crucial aspect to consider is the use or not of the CTA. In previous experiments conducted without the use of transfer agents, difficulties in measuring MFI values were observed. Given the creation of both extremely long chain branching polymers and ionic crosslinking, this behavior is easily explained. It is important to note that the final product's unusually high viscosity causes processing issues, therefore using CTA to control the chain length during synthesis is a critical feature to achieve the proper mechanical and processing qualities. Control experiments were carried out without the addition of CTA and as expected, the ionomers generated by adding a low content of CTA (0.07 mol%) in the feed, have an MFI so low that cannot be measured. Even without the presence of a CTA, the MFI value increases with increasing IPC content in the feed (0.1 and 0.2 mol%), indicating that the IPC can operate as a change transfer agent itself. Of course, also the temperature influences the viscosity of the final product as well. A clear trend is visible in the diagram below: the MFI increases whit the increasing IPC content in the feed and with the increasing of the reaction temperature.

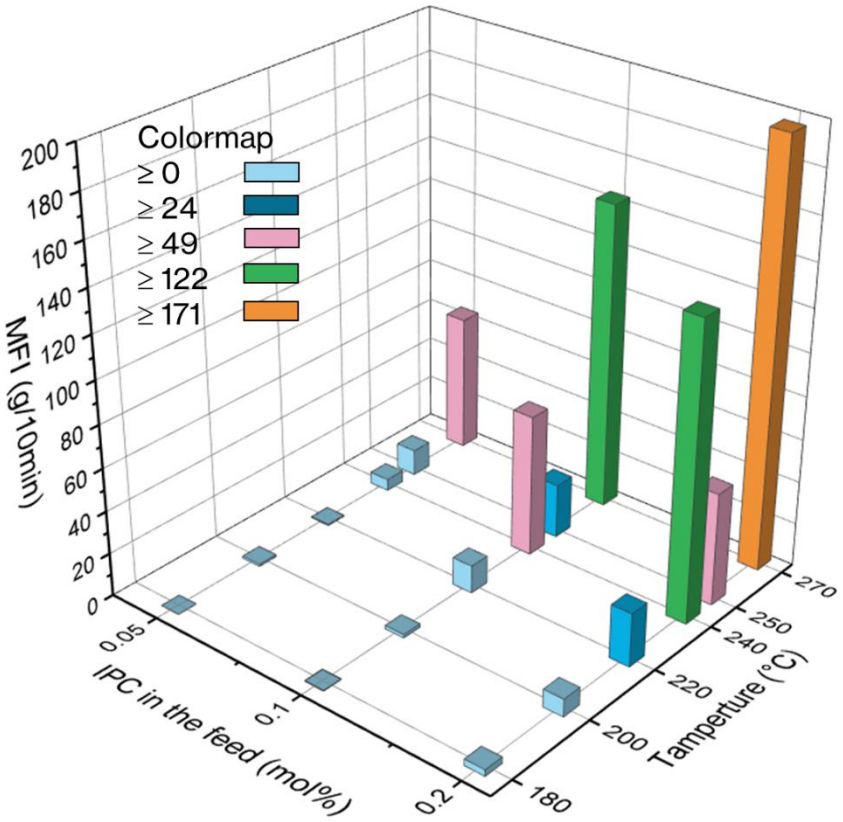

Graph 1. Effect of the temperature and IPC content in the feed on the MFI of the final polymer.

1.3.4 Processability of the ionomers.

The viscosity of the polymer, and consequently its MFI value, are critical factors to consider because they have an impact on the manufacturing stage. Cast film extruder testing was performed at temperatures between 150 °C and 190 °C (temperatures commonly used to

extrude LDPE),[37] to determine their processability. The temperature of the extruder was chosen depending on the MFI of the polymer: with a high MFI, the temperature needed to make the polymer flow is lower with respect to the polymer with a lower MFI (Figure 8 shows the temperatures used).

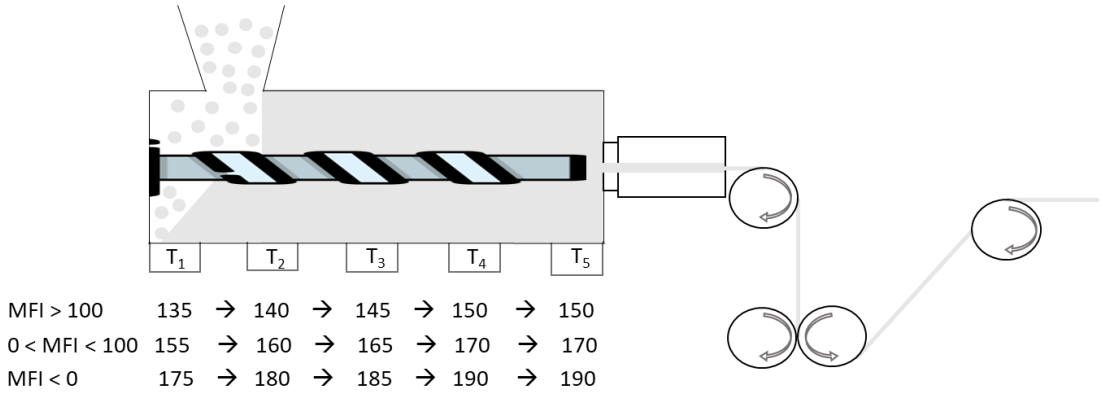

Figure 8. Setup of the cast film extruder, and temperatures used according to the MFI of the polymer.

The ionomers with an MFI > 100 (**P15**, **P19**, and **P21**) had such low viscosity that film formation was impossible. For a diametrically opposite reason, the ionomer **P2** was not processable, because too viscous and was not able to flow through the die. For these reasons, these polymers will not be discussed further after this point. The films obtained (~ 50 μm of thickness) are uniform except for the presence of some gels spread along the volume inherent to the small autoclave process caused by branching reactions (see Figure S1).[38]

1.3.5 Characterization of the ionomer

The ionomers produced with the autoclave were recovered and characterized through ^{1}H-NMR spectroscopy, FT-IR spectroscopy, and elemental analysis. The ^{1}H-NMR spectra were conducted at high temperatures, using TCE-d_2 as solvent. The spectrum of P10 is reported in Figure 9 as an example, where it is possible to identify the diagnostic peaks of the methyl belonging to the amino moieties, as well as the methylene connecting the ester and the amino group, and the polyethylene backbone in the aliphatic region.

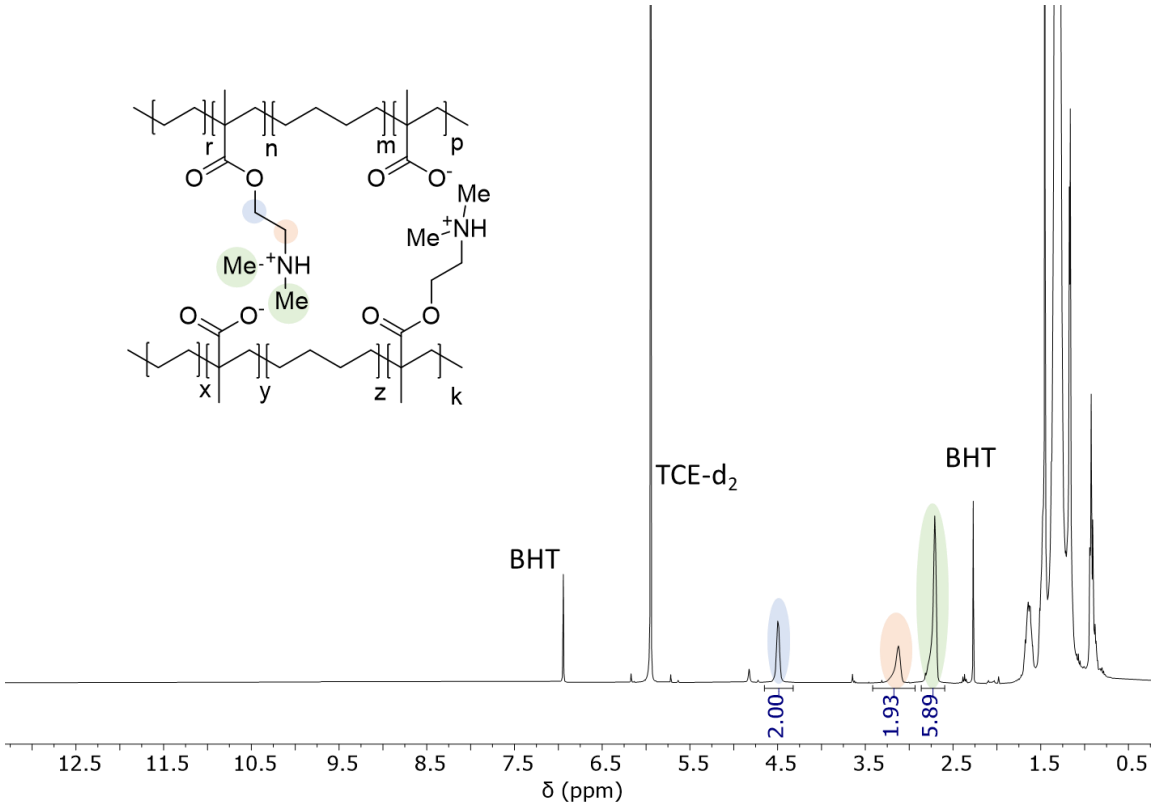

Figure 9. ^{1}H NMR (500 MHz, 120 °C) of P1 in TCE-d2 (10 mg of butylated hydroxytoluene BHT were added in the NMR tube).

The NMR spectrum confirms the absence of unreacted monomers (no vinyl groups present) and also highlights that the polymerization reaction proceeds without the formation of side products providing a relatively pure polymer. These specific peaks can be used to determine the IPC content in the polymer through the relation between their integral and the integral of the aliphatic backbone.

However, to accurately quantify the content of IPC inside the final polymer, elemental analysis was instead used to obtain the exact content of nitrogen, present only in the comonomer. As shown in Table 2, the content of IPC is dependent on the initial content of IPC added and the temperature of the reaction. Increasing the IPC content in the feed of the reactor increases the IPC content in the polymer while increasing the temperature has the opposite effect. Indeed, at low temperatures the reactivity of the methacrylate is higher than the reactivity of ethylene,[39] instead increasing the temperature, the reactivity turns in favor of ethylene, leading to a polymer with a lower content of IPC.

Table 2. The content of IPC was calculated *via* nitrogen elemental analysis, melting temperature (T_m), the heat of fusion (ΔH_f), and crystallinity (X_C) obtained *via* DSC. As references, a commercial LDPE ($LDPE_C$) and an LDPE made in the same autoclave of the ionomers ($LDPE_A$) are used.

Name	***Content of IPC (wt%)***	T_m ***(°C)***	ΔH_f ***(J g^{-1})***	X_C ***(%)***[a)]
$LDPE_C$	-	105	131.9	46
$LDPE_A$	-	115	167.5	58
P1	4.2	114	157.0	53
P3	3.8	112	157.8	54
P4	3.1	111	147.0	50
P5	2.6	110	189.9	65
P6	2.8	111	150.3	51
P7	4.1	110	154.0	53
P8	3.3	108	144.5	49
P9	2.8	108	142.1	48
P10	6.6	111	145.7	50
P11	5.7	110	143.7	49
P12	6	109	152.8	52
P13	5.8	107	147.3	50
P14	2.8	106	137.3	47
P16	11.4	106	128.1	44
P17	10	105	125.3	43
P18	10.5	105	135.4	46
P20	6.1	103	123.2	42

a) Calculated considering the heat of fusion of 100% crystalline polyethylene ΔH_f^0 = 286.2 J g^{-1}.[40]

To determine the molecular weight, gel permeation chromatography (GPC) has been attempted on P5 by dissolving it in 1,2-dichlorobenzene at 80 °C. The resulting chromatogram (Figure S2) shows the presence of ionic aggregates, that persist also in solution, giving an apparent molecular weight M_w = 324400 g/mol and a polydispersity index (DPI) M_w/M_n= 39. We believe that these values do not reflect reality, but are due to the presence of the ionic clusters, that provide an apparent abnormal high molecular weight.

1.3.6 Thermal and mechanical characterization

Differential Scanning Calorimetry (DSC) was used to acquire a better understanding of the microstructure and thermal properties of the produced ionomers. Table 2 shows the thermal data, obtained *via* DSC, of the ionomers and as references a commercial LDPE ($LDPE_C$) and an LDPE made in the same autoclave of the ionomers ($LDPE_A$). All the ionomers show similar thermograms, comparable to the one of $LDPE_A$ (see Figure S3). The melting temperatures obtained from the second heating, range from 103 °C to 114 °C in line with the crystallinity % (42% to 65%) that decreases with the increasing content of IPC. Indeed, a higher IPC content is expected to increase the amorphous domains of LDPE

To investigate the microstructure of the polymer, the average lamellar thickness (Table S1) has been calculated following the Gibbs-Thomson equation (equation 1):[41]

$$l_c = \frac{2\sigma_e}{\rho \cdot \Delta H_f^0} \cdot \frac{T_m^0}{T_m^0 - T_m} \quad (1)$$

Where σ_e = 90.4 mJ m^{-2} is the surface energy for polyethylene,[42],[43] ρ =1 g cm^{-3} is the density of the crystal phase. ΔH_f^0 = 286.2 g J^{-1} is the heat of fusion,[40] and T_m^0 = 418.6 K is the equilibrium melting temperature of polyethylene. The obtained lamellar thickness values, between 8.4 nm and 8.7 nm are consistent with the typical values of LDPE,[44] suggesting that the inclusion of the IPC does not affect in a meaningful way the microstructure of the polymer, even if it is also evident that both the higher addition of IPC in the feed and the higher reaction temperature results in slightly smaller crystallinity structure of polyethylene.

The most significant and desired effect of the addition of IPC into the polyethylene backbone consists of the cross-linking of the chains through the ionic bond between the carboxylate and ammonium groups. Such an effect, results in an improvement in the mechanical properties of the polymer compared to ordinary LDPEs, obtaining performances tending to thermoset materials without sacrificing the processability of the thermoplastic thanks to the non-covalent network. A direct effect of the formation of this network is the increased Young modulus value and the capability to not melt easily but retain a modulus after the melting temperature.

With these lenses, dynamic mechanical thermal analysis (DMTA) was performed to analyze the thermo-mechanical behavior of the ionomers with respect to $LDPE_C$. The thermograms were recorded in the tensile mode (Figure 10d) from 30 °C to 200 °C. The measurement of $LDPE_C$ (black line in Figure 10) stopped nearby its melting temperature where a sudden collapse of the storage modulus is registered. Most of the ionomers behave like $LDPE_C$ and the rupture of the sample is reached at the melting point. Visibly in both the three graphs (Figure 10a,b,c) the samples able to retain a modulus after the melting temperature are the ones obtained using lower reaction temperature, and thus the polymers with lower MFI values (between 0 and 8 g/10 min). Moreover, among these six polymers, only P1 and P4 show good modulus values at 150 °C of 0.6 and 0.8 Mpa respectively, afterward the modulus decrees to 0.1 Mpa for P5, 0.5 Mpa for P10 and P16, and 0.4 Mpa for P17.

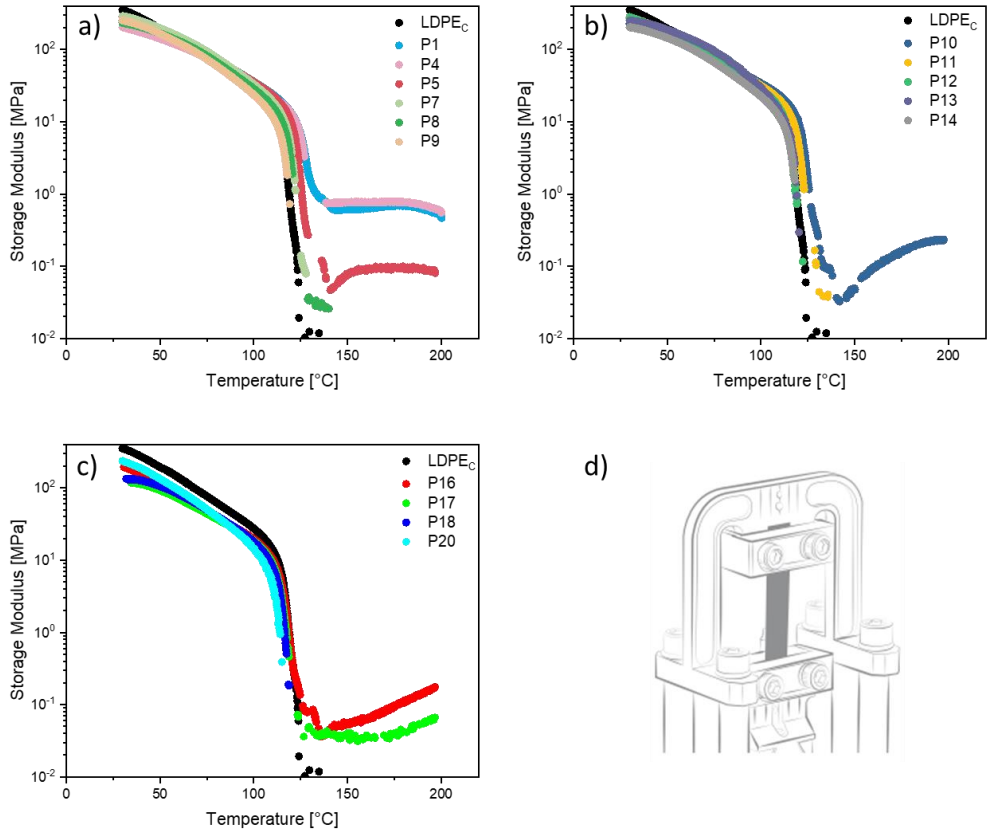

Figure 10. DMTA thermograms of a) $LDPE_C$, P1-9, b) $LDPE_C$, P10-14, c) $LDPE_C$, P16-20, and d) setting of the measurement conducted in the tensile mode.

Especially for the polymers with a high content of IPC, like P16, and P17, the entropic effect of the crosslink in the increasing inclination of the plateau segment is clearly visible. This effect consists of an entropic reduction in the gyration radius of the polymer that causes the

approach of the crosslinking points and thus the rise of the plateau. This transition is related to crystallization phenomena, that can be seen in the rubbery plateau region upon heating. The chains gain enough mobility to rearrange into crystallites, which causes sporadically an increase in modulus.[45]

These results highlighted that the effect of crosslinking is detectable through DMTA only for polymers with high viscosity. To obtain further information, the mechanical properties in the solid state were studied by performing tensile tests on the films.

Five specimens for each material were analyzed and preliminary observations can be made by comparing the stress-strain curve profiles of $LDPE_C$ and an ionomer (P18) in Figure 11.

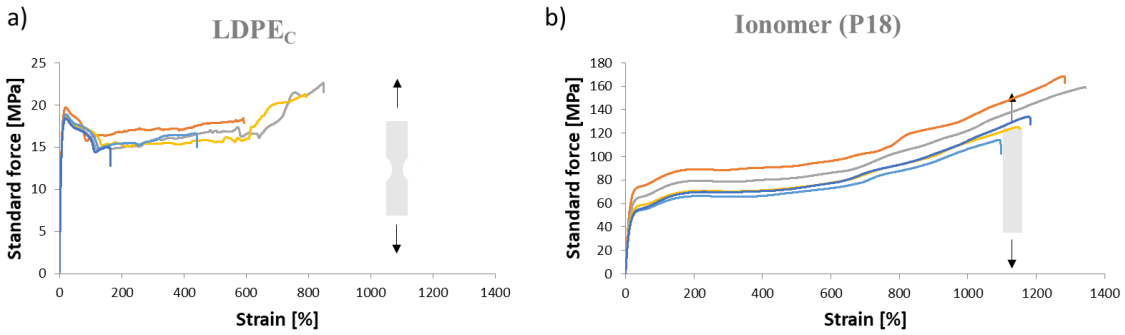

Figure 11. Stress-strain curves of a) $LDPE_C$ and b) P18.

Important evidence is the way the ionomer and $LDPE_C$ deform once reaching the yield point, $LDPE_C$ immediately neck, while the ionomer films deform mostly uniformly across its whole surface. The improved ability of the ionomers films to be extended before breaking is another feature seen in Figure 11 and Figure 12a, which is remarkable since the stiffness of the films is also increased (Figure 12b). Analyzing elongation and stress at break charts a trend in connection to polymerization temperature, and as a result, also to the polymers' MFI value is noticed. In comparison to both LDPEs, all ionomers can be pulled further before breaking, however, the ionomers with greater viscosities are rightly stiffer and can be extended less.

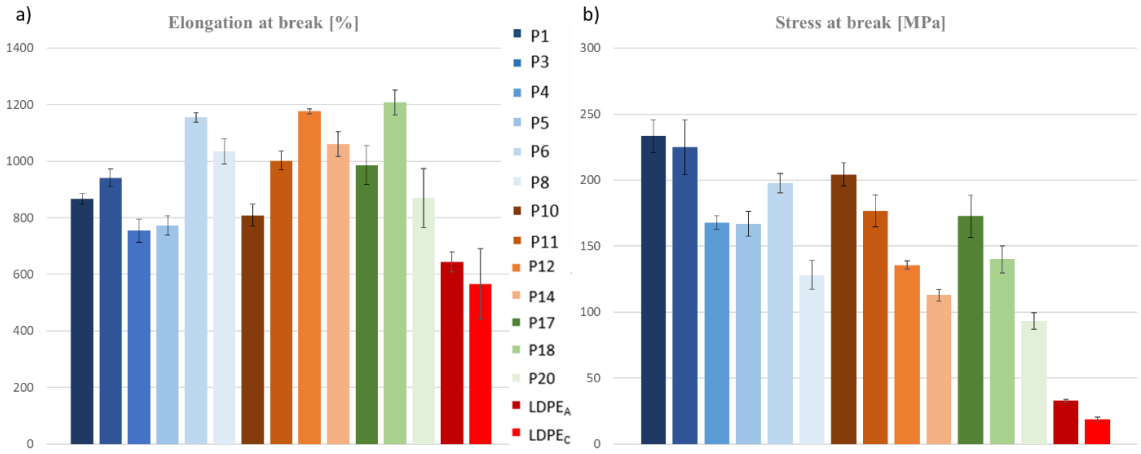

Figure 12. Column chart of a) elongation at break, and b) stress at break.

The stiffness of the ionomers is confirmed by the increased values of Young modulus (Figure 13), especially for the polymers made at lower temperatures and with less IPC content incorporated. These results are in line with the expectations since the IPC works as CTA: the higher the IPC content, the smaller the chains of the polymer (and thus the rigidity) are. The only explanation for this behavior, given that both the melting point and crystallinity are comparable to the one of pure LDPE, is the crosslinking provided by the functionalization, which improves their stiffness.

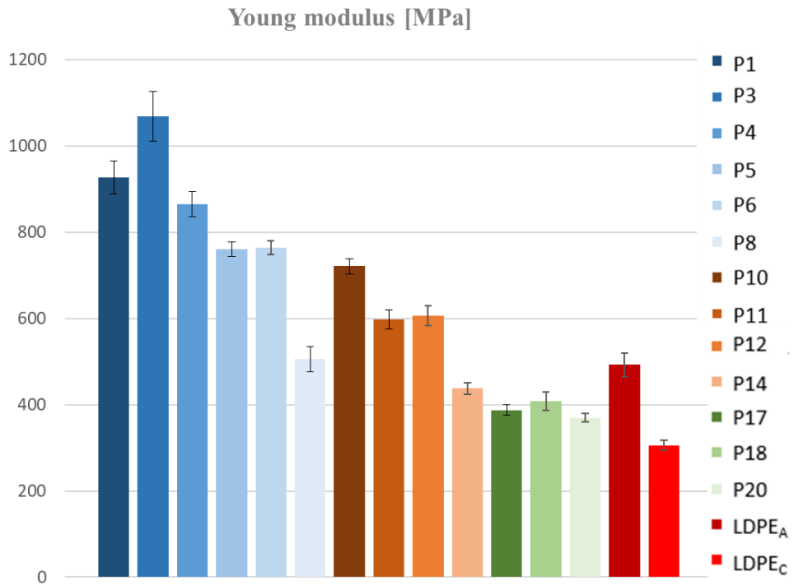

Figure 13. Column chart of Young modulus values.

The aforementioned discussion has left out four ionomers (P7, P9, P13, and P16) because they have consistently different mechanical behavior (see Figure S4). P13 and P16 results to be extremely inhomogeneous, most likely due to the high content of gels throughout

the films. P7 and P9, on the other hand, display two opposite properties. P7 displays an elongation equivalent to the ionomers seen before (~900%) but a very low stress, while P9 exhibits the opposite behavior, a high stress with a very low elongation at break. At this point, there is no clear explanation for these discrepancies, which could not be explained by their characterization.

1.4 Ionomers adhesion properties

As already mentioned in paragraph 1.1, a drawback of polyethylene is its hydrophobic nature, which makes it less suited for a wide range of applications, like heat sealing, extrusion coating, printing, or adhesive bonding when untreated. When treated, polyethylene is used to connect a variety of materials, including paper, plastics, metal, inks, etc. surface traits of adherents have a significant impact on the quantity of adhesive strength. As a means of obtaining stronger joints, the surface of PE has to be treated, with a variety of methods. These techniques typically involve ways to chemically alter very thin surface layers without altering the bulk and typically consist of corona discharge,[46] flame treatment,[47] oxidation by acids,[48] and chlorination.[49] However, only the first two techniques have received substantial commercial recognition, and it is now normal practice in industrial methods to surface-treat polyolefins this way. Because of the commercial importance of polyethylene and polypropylene and the frequency of adhesion problems with these polymers, a great amount of adhesion research has been carried out on them. In order to meet the demands for automobile light weighing, the variety of metals in today's vehicles will continue to increase, favoring the use of aluminum. To efficiently seal these mixed materials while ensuring long-term performance and durability, solid solutions are essential. The goal in the automotive sector is to reduce vehicle weight while maintaining or enhancing long-term performance and durability and promoting sustainability using eco-friendly products and procedures. Automotive structural adhesives, such as rubber and epoxy adhesives, have special qualities that make them suitable for use in a variety of vehicle applications but exclude the possibility of being reprocessed.

Here, we describe how the addition of ionic groups to the PE matrix is an effective method to increase PE adherence properties to aluminum. Ionomers increase the hydrophilicity of polyethylene backbone and as such have great potential in extrusion coating applications as a result of their enhanced adhesion properties. To study how the introduction of ionic moieties changes the adhesion properties of LDPE, lap shear tests were performed according to ASTM D3163, a method standardized to evaluate the adhesion strength of polymers on a tensometer. Several ionomers with different IPC content and viscosity have been tested, all the samples were prepared using the same setup illustrated in Figure 14. Aluminum bars (dimensions of 100

mm x 25 mm x 1.5 mm) were used as adherent, and the surface was carefully cleaned with EtOH. To prepare the polymer joint, 10 g of powder was pressed in a mold of 10 cm x 10 cm x 0.5 mm at 180 °C, and three rectangular stripes (12.5 mm x 25 mm x 0.5 mm) were cut and cleaned with EtOH. Three specimens for each sample were prepared by placing the ionomer in two bars (Figure 14b) and subsequently pressing them at 180 °C.

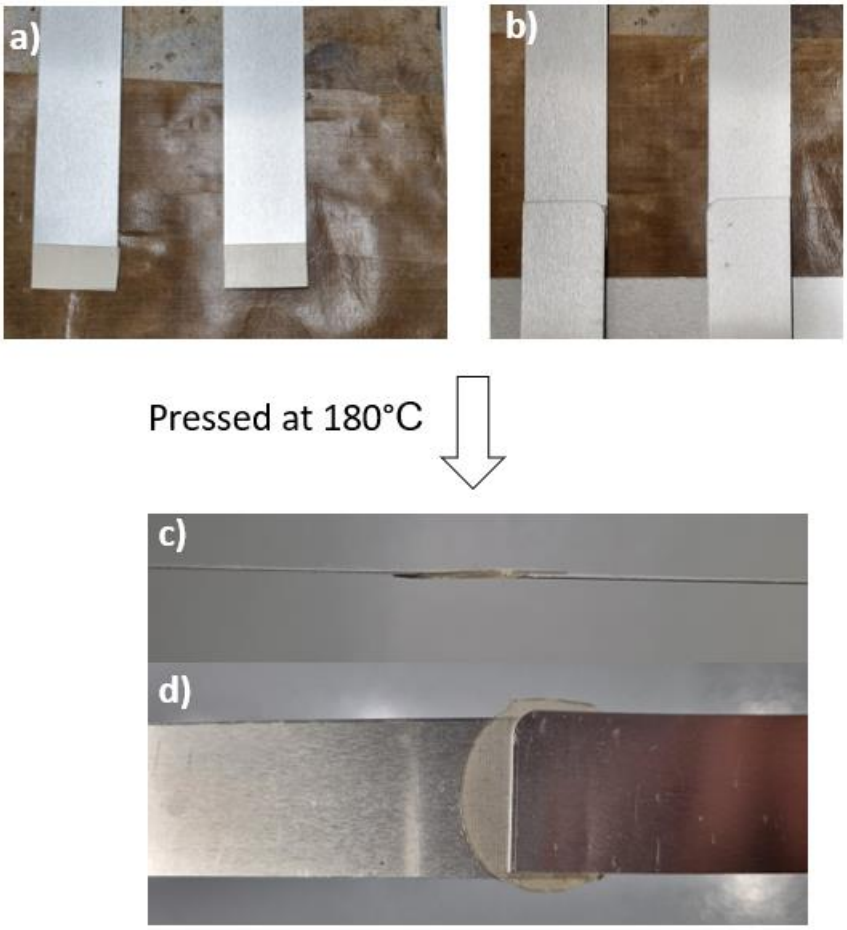

Figure 14. Typical sample setup process for adhesion tests, a) view from above of aluminum bars with the ionomer sample placed on the end and b) sandwich formation before pressing; c) and d) show the view from the side and from above, respectively, of a specimen obtained after compression molding at 180 °C.

Table 3 shows the results relative to six selected ionomers. These particular samples were chosen to compare the adhesive qualities of samples with low (P14 and P4), medium (P12 and P20), and high IPC contents (P17 and P18). The molecular weight of the polymers and, consequently, their viscosity, are additional parameters that must be taken into account; for this reason, a broad range of MFI values have also been considered.

Table 3. Samples used for adhesive tests.

Name	*Content of IPC (wt%)*	*MFI (g/10 min)*	T_m *(°C)*	X_C *(%)*[a)]
P14	2.8	25.3	106	47
P4	3.1	n.d.	111	50
P12	6.0	13	109	52
P20	6.1	52.5	103	42
P17	10	8.3	105	43
P18	10.5	25	105	46

There are three types of failures to be considered, cohesive, adhesive, and substrate failure. Failure owing to limited adherence between the glue and the adherent is referred to as an adhesive failure and is usually named delamination. Cohesive failure occurs when the structural integrity of the glue is not as strong as its adherence to the substrates, and the breakdown of the adhesive itself occurs. The last possible failure consists of the breakdown of the substrate, indicating that the proper strength of the adhesive bond with the substrate is achieved (Figure 15).

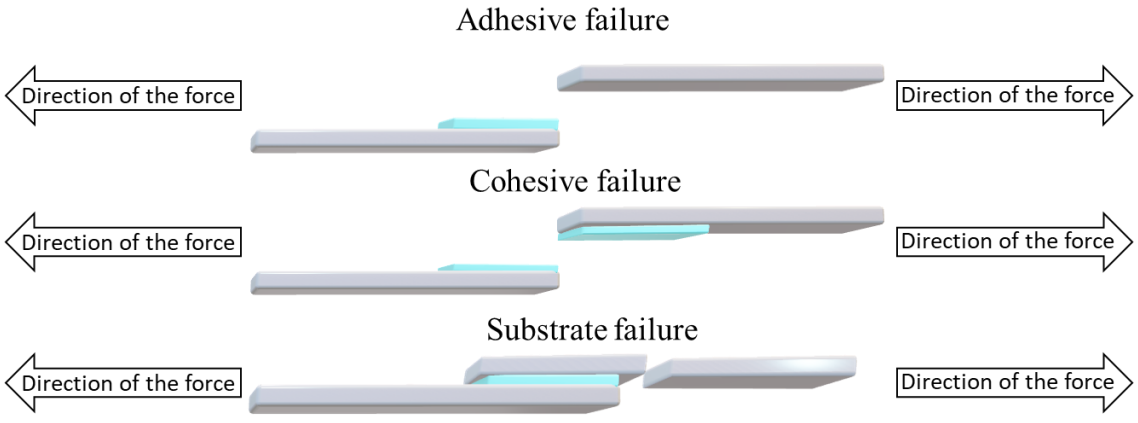

Figure 15. representation of the three types of failures: adhesive (top), cohesive (middle), and substrate failure (bottom).

In Figure 16, the stress-strain curves of $LDPE_C$ and the ionomers tested are displayed where the failure of the joint can be deducted by the stress-strain profiles. Figure 16b shows

how $LDPE_C$ is ineffective in adhering to aluminum since only a small stress led to the separation of the two metal slabs through an adhesive failure. Specimens from P14 undergo an adhesive failure since they broke after a short strain and a sudden increase in stress (Figure 16f). In contrast, specimen 3 of P17 exhibited a cohesive failure which is characterized by a slow increase in stress and maximum stress at larger strain (Figure 16e). All the ionomer joints exhibit a considerable increase in adhesion when compared to LDPE (at least twice), showing that even a small number of ionic groups can significantly enhance PE's hydrophobic properties. The ionomer with less IPC content, P14, has the worst performance, all showing early adhesive failure. P12, P18, and P20 taking the errors into account, were slightly better than P14 as both cohesive and adhesive failures were observed. P4 and P17 remarkably caused a substrate failure indicating a very strong adhesion to the substrate (Figure S24). While we expected a clear correlation between IPC content in the polymer and adhesive strength, we did not observe such a relationship. Instead, both IPC content and the materials' viscosity are key factors in the adhesion strength.

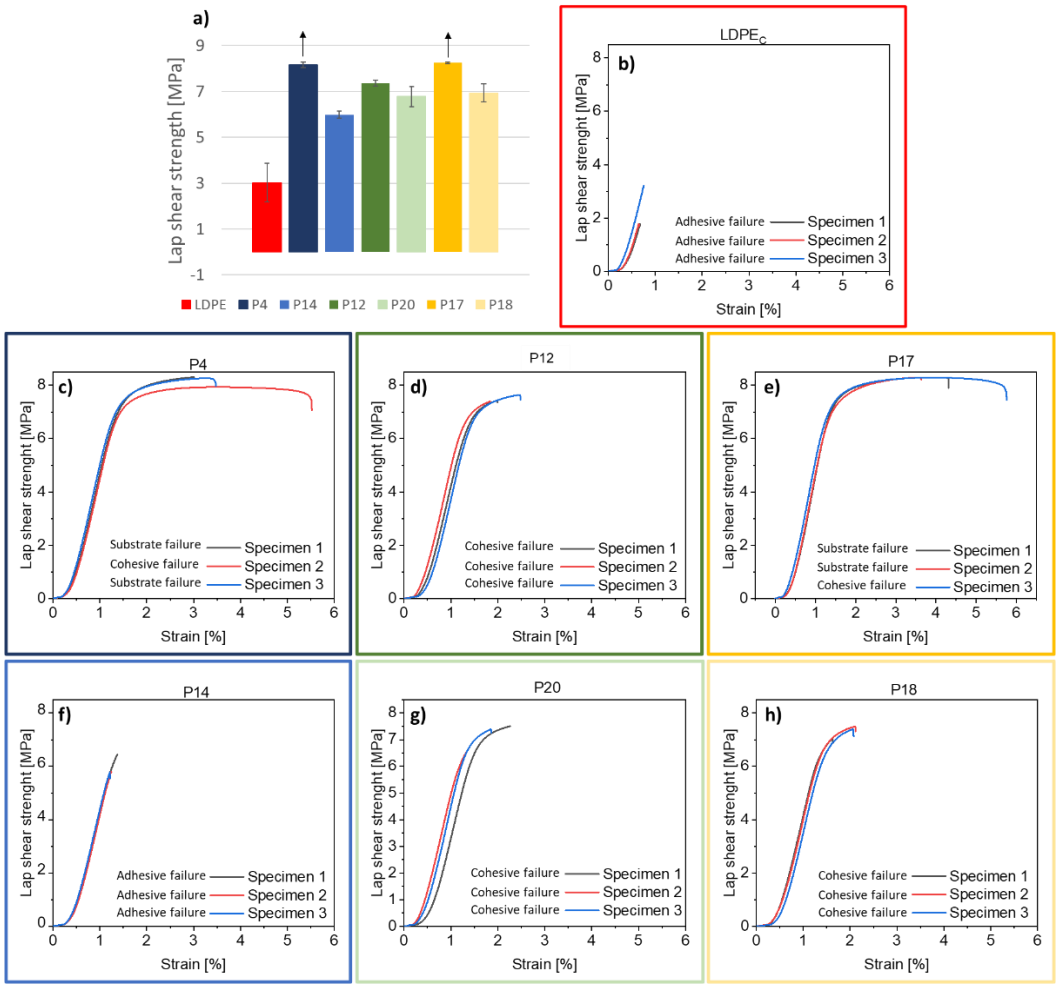

Figure 16. a) Average maximum lap shear strength b)-h) stress-strain curves of $LDPE_C$ and of the ionomers obtained from lap shear tests.

1.4.1 Cataplasma Aging

Cataplasma aging was employed to speed up the degradation of the adhesive joint caused by temperature and moisture. This test will subject the adhesive PE layer to conditions similar to those to which the finished product may be exposed. For example, in the automotive segment, the research of joints is accelerating in order to find effective joints to seal metals ensuring long-term durability and performance. To achieve the aging of the joint lap shear specimens were prepared as shown in the previous paragraph and subjected to one-day conditioning at 23 °C and 50% of humidity. Afterward, the specimens were wrapped individually in cotton soaked with deionized water and packaged in aluminum foil. The prepared specimens were placed in a PE beg and subsequently welded completely airtight. At this time, the following cycles were conducted to perform the climate durability test:

- The packaged sample is stored at (70±2) °C and (100±6) %RH for 168 hours (7 days)
- Then immediately exposed to (-20±2) °C for 16 hours
- Thereafter, the sample is thawed at room temperature, the package removed, and the test piece reconditioned for 2 hours at (23±2) °C and (50±6) %RH.

The lap shear procedure discussed before was then used to evaluate whether the glue has withstood the aging test. Figure 17 shows the average strength of three specimens for each sample before and after the aging process.

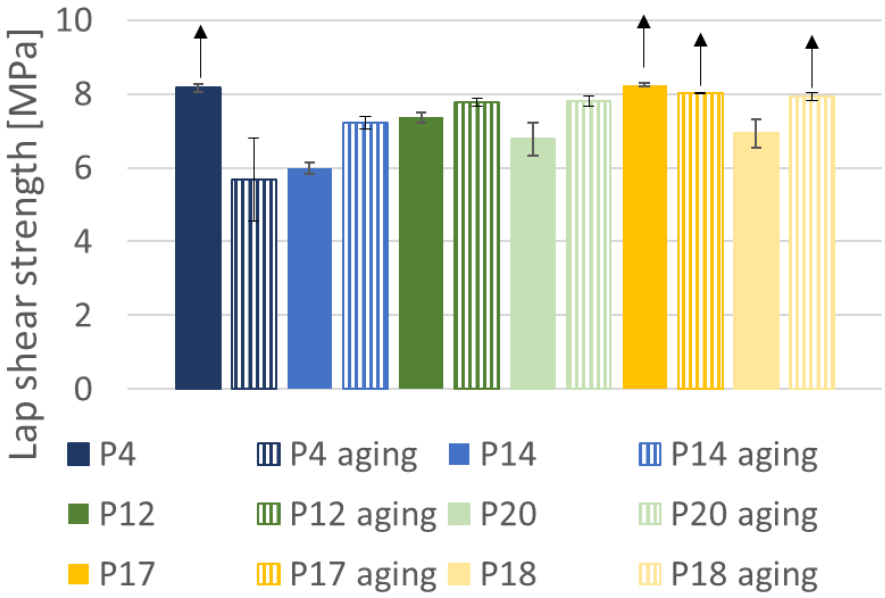

Figure 17. Lap shear strength for the ionomers before (solid-colored bars) and after (striped-colored bars) aging procedure.

Surprisingly, the strength of the adhesives was mostly unaltered or even increased for some samples (P14, P18, and P20) after the climate durability test, except for P4, which changes its behavior from a substrate failure to an adhesive one. Finally, from the stress-strain curves displayed in Figure 18, a clear trend consistent with the IPC content of the ionomer can be observed. P4 and P14, the polymers with less ionic moieties (3.1 wt% and 2.8 wt% respectively), show the worst adhesive performance ~6 Mpa, increasing the ionic content (6.0 wt% for P12 and 6.1 wt% for P20) leads to the adhesive strength to increase, reaching values around 8 MPa. Lastly, P17 and P18 with the highest content of IPC (10 wt% and 10.5 wt% respectively) displayed the highest adhesive strength with consequent substrate failure (Figure S25).

To explain the better performance after aging, we speculate that the seven days spent at 70 °C during the aging process may have caused a slow reorganization of the ionic moieties close to the metal's surface, favoring the ionomers with the highest IPC content.

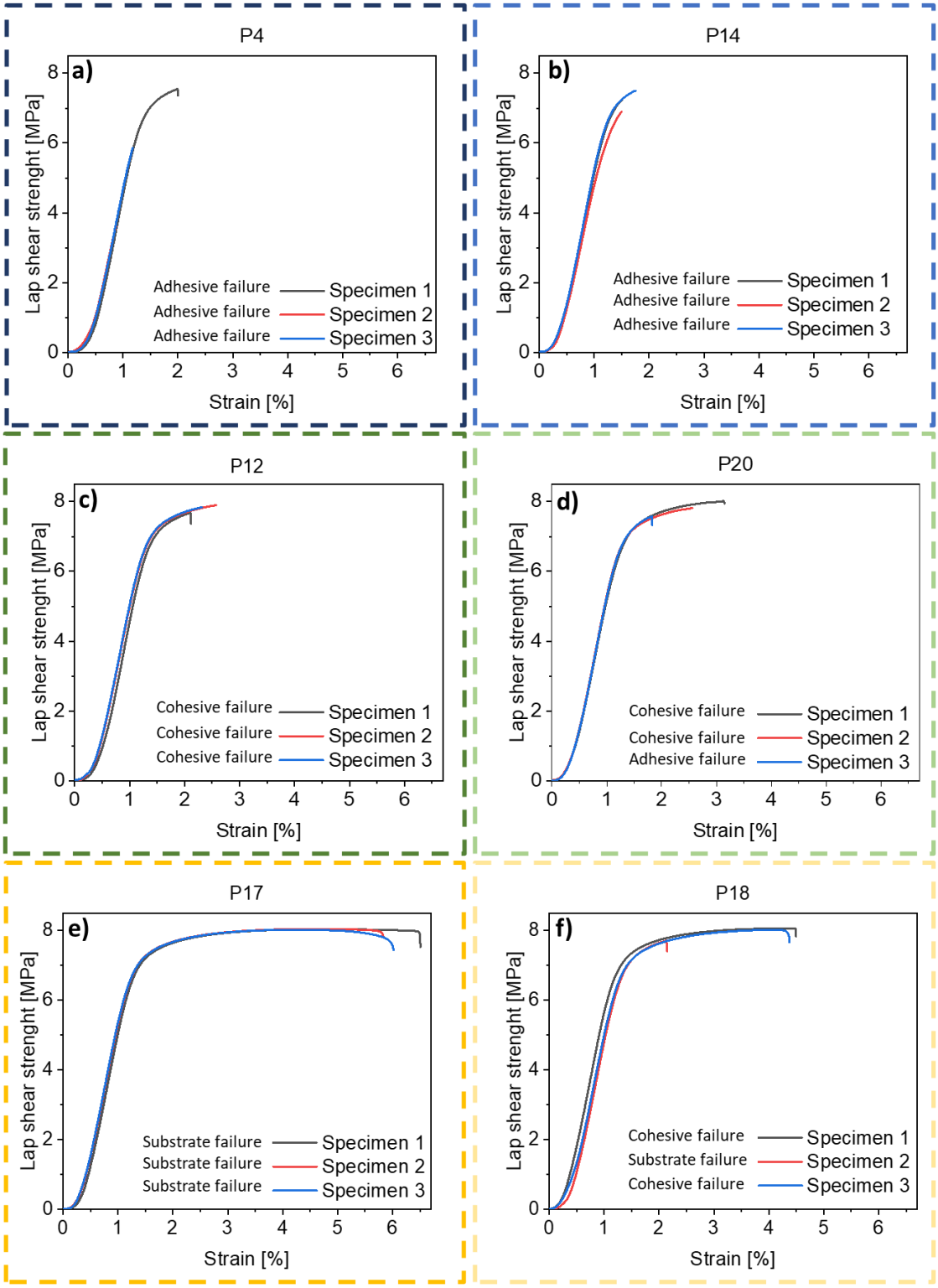

Figure 18. Stress-strain curves of a) P4, b) P14, c) P12, d) P20, e) P17, and f) P18 obtained after aging of the samples.

1.5 Conclusions

Several ionomers have been synthesized *via* high-pressure/high-temperature free radical copolymerization by reacting ethylene directly with an ion-pair comonomer (IPC). The IPC is an ionic couple formed by a dimethyl-amino terminated methacrylate cation and a methacrylate as anion obtained *via* an acid/base reaction of the reactants.

The polymerization reaction conditions were varied to investigate the effects of modifying factors like temperature, IPC content, and chain transfer agent (CTA) content on the resultant polymer. As expected, increasing the temperature causes a minor inclusion of the methacrylate comonomer and a decrease in the growth of the chains. The increase in IPC content led to ionomers with higher ionic moieties and proved to be benefic to lower the viscosity of the polymer where a measurable MFI was obtained due to the CTA effect of the IPC. Most of the ionomers results to be processable *via* casting film extrusion by setting the adequate temperature of extrusion according to the viscosity of the polymer. While the thermal properties of the ionomers reflect the properties of a typical LDPE, the mechanical properties differ dramatically. The tensile tests show an improved ability of the ionomers films to be extended before breaking and a higher stiffness in comparison to LDPE, confirmed also by the increased values of Young modulus. Given that the melting temperature and crystallinity are comparable to those of pure LDPE, we assumed that the reason for this behavior is the ionomer crosslinking that strongly influences the stiffness of the polyolefin.

Six of these ionomers have been selected to study their adhesion performances on aluminum slabs driven by the enhanced hydrophilicity of the polymer with respect to LDPE. Adhesive properties of samples with low (P14 and P4), medium (P12 and P20), and high IPC levels (P17 and P18), considering a wide range of MFI values as additional factors, were studied. Preliminary adhesion tests on the virgin polymers show that the insertion of IPC leads to improved adhesion performances, but there is not a clear relationship between the IPC content and the strength of the joint. At this stage, the key factor seems to be the viscosity of the material, since lower MFI P4 and P17 caused a substrate failure.

In the last section of the chapter, aging tests of the joints have been reported. Cataplasma aging was employed to hasten the adhesive joint's deterioration by moisture and temperature. The lap shear procedure was then used to evaluate whether the ionomer has withstood the aging test. Remarkably, the lap shear strength tests reveal a clear trend with the IPC content of the ionomers showing that:

- the polymers with less ionic moieties, P4 (3.1 wt%) and P14 (2.8 wt%), show the worst adhesive performance (~ 6),

- P12 (6.0 wt%) and P20 (6.1 wt%) display increased adhesive strength reaching values of around 8.
- P17 (10 wt%) and P18 (10.5 wt%) exhibit higher adhesive strength with consequent substrate failure.

This behavior can be explained by the reorganization of the ionic moieties from the bulk to the surface of the polymer, triggered by the seven days spent at 70 °C during the aging process.

1.6 Experimental Section

Methods

Nuclear magnetic resonance (NMR): NMR spectra were recorded using a Bruker Advance 400 (400 MHz) spectrometer at room temperature. Chemical shifts are reported in parts per million (ppm). ^{1}H-NMR chemical shifts are given in reference to the residual solvent peak at 7.26 ppm in $CDCl_3$. High-temperature NMR spectra were recorded on a Bruker AVANCE III (500 MHz) equipped with a cryogenically cooled probe head at 80 °C or 120 °C in TCE-d_2.

Elemental Analysis (EA): Elemental analysis was carried out with a CHNS Thermo Fisher FlashSmart instrument. Samples were burned in the presence of oxygen. The nitrogen content was determined by means of thermal conductivity (TC) and volumetric analysis.

Dynamic mechanical thermal analysis (DMTA): DMTA was carried out in tensile mode using a TA Q800 DMA in tensile mode on 30 mm × 11 mm pieces cut from 0.7 mm thick melt-pressed films. Variable-temperature measurements from 25 to 200 °C were done at a heating rate of 3 °C min^{-1}, with a preload force of 0.01 N, a maximum strain of 0.05 % and a frequency of 1 Hz. The given values are related to the second heating curve.

Differential scanning calorimetry (DSC): Differential scanning calorimetry was performed on a *TA Instruments* Q20 equipped with a RCS 90 cooling system. About 2- 4 mg of polymeric sample was weighed inside an aluminum pan. DSC measurements were carried out under nitrogen atmosphere between -40 °C to 200 °C at a constant heating/cooling rate of 10 °C min^{-1}. Enthalpy, melting, and crystallization temperatures were determined from the second heating and cooling cycle.

Tensile tests: Tensile tests were performed with a *Zwick* type Z020 tensile tester equipped with a 1 kN load cell. The tests were performed on film strips with dimensions of 40 mm (length) x 5 mm (height) x 0.05 mm (width). A grip-to-grip separation of 20 mm was used.

The samples were pre-stressed to 0.1 N and then loaded with a constant crosshead speed of 500 $mm \cdot min^{-1}$.

Preparation of tests specimens for lap shear tests according to ASTM D3163: The aluminum slabs were stuck together with LDPE or ionomers using compression molding. Films of compression molded polymers were cut to size (12.5 mm x 25 mm), so that their surface area corresponds to the overlap of the substrate metal slabs. The metal slabs were placed so that they overlapped with the appropriate area and the polymer films were placed between them. Metal slabs of the same thickness were employed to support the upper aluminum slabs in order to align them in a plane. The entire setup was placed inside the compression molding machine, and then a force of 100 N and a temperature of 180 C were applied for 5 minutes.

Aging test procedure: initial conditions: 168 hours at (23 ± 2) °C and (50 ± 6) %RH. After initial conditions, the joints were exposed to the following aging tests, *Porsche Cataplasma PPV 7000:* the samples are completely wrapped with cotton. Then the wrapped sample is wetted evenly with demineralized water. The sample is completely wrapped in aluminum foil before it enters a PE bag. Subsequently, the air is pressed out of the PE bag by hand and the polyethylene bag is welded completely airtight.

- The package sample is stored at (70 ± 2) °C and (100 – 6) %RH for 168 hours (7 days)
- and immediately exposed to (-20 ± 2) °C for 16 hours.
- Thereafter, the sample is thawed at room temperature, the package removed and the test piece reconditioned for 2 hours at (23 ± 2) °C and (50 ± 6) %RH.

Materials

Ionomers P1-21 were synthesized by free radical polymerization of ethylene in the presence of the IPC (see Table 1 for details). SABIC® LDPE 1922N0Now, with a melt flow rate (MFR) of 22 g / 10 min (190 ºC; 2.16 kg) and density of 0.919 g cm^{-3} was obtained from SABIC. Unless otherwise specified, solvents and chemicals used for the synthesis of the IPC and all the ionomers were purchased from Sigma Aldrich and used as received. All solvents employed were laboratory grade and used as received.

Synthesis

Synthesis of IPC.

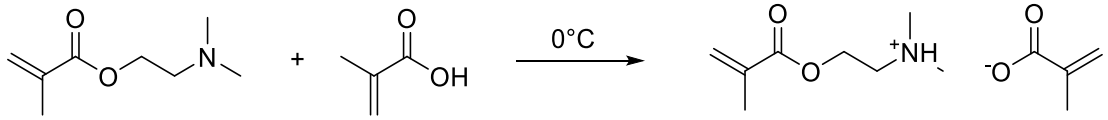

Methacrylic acid (40.5 mL, 0.48 mol) was dropped into 2-(dimethylamino)ethyl methacrylate (81 mL, 0.48 mol) in a 2- neck flask equipped with an ice bath and a mechanical stirrer. The mixture was stirred at 0 °C and after 30 minutes a gel was formed. The formation of the product was confirmed *via* NMR.

^{1}H NMR (400 MHz, $CDCl_3$, δ) 1.94 (6H, m), 2.45 (6H, s), 2.86 (2H, t, J= 5.6 Hz), 4.36 (2H, td, J = 5.6, 1.6 Hz), 5.52 (1H, m), 5.58 (1H, m), 6.07 (1H, m), 6.13 (1H, m), 7.05 (1H, bs).

^{13}C NMR (101 MHz, $CDCl_3$, δ): 18.37; 18.69; 44.09; 56.36; 60.88; 124.44; 126.33; 135.90; 138.22; 167.15; 171.96.

Synthesis of ionomers *via* radical polymerization.

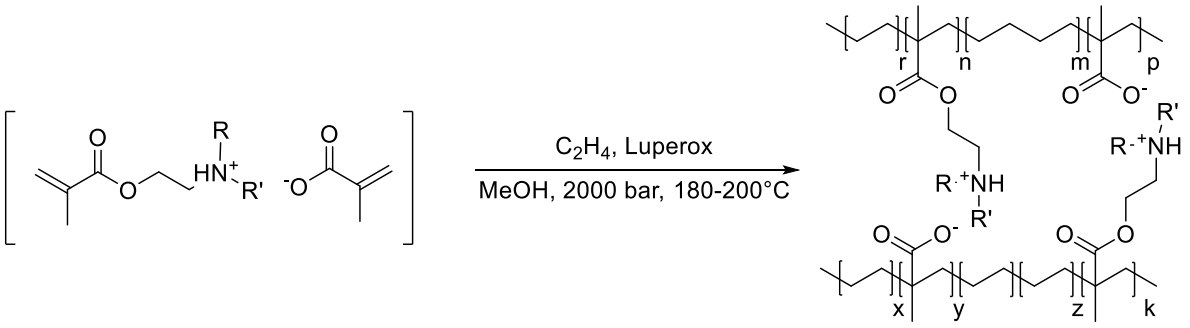

The ionomers were synthesized through a copolymerization between ethylene and the ionomeric monomers according to the following general procedure: the polymerization was carried out in an autoclave reactor by using a pressure of 2000 bars with an impeller velocity fixed at 1540 rpm, at a different temperature (180, 200, 220, 240, 250, 270 °C) for 30 minutes. Before being injected with high-pressure ethylene, the IPC (1 eq. of ethylene for 0.05, 0.1 or 0.2 of IPC) was dissolved in methanol (50 wt%). Luperox®11M75 (1.5 g/L), dissolved in heptane, was added as initiator together with propanal, used as CTA. The polymers were recovered from the bottom of the autoclave directly to a recuperation vessel through a let-down valve. Two recuperation vessels were used: the first one was used when stabilizing the

conditions and then switched to the 2nd recuperation vessel once the polymerization conditions were steady for collecting the copolymer. The ionomer was recovered in a fine powder form. Elemental analysis (EA) was used to determine the composition of the copolymer through nitrogen quantification. The specific conditions and quantities of IPC are specified in Table 1.

1.7 Supporting information

Processing

Figure S1. image of the film of P4, little gels are visible along the entire volume.

GPC

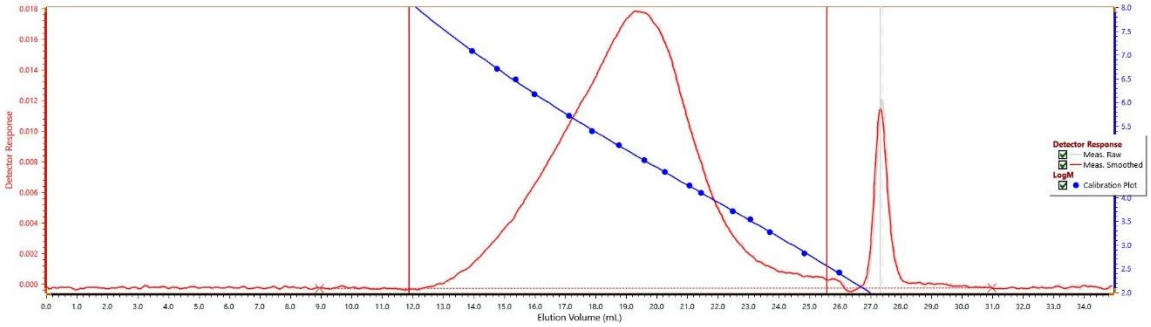

Figure S2. GPC of P5.

DSC

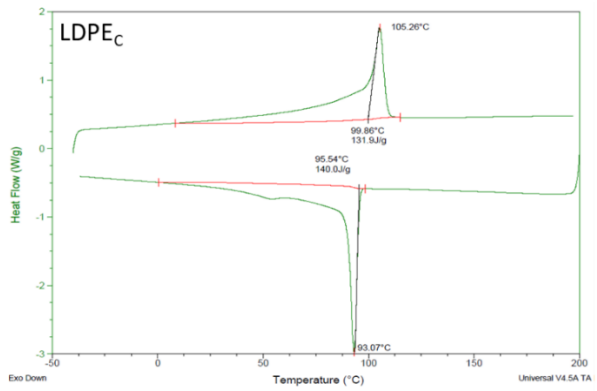
LDPE$_C$
105.26°C
99.86°C
131.9J/g
95.54°C
140.0J/g
93.07°C
Heat Flow (W/g)
Temperature (°C)
Exo Down
Universal V4.5A TA

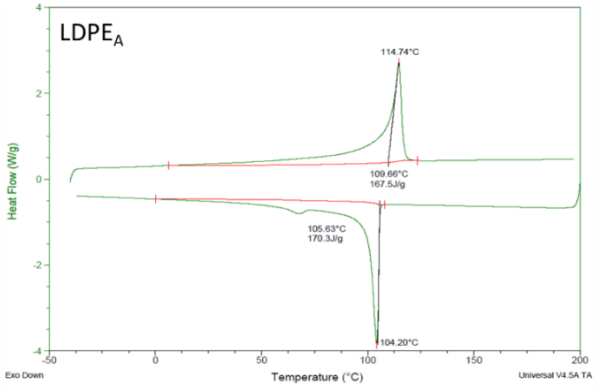
LDPE$_A$
114.74°C
109.66°C
167.5J/g
105.63°C
170.3J/g
104.20°C
Heat Flow (W/g)
Temperature (°C)
Exo Down
Universal V4.5A TA

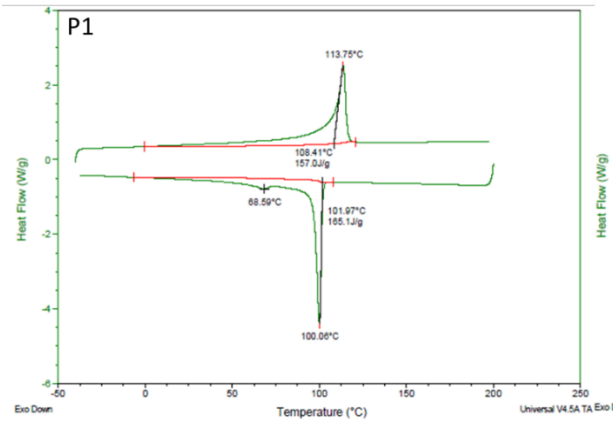
P1
113.75°C
108.41°C
157.0J/g
68.59°C
101.97°C
165.1J/g
100.06°C
Heat Flow (W/g)
Temperature (°C)
Exo Down
Universal V4.5A TA

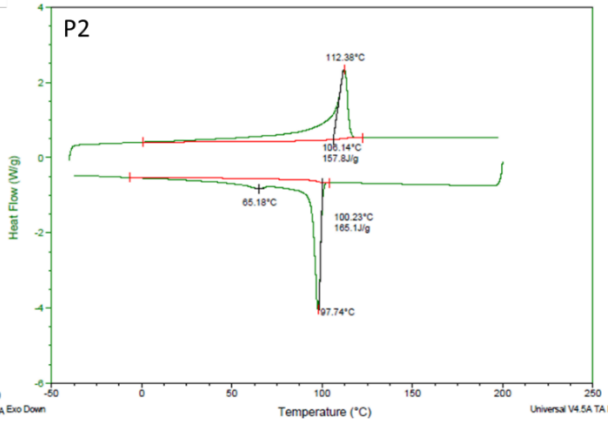
P2
112.38°C
108.14°C
157.8J/g
65.18°C
100.23°C
165.1J/g
97.74°C
Heat Flow (W/g)
Temperature (°C)
Exo Down
Universal V4.5A TA

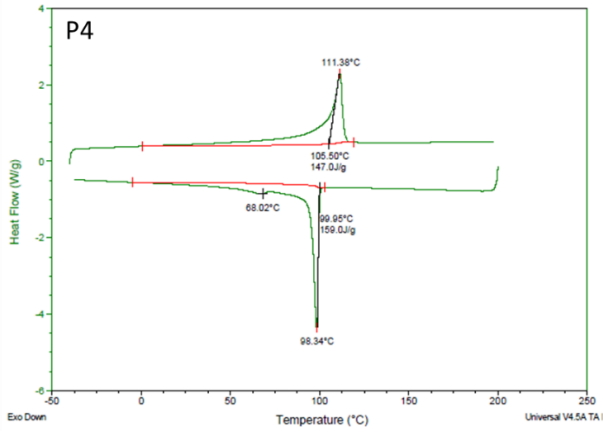
P4
111.38°C
105.50°C
147.0J/g
68.02°C
99.95°C
159.0J/g
98.34°C
Heat Flow (W/g)
Temperature (°C)
Exo Down
Universal V4.5A TA

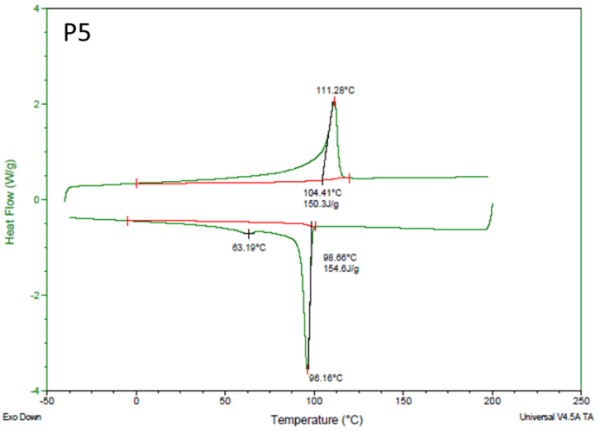
P5
111.28°C
104.41°C
150.3J/g
63.19°C
98.66°C
154.6J/g
96.16°C
Heat Flow (W/g)
Temperature (°C)
Exo Down
Universal V4.5A TA

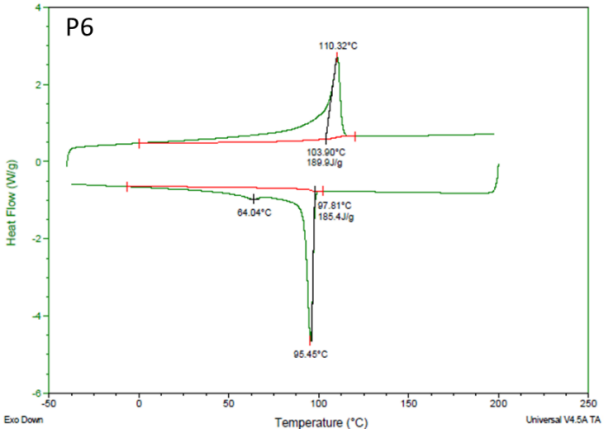
P6
110.32°C
103.90°C
169.9J/g
64.04°C
97.81°C
185.4J/g
95.45°C
Heat Flow (W/g)
Temperature (°C)
Exo Down
Universal V4.5A TA

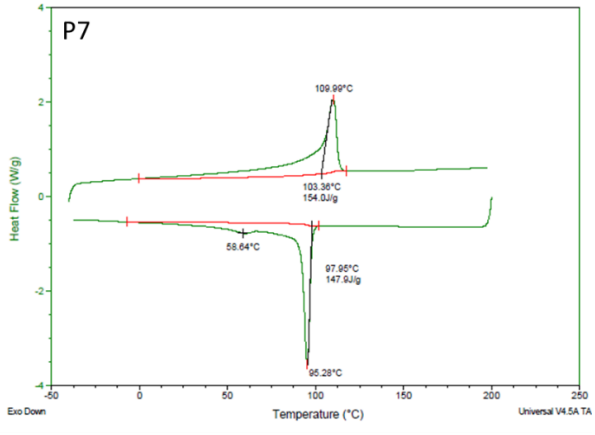
P7
109.99°C
103.36°C
154.0J/g
58.64°C
97.95°C
147.9J/g
95.28°C
Heat Flow (W/g)
Temperature (°C)
Exo Down
Universal V4.5A TA

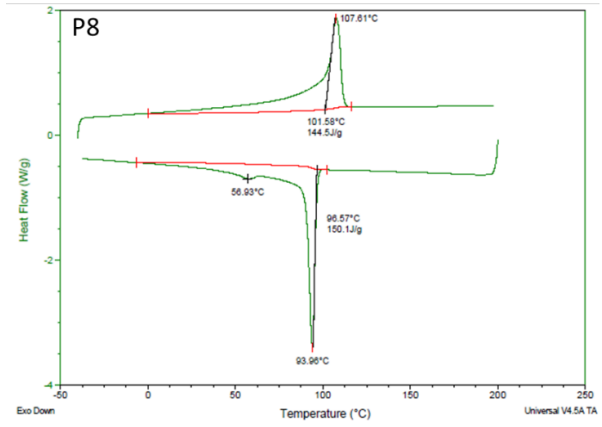
P8
107.61°C
101.58°C
144.5J/g
56.93°C
96.57°C
150.1J/g
93.96°C
Heat Flow (W/g)
Temperature (°C)
Exo Down
Universal V4.5A TA

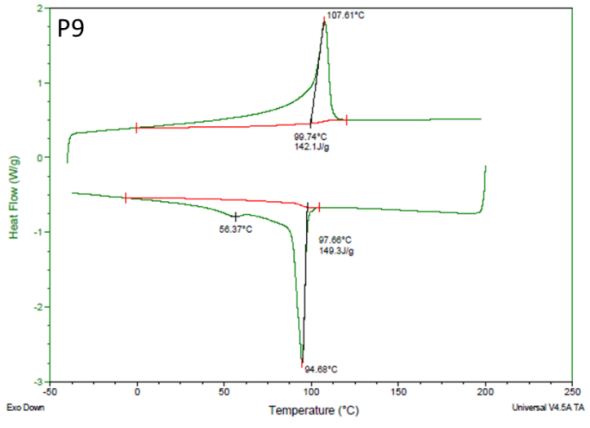
P9
107.61°C
99.74°C
142.1J/g
56.37°C
97.66°C
149.3J/g
94.68°C
Heat Flow (W/g)
Temperature (°C)
Exo Down
Universal V4.5A TA

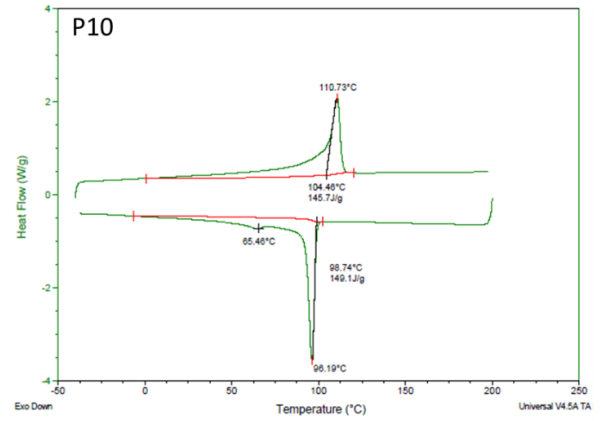
P10
110.73°C
104.46°C
145.7J/g
65.46°C
98.74°C
149.1J/g
96.19°C
Heat Flow (W/g)
Temperature (°C)
Exo Down
Universal V4.5A TA

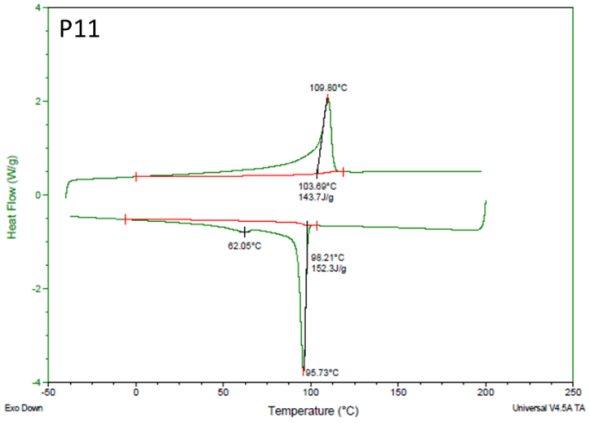
P11
109.80°C
103.69°C
143.7J/g
62.05°C
98.21°C
152.3J/g
95.73°C
Heat Flow (W/g)
Temperature (°C)
Exo Down
Universal V4.5A TA

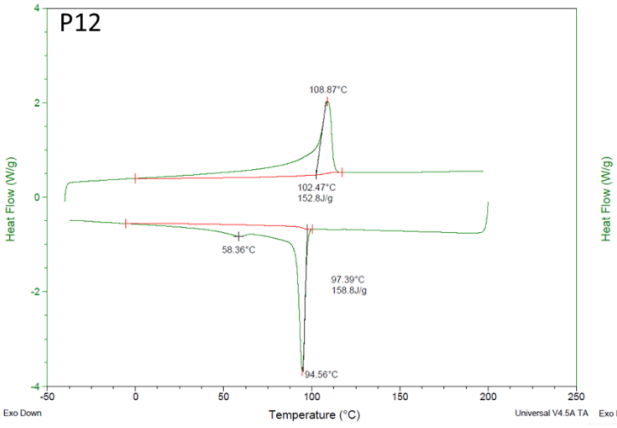
P12
108.87°C
102.47°C
152.8J/g
58.36°C
97.39°C
158.8J/g
94.56°C
Heat Flow (W/g)
Temperature (°C)
Exo Down
Universal V4.5A TA

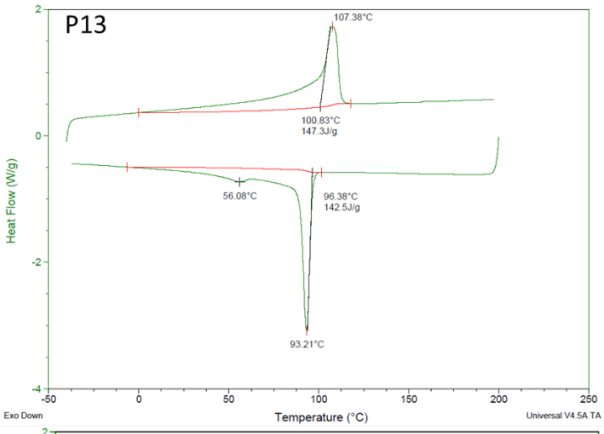
P13
107.38°C
100.83°C
147.3J/g
56.08°C
96.38°C
142.5J/g
93.21°C
Heat Flow (W/g)
Temperature (°C)
Exo Down
Universal V4.5A TA

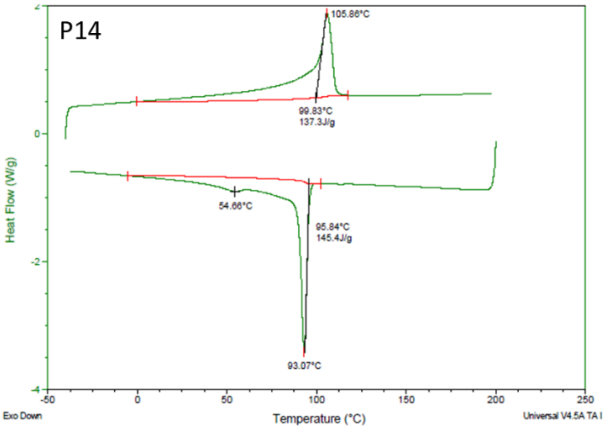
P14
105.86°C
99.83°C
137.3J/g
54.66°C
95.84°C
145.4J/g
93.07°C
Heat Flow (W/g)
Temperature (°C)
Exo Down
Universal V4.5A TA

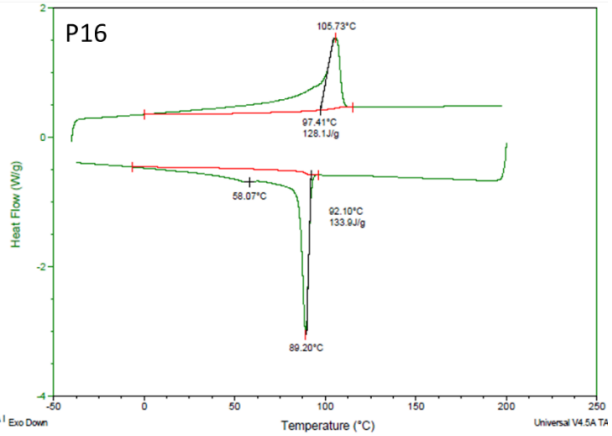
P16
105.73°C
97.41°C
128.1J/g
58.07°C
92.10°C
133.9J/g
89.20°C
Heat Flow (W/g)
Temperature (°C)
Exo Down
Universal V4.5A TA

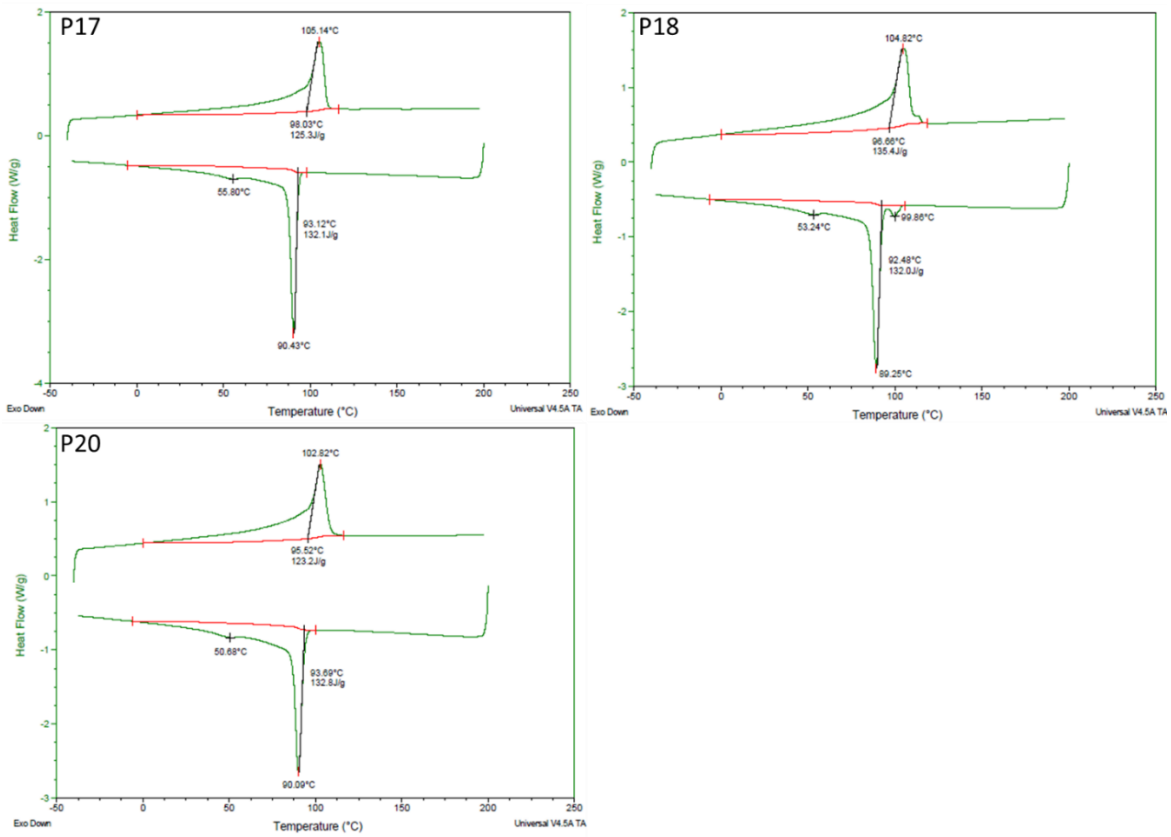

Figure S3. DSC curves.

Lamellar thickness

Table S1. Lamellar thickness (l_c) values of the ionomers. Melting temperature (T_m), and the heat of fusion (ΔH_m) were obtained *via* DSC, σ_e is the surface energy for polyethylene, and T_m^0 is the equilibrium melting temperature of polyethylene.

Polymer	T_m (K)	T_m (°C)	σ_e	ΔH_f^0	T_m^0 (K)	l_c
P1	387	114	90.4	286.2	418.6	0.87
P3	385	112	90.4	286.2	418.6	0.86
P4	384	111	90.4	286.2	418.6	0.86
P5	383	110	90.4	286.2	418.6	0.86
P6	384	111	90.4	286.2	418.6	0.86
P7	383	110	90.4	286.2	418.6	0.86
P8	381	108	90.4	286.2	418.6	0.85
P9	381	108	90.4	286.2	418.6	0.85
P10	384	111	90.4	286.2	418.6	0.86
P11	383	110	90.4	286.2	418.6	0.86
P12	382	109	90.4	286.2	418.6	0.85
P13	380	107	90.4	286.2	418.6	0.85
P14	379	106	90.4	286.2	418.6	0.85
P16	379	106	90.4	286.2	418.6	0.85
P17	378	105	90.4	286.2	418.6	0.84
P18	378	105	90.4	286.2	418.6	0.84
P20	376	103	90.4	286.2	418.6	0.84

Tensile tests

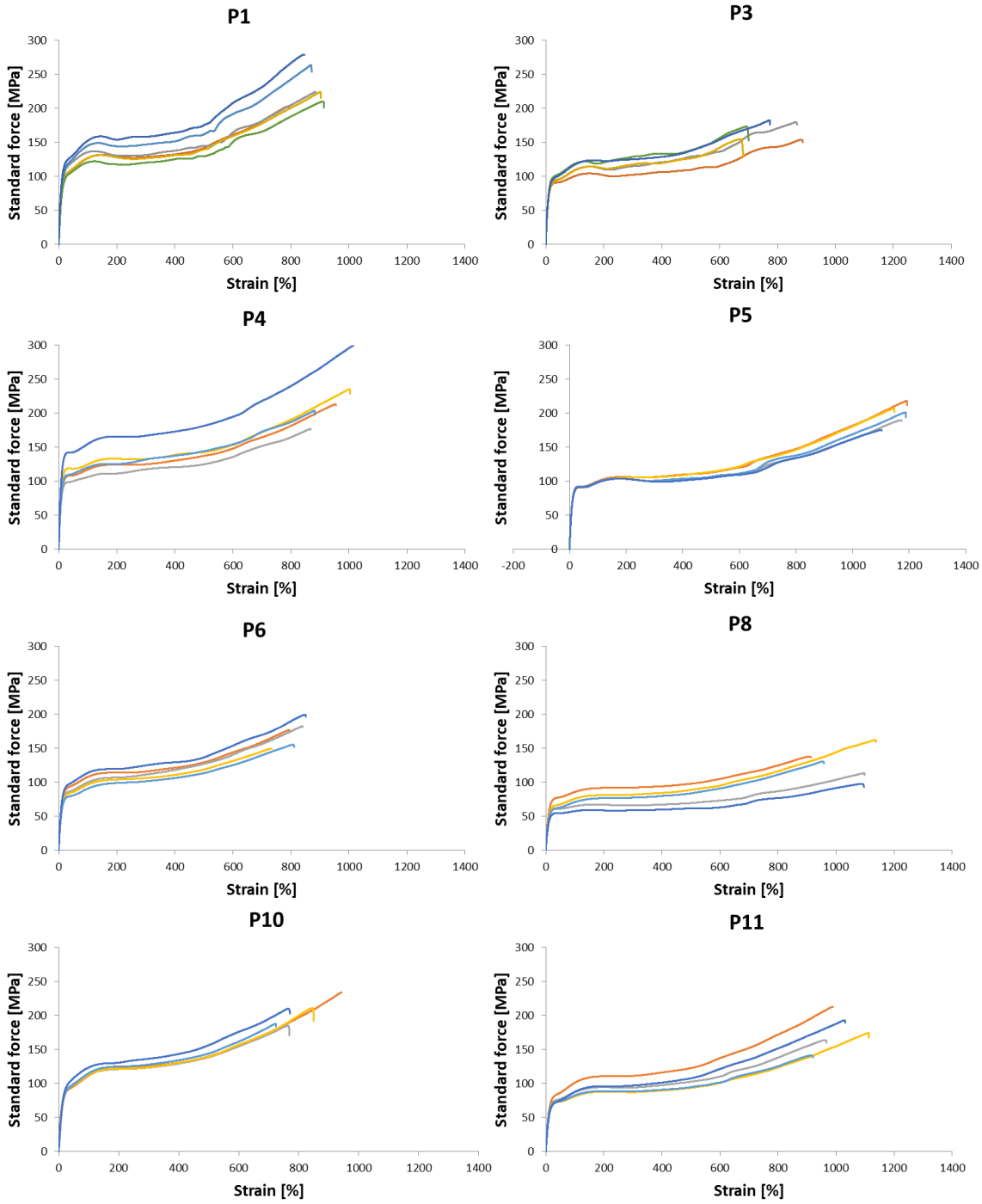

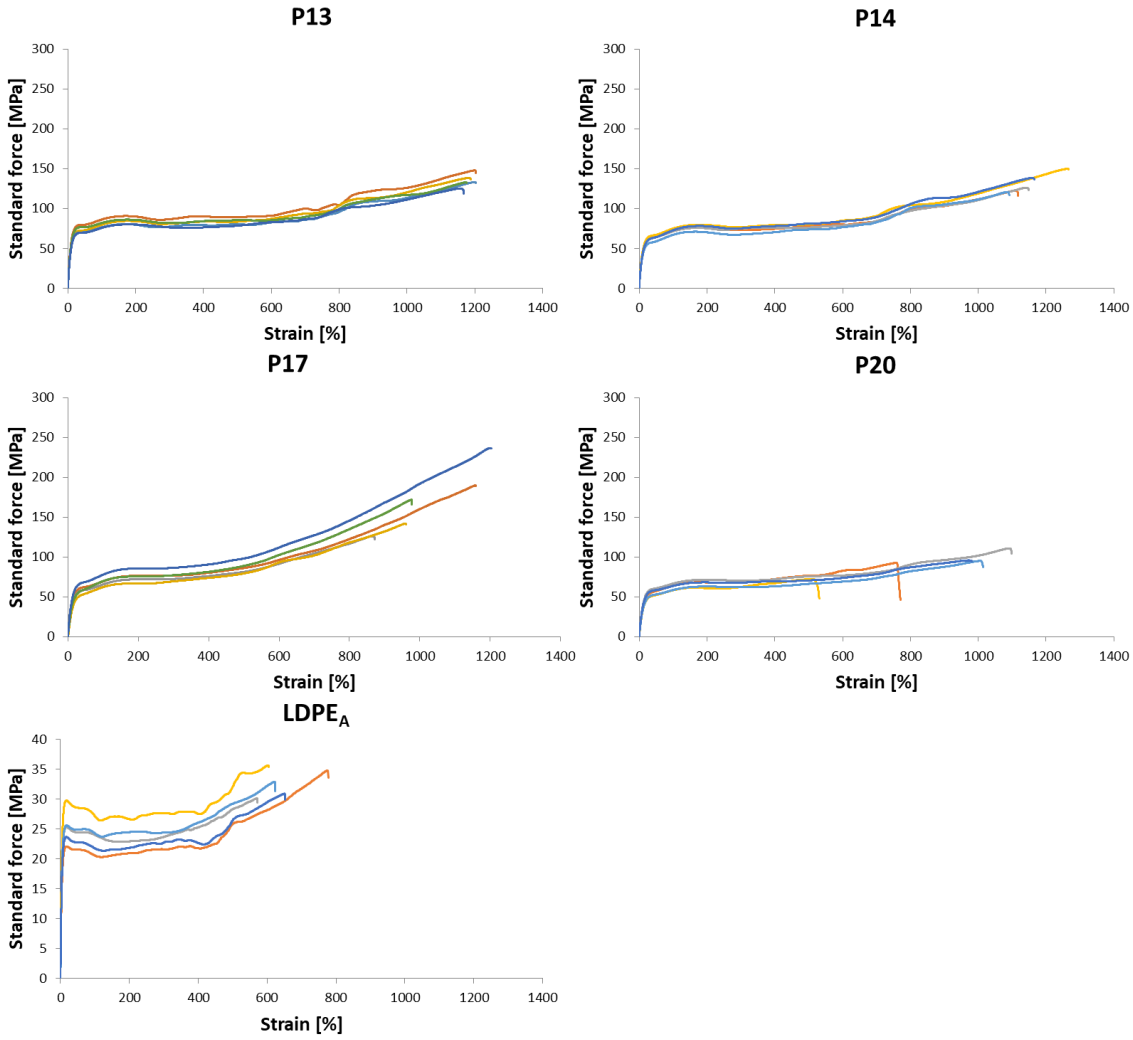

Figure S4. Stress-strain curves obtained *via* tensile tests of ionomers and $LDPE_A$.

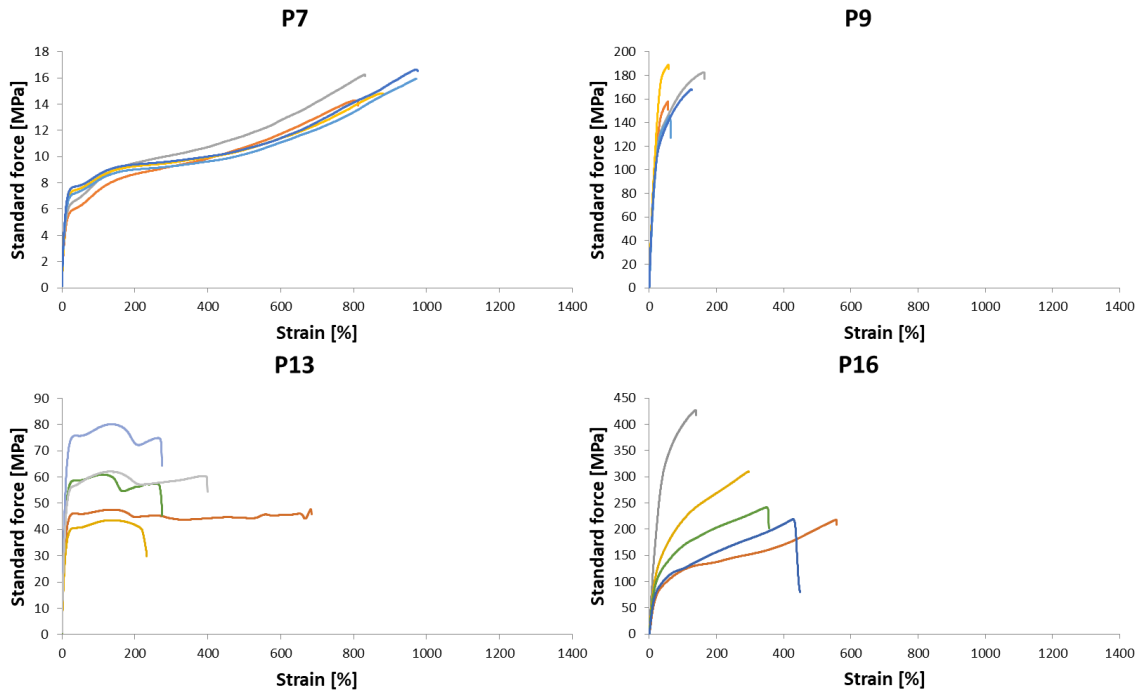

Figure S5. Stress-strain curves obtained *via* tensile tests of P7, P9, P13 and P16.

NMR

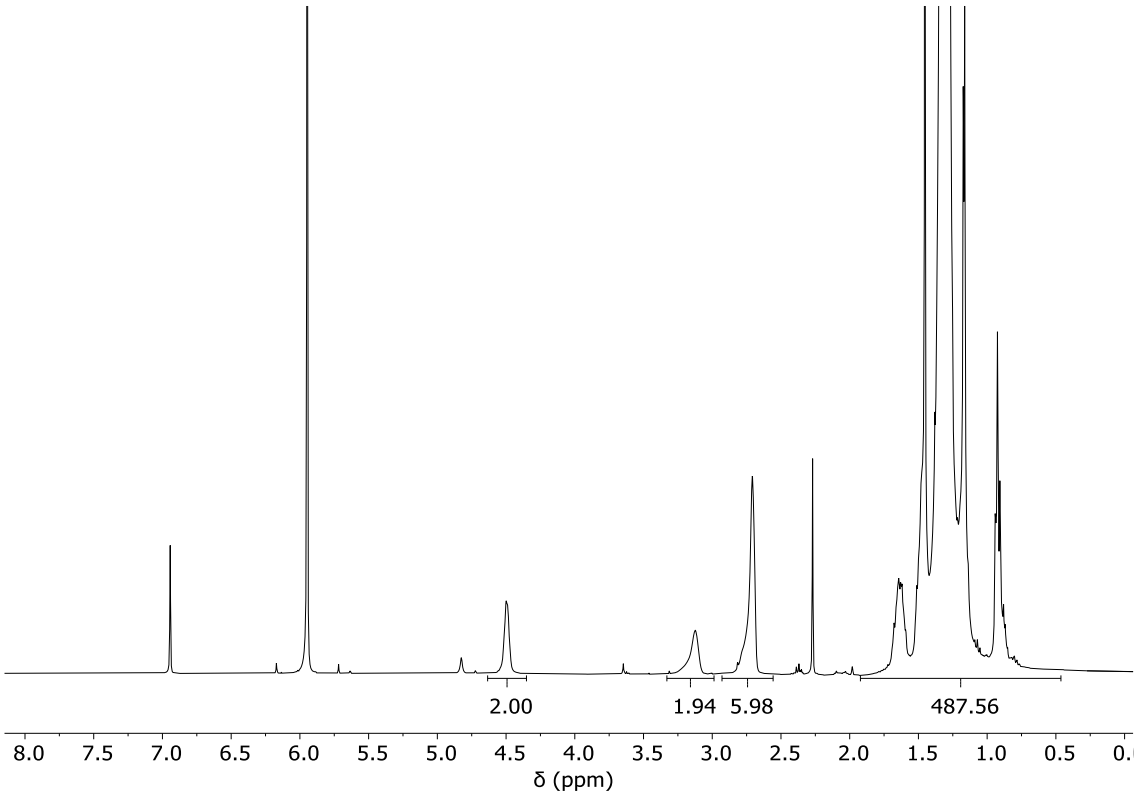

Figure S6. ^{1}H-NMR of P1 (TCE-d2, 500 MHz, 80 °C).

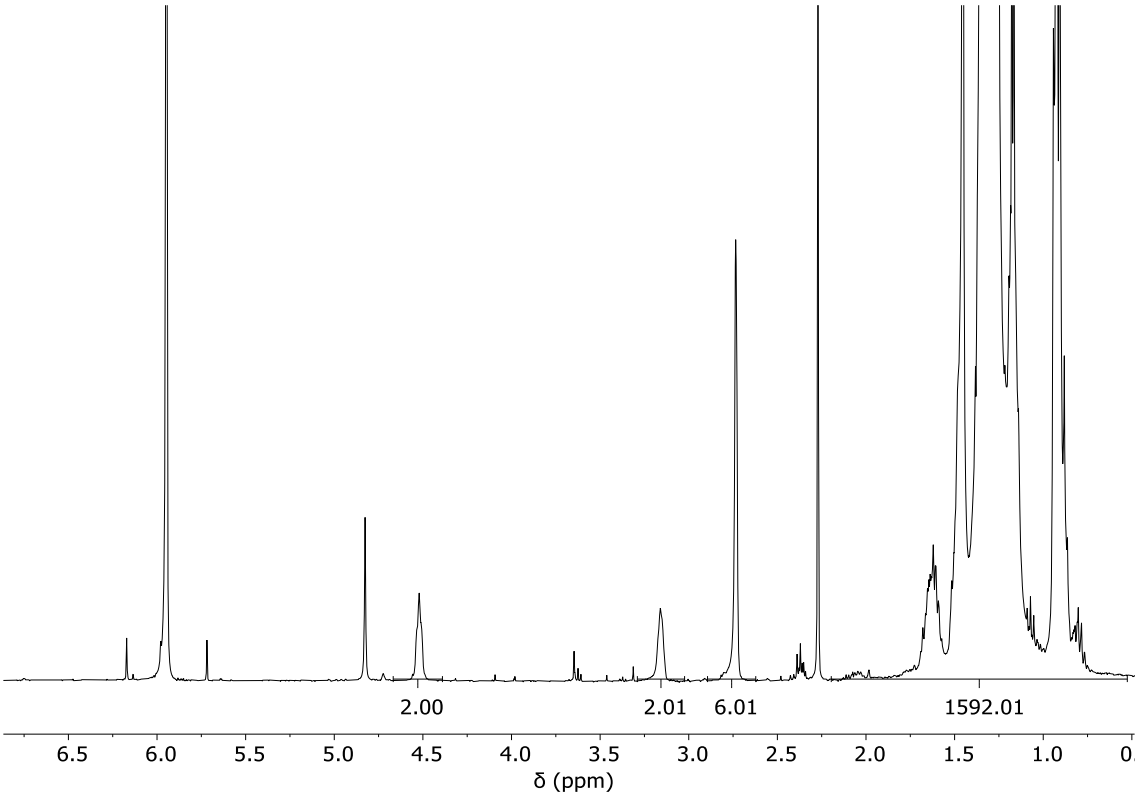

Figure S7. ^{1}H-NMR of P3 (TCE-d2, 500 MHz, 80 °C).

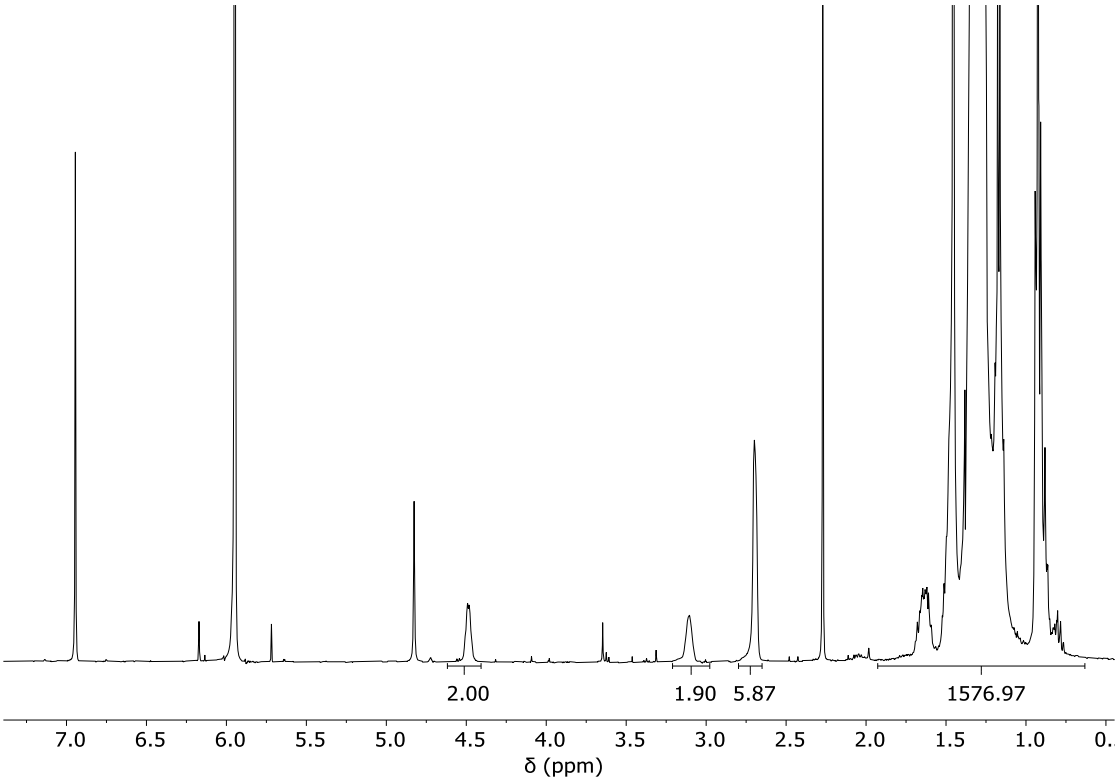

Figure S8. ^{1}H-NMR of P4 (TCE-d2, 500 MHz, 80 °C).

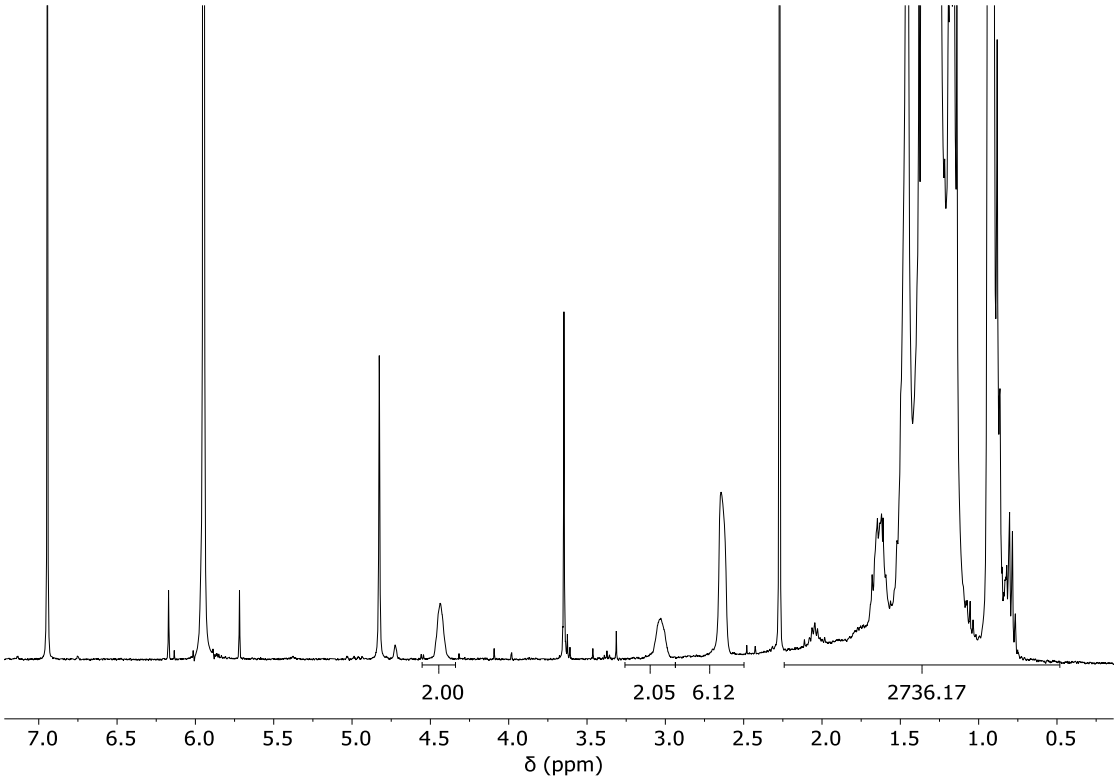

Figure S9. ^{1}H-NMR of P6 (TCE-d2, 500 MHz, 80 °C).

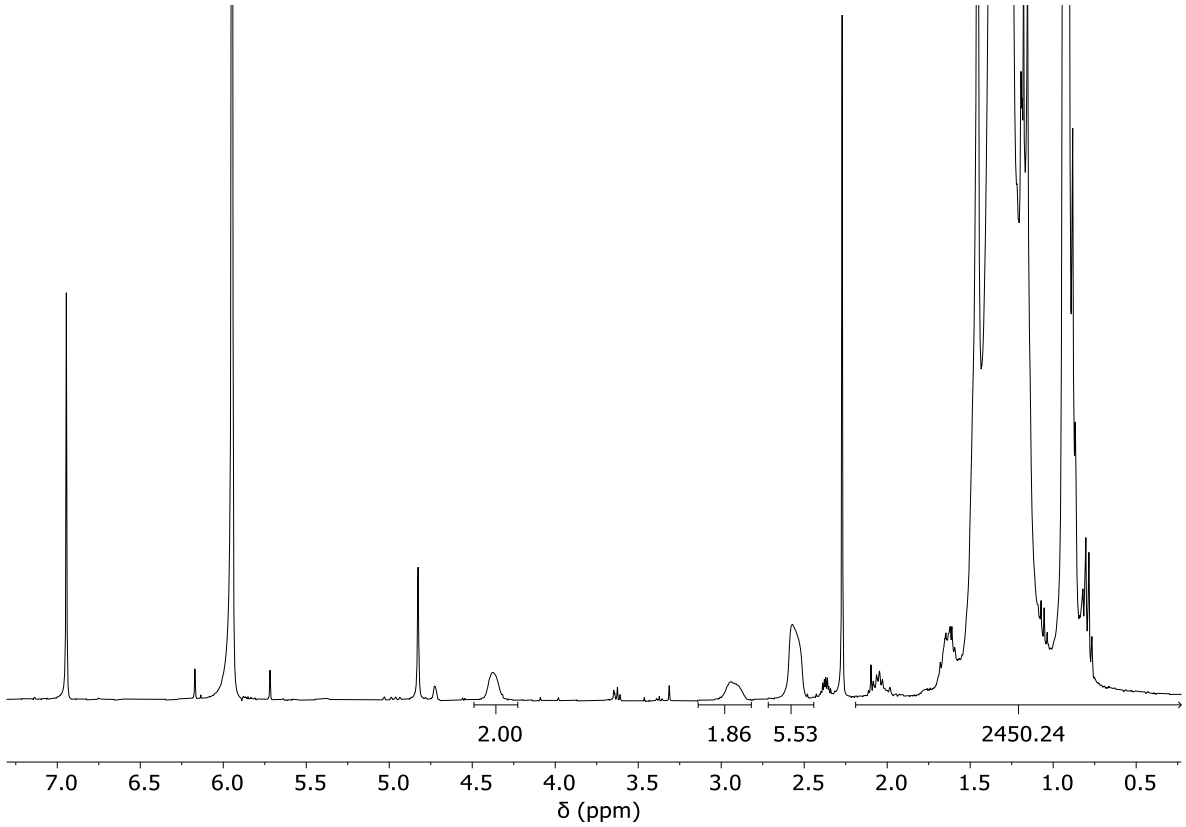

Figure S10. ^{1}H-NMR of P9 (TCE-d2, 500 MHz, 80 °C).

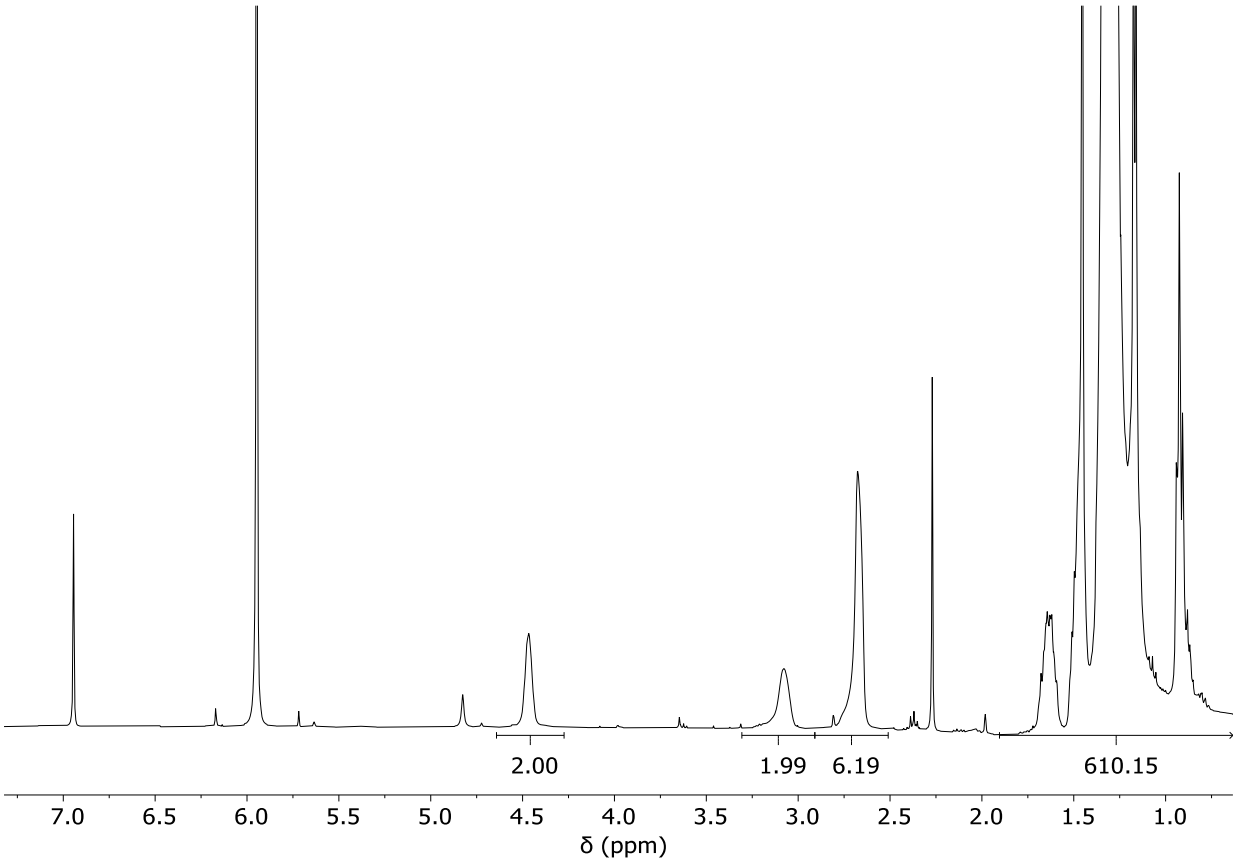

Figure S11. ^{1}H-NMR of P10 (TCE-d2, 500 MHz, 80 °C).

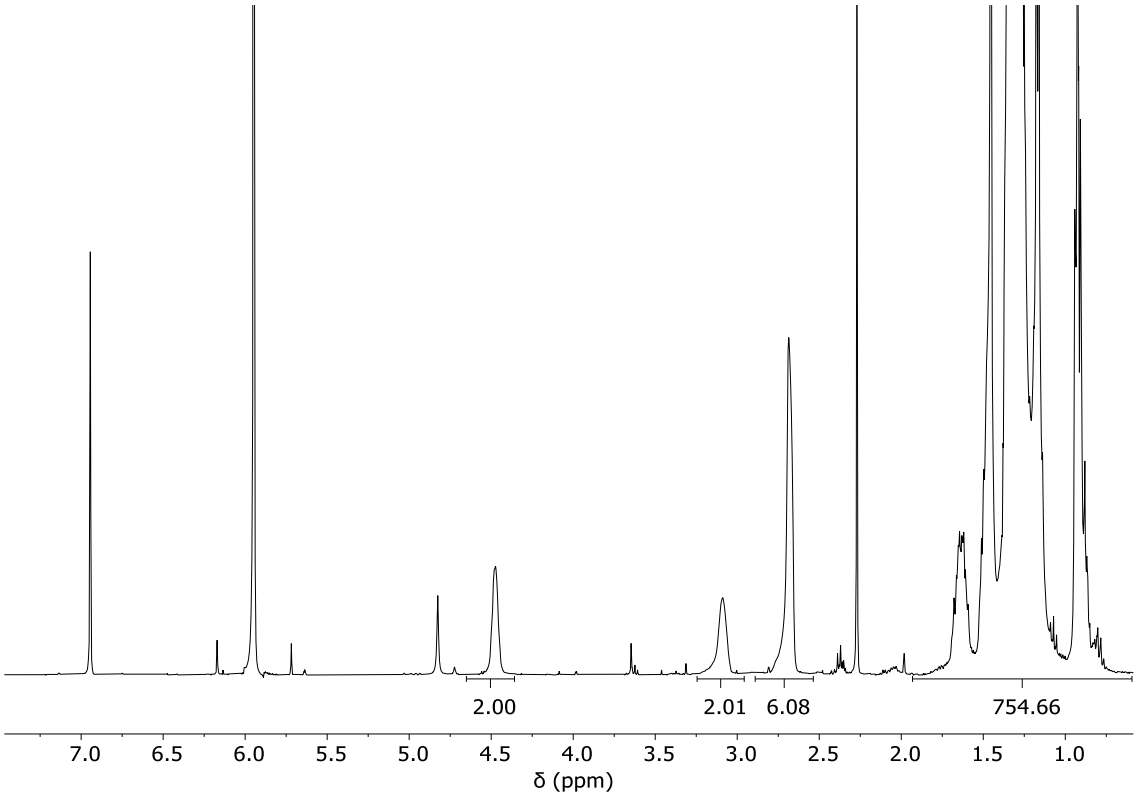

Figure S12. ^{1}H-NMR of P11 (TCE-d2, 500 MHz, 80 °C).

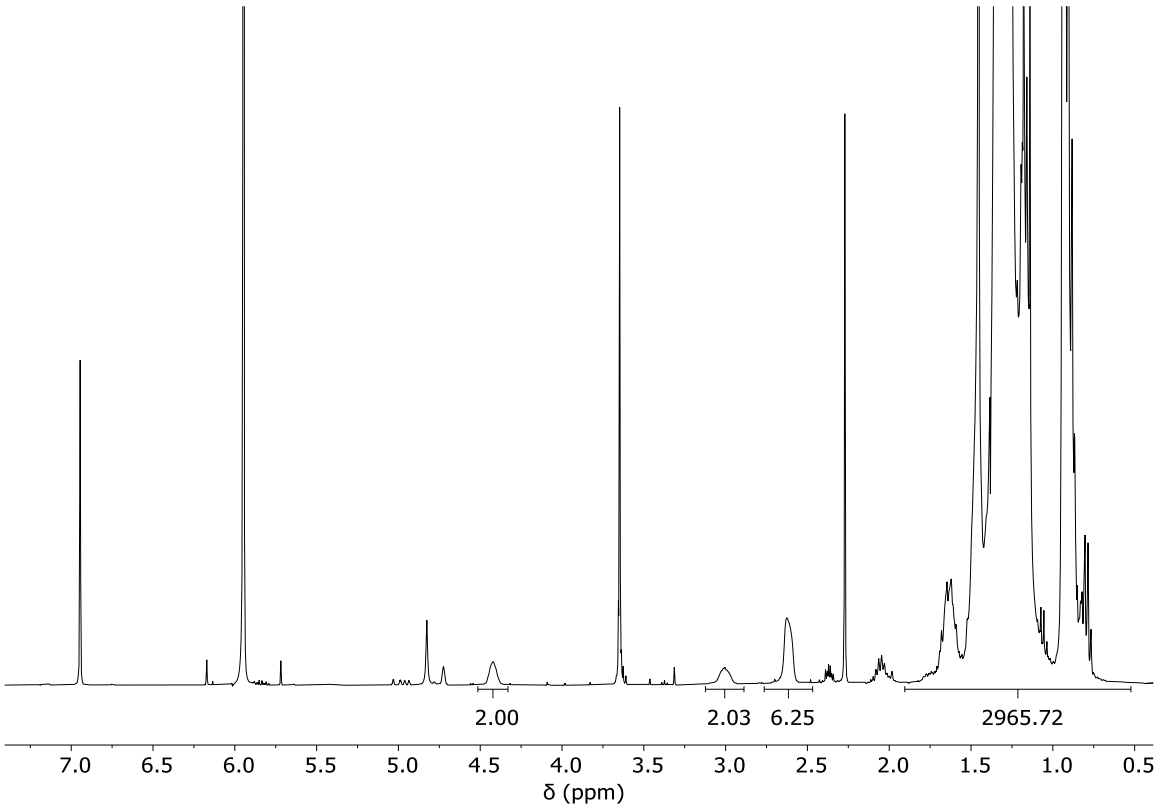

Figure S13. ^{1}H-NMR of P14 (TCE-d2, 500 MHz, 80 °C).

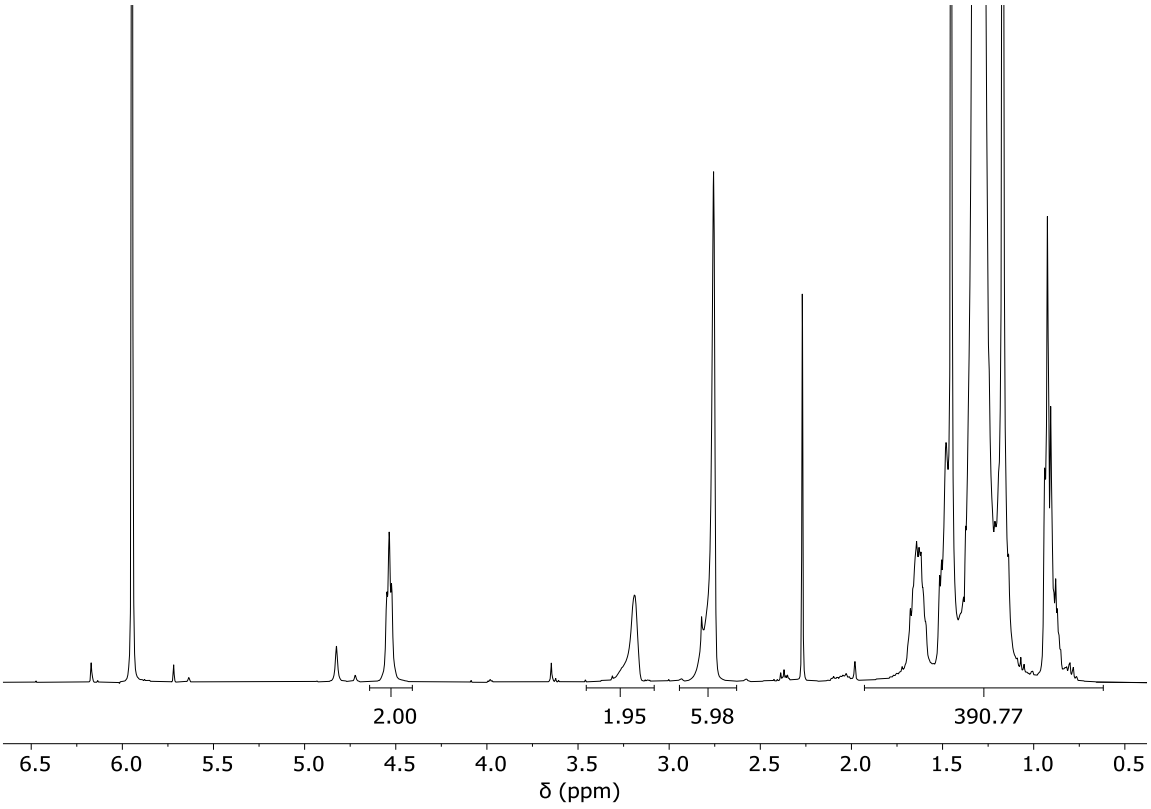

Figure S14. ^{1}H-NMR of P17 (TCE-d2, 500 MHz, 80 °C).

TGA

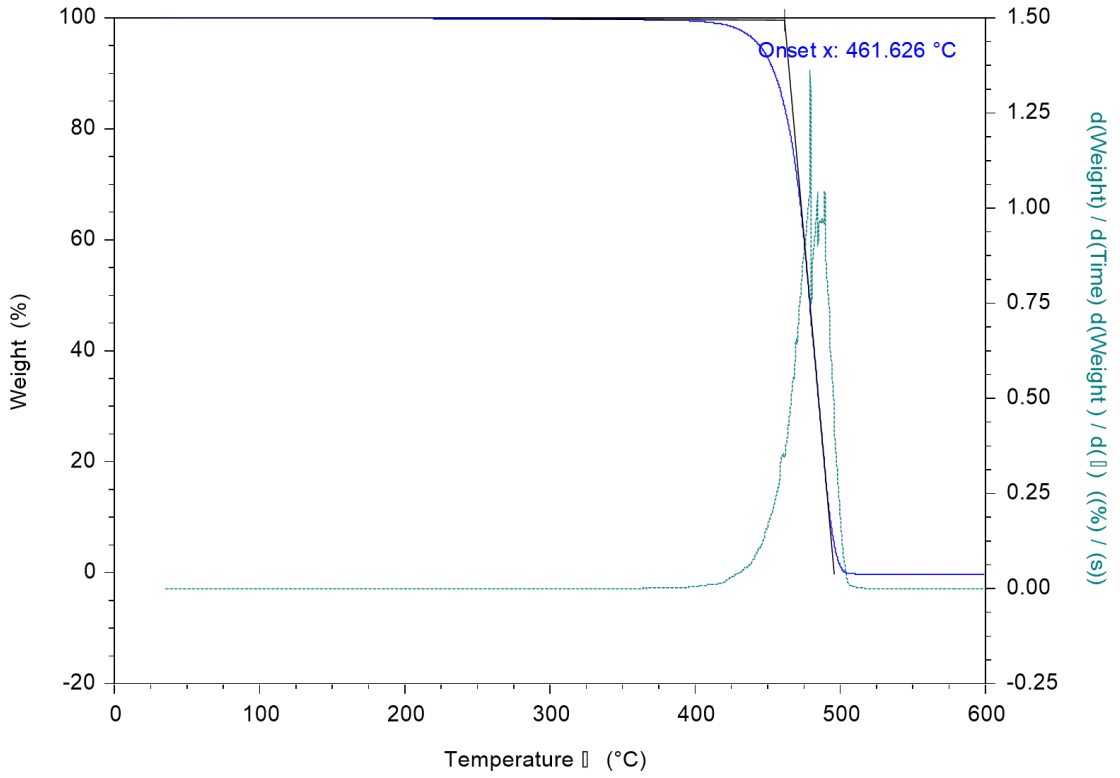

Figure S15. TGA thermogram of P4.

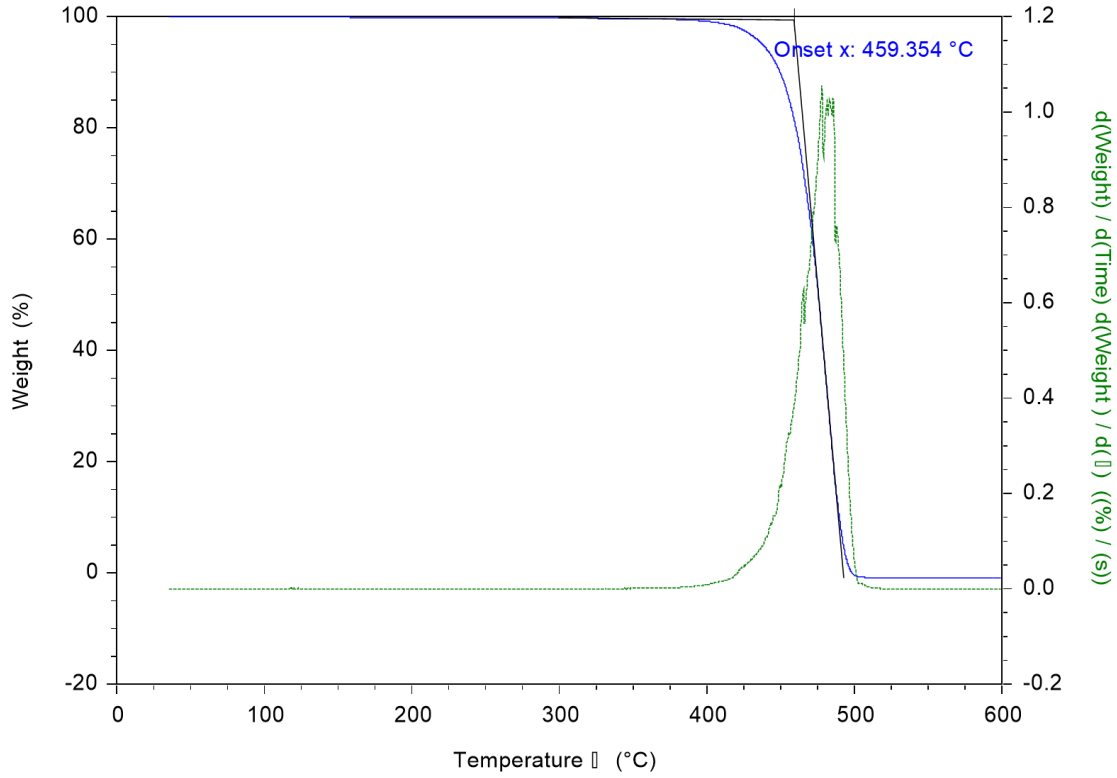

Figure S16. TGA thermogram of P6.

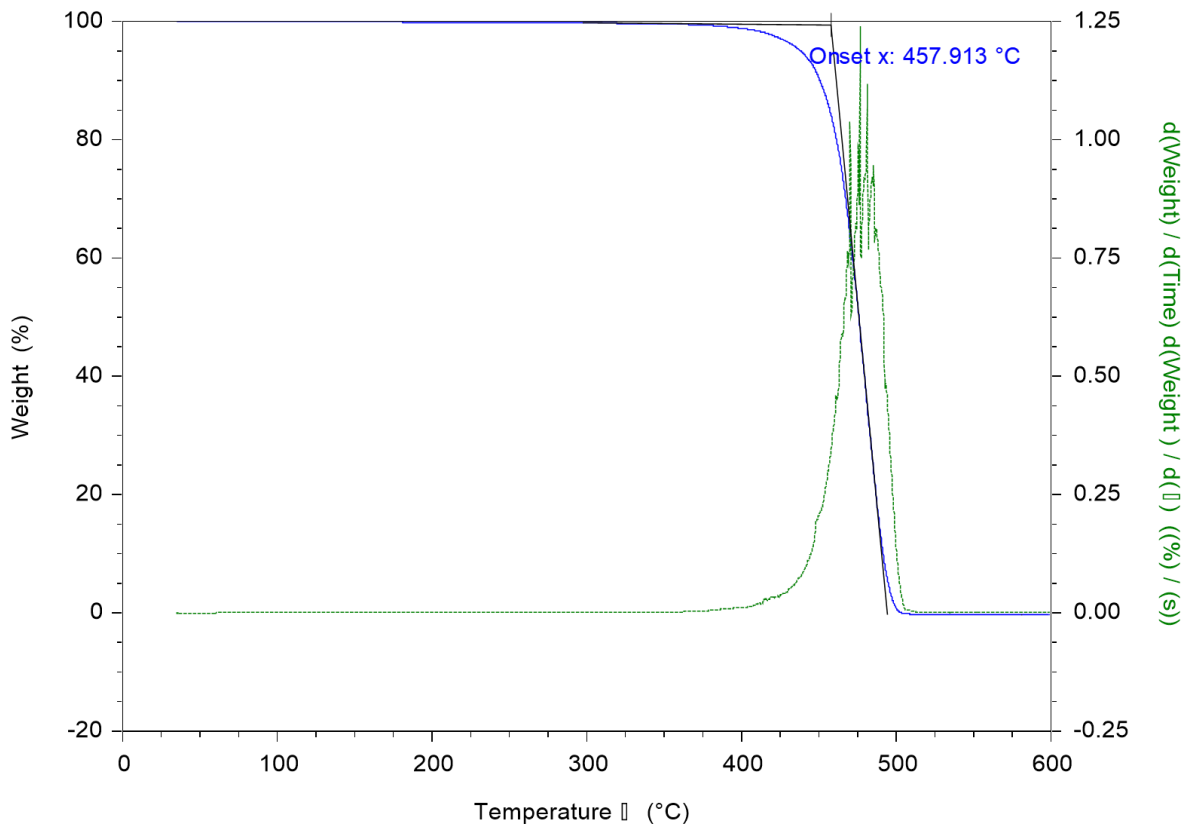

Figure S17. TGA thermogram of P10.

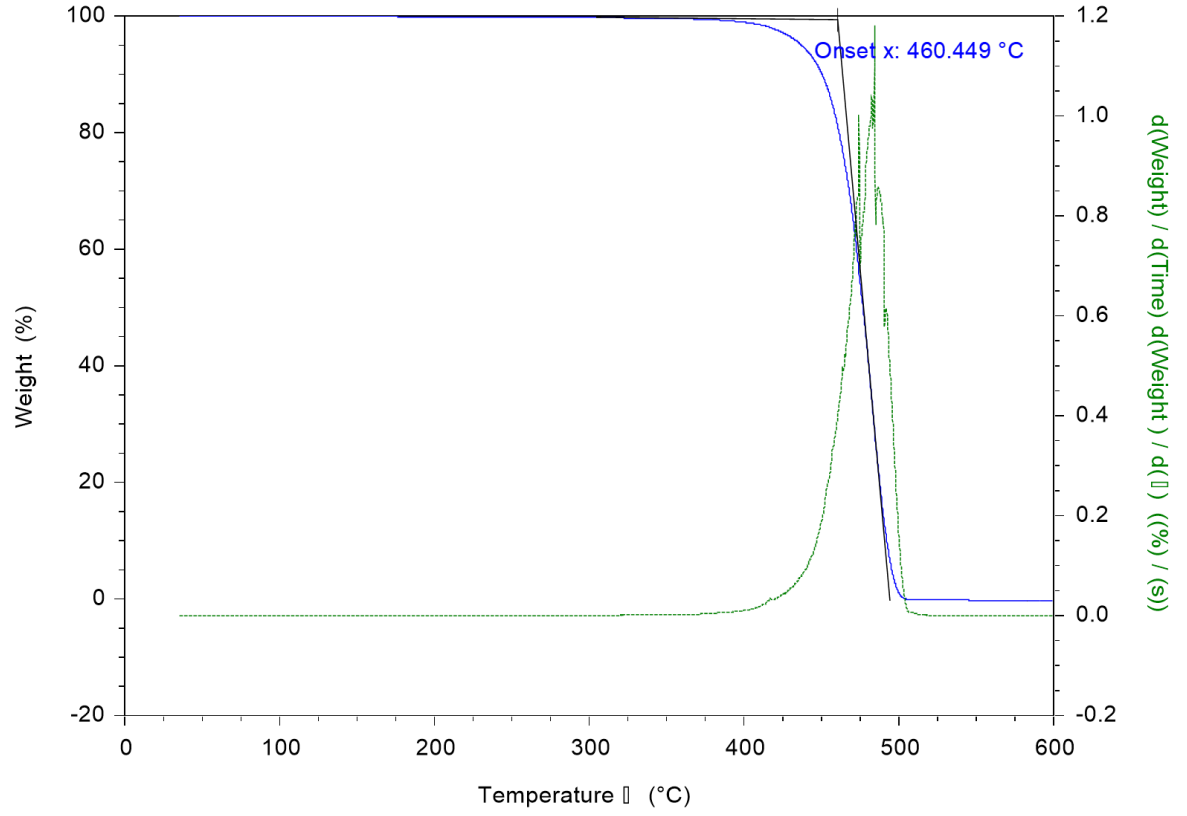

Figure S18. TGA thermogram of P11.

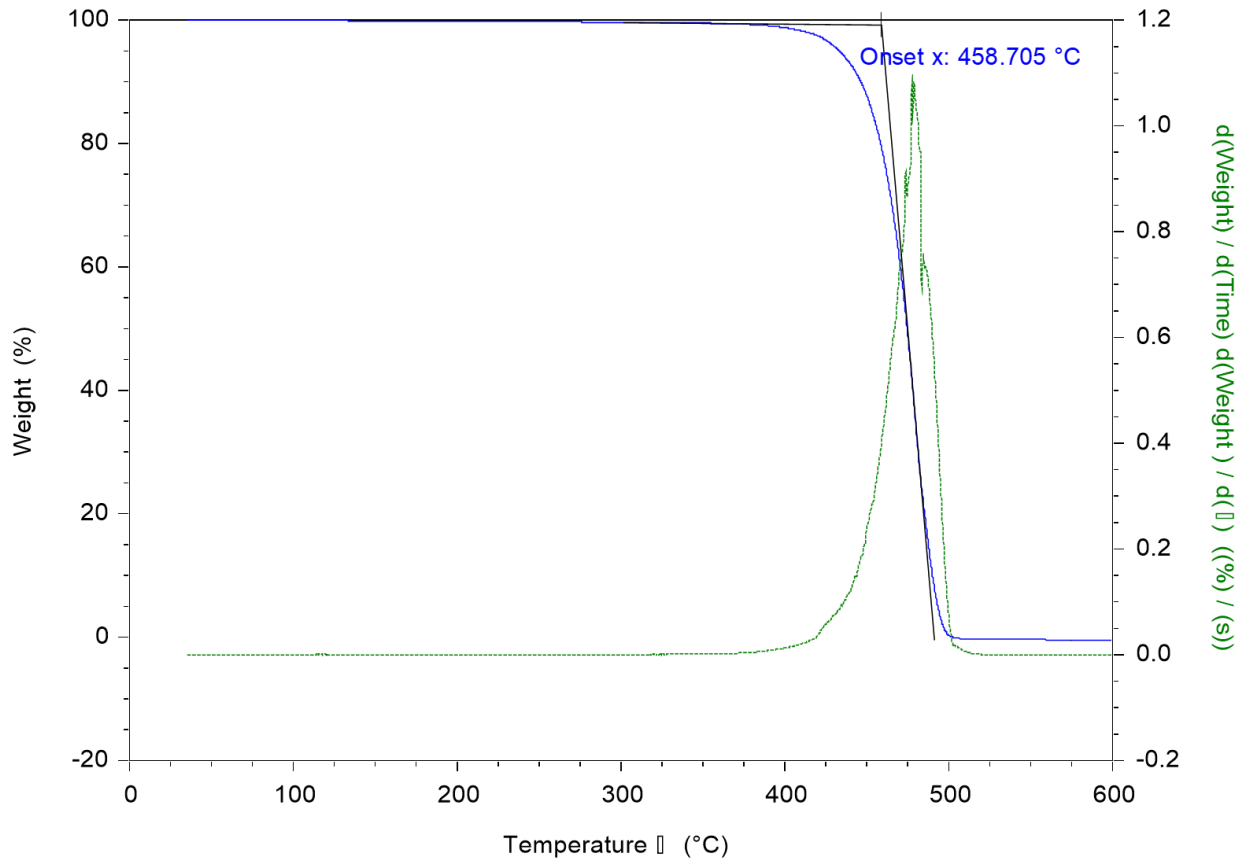

Figure S19. TGA thermogram of P8.

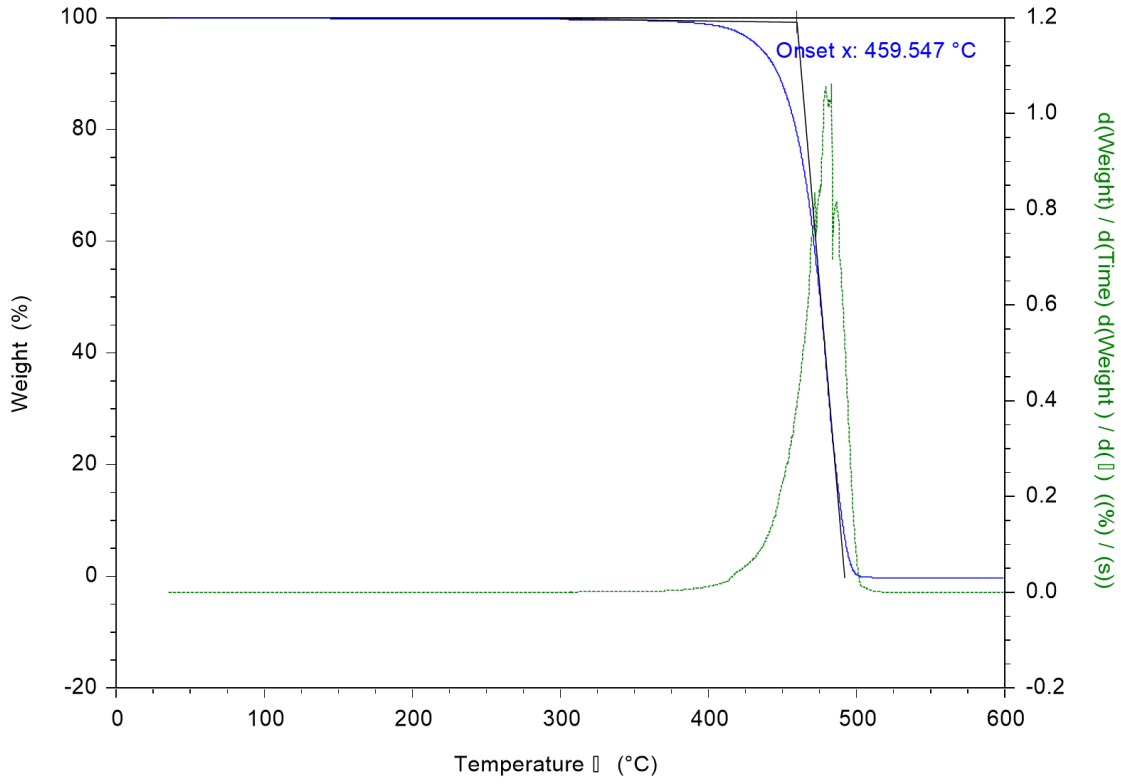

Figure S20. TGA thermogram of P9.

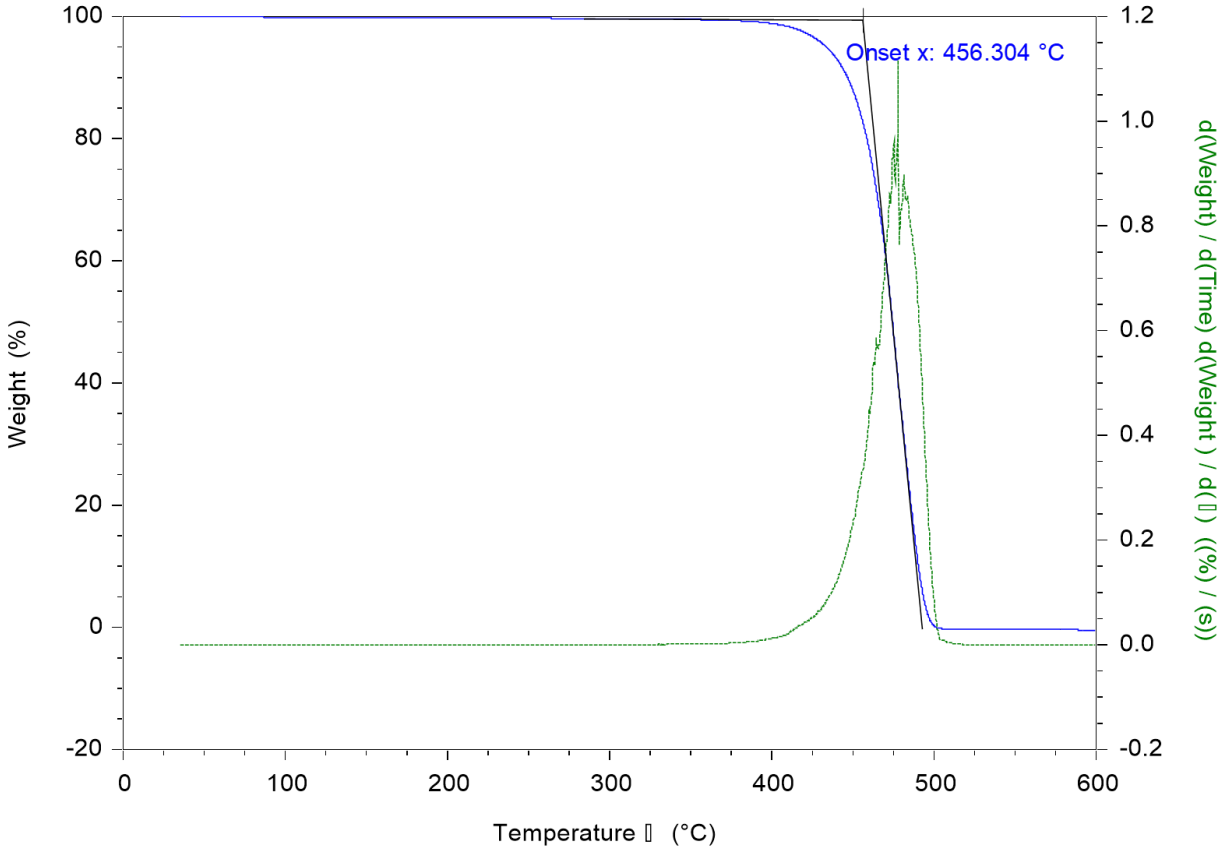

Figure S21. TGA thermogram of P14.

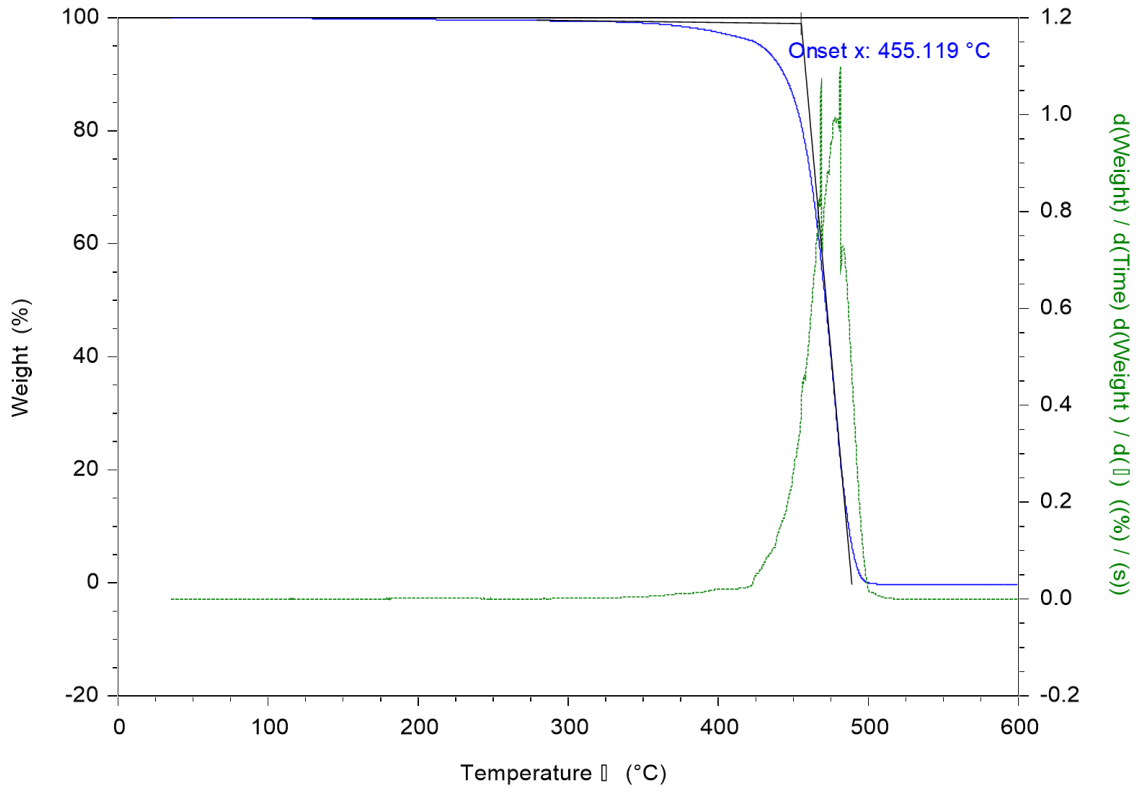

Figure S22. TGA thermogram of P16.

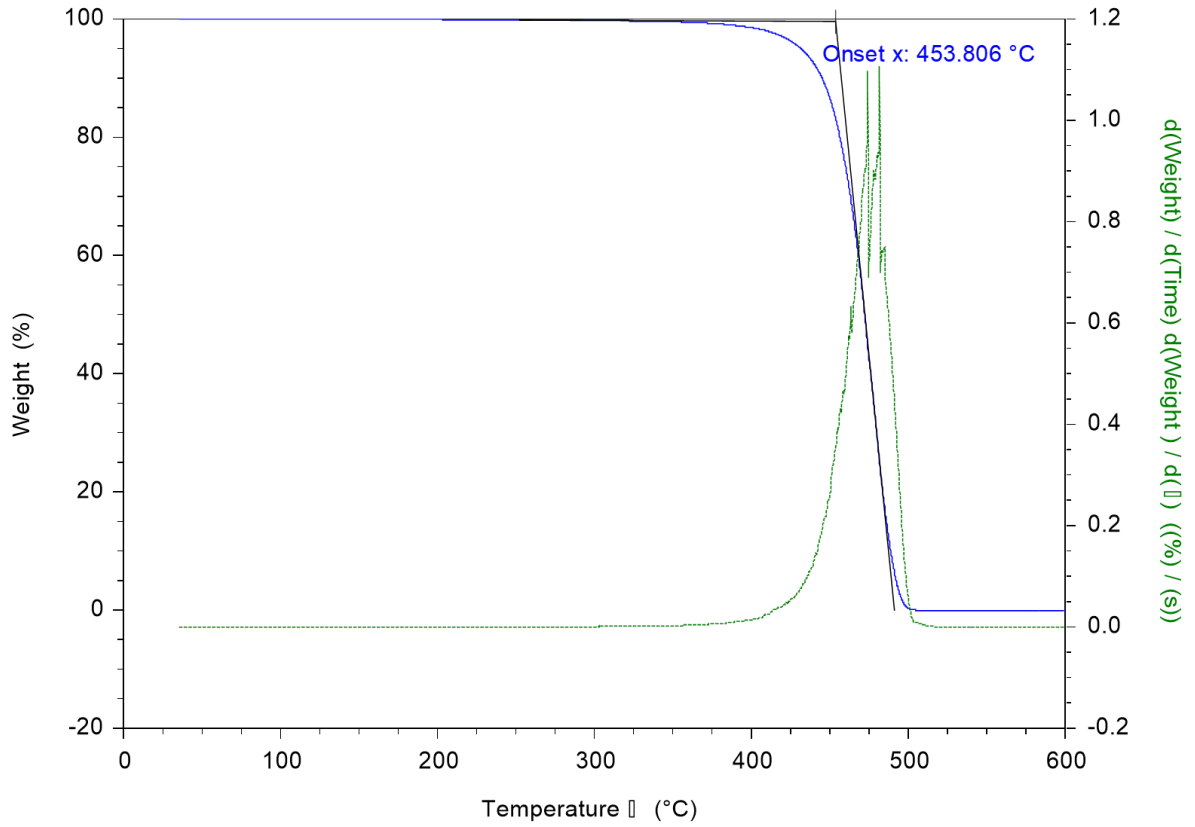

Figure S23. TGA thermogram of P20.

Adhesion specimens

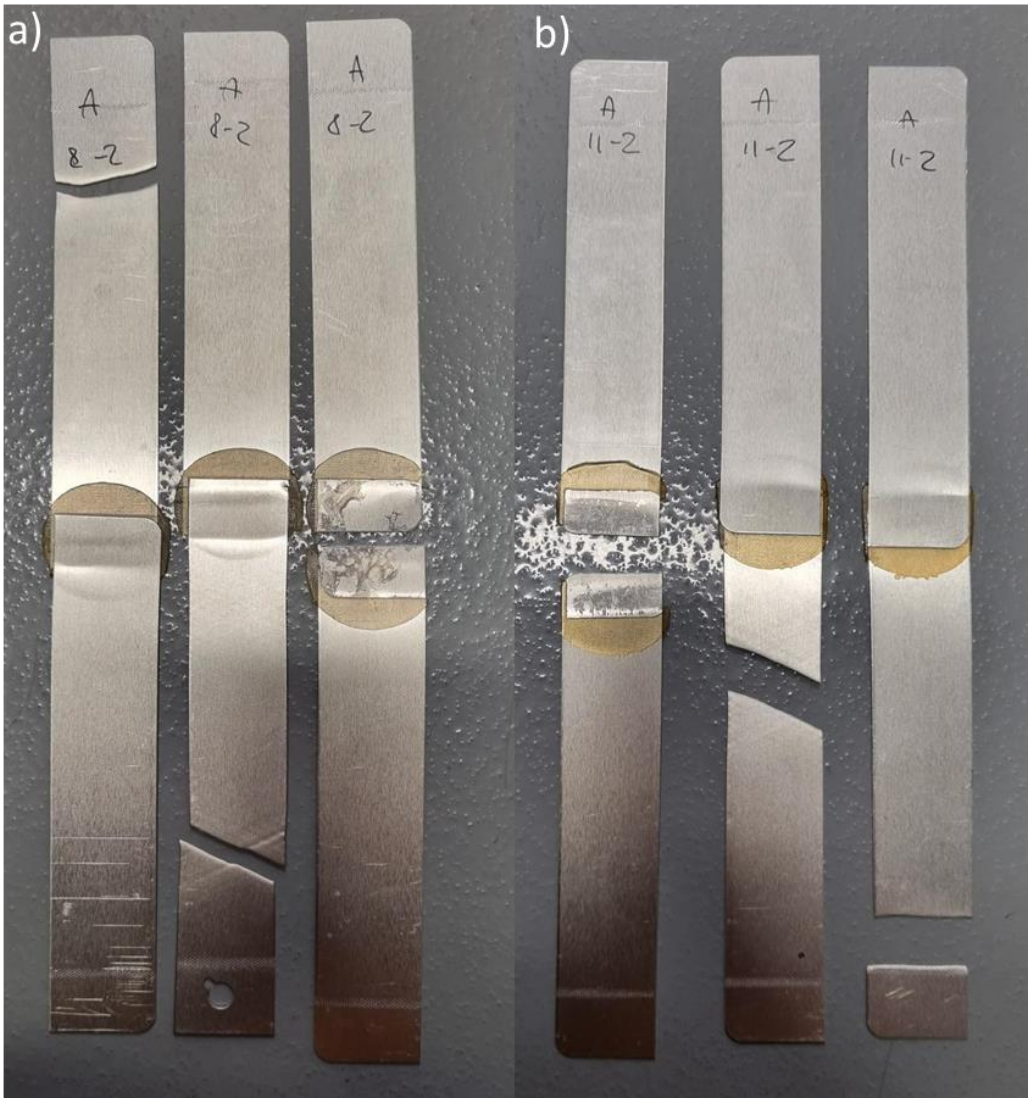

Figure S24. Failure of adhesive specimens of a) P4 and b) P17.

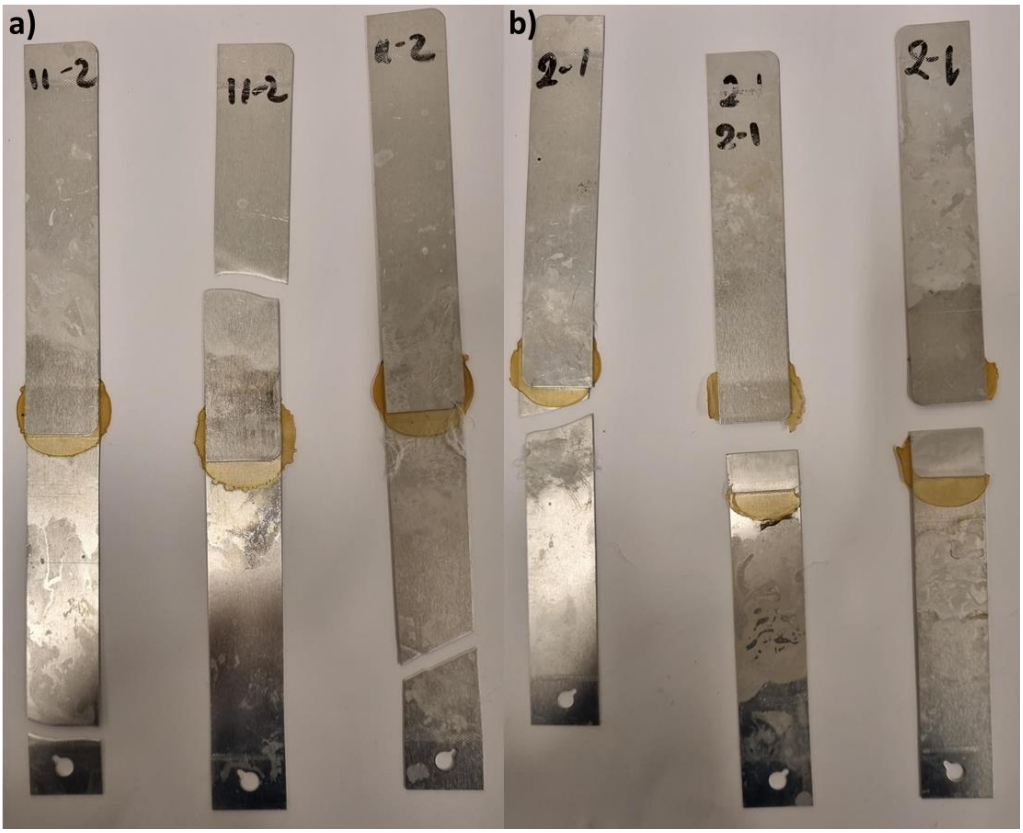

Figure S25. Failure of the specimens after aging tests of the samples a) P17 and b) P18.

1.8 References

[1] C. Vasile, Ed., *Handbook of Polyolefins*, Marcel Dekker, New York, **2000**.
[2] W. Kaminsky, Ed., *Polyolefins: 50 Years after Ziegler and Natta II: Polyolefins by Metallocenes and Other Single-Site Catalysts*, Springer Berlin Heidelberg, Berlin, Heidelberg, **2013**.
[3] S. Dadbin, M. Frounchi, M. Sabet, *Polym. Int.* **2005**, *54*, 686.
[4] M. Narkis, I. Raiter, S. Shkolnik, A. Siegmannz, P. Eyerer, *Journal of Macromolecular Science, Part B* **1987**, *26*, 37.
[5] U. W. Gedde, M. Ifwarson, *Polym. Eng. Sci.* **1990**, *30*, 202.
[6] J. Morshedian, P. M. Hoseinpour, *Iran. Polym. J.* **2009**, *18*, 104.
[7] R. P. de Melo, V. de O. Aguiar, M. de F. V. Marques, *Mat. Res.* **2015**, *18*, 313.
[8] A. Smedberg, T. Hjertberg, B. Gustafsson, *Polymer* **1997**, *38*, 4127.
[9] G. M. Gale, *Appl. Organomet. Chem.* **1988**, *2*, 17.
[10] A. Eisenberg, J.-S. Kim, *Introduction to Ionomers*, Wiley, New York, **1998**.
[11] M. R. Tant, G. L. Wilkes, in *Structure and Properties of Ionomers* (Eds.: M. Pineri, A. Eisenberg), Springer Netherlands, Dordrecht, **1987**, pp. 191–226.
[12] L. Leibler, M. Rubinstein, R. H. Colby, *Macromolecules* **1991**, *24*, 4701.
[13] A. Eisenberg, *Macromolecules* **1970**, *3*, 147.
[14] E. J. Roche, R. S. Stein, T. P. Russell, W. J. Macknight, *J. Polym. Sci. Polym. Phys. Ed.* **1980**, *18*, 1497.
[15] S. Yano, N. Nagao, M. Hattori, E. Hirasawa, K. Tadano, *Macromolecules* **1992**, *25*, 368.
[16] A. Eisenberg, B. Hird, R. B. Moore, *Macromolecules* **1990**, *23*, 4098.
[17] K. Tadano, E. Hirasawa, H. Yamamoto, S. Yano, *Macromolecules* **1989**, *22*, 226.
[18] M. Hara, J. A. Sauer, *J. Macromol. Sci., Part C: Polymer Reviews* **1994**, *34*, 325.
[19] W. Cooper, *J. Polym. Sci.* **1958**, *28*, 195.
[20] Y. Li, Z. Yao, Z. Chen, S. Qiu, C. Zeng, K. Cao, *Polymer* **2015**, *70*, 207.
[21] R. W. Rees, *Ionic Hydrocarbon Polymers*, **n.d.**, US Patent 3,264,272.
[22] M. Tolinski, *Additives for Polyolefins, Getting the Most Out of Polypropylene, Polyethylene and TPO, Elsevier, Oxford, UK 2015.*, **n.d.**
[23] H. Okamura, Y. Takatori, M. Tsunooka, M. Shirai, *Polymer* **2002**, *43*, 3155.
[24] L. Feng, K. A. Cavicchi, B. C. Katzenmeyer, C. Wesdemiotis, *J. Polym. Sci. A Polym. Chem.* **2011**, *49*, 5100.
[25] B. S. Aitken, M. Lee, M. T. Hunley, H. W. Gibson, K. B. Wagener, *Macromolecules* **2010**, *43*, 1699.
[26] C. R. López-Barrón, J. A. Throckmorton, T.-P. Lin, *J. Rheol.* **2022**, *66*, 657.
[27] J. Vachon, P. Neuteboom, J. Tellers, (SABIC GLOBAL TECHNOLOGIES B.V.), *NL WO 2021009274 A1*, **2020**.
[28] J. C. Salamone, C. C. Tsai, A. P. Olson, A. C. Watterson, *J. Polym. Sci. Polym. Chem. Ed.* **1980**, *18*, 2983.
[29] J. C. Salamone, N. A. Mahmud, M. U. Mahmud, T. Nagabhushanam, A. C. Watterson, *Polymer* **1982**, *23*, 843.
[30] S. Jana, V. A. Vasantha, L. P. Stubbs, A. Parthiban, J. G. Vancso, *J. Polym. Sci. Part A: Polym. Chem.* **2013**, *51*, 3260.
[31] G. Deng, K. A. Cavicchi, *Macromolecules* **2017**, *50*, 9473.

[32] M. Tolinski, *Additives for Polyolefins: Getting the Most out of Polypropylene, Polyethylene and TPO*, Elsevier, William Andrew Is An Imprint Of Elsevier, Kidlington, Oxford, UK, **2015**.
[33] L. Cortes, F. Li, J. Tippet, K. Blackmon, M. Myhall, L. Daniels, J. Ashbaugh, (Fina Technology, Inc.), *Patent WO 2016114802*, **2015**.
[34] H. Yasuda, R. Nakano, S. Ito, K. Nozaki, *J. Am. Chem. Soc.* **2018**, *140*, 1876.
[35] P. Ehrlich, G. A. Mortimer, in *Fortschritte Der Hochpolymeren-Forschung*, Springer-Verlag, Berlin/Heidelberg, **1970**, pp. 386–448.
[36] G. A. Mortimer, *J. Polym. Sci. A-1 Polym. Chem.* **1966**, *4*, 881.
[37] J. R. Wagner, E. M. Mount, H. F. Giles, in *Extrusion*, Elsevier, **2014**, pp. 181–192.
[38] W.-M. Chan, P. E. Gloor, A. E. Hamielec, *AIChE J.* **1993**, *39*, 111.
[39] Y. Suzuki, R. Mishima, A. Matsumoto, *Int J. Chem. Kinetics* **2022**, *54*, 361.
[40] B. Wunderlich, C. M. Cormier, *J. Polym. Sci. A-2 Polym. Phys.* **1967**, *5*, 987.
[41] Y. Furushima, M. Nakada, M. Murakami, T. Yamane, A. Toda, C. Schick, *Macromolecules* **2015**, *48*, 8831.
[42] J. D. Hoffman, R. L. Miller, H. Marand, D. B. Roitman, *Macromolecules* **1992**, *25*, 2221.
[43] J. D. Hoffman, R. L. Miller, *Polymer* **1997**, *38*, 3151.
[44] D. V. Rees, D. C. Bassett, *Nature* **1968**, *219*, 368.
[45] K. Menard, in *Handbook of Plastics Analysis* (Eds.: H. Lobo, J. Bonilla), CRC Press, **2003**.
[46] R. H. Hansen, H. Schonhorn, *J. Polym. Sci. B Polym. Lett.* **1966**, *4*, 203.
[47] P. Fabbri, M. Messori, in *Modification of Polymer Properties*, Elsevier, **2017**, pp. 109–130.
[48] Y.-L. Hsieh, Shanqing Xu, M. Hartzell, *J. Adhesion Sci. Tech.* **1991**, *5*, 1023.
[49] H. N. A. M. Steenbakkers-Menting, P. E. L. Voets, P. J. Lemstra, *J. Adhesion Sci. Tech.* **1995**, *9*, 889.

Chapter 2

Polyethylene Based Ionomers as High Voltage Insulation Materials

Part of this work was carried out in collaboration with Prof. Christian Muller (Chalmers University)

Abstract

Polyethylene based ionomers are demonstrated to feature a thermo-mechanical and dielectric property portfolio that is comparable to crosslinked polyethylene (XLPE), which may enable the design of more sustainable high-voltage direct-current (HVDC) power cables, a crucial component of future electricity grids that seamlessly integrate renewable sources of energy. A new type of ionomer is obtained *via* high-pressure/high-temperature free radical copolymerization of ethylene in the presence of small amounts of ion-pair comonomers comprising amino terminated methacrylates and methacrylic acid. The synthesized ionomers feature a crystallinity, melting temperature, rubber plateau modulus and thermal conductivity similar to XLPE but remain melt-processable. Moreover, the preparation of the ionomers is free of byproducts, which readily yields a highly insulating material with a low direct-current (DC) electrical conductivity of 1 to $6 \cdot 10^{-14}$ S m^{-1} at 70 °C and an electric field of 30 V mm^{-1}. Evidently, the here investigated ionomers represent a promising alternative to XLPE-based high voltage insulation, which may permit to ease the production as well as end-of-use recycling of HVDC power cables by combining the advantages of thermoset and thermoplastic materials while avoiding the formation of byproducts.

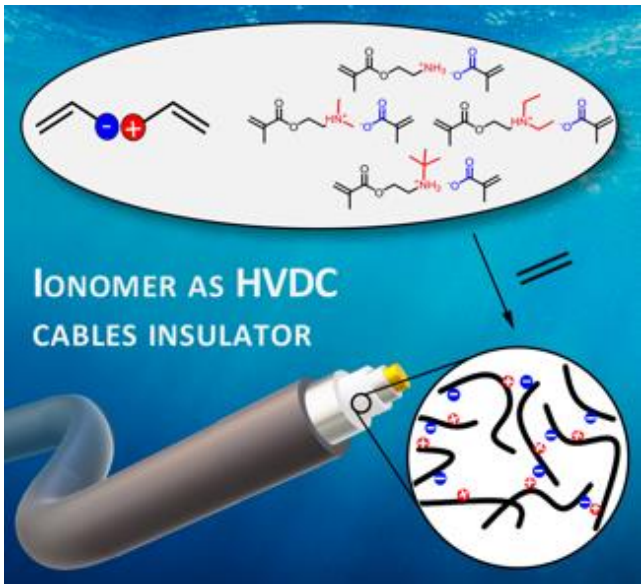

The content of this chapter is partially adapted from a manuscript under second revision on Advanced Functional Materials.

2. Introduction

High voltage direct-current (HVDC) power cables are an integral part of modern electrical power grids that integrate renewable sources of energy.[1] The most advanced type of HVDC cable comprises an extruded insulation layer between the inner conductor and outer shielding, which allows the cable to be buried underground or placed at the bottom of the sea.[2] The most common insulation material of extruded HVDC cables is composed of low-density polyethylene (LDPE), which is crosslinked with peroxides to form an infusible material that maintains dimensional stability above the melting temperature of LDPE, $T_m^{LDPE} \approx 110$ °C. Peroxide crosslinking, however, results in the formation of byproducts, such as water, methane, cumyl alcohol and α-methyl styrene,[3] which represent a health hazard and cause premature aging of dielectrics under service conditions.[4] Hence, these byproducts must be removed from crosslinked polyethylene (XLPE), which can be achieved through a time and energy intensive degassing process.[4] Degassed XLPE features a low $\sigma_{DC} \approx 3 \cdot 10^{-14}$ S m^{-1} at an electric field of 30 kV mm^{-1} and 70 °C,[5] which is a typical HVDC cable operating temperature.

Alternative materials concepts that avoid the formation of byproducts during the cable manufacturing process, while maintaining the thermo-mechanical and dielectric properties of XLPE, are highly sought after.[6] The ability to dissipate the heat generated by the conducting core to avoid the risk of thermal runway and breakdown of the insulation material is another key parameter to be considered for high-voltage insulation materials.[1]

Two types of strategies have been explored that either aim to replace peroxide curing or avoid crosslinking altogether. Byproduct-free curing processes exploit click-chemistry type reactions between polyethylene copolymers, where permanent covalent bonds form upon the reaction of functional groups such as carboxylic acids and epoxides.[7, 8] A second strategy is to use polypropylene copolymers or blends,[6, 9-12] which thanks to the high melting temperature of polypropylene of up to $T_m^{PP} \approx 170$ °C maintain dimensional stability at elevated temperatures despite the absence of crosslinks. Both, types of blends feature electrical conductivities that are comparable to or even less than values reported for XLPE. The dielectric properties of novel insulation materials can be tuned further through the addition of additives such as metal oxide nanoparticles,[13, 14] aromatic molecules[15] and organic semiconductors.[16, 17] One additional advantage of thermoplastic formulations is the possibility to reprocess the material by remelting, which may ease recycling of the cable insulation for other applications once a cable has reached the end of its lifetime.

One approach that has not yet received much attention in the context of HVDC cable insulation is the use of dynamic bonds, presumably because of concerns that the introduction of additional chemical moieties may negatively affect the dielectric properties. One recent study[18] proposed the use of a dynamic network as a cable insulation material and explored the thermo-mechanical and dielectric properties of a polyethylene vitrimer comprising hydroxy ester crosslinks formed through a byproduct free reaction of a dicarboxylic acid and epoxides that underwent transesterification in the presence of zinc acetate.[19, 20] In terms of thermo-mechanical behavior dynamic networks have the potential to combine the advantages of both thermoset and thermoplastic insulation materials, i.e. an XLPE type rubber plateau above T_m^{PE}, as well as the possibility to reprocess the material at more elevated temperatures.

The here described type of ionomer features a low σ_{DC} = 1 to 6·10^{-14} S m^{-1} at an electric field of 30 kV mm^{-1} and 70 °C, comparable to XLPE, together with a similar or even higher thermal conductivity around $\kappa \geq$ 0.36 W m^{-1} K^{-1}. Evidently, all-organic ionomers represent a new design strategy for high-voltage insulation materials that combine the advantages of both thermosets and thermoplastics while avoiding the formation of byproducts.

2.1 Results and discussion

A wide range of IPCs were synthesized, either through an acid-base reaction, when secondary or tertiary amines were used, or through ion exchange metathesis in case of primary amines. IPCs based on secondary or tertiary amines were obtained by mixing the two starting reagents without the use of solvents (Scheme 1a). To realize IPCs based on primary amines, protonation was necessary (typically with HCl) to avoid transamidation reactions followed by co-dissolution of the two reagents in a mixture of methanol and dichloromethane and removal of the resulting insoluble inorganic salt to shift the equilibrium toward the product (Scheme 1b).

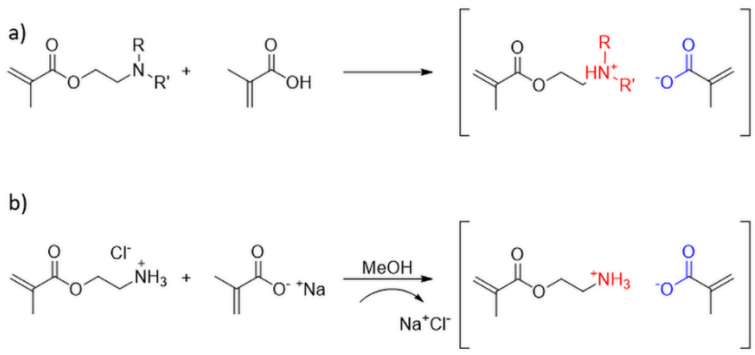

Scheme 1. a) Acid-base reaction in the case of secondary and tertiary amines and b) exchange metathesis reaction in the case of a primary amine.

Structural variations of the starting monomers were devised to probe the influence of different ion pairs on the thermal, mechanical and dielectric properties of the resulting copolymers. In particular, we used cationic comonomers with diverse degrees of alkylation of the amino moiety or different alkylating groups, while for the anionic comonomers we used exclusively methacrylic acid (see Figure 2a, monomers M1-4). To confirm the formation of the ion pair, we used ^{1}H-NMR spectroscopy. An upfield shift of the vinyl protons belonging to the methacrylate unit is observed, while the ethane protons connecting the ester to the amino group and the methyl of the latter experience a downfield shift, as expected (Figures S1-S7).

All ionomers (Figure 2c) were prepared through free radical polymerization by reacting the IPC and ethylene at a high pressure of about 2000 bars and high temperature of 180 °C or 200 °C in an autoclave using a peroxide initiator (Figure 2b; see Table 1 for reaction conditions). The IPCs were dissolved in methanol (50 wt%) and co-injected together with high-pressure ethylene in the autoclave through a static mixer. Methanol was chosen as a solvent since it does not have a large effect on the polymerization thanks to its very low chain transfer constant.

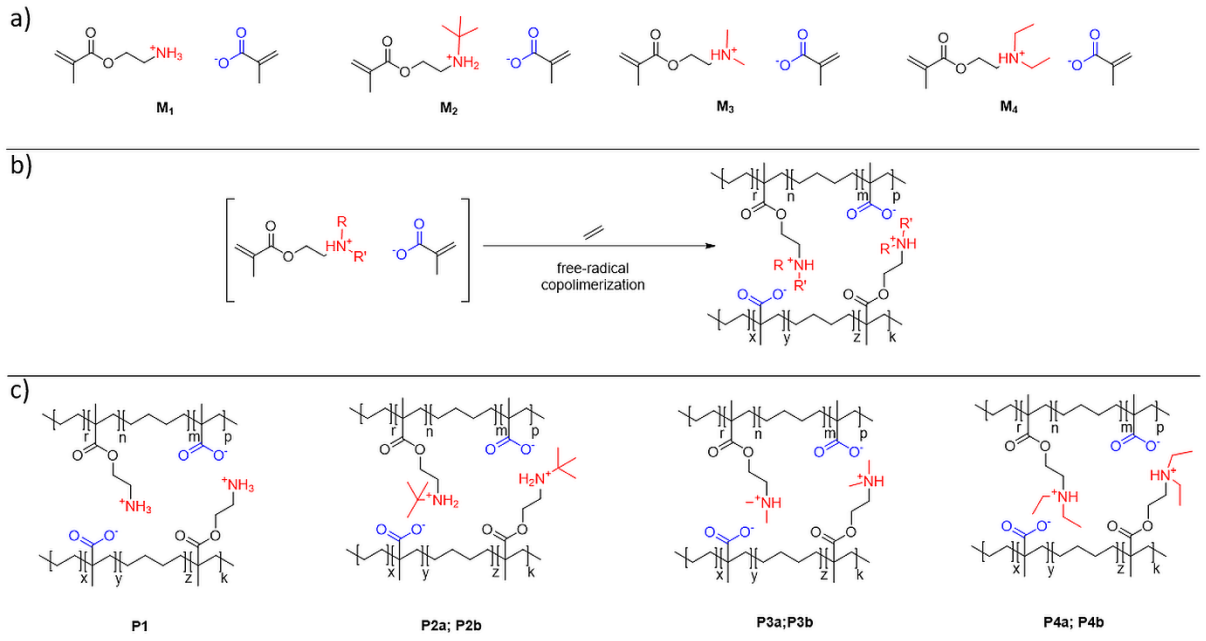

Figure 2. a) The synthetized ion pair comonomers (IPCs), b) free radical polymerization reaction, and c) corresponding ionomers.

At the end of the reaction, the desired ionomers were recovered as a fine powder from the recuperation vessel and characterized through ^{1}H NMR spectroscopy (Figures S8-S15), FTIR spectroscopy (Figure S16), and elemental analysis. The ^{1}H NMR spectra of polymers P2-4 featured diagnostic peaks belonging to the amino moieties, as well as to the polyethylene backbone. The obtained polymers were quite pure, without the presence of any side product.

On the contrary, for P1 the ^{1}H NMR spectrum indicated the presence of both unreacted monomers and side products, the latter due to unwanted amidation reactions (Figure S9). We speculate that since M2-4 carry substituents on the amino group, amidation reactions are less likely to occur due to steric hindrance compared with M1. Moreover, the degree of conversion of M1 to P1 was found to be lower compared with M2-4 (Table S1) and varied between different synthetic runs. Therefore, we decided to dismiss P1 during the remainder of this study.

The nitrogen content in the resulting polymers is diagnostic of the presence of IPCs and allows their quantification. Therefore, elemental analysis was used to determine the IPC content, which was found to be about 3 wt% for P2-4 and 4.5 wt% for P1. The calculated IPC content per 1000 carbons (-CH_2-) was similar for all synthesized ionomers, except P1 (see Table 1).

Table 1. IPC molecular weight M_{IPC}, IPC content in the feed and temperature *T* used for free radical polymerization of ionomers, IPC content of the synthesized ionomers from elemental analysis of the nitrogen content given in wt%, mol% and per 1000 CH_2.

IPC	M_{IPC} [g mol^{-1}]	IPC feed [mol%]	*T* [°C]	ionomer	IPC content [wt%]	IPC content [mol%]	IPC content per 1000 CH_2
M1	215.25	0.1	200	**P1**	4.5	0.61	3.1
M2	271.35	0.05	180	**P2a**	3.1	0.33	1.7
			200	**P2b**	2.9	0.31	1.5
M3	243.30	0.05	180	**P3a**	2.9	0.34	1.7
			200	**P3b**	2.8	0.33	1.7
M4	271.35	0.05	180	**P4a**	2.9	0.31	1.5
			200	**P4b**	2.9	0.31	1.5

We also confirmed that both the as synthesized ionomers as well as melt-pressed films could be dissolved in p-xylene at 100 ºC, which suggests that the material does not form one inseparable network. Size exclusion chromatography (SEC) of the ionomers using 1,2-dichlorobenzene as the solvent indicated the presence of aggregates with apparent molecular weights of more than 10^6 g mol^{-1} (not shown), which likely consist of several polyethylene backbones linked *via* ion pairs. We argue that the ionomers should not be thought of as individual macromolecules but rather clusters of macromolecules whose makeup can evolve due to exchange reactions between different ion pairs.

Differential Scanning Calorimetry (DSC) was performed to gain further insight into the microstructure of the synthesized ionomers and to assess their thermal properties. Second heating thermograms of all ionomers feature a similar crystallinity of about 40 % and peak melting temperature T_m = 113 to 114 ºC, comparable to reference LDPE (Table 2 and Figure S17), indicating that the IPCs do not significantly affect the microstructure of the polymer matrix. We also note that all DSC thermograms feature a single melting endotherm, which is consistent with a relatively even distribution of the comonomers along the polymer backbone.

As mentioned in the chapter 1, the Gibbs-Thomson equation (equation 1, chapter 1) was used to calculate the average lamellar thickness (see table S2).

Dynamic mechanical thermal analysis (DMTA) in tensile mode was used to analyze the thermo-mechanical properties of melt-pressed films of the ionomers up to 200 ºC (thermal gravimetric analysis (TGA) shows no weight loss up to 200 ºC, see Figures S17-23). All materials display a storage modulus E' between 200 and 500 MPa at room temperature (Figure 3). DMTA thermograms of reference LDPE and Surlyn™ feature a significant decrease in E' above their melting temperature(s), resulting in a molten material above 120 ºC (Figure 3). In contrast, XLPE (see experimental section for details) with a gel content of 68 % gave rise to a rubber plateau above its T_m = 108 ºC with a value of $E' \approx 3.7$ MPa at 150 ºC (Table 2). Likewise, DMTA thermograms of the synthesized ionomers feature a distinct rubber plateau above T_m^{PE}, confirming that the introduction of IPCs leads to the formation of a network (Figures 3a and b). Except for P2a, the moduli of the polymers synthesized at 200 °C are lower compared with the modulus of the corresponding polymers synthesized at 180 °C. In particular P3a exhibits a rubber plateau modulus of $E' \approx 2.6$ MPa at 150 °C (Table 2), which is similar to the value obtained for XLPE.

Table 2. Peak melting temperature T_m and crystallinity $X_c = \Delta H_f / \Delta H_f^0$ from DSC, where ΔH_f is the melting enthalpy and ΔH_f^0 = 286.2 J g^{-1}, storage modulus E' at 150 °C from DMTA, molecular weight between crosslinks M_c according to equation 2, number of crosslinks N_c per 1000 CH_2, thermal conductivity κ at room temperature, electrical conductivity σ_{DC} at 70 ºC and an electric field of 30 kV mm^{-1} of LDPE, XLPE, Surlyn™ as well as the synthesized ionomers; the error in σ_{DC} is estimated to be 30%.[12]

Material	T_m [°C]	X_c [%]	E' at 150 °C [MPa]	M_c [kg mol^{-1}]	N_c per 1000 CH_2	κ at r. t. [W m^{-1} K^{-1}]	σ_{DC} at 70 °C [10^{-14} S m^{-1}]
LDPE	110	39	-	-	-	0.41 ± 0.08	7.0 ± 2.1
XLPE	108	42	3.7	2.3	6.2	0.36 ± 0.004	4.5 ± 1.4
Surlyn™	90	10	-	-	-	0.29 ± 0.002	3.4 ± 1.0
P2a	114	40	0.8	10.8	1.3	0.39 ± 0.006	1.0 ± 0.3
P2b	113	41	1.01	8.2	1.7	0.38 ± 0.006	6.0 ± 1.8
P3a	114	42	2.6	3.2	4.4	0.37 ± 0.001	3.1 ± 0.9
P3b	113	41	1.14	7.3	1.9	0.35 ± 0.006	5.3 ± 1.6
P4a	114	39	1.4	6.0	2.3	0.39 ± 0.001	1.6 ± 0.5
P4b	113	42	0.85	9.8	1.4	0.36 ± 0.009	1.7 ± 0.5

The molecular weight between consecutive crosslinks M_c was estimated according to equation 2:

$$M_c = \frac{\rho RT}{G'} \quad (2)$$

Where ρ = 0.790 g cm^{-3} is the density at temperature T = 150 °C (423 K), R the universal gas constant and $G' = E'/[2(1+\upsilon)] = E'/3$ the shear modulus at T = 150 °C assuming a Poisson's ratio υ = 0.5. The number of network points N_c per 1000 carbons (−CH_2−) was then estimated by dividing 14 kg mol^{-1} with M_c (Table 2). For XLPE we obtain a value of $M_c \approx$ 2.3 kg mol^{-1}, which corresponds to $N_c \approx$ 6.3 per 1000 carbons. Ionomer P3a yields similar values of $M_c \approx$ 3.2 kg mol^{-1} and $N_c \approx$ 4.4 per 1000 carbons (Table 2), which suggests that the amount of comonomer and type of amine group can be selected to match the thermo-mechanical properties of XLPE. In general, for P2-4 the estimated value for N_c is comparable to or larger

than the number of IPCs per 1000 carbons (cf. Tables 1 and 2), which suggests that the majority of IPCs, in addition to long-chain branches and trapped entanglements, form a network point. The overall picture emerging from these data is the presence of ionic network points that reinforce the molten ionomers.

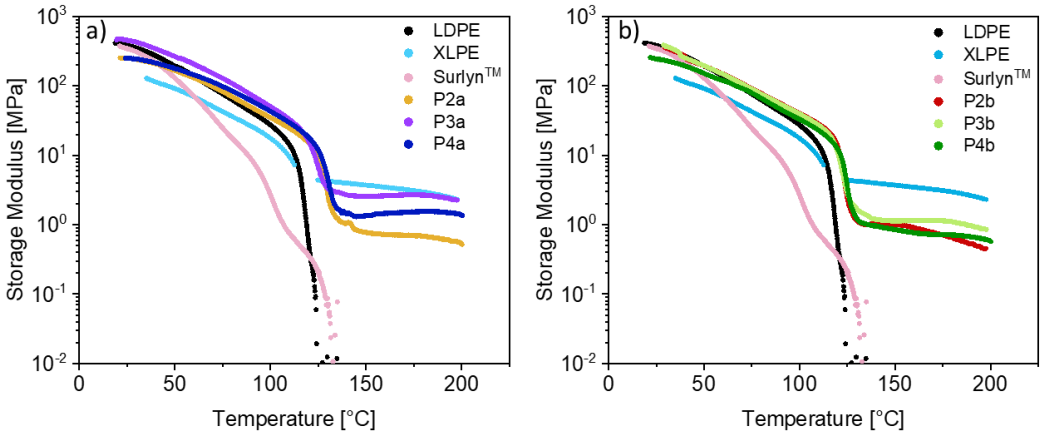

Figure 3. DMTA thermograms of: a) LDPE, XLPE, Surlyn™, P2-4a and b) LDPE, XLPE, Surlyn™, P2-4b.

In a further set of experiments dynamic oscillatory shear and extensional rheology measurements were carried out to gain further inside into the viscoelastic properties of the ionomer melts. Dynamic oscillatory shear measurements at 150 °C of LDPE and Surlyn™ reveal a crossover frequency where the shear storage and loss modulus are of equal magnitude, i.e. $G' = G''$, indicating a transition from an elastic- to a viscous-dominated behavior with decreasing frequency (Figure S24). The longest relaxation time of the polymer melt $\tau_d = 1/\omega_{G'=G''}$ was found to be 5.6 s for LDPE and 0.7 s for Surlyn™. In contrast, XLPE shows an elastic-dominated behavior in the entire tested frequency range from ω = 0.01 to 600 rad s^{-1}, i.e. $G' > G''$ as expected for a crosslinked polymer. Likewise, the ionomers P2-4a,b have virtually identical viscosity functions compared to XLPE both in terms of magnitude and shear thinning slope, retaining their elastic network character across the tested frequency range, in agreement with the DMTA measurements (see Figure 3). For all ionomers but P3a we observe that the difference between G' and G'' decreases at lower frequencies, and thus a crossover point may exist at ω << 0.01 rad s^{-1} where $G' = G''$ implying longest relaxation times of τ_d >> 600 s (Figure S24).

Extensional rheology measurements allowed us to monitor the transient uniaxial extensional viscosity as a function of Hencky strain rate from $\dot{\varepsilon}$ = 10^{-2} to 10^{1} s^{-1} (Figure S25). LDPE displays significant strain hardening, as expected due to its long-chain branched

molecular topology. A similar degree of strain hardening is observed in case of XLPE as well as the ionomers P3a,b and P4a,b indicating that strain stretching occurs between the covalent network points in case of XLPE and ionic network points in case of the ionomers. In contrast, the ionomers P2a,b with a tert-butyl group on the secondary amine feature minimal strain hardening. Since these two materials feature a similar N_c as, e.g., P3b and P4b (see Table 2), we argue that chain stretching between crosslinks and thus strain hardening is absent because the ionic network points are able to reorganize to a greater extent. This observation is consistent with a lower dissociation energy of ion-pairs due to the presence of the bulky alkyl group at the ammonium cation, which increases the anion/cation distance.[21-23]

The transient plane source method was used to determine the thermal diffusivity α and heat capacity C_p at room temperature, and the thermal conductivity was calculated according to:

$$\kappa = \alpha \rho C_p \quad (5)$$

using a density of ρ = 0.921 g cm^{-3}. We find that LDPE has a thermal conductivity at room temperature of κ = 0.41 W m^{-1} K^{-1} while XLPE shows a lower value of κ = 0.36 W m^{-1} K^{-1} (Table 2). Surlyn^{TM} features a significantly lower thermal conductivity, which we assign to the lower crystallinity of the material. Ionomers P2-4 display slightly larger values than XLPE, e.g. κ = 0.39 W m^{-1} K^{-1} for P4a, which we explain with the similar crystallinity but slightly larger lamellar thickness as indicated by the larger T_m compared with XLPE.

In a final set of experiments, we determined the electrical conductivity of the ionomers. Films with thicknesses of 0.14 to 0.16 mm were placed between two planar electrodes, with the measuring electrode surrounded by a shielding electrode, and the electrode system was placed in an oven to maintain a temperature of 70 °C (Figure 4a). We applied a DC voltage for 18 h that gave rise to an electric field of 30 kV mm^{-1}, followed by an intermittent interval during which the applied voltage was turned off for 6 h to simulate a discharging event, and finally the same DC voltage was reapplied for another 18 h. After reapplication of the voltage the leakage currents and hence the apparent conductivity rapidly approached quasi steady-state behavior, indicating that polarization did not significantly affect the here studied materials (Figure 4). The apparent conductivity gradually decayed, approaching quasi steady-state conditions at the end of the measurement and the value obtained at the end of the second 18 h period was used as an estimate for σ_{DC}. For LDPE and XLPE we obtained values of σ_{DC} = 7.0 and 4.5·10^{-14} S m^{-1}, respectively (Table 2), the latter being similar to values reported for XLPE used for high voltage insulation.[8] Remarkably, despite the presence of polar functional groups, ionomers P2-4a synthesized at 180 °C feature a low σ_{DC} = 1 to 3.1·10^{-14} S m^{-1}, which is close to the value

obtained for XLPE. Instead, P2-4b, which were synthesized at 200 °C, display slightly higher values of σ_{DC} = 1.7 to 6·10^{-14} S m^{-1}. Evidently, the selection of a judicious amount of IPCs in combination with tuning of the polymerization conditions results in materials that display a promising combination of thermo-mechanical and dielectric properties. The ionomers P2a and P4a, for example, offer a desirable combination of a low σ_{DC} < 2·10^{-14} S m^{-1} but high κ = 0.39 W m^{-1} K^{-1}, while the tensile storage modulus at 150 °C ranges from $E' \approx$ 0.8 to 1.4 MPa, slightly less than reference XLPE (Table 2).

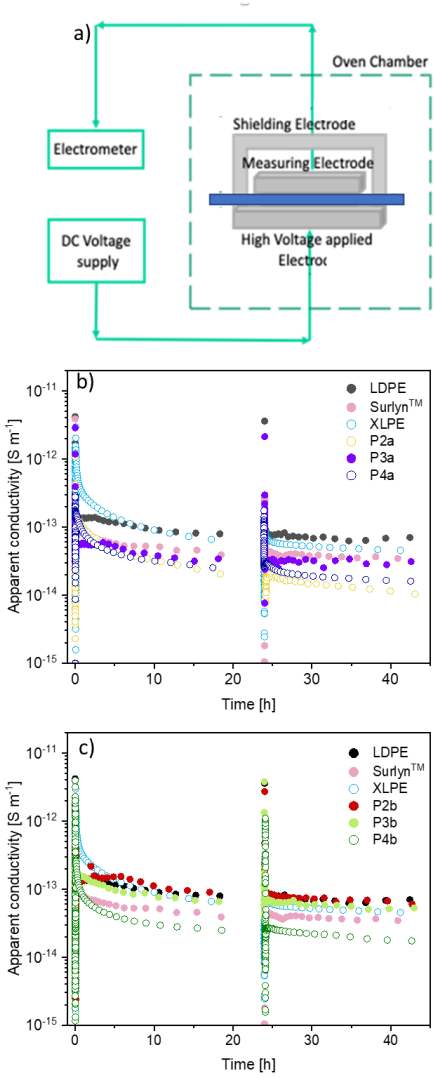

Figure 4. a) Schematic of setup used for leakage current measurements, and apparent conductivity $\sigma = IV^{-1} \cdot 4L(\pi D^2)^{-1}$ where L is the distance between the measuring and high voltage electrode (i.e. the sample thickness), D the diameter of the measuring electrode, V the applied voltage and I the leakage current recorded at 70 °C and 30 kV mm^{-1} with an intermittent step of 6 h during which the applied voltage was turned off for b) LDPE, XLPE, Surlyn™ and ionomers P2-4a and c) LDPE, XLPE, Surlyn™ and ionomers P2-4b. Open symbols: D = 28 mm; closed symbols: D = 59 mm.

2.2 Conclusions

In this work, we introduce polyethylene based ionomers as potential insulation materials for high voltage power cables. The studied ionomers were synthesized *via* high-pressure/high-temperature free radical copolymerization in the presence of a suitable initiator by directly reacting various ion-pair comonomers (IPCs) with ethylene. The IPCs comprise amino terminated methacrylates and methacrylic acid that differ in the type and number of substituents on the amino group. This approach resulted in melt-processable materials with thermo-mechanical properties similar to XLPE, while avoiding the presence of mobile inorganic cations or crosslinking side products that can affect the dielectric properties. The synthesized ionomers exhibit a melting temperature and crystallinity similar to XLPE and LDPE, indicating that the IPCs do not significantly affect the microstructure of the polymer matrix. Dynamic mechanical thermal analysis (DMTA) indicated that all investigated ionomers feature a rubber plateau above their melting temperature, similar to XLPE. Despite the presence of ionic moieties, the obtained ionomers display promising insulating properties, as evidenced by a low electrical conductivity of σ_{DC} = 1 to $6 \cdot 10^{-14}$ S m^{-1}, comparable to or lower than the value measured for XLPE, σ_{DC} = $4.5 \cdot 10^{-14}$ S m^{-1}, the most common insulation material used for extruded high voltage cables. Moreover, the ionomers exhibit a relatively high thermal conductivity κ = 0.35 to 0.39 W m^{-1} K^{-1} compared with XLPE (κ = 0.36 W m^{-1} K^{-1}). Importantly, properties like the elastic modulus at elevated temperatures as well as the electrical and thermal conductivity can be tuned by a judicious selection of the amino group of the IPC, which offers the opportunity optimize the here presented ionomer concept for specific application requirements. Overall, the here investigated type of ionomers show potential as a viable alternative to XLPE for high voltage power cable insulation.

2.3 Experimental Section

Methods

Sample preparation: Samples for DMTA and DC conductivity measurements were prepared by melt-pressing the ionomers or LDPE at 150 °C, including a 5 min melting step followed by application of 150 kN for 10 min. Some melt-pressed ionomer films contained physical impurities that were removed by cutting followed by melt-pressing of the remaining material for a second time. To prepare XLPE, milled LDPE was dispersed in a solution of dicumyl peroxide (DCP) in methanol at 40 °C and stirred for 1 h, followed by solvent evaporation. The resulting milled LDPE infused with 1 wt% DCP was melt-pressed at 120 °C for 5 min. The temperature was then increased to 180 °C, where the sample was allowed to crosslink for 10 min before cooling. The gel content was measured by submerging 150 mg of material in 500 mL of decalin for 20 h followed by drying and weighing of the insoluble fraction.

Nuclear magnetic resonance (NMR): NMR spectra were recorded using a Bruker Advance 400 (400 MHz) spectrometer at room temperature. Chemical shifts are reported in parts per million (ppm). ^{1}H-NMR chemical shifts are given in reference to the residual solvent peak at 7.26 ppm in $CDCl_3$, at 6.00 ppm for tetrachloroethane-d_2 (TCE-d_2), and at 2.50 ppm in dimethyl sulfoxide-d_6 (DMSO-d_6), High-temperature NMR spectra were recorded on a Bruker AVANCE III (500 MHz) equipped with a cryogenically cooled probe head at 80 °C or 120 °C in TCE-d_2.

Elemental Analysis (EA): Elemental analysis was carried out with a CHNS Thermo Fisher FlashSmart instrument. Samples were burned in the presence of oxygen. The nitrogen content was determined by means of thermal conductivity (TC) and volumetric analysis.

Fourier transform infrared spectroscopy (FTIR): FTIR in attenuated total reflectance (ATR) mode was performed on powder samples with a Perkin Elmer FTIR Spectrum Two instrument equipped with a GladiATR attachment from Pike Technologies. The background was subtracted from every recorded spectrum.

Thermogravimetric analysis (TGA): was performed under nitrogen atmosphere using a Perkin Elmer TGA 8000. Samples were heated to 800 °C at a heating rate of 10 °C min^{-1}.

Differential scanning calorimetry (DSC): DSC measurements were carried out under nitrogen between -50 and 150 °C at a scan rate of 10 °C min^{-1}, using a Mettler Toledo DSC2 calorimeter. The sample weight was 5-10 mg.

Dynamic mechanical thermal analysis (DMTA): DMTA was carried out in tensile mode using a TA Q800 DMA in tensile mode on 30 mm × 11 mm pieces cut from 0.7 mm thick melt-pressed films. Variable-temperature measurements from 25 to 200 °C were done at a heating rate of 3 °C min^{-1}, with a preload force of 0.01 N, a maximum strain of 0.05 % and a frequency of 1 Hz. The given values are related to the second heating curve.

Rheology: Rheological properties in simple shear and uniaxial extension were determined using an Anton Paar MCR702e Space rheometer equipped with a convection oven for temperature control. All tests were performed at 150 °C. Shear rheological properties were measured in oscillatory shear using a 8 mm plate-plate measuring geometry (and 15 mm plate-plate geometry for LDPE and Surlyn™) in counter-oscillation separate motor-transducer configuration. The angular frequency was varied from 0.01 to 600 rad s^{-1} at shear strain amplitudes adjusted between 0.03-0.3 % to contain the measurements within the linear viscoelastic regime. Oscillatory shear measurements were performed in a nitrogen atmosphere. The extensional rheological properties were measured using an extensional fixture for rotational rheometry in separate motor-transduced configuration. Thus, the transient uniaxial extensional viscosity, $\eta_E^+(t,\dot{\varepsilon})$, was recorded at four Hencky strain rates,[24] $\dot{\varepsilon} = 10^{-2}, 10^{-1}, 10^{0}, 10^{1}$ s^{-1} at 150 °C, where the extensional viscosity is defined at steady state as $\eta_E(\dot{\varepsilon}) = \lim_{t\to\infty} \eta_E^+(t,\dot{\varepsilon})$.

Thermal conductivity measurements: The thermal conductivity was measured with a TPS 2500 S instrument from Hot Disk. A 7854 Kapton sensor was sandwiched between two 4.6-mm-thick specimen films with a diameter of 3.0 mm, fixed between two steel blocks. During each measurement, 4 mW of heating power was supplied over 2 s, resulting in a probing depth of about 2 mm.

DC conductivity measurements: The test cell consisted of a three-electrode setup that was placed in an oven at 70 C and connected to a high-voltage power supply (Keithley 2290). The high-voltage electrode had a diameter of 60 mm; a measuring electrode with a diameter of D = 28 or 59 mm was used, as indicated. A DC voltage of V = 4.2 to 4.8 kV was applied across L = 0.14 to 0.16 mm thick specimen films for about 18 h, yielding an electric field of 30 kV mm-1, and then the voltage was switched-off for about 6 h. The same voltage was subsequently reapplied for another 18 h. The DC conductivity was calculated based on the charging currents obtained at the end of the second 18 h period. The volume leakage current was recorded with a Keithley 6517B electrometer, and dynamically averaged.

Materials

Ionomers P1-4a,b were synthesized by free radical polymerization of ethylene in the presence of the IPCs M1-4 (see Table 1 and Supporting Information for details). LDPE with a melt flow rate (MFR) of 0.85 g / 10 min (190 ºC; 2.16 kg) and density of 0.921 g cm^{-3} was obtained from SABIC. An ethylene-methacrylic acid ionomer neutralized with NaOH Surlyn™ (14.5 wt% of MAA and 2.02 wt% of Na^+) was obtained from Dow. Unless otherwise specified, solvents and chemicals used for the synthesis of the IPC M1-4 and all the ionomers were purchased from Sigma Aldrich and used as received. All solvents employed were laboratory grade and used as received.

Synthesis

Synthesis of M1.

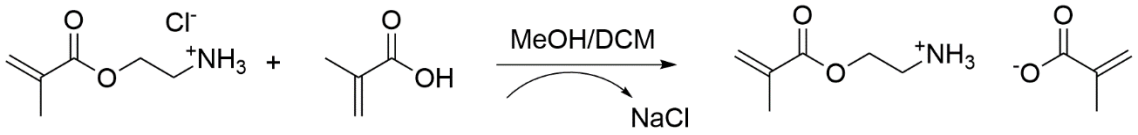

2-(methacryloyloxy)-ethylethanamonium chloride (79.5 g,1eq.) was dissolved in DCM (40 mL) and few drops of MeOH (till dissolution), then sodium methacrylate (52 g, 1eq.) dissolved in MeOH was added to the mixture. During the reaction proceeding, the formation and precipitation of sodium chloride is visible. The mixture was stirred at 0°C and after 30 minutes sodium chloride was removed by filtration. The product was collected after the evaporation of the solvent.

The formation of the product was confirmed *via* NMR.

^{1}H NMR (400 MHz, $CDCl_3$, δ): 1.87 (3H, s), 1.92 (3H, s), 3.11 (2H, t, J= 5.4 Hz), 4.28 (2H, t, J = 5.4 Hz), 5.38 (1H, m), 5.57 (1H, m), 5.92 (1H, m), 6.15 (1H, m).

^{13}C NMR (101 MHz, $CDCl_3$, δ): 18.09; 18.53; 42.37; 61.41; 120.20; 124.67; 138.24; 139.51; 169.58; 172.24.

Synthesis of M2.

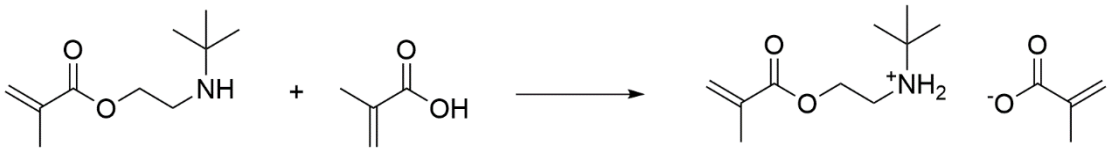

Methacrylic acid (40.5 mL, 0.48 mol) was dropped into 2-(tert-buthylamino)ethyl methacrylate (81.5 mL, 0.48 mol) in a 2- neck flask equipped with an ice bath and a mechanical stirrer. The mixture was stirred at 0°C and after 30 minutes a gel was formed. The formation of the product was confirmed *via* NMR.

^{1}H NMR (400 MHz, DMSO-d_6, δ): 1.05 (9H, s), 1.83 (3H, s), 1.89 (3H, s), 2.79 (2H, t, J= 5.8 Hz), 4.10 (2H, t, J= 5.8 Hz), 5.50 (1H, m), 5.57 (1H, m), 5.91 (1H, m), 6.05 (1H, m).

^{13}C NMR (101 MHz, DMSO-d_6, δ): 17.91; 19.94; 28.81; 41.04; 50.08; 65.55; 123.29; 125.39; 137.46; 139.90; 167.02; 169.28.

Synthesis of M3.

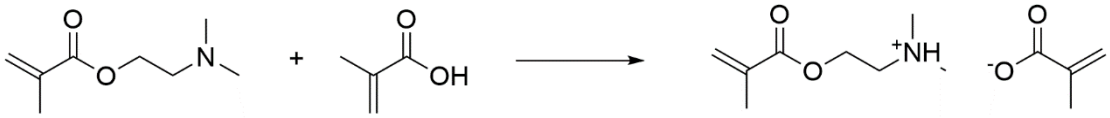

Methacrylic acid (40.5 mL, 0.48 mol) was dropped into 2-(dimethylamino)ethyl methacrylate (81 mL, 0.48 mol) in a 2- neck flask equipped with an ice bath and a mechanical stirrer. The mixture was stirred at 0°C and after 30 minutes a gel was formed. The formation of the product was confirmed *via* NMR.

^{1}H NMR (400 MHz, $CDCl_3$, δ) 1.94 (6H, m), 2.45 (6H, s), 2.86 (2H, t, J= 5.6 Hz), 4.36 (2H, td, J = 5.6, 1.6 Hz), 5.52 (1H, m), 5.58 (1H, m), 6.07 (1H, m), 6.13 (1H, m), 7.05 (1H, bs).

^{13}C NMR (101 MHz, $CDCl_3$, δ): 18.37; 18.69; 44.09; 56.36; 60.88; 124.44; 126.33; 135.90; 138.22; 167.15; 171.96.

Synthesis of M4.

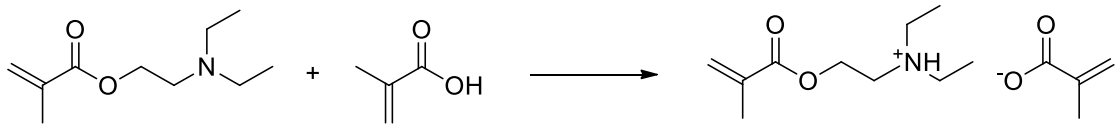

Methacrylic acid (40.5 mL, 0.48 mol) was dropped into 2-(diethylamino)ethyl methacrylate (88.9 mL, 0.48 mol) in a 2- neck flask equipped with an ice bath and a mechanical stirrer. The mixture was stirred at 0°C and after thirty minutes a gel was formed. The formation of the product was confirmed *via* NMR.

^{1}H NMR (400 MHz, $CDCl_3$,δ) 1.17 (6H, t, J= 7.3 Hz), 1.97 (6H, m), 2.86 (2H, q, J= 7.3 Hz), 3.04 (2H, t, J = 6.7 Hz), 4.39 (2H, t, J = 6.7 Hz), 5.54 (1H, m), 5.60 (1H, m), 6.13 (2H, m), 9.00 (1H, bs).

^{13}C NMR (101 MHz, $CDCl_3$, δ): 10.17; 18.28; 18.50; 46.63; 49.62; 61.24; 124.81; 125.96; 136.32; 137.97; 167.15; 171.97.

Synthesis of ionomers *via* radical polymerization.

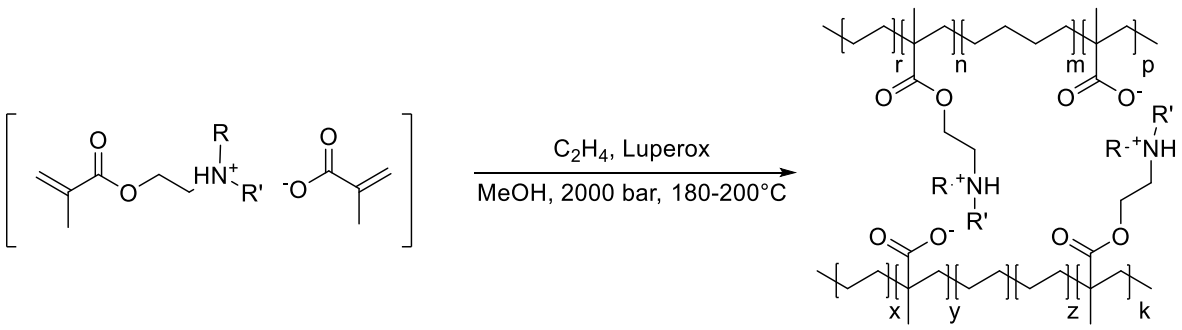

The ionomers were synthesized through a copolymerization between ethylene and the ionomeric monomers according to the following general procedure: the polymerization was carried out in an autoclave reactor by using a pressure of 2000 bars with an impeller velocity fixed at 1540 rpm, at a temperature of 180 or 200 °C for 30 minutes. Before being injected with high pressure ethylene, the IPCs (1 eq. of ethylene for 0.05 or 0.1 eq of IPC) were dissolved in methanol (50 wt%) and Luperox®11M75 (1.5 g/L), dissolved in heptane, was added as initiator. The polymers were recovered from the bottom of the autoclave directly to a recuperation vessel through a let-down valve. Two recuperation vessels were used: the first one was used when stabilizing the conditions and then switched to the 2nd recuperation vessel once the polymerization conditions were steady for collecting the copolymer. The ionomer was recovered in a fine powder form. Elemental analysis (EA) was used to determine the composition of the copolymer through nitrogen quantification. The presence of the ionic comonomers in the polymer chains was easily confirmed through ^{1}H NMR, monitoring the presence of the diagnostic peaks nearby the amino and ester groups (Figures S8-S11). The specific conditions and quantities of IPC are specified in Table 1.

P1.

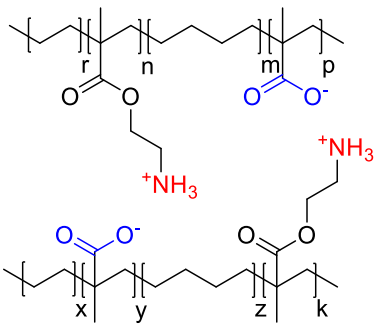

^{1}H NMR (500 MHz, TCE-d_2, 120°C, δ) from 0.65 to 1.80 (polymer chain, m), 3.39 (ethane protons nearby amino group, m), 3.67 (ethane protons nearby ester group, m)

EA: 4.5 wt% of ion pair comonomer calculated by the content of nitrogen (C 86.69%; H 13.01%; N 0.30%).

P2

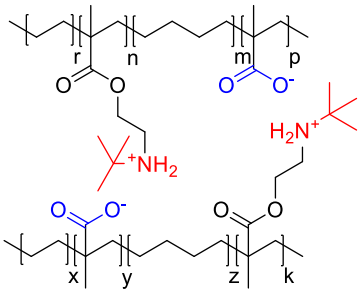

P2a. ^{1}H NMR (500 MHz, TCE, 120°C, δ) from 0.75 to 1.93 (polymer chain, m), 3.16 (ethane protons nearby amino group, m), 4.54 (ethane protons nearby ester group, m)

EA: 3.1 wt% of ion pair comonomer calculated by the content of nitrogen (C, 85.58; H, 14.45; N, 0.16).

P2b. ^{1}H NMR (500 MHz, TCE, 120°C, δ) from 0.75 to 1.90 (polymer chain, m), 3.11 (ethane protons nearby amino group, m), 4.46 (ethane protons nearby ester group, m)

EA: 2.9 wt% of ion pair comonomer calculated by the content of nitrogen (C, 85.39; H, 14.44; N, 0.15)

P3

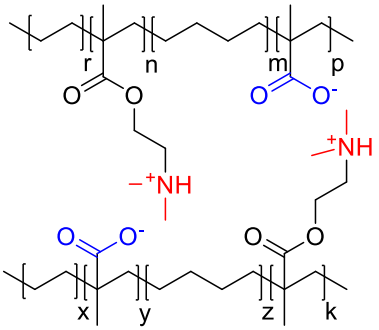

P3a. ^{1}H NMR (500 MHz, TCE, 120°C, δ) from 0.75 to 1.72 (polymer chain, m), 2.58 (methyl groups bonded to the nitrogen, bs), 2.89 (ethane protons nearby amino group, m), 4.35 (ethane protons nearby ester group, m)

EA: 2.9 wt% of ion pair comonomer calculated by the content of nitrogen (C, 85.42; H, 14.40; N, 0.17).

P3b. ^{1}H NMR (500 MHz, TCE, 120°C, δ) from 0.75 to 1.90 (polymer chain, m), 2.51 (methyl groups bonded to the nitrogen, bs), 2.87 (ethane protons nearby amino group, m), 4.35 (ethane protons nearby ester group, m)

EA: 2.8 wt% of ion pair comonomer calculated by the content of nitrogen (C, 85.43; H, 14.42; N, 0.16).

P4

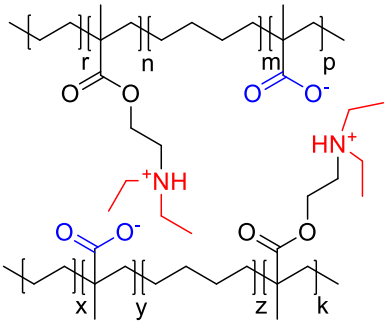

P4a. ^{1}H NMR (500 MHz, TCE, 120°C, δ) from 0.75 to 1.90 (polymer chain, m), 3.07 (ethane protons nearby to the nitrogen, m), 3.22 (ethane protons nearby amino group, m), 4.37 (ethane protons nearby ester group, m)

EA: 2.9 wt% of ion pair comonomer calculated by the content of nitrogen (C, 85.42; H, 14.42; N, 0.15).

P4b. ^{1}H NMR (500 MHz, TCE, 120°C, δ) from 0.75 to 1.90 (polymer chain, m), 3.01 (ethane protons nearby to the nitrogen, bs), 3.12 (ethane protons nearby amino group, m), 4.48 (ethane protons nearby ester group, m)

EA: 2.9 wt% of ion pair comonomer calculated by the content of nitrogen (C, 85.42; H, 14.44; N, 0.15).

Table S1. Degree of conversion of the monomers M1-M4 to the desired polymers P1-P4.

Polymers	**Pressure** (bar)	**Temperature** (°C)	**Conversion** (%)
P1a	2000	180	4.07
P1b	2000	200	1.74
P2a	2000	180	7.31
P2b	2000	200	7.54
P3a	2000	180	6.88
P3b	2000	200	5.61
P4a	2000	180	7.77
P4b	2000	200	7.51

2.4 Supporting information

^{1}H NMR of the synthesized comonomers

M1:

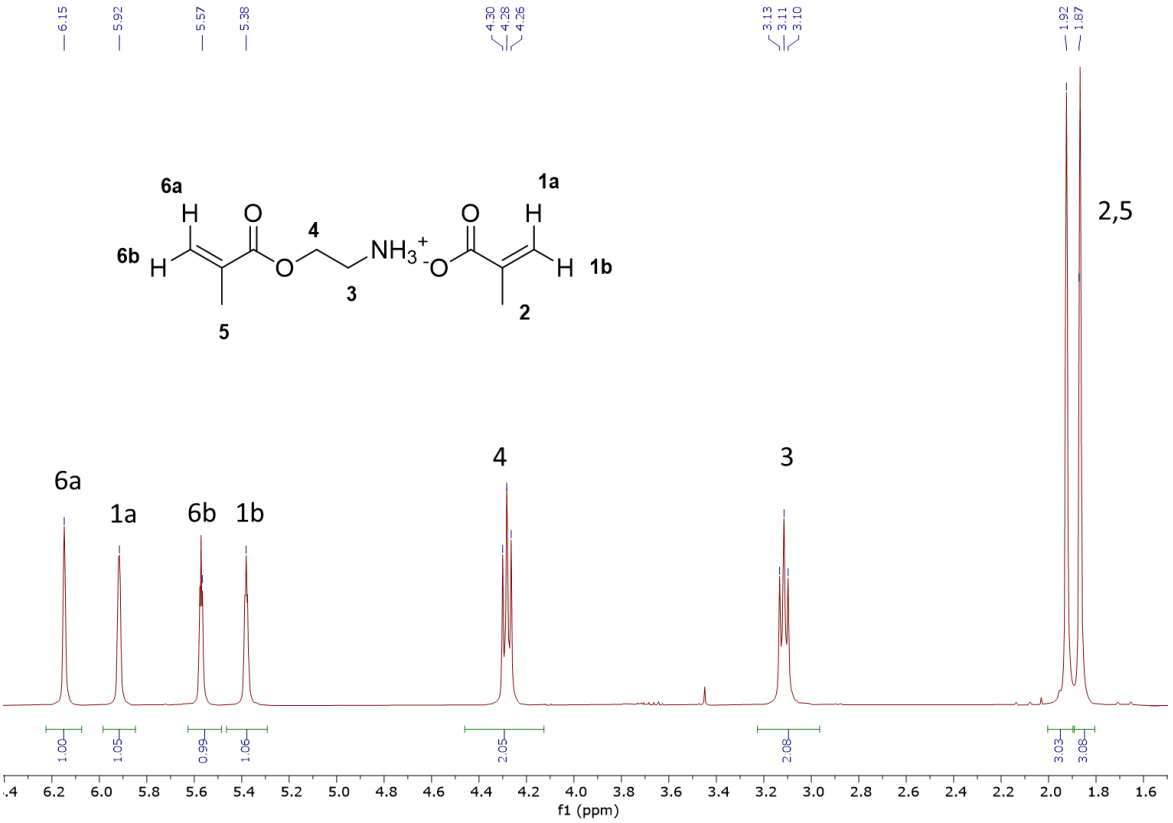

Figure S1. ^{1}H NMR (400 MHz, r.t.) of M1 in $CDCl_3$.

M2:

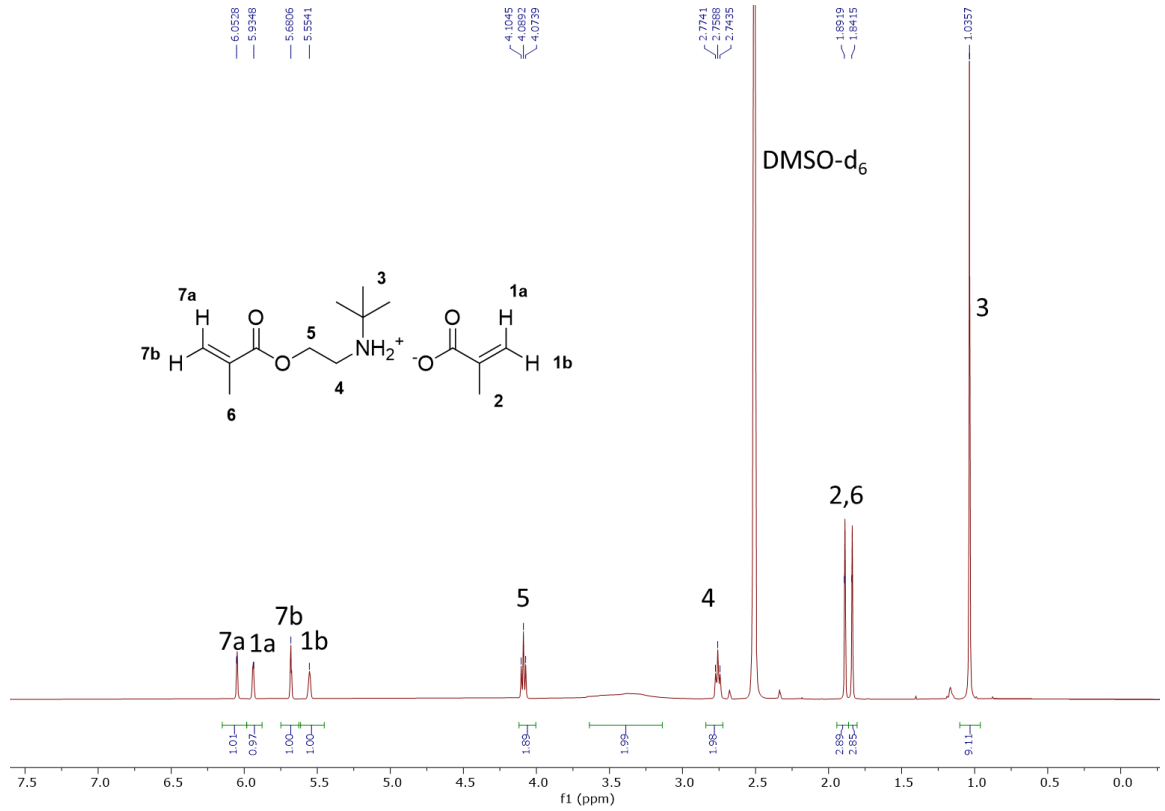

Figure S2. ^{1}H NMR (400MHz, r.t.) of M2 in DMSO-d$_6$.

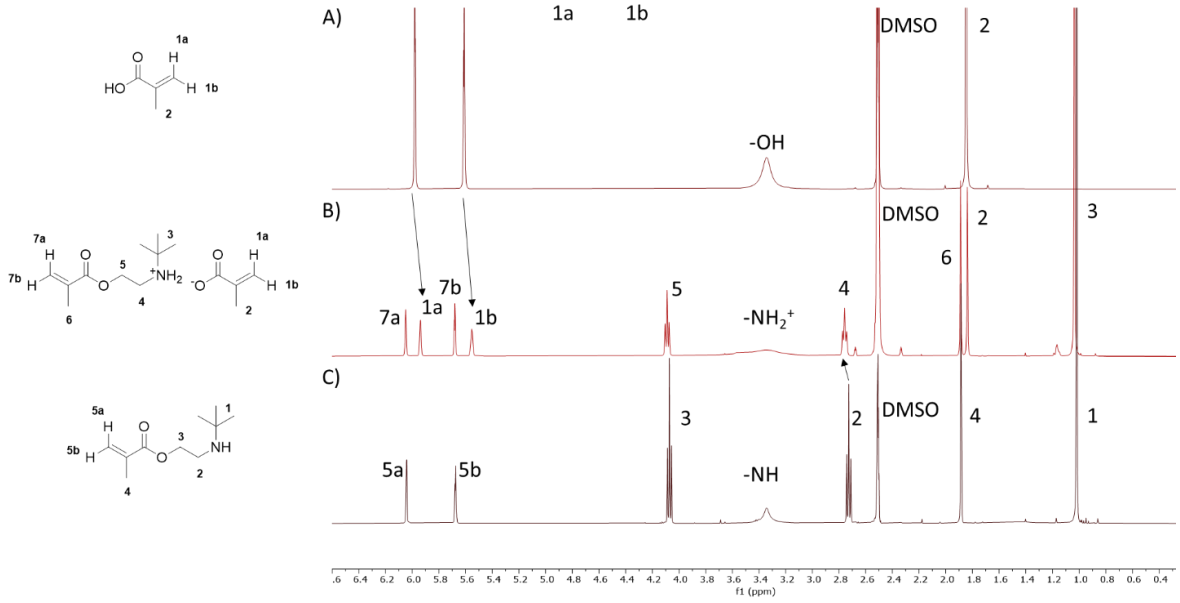

Figure S3. Comparison between ^{1}H NMR (400 MHz, r.t.) of (A) Methacrylic acid, (B) M2, (C) and 2-(*tert*-butylamino)ethyl methacrylate in DMSO-d$_6$.

M3:

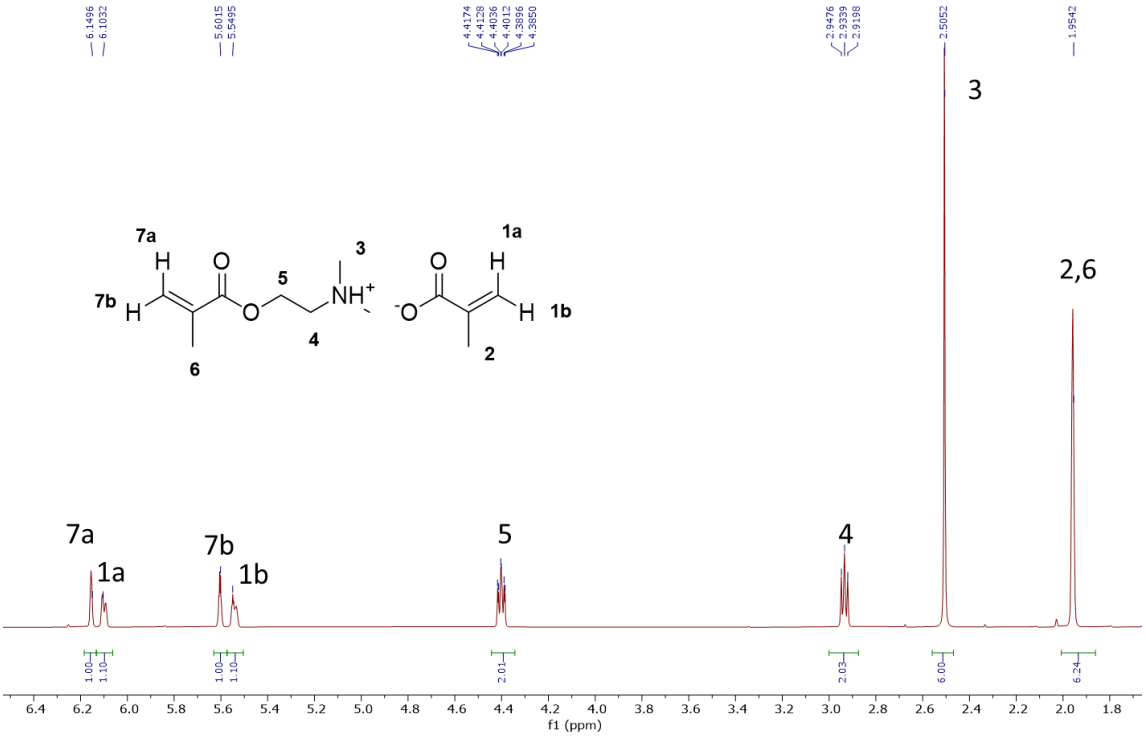

Figure S4. ^{1}H NMR (400MHz, r.t.) of M3 in $CDCl_3$.

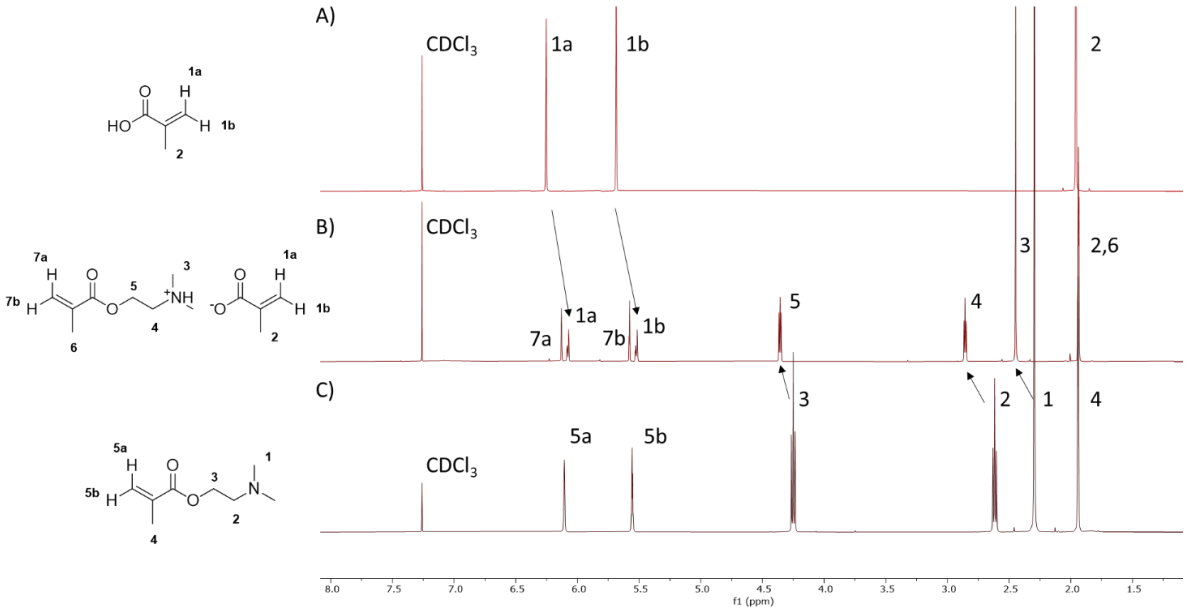

Figure S5. Comparison between ^{1}H-NMR (400MHz, r.t.) of (A) Methacrylic acid, (B) M3, (C) and 2-(dimethylamino)ethyl methacrylate in $CDCl_3$.

M4:

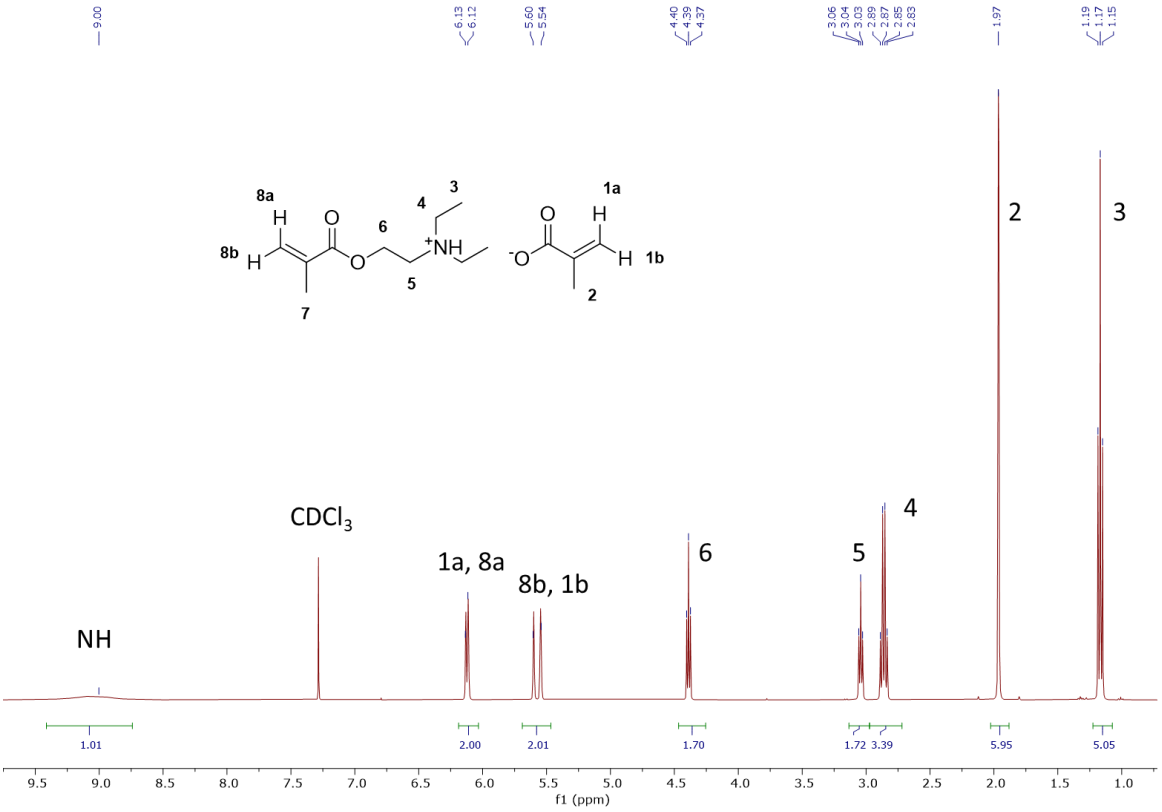

Figure S6. ^{1}H NMR (400MHz, r.t.) of M4 in $CDCl_3$.

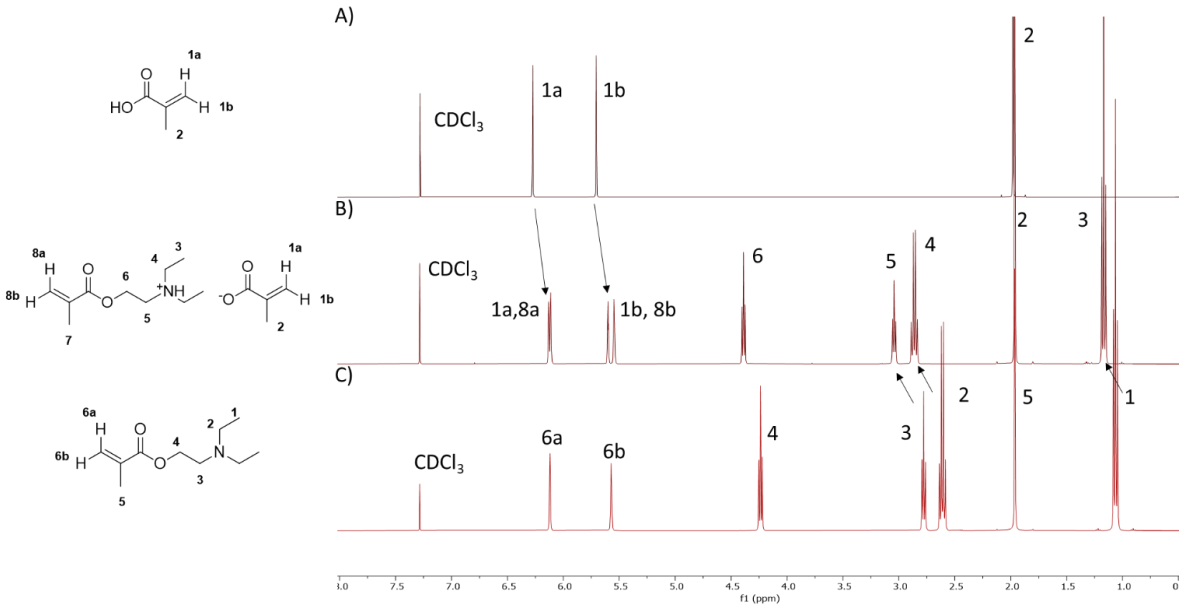

Figure S7. Comparison between ^{1}H NMR (400MHz, r.t.) of (A) Methacrylic acid, (B) M4, (C) and 2-(diethylamino)ethyl methacrylate in $CDCl_3$.

^{1}H NMR of the synthesized ionomers

P1-180°C

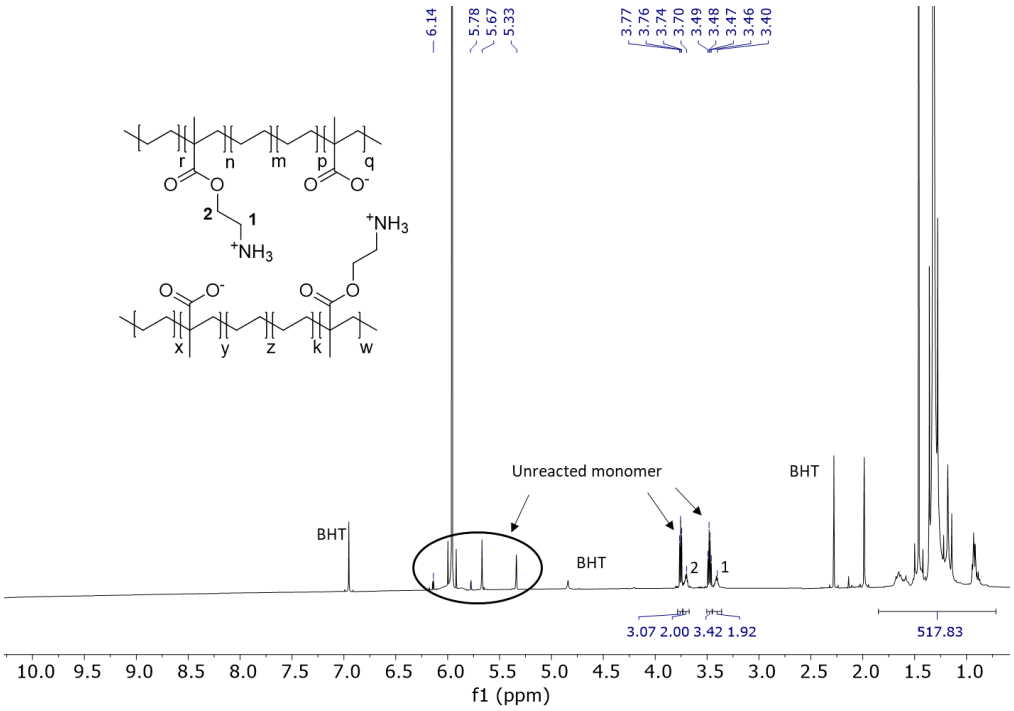

Figure S8. ^{1}H NMR (500 MHz, 120°C) of P1-180°C in TCE-d_2 (10 mg of BHT were added in the NMR tube).

P1-200°C

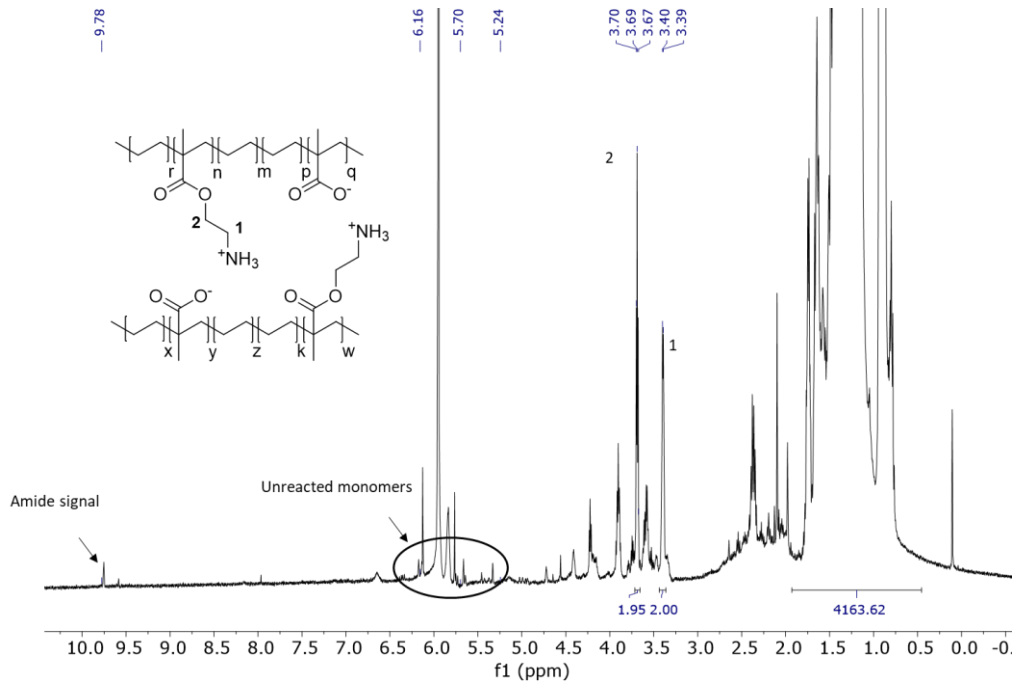

Figure S9. ^{1}H NMR (500 MHz, 120°C) of P1-200°C in TCE-d_2.

P2a

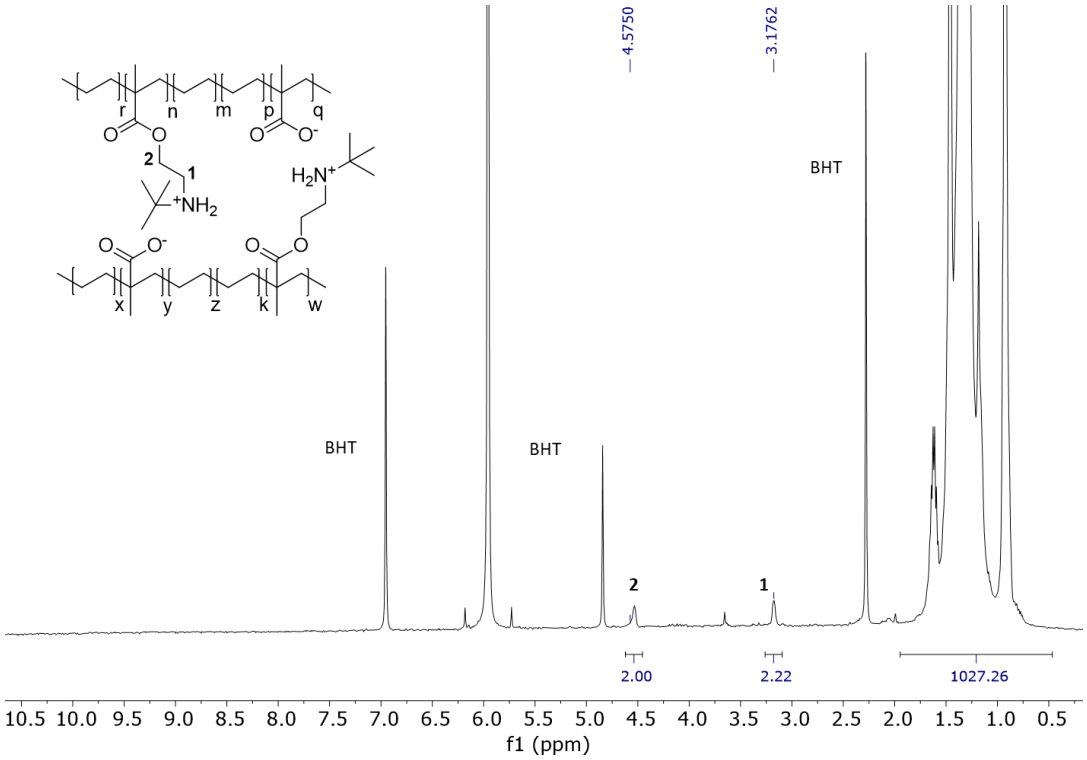

Figure S10. ^{1}H NMR (500 MHz, 120°C) of P2a in TCE-d_2 (10 mg of BHT were added in the NMR tube).

P2b

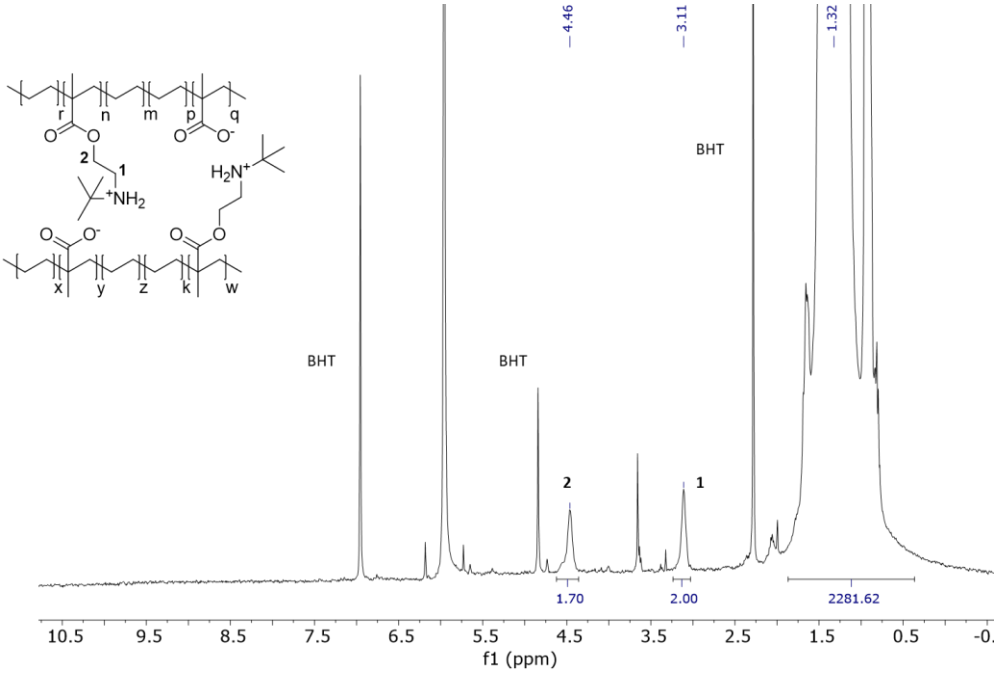

Figure S11. ^{1}H NMR (500 MHz, 120°C) of P2b in TCE-d_2 (10 mg of BHT were added in the NMR tube).

P3a

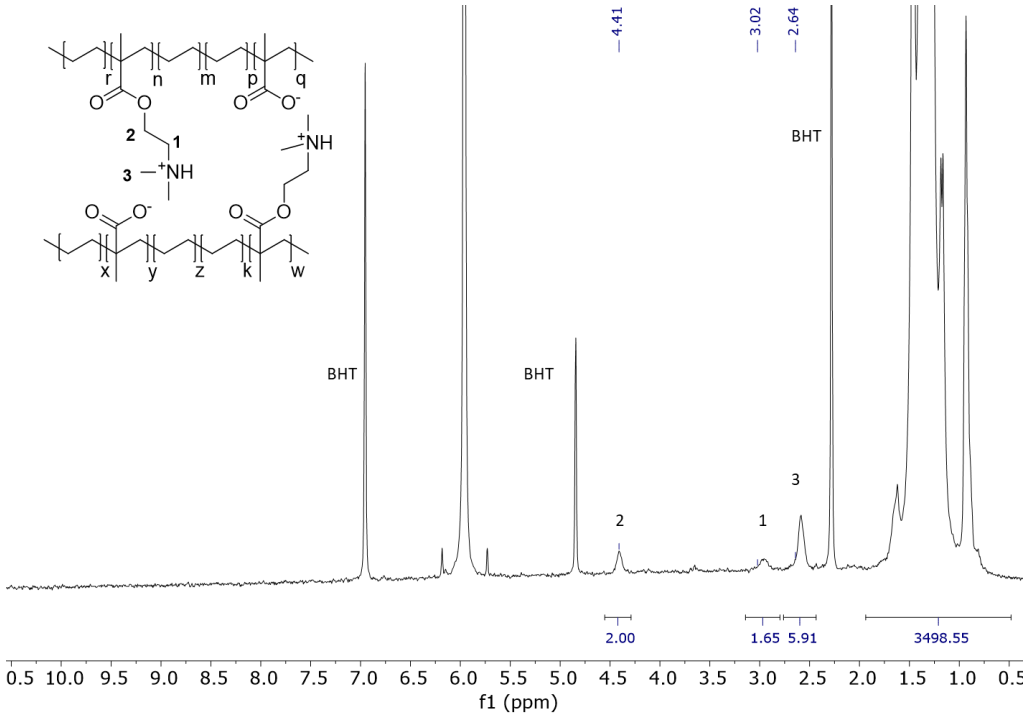

Figure S12. ^{1}H NMR (500 MHz, 120°C) of P3a in TCE-d_2 (10 mg of BHT were added in the NMR tube).

P3b

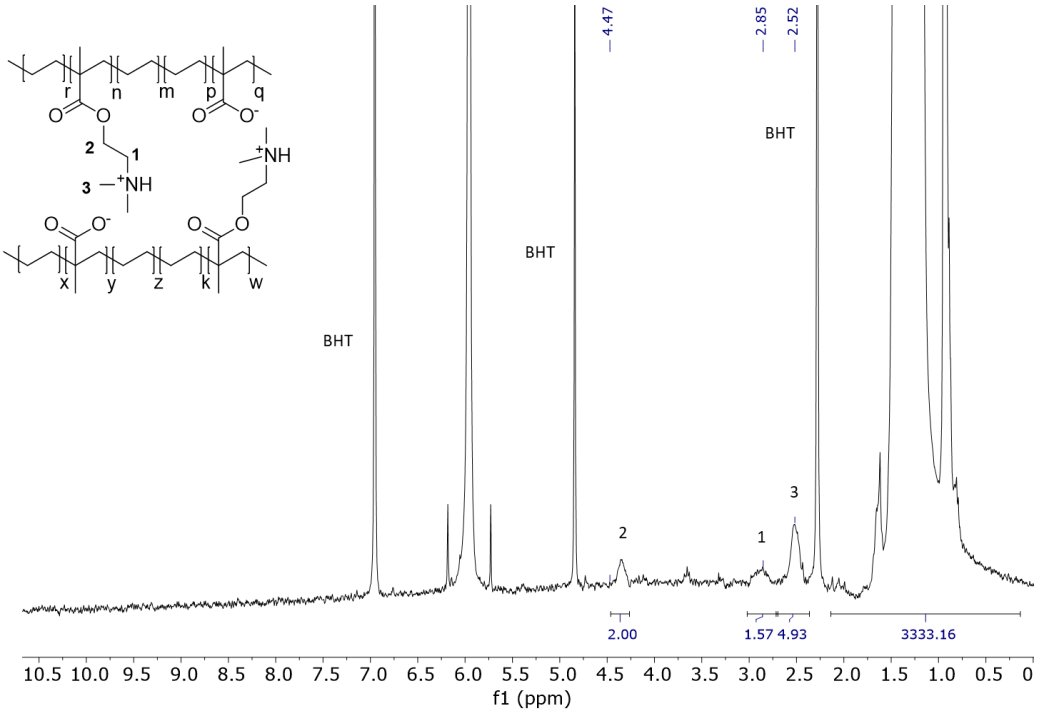

Figure S13. ^{1}H NMR (500 MHz, 120°C) of P3b in TCE-d_2 (10 mg of BHT were added in the NMR tube).

P4a

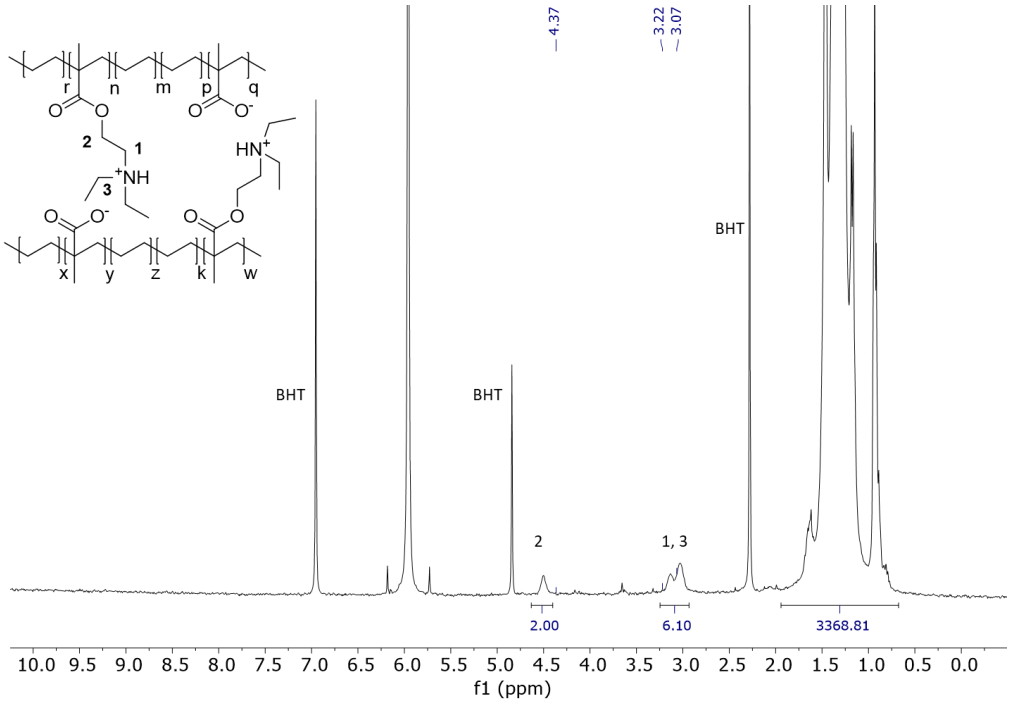

Figure S14. ^{1}H NMR (500 MHz, 120°C) of P4a in TCE-d_2 (10 mg of BHT were added in the NMR tube).

P4b

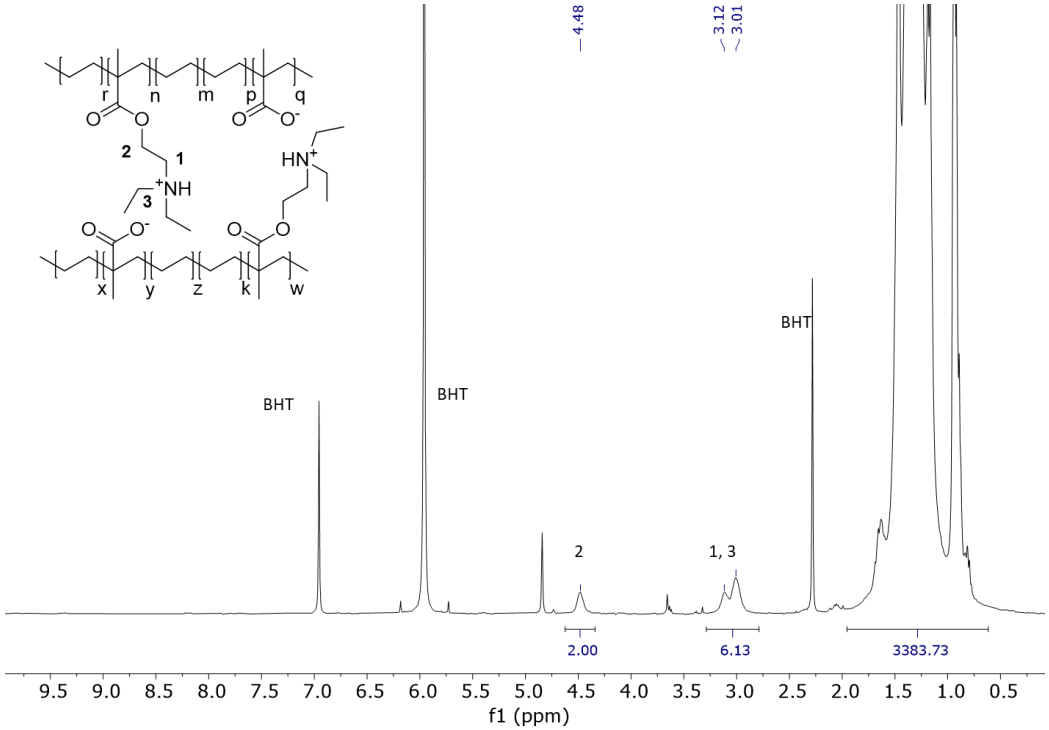

Figure S15. ^{1}H NMR (500 MHz, 120°C) of P4b in TCE-d_2 (10 mg of BHT were added in the NMR tube).

FT-IR analyses

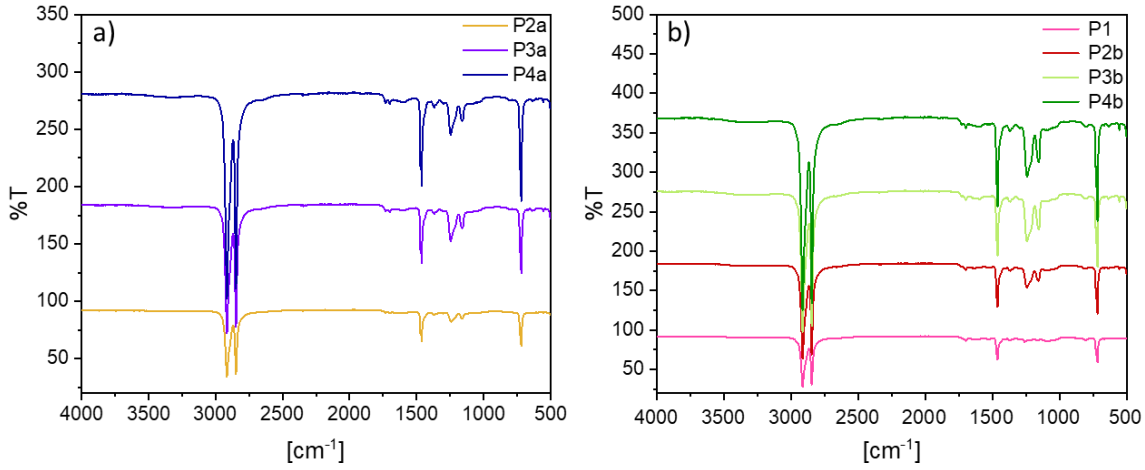

Figure S16. FT.IR spectra of ionomers a) P2a, P3a and P4a b) P1, P2b, P3b, P4b.

DSC analyses

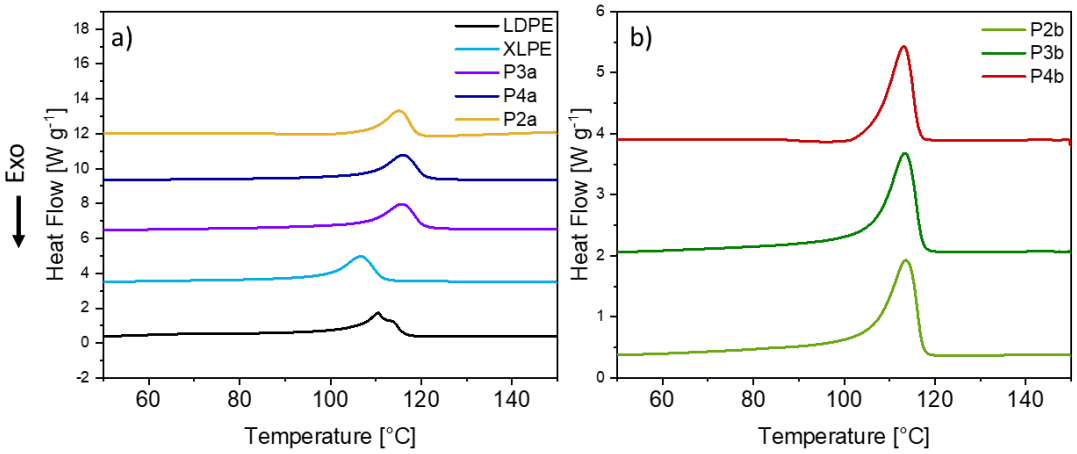

Figure S17. Heating curves (2nd heating) of ionomers a) P2a, P3a and P4a, and as references LDPE and XLPE and b) P2b, P3b, P4b.

TGA Analyses

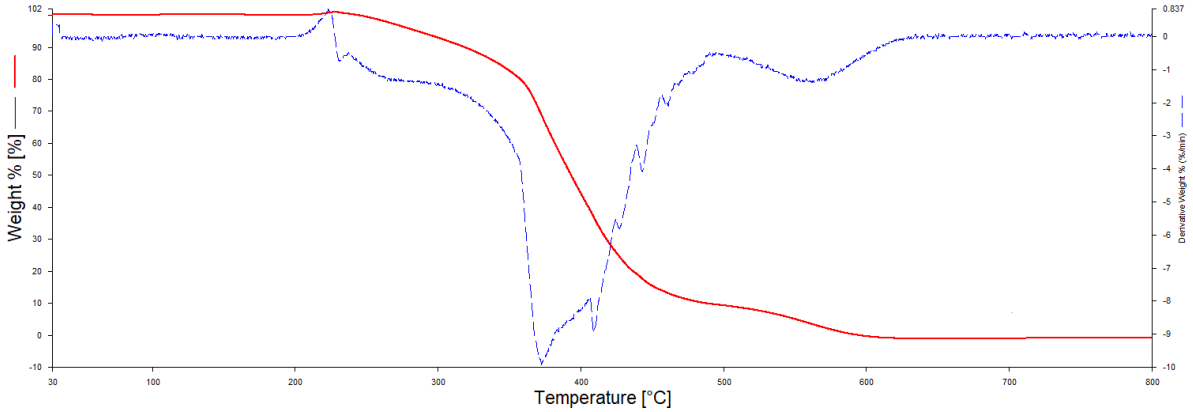

Figure S18. Thermogram of P2a.

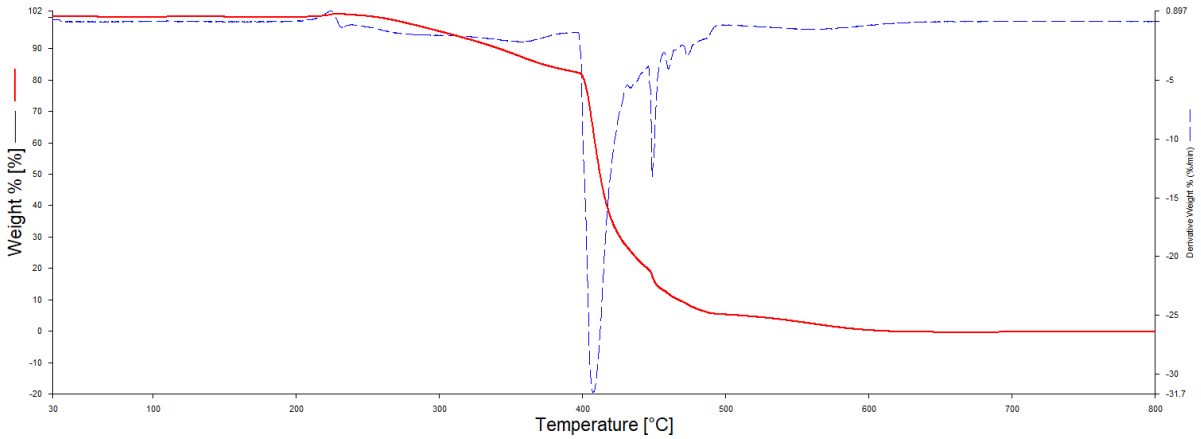

Figure S19. Thermogram of P2b.

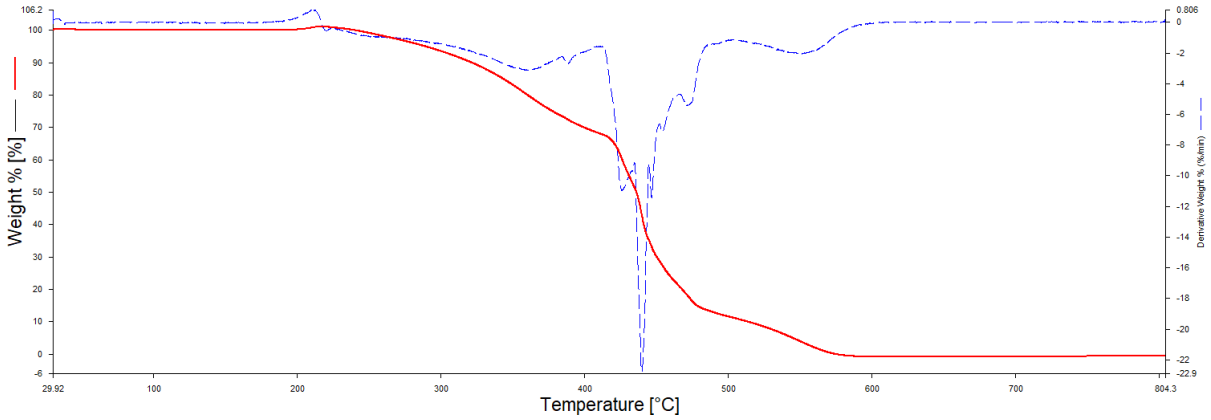

Figure S20. Thermogram of P3a.

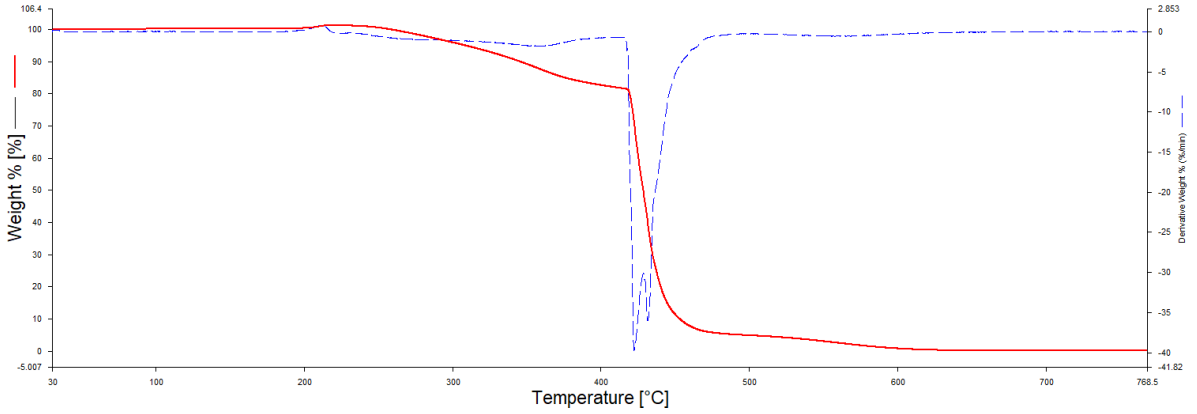

Figure S21. Thermogram of P3b.

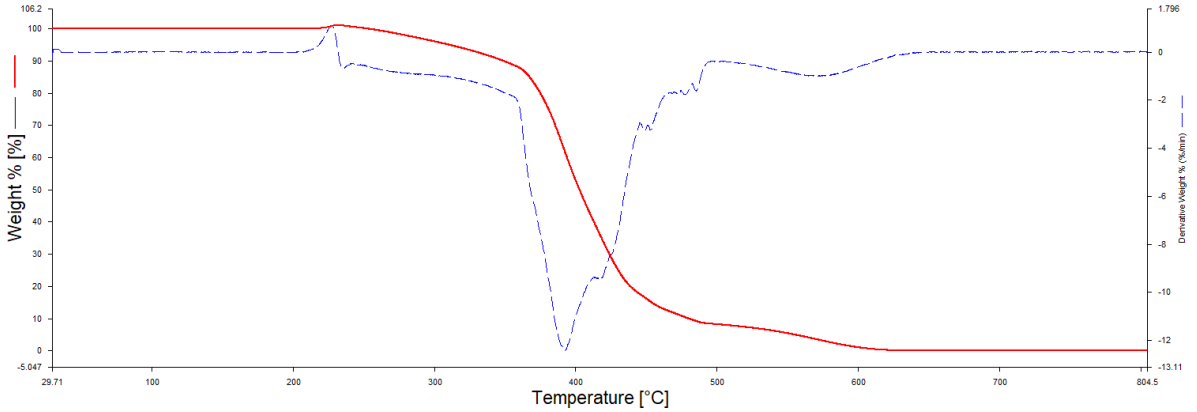

Figure S22. Thermogram of P4a.

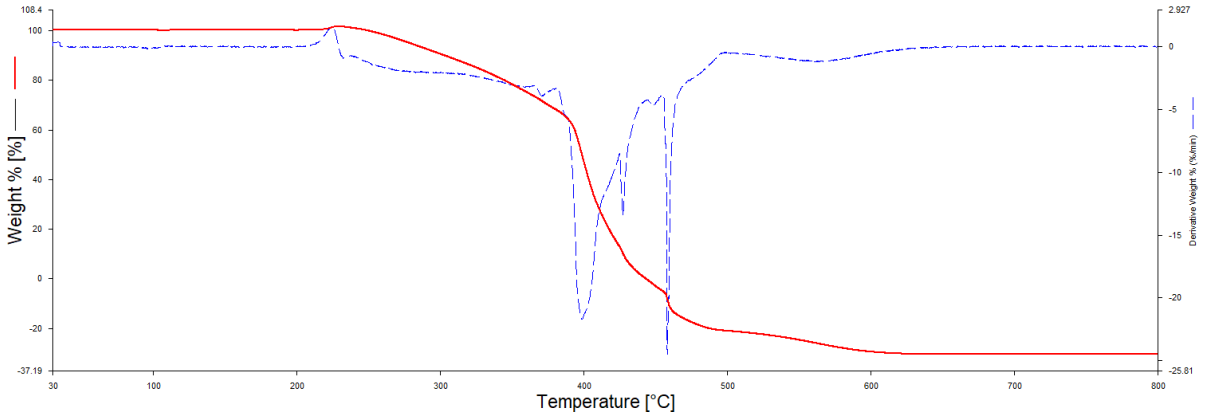

Figure S23. Thermogram of P4b

Rheology data

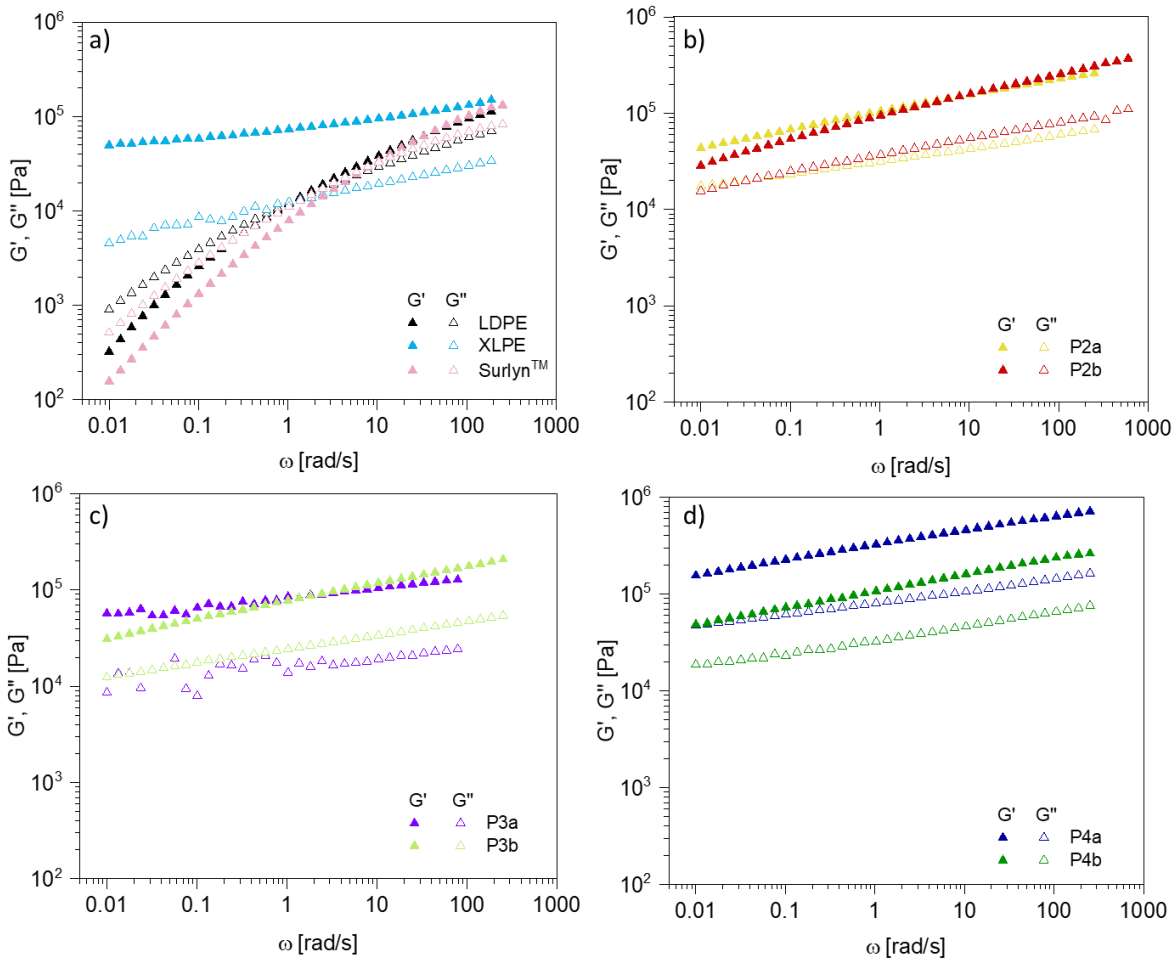

Figure S24. Dynamic moduli, storage *G'* and loss *G''*, functions from oscillatory shear tests for a) the reference materials, b) P2a-b, c) P3a-b, d) P4a-b.

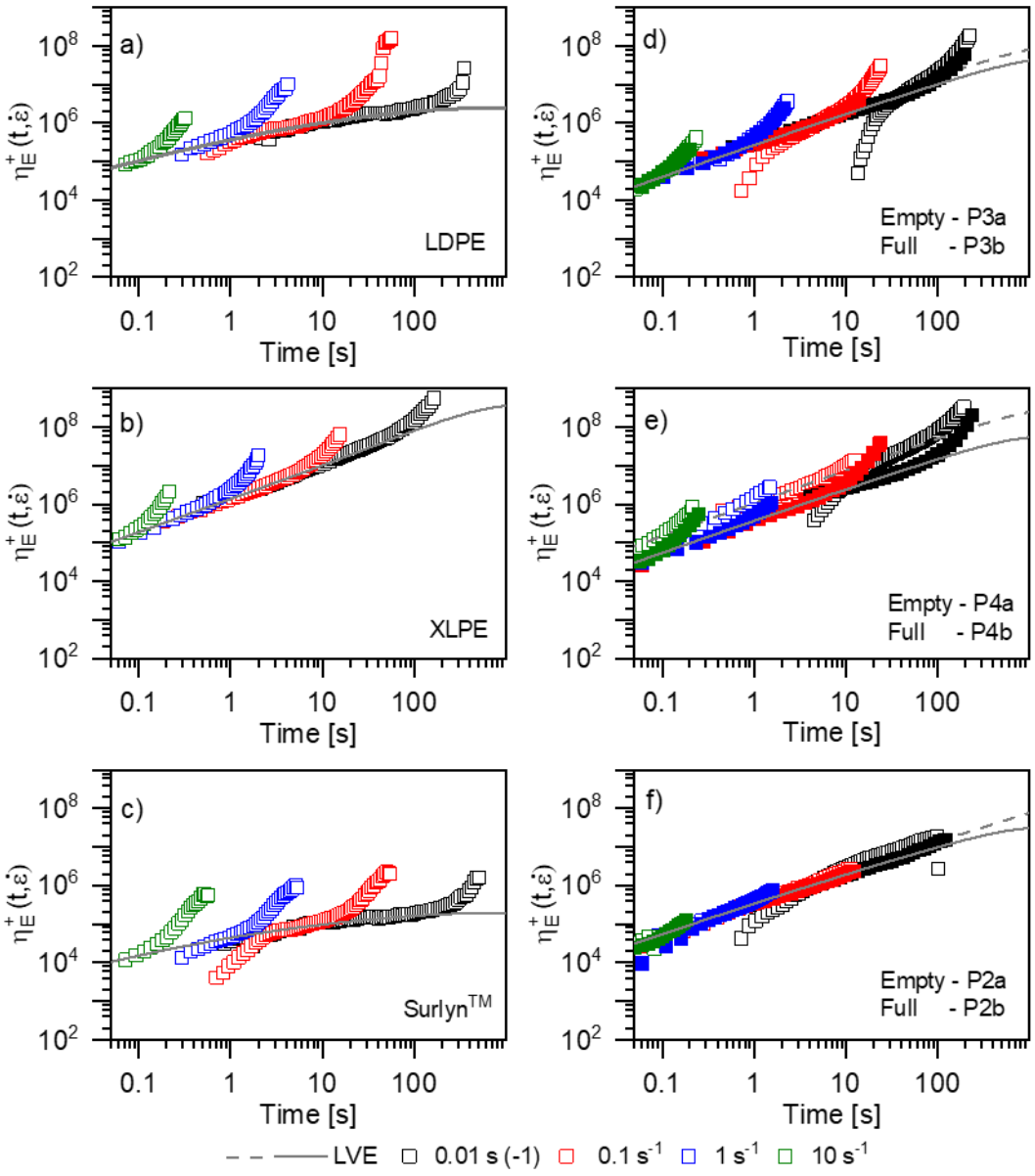

Figure S25. Transient extensional measurements at 150 °C for a) LDPE b) XLPE, c) Surlyn™ , d) P3a-b, e) P4a-b, f) P2a-b. The dotted and continuous lines show the linear viscoelastic envelope (LVE), η^+_{LVE} .

M_c and N_c calculations

$M_c = \rho RT/G$

ρ (LDPE) at 150°C = 790 [Kg/m^3]

R = 8.314 [J/(mol·K)]

T = 423.15 [K]

G at 150°C = E'/3 [J/m^3]

As an example, we show the calculations of P2a:

$M_c = \frac{3 \cdot 8.314 \cdot 423.15 \cdot 790}{770000} = 10.83$ [Kg/mol]

$N_c = \frac{14}{10.83} = 1.29$

IPC content per 1000 CH_2

As an example, we show the calculations of P1:

IPC content per 1000 CH_2: $\frac{\text{IPC N wt\%/ IPC Mw}}{PE\ wt\%/Mw\ of\ 1000\ CH2} = \frac{4.5/215.25}{95.5/14000} = 3.1$

Conversion wt% to mol% calculations

IPC mol% content can be express like:

mol%= (1 IPC/nCH_2) *100

nCH_2= M_w (PE)/M_w (CH_2)

Mw (PE) is obtained by the equation:

wt%= [Mw (IPC)/ (Mw (IPC) + Mw (PE))] *100

Lamellar thickness

Table S2. Lamellar thickness values of the polymers P1-P4.

Ionomer	Lamellar thickness l_c (nm)
P1	7.9
P2a	8.4
P2b	8.1
P3a	8.4
P3b	8.1
P4a	8.4
P4b	8.1

Thermal conductivity measurement at room temperature

Table S3. Thermal conductivity, thermal diffusivity, thermal effusivity and specific heat of ionomers P2-P4 and LDPE, XLPE and Surlyn as references.

Compound	Thermal Conductivity ($W\ m^{-1}K^{-1}$)	Thermal Diffusivity ($mm^2\ s^{-1}$)	Thermal Effusivity ($W\ s^{1/2}\ m^{-2}K^{-1}$)	Specific Heat ($M\ J\ m^{-3}K^{-1}$)
LDPE	0.4050	0.4258	620.7	0.9515
XLPE	0.3612	0.3316	627.7	1.091
Surlyn™	0.2939	0.3489	497.9	0.8440
P2a	0.3850	0.3743	629.9	1.031
P2b	0.3893	0.4017	614.4	0.9700
P3a	0.3693	0.3932	588.8	0.9390
P3b	0.3539	0.3771	577.6	0.9437
P4a	0.3938	0.3830	636.6	1.029
P4b	0.3654	1.0702	353.5	0.3421

References

[1] G. C. Montanari, P. H. F. Morshuis, M. Zhou, G. C. Stevens, A. S. Vaughan, Z. Han, D. Li, *High Volt.* **2018**, *3*, 90.
[2] G. Mazzanti, M. Marzinotto, *Extruded Cables for High-Voltage Direct-Current Transmission*, Wiley, New Jersey 2013.
[3] T. H. A. Smedberg, B. Gustafsson, *Polymer* **1997**, *38*, 4127.
[4] T. Andrews, R. N. Hampton, A. Smedberg, D. Wald, V. Waschk, W. Weissenberg, *IEEE Electr. Insul. Mag.* **2006**, *22*, 5.
[5] S. Kumara, X. D. Xu, T. Hammarström, Y. W. Ouyang, A. M. Pourrahimi, C. Müller, Y. V. Serdyuk, *Energies* **2020**, *13*, 1434.
[6] T. Andritsch, A. Vaughan, G. C. Stevens, *IEEE Electr. Insul. Mag.* **2017**, *33*, 27.
[7] M. Mauri, A. Peterson, A. Senol, K. Elamin, A. Gitsas, T. Hjertberg, A. Matic, T. Gkourmpis, O. Prieto, C. Müller, *J. Mater. Chem. C* **2018**, *6*, 11292.
[8] M. Mauri, A. I. Hofmann, D. Gomez-Heincke, S. Kumara, A. M. Pourrahimi, Y. W. Ouyang, P. O. Hagstrand, T. Gkourmpis, X. D. Xu, O. Prieto, C. Müller, *Polym. Int.* **2020**, *69*, 404.
[9] C. D. Green, A. S. Vaughan, G. C. Stevens, A. Pye, S. J. Sutton, T. Geussens, M. J. Fairhurst, *IEEE Trans. Dielectr. Electr. Insul.* **2015**, *22*, 639.
[10] X. Y. Huang, Y. Y. Fan, J. Zhang, P. K. Jiang, *IEEE Trans. Dielectr. Electr. Insul.* **2017**, *24*, 1446.
[11] S. Yu, S. H. Lee, J. A. Han, M. S. Ahn, H. Park, S. W. Han, D. H. Lee, *Polymer* **2020**, *202*, 122674.
[12] Y. W. Ouyang, A. M. Pourrahimi, I. Östergren, M. Mellqvist, J. Anevall, A. Soroudi, A. Lund, X. D. Xu, T. Gkourmpis, P. O. Hagstrand, C. Müller, *High Volt.* **2022**, *7*, 251.
[13] A. M. Pourrahimi, R. T. Olsson, M. S. Hedenqvist, *Adv. Mater.* **2018**, *30*, 1703624.
[14] A. Soroudi, Y. W. Ouyang, F. Nilsson, I. Östergren, X. D. Xu, Z. R. Li, A. M. Pourrahimi, M. Hedenqvist, T. Gkourmpis, P. O. Hagstrand, C. Müller, *Nanoscale* **2022**, *14*, 7927.
[15] Z. J. Wei, H. Y. Liu, L. W. Yu, S. W. Xiao, Y. X. Hou, X. R. Chen, *J. Appl. Polym. Sci.* **2020**, *137*.
[16] A. M. Pourrahimi, S. Kumara, F. Palmieri, L. Y. Yu, A. Lund, T. Hammarström, P. O. Hagstrand, I. G. Scheblykin, D. Fabiani, X. D. Xu, C. Müller, *Adv. Mater.* **2021**, *33*, 2100714.
[17] B. Dang, J. Hu, Y. Zhou, J. L. He, *J. Phys. D Appl. Phys.* **2017**, *50*.
[18] Y. Zhao, H. Mao, T. Zhang, Z. Guo, D. Bai, H. Bai, Q. Zhang, H. Xiu, F. Q, *Ind. Eng. Chem. Res.* **2022**, *61*, 13126.
[19] D. Montarnal, M. Capelot, F. Tournilhac, L. Leibler, *Science* **2011**, *334*, 965.
[20] T. Liu, B. M. Zhao, J. W. Zhang, *Polymer* **2020**, *194*, 122392.
[21] P. I. Nagy, P. W. Erhardt, *J. Phys. Chem. B* **2012**, *116*, 5425.
[22] C. Houriez, V. Vallet, F. Réal, M. Meot-Ner, M. Masella, *J. Chem. Phys.* **2017**, *147*, 161720.
[23] I. V. Fedorova, L. P. Safonova, *J. Phys. Chem. A* **2020**, *124*, 3170.
[24] R. Kádár, M. Abbasi, R. Figuli, M. Rigdahl, M. Wilhelm, *Nanomaterials* **2017**, *7*, 23.

Chapter 3

Two-photon Microscopy as visual tool for polymer compatibilization monitoring: The PE-EVOH case

Part of this work was carried out in collaboration with Prof. Cristina Sissa (University of Parma)

Abstract

In this study, we present two-photon microscopy (2PM) as an original technique to investigate the compatibilization between PE-HEMA and EVOH at the sub-micrometer level, both on the surface and in the bulk. 2PM is a nonlinear fluorescence imaging technique commonly exploited for thick biological tissues analysis. Here, we use 2PM to visualize polymer blending through 3D images of the obtained films. Compatibilization was performed in solution, upon functionalization of PE-HEMA with 1.4% molar of ODIN, a fluorescent molecule able to form multiple hydrogen bonding with EVOH and to act as fluorescent probe. Different blends were synthesized, and the obtained films analyzed by 2PM. For all compositions, it was demonstrated that ODIN is evenly distributed both on the surface and in the bulk. 2PM analysis of the thermally reprocessed specimen revealed that repeated reprocessing allows the reformation of ODIN dimers as the most stable H-bonding array in the solid state, partially reversing the compatibilization.

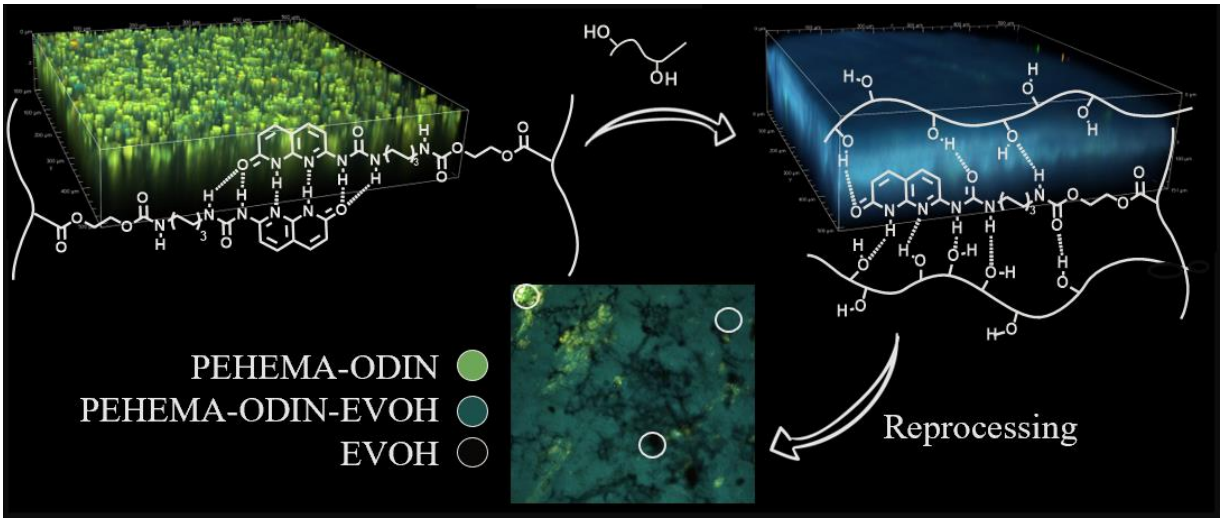

The content of this chapter is partially adapted from:

S.D'Auria, A. Pedrini, I. Ferraboschi, J. Vachon, C. Sissa and R. Pinalli, E. Dalcanale, Soft Matter, 2023, DOI:10.1039/D2SM01577C.

3. Introduction.

Polymer compatibilization is a long-standing issue in polymer science,[1] with relevant technological implications, being polymer blending the most efficient method to produce new polymeric materials having intermediary properties among their components. In most cases, polymers are immiscible because their entropy of mixing is so small that compatibilization relies entirely on the presence of enthalpically favorable intermolecular interactions.

Among the many different approaches used for polymer blending,[2] H-bonding stands out for its ability to boost intermolecular interactions among widely different polymers.[3] In this context, the use of multiple H-bond arrays has showed to be a very efficient way to mix[4],[5] and cross-link[6] polymers.

We recently introduced ODIN (Figure. 1),[7] a sextuple H-bonding array motif, capable of self-dimerizing in its most stable keto tautomer,[8] both in solution and in a polymeric matrix. With respect to the widely used UPy analogue,[9] ODIN features a slightly smaller self-dimerization constant and a higher thermal stability.[7] Furthermore, ODIN is a fluorescent molecule, therefore suitable as probe to test its distribution in a polymer matrix *via* fluorescence imaging. Following this reasoning, we considered using ODIN for the compatibilization of polyethylene (PE) with ethylene vinyl alcohol (EVOH) exploiting its ability to form multiple H-bonds and, at the same time, its fluorescence to investigate the homogeneity of blending. Poly(2-hydroxyethyl) methacrylate (PE-HEMA), the copolymer of ethylene and 2-hydroxyethyl methacrylate,[10] was chosen as PE substrate for ODIN insertion, while commercial EVOH was used as purchased. The pendant hydroxyl groups of HEMA allow for easy grafting of ODIN isocyanate (Figure. 1).[7]

The standard way to prove polymer blending relies on thermal (DSC)[11] and surface morphology (TEM, AFM)[5],[12] measurements. At present, experimental techniques capable to investigate the composition and the formation of homogenous blends in the bulk are based on the combined use of X-ray scattering (WAXS and SAXS) and small-angle neutron scattering (SANS).[13],[14] However, SANS requires the deuteration of one of the components of the blend. In this work, we propose to exploit the advantages of two-photon microscopy (2PM) in the new context of polymeric blends using ODIN both as molecular compatibilizer and as fluorescent probe.

2PM is a powerful tool to reconstruct 3D images of films and retrieve information about the (dis)homogeneity of polymer blends not only on the surface, but also from the bulk. 2PM is a nonlinear fluorescence imaging technique, which is commonly exploited for the imaging of thick biological tissues.[15] In the field of polymer science, only an example of 2PM is reported in the literature, for the morphological characterization of polymeric multiphase samples.[16] The compatibilization of PE-HEMA-ODIN and EVOH through the formation of H bonds represents an ideal system for evaluating the potentialities of the 2PM technique for the characterization of polymer blends. In fact, ODIN can be exploited as a fluorescent probe, and the visual localization of its fluorescence signal within the sample gives direct information about its aggregation form (monomer vs dimer) and distribution in the polymer blend.

3.1 Results and discussion.

3.1.1 Synthesis and characterization of PE-HEMA-ODIN (P1).

1-(7-**o**xo-7,8-**di**hydro-1,8-**n**aphthyridin-2-yl)urea (see ODIN isocyanate, Figure 1A) is a multiple hydrogen bonding motif able to form dimers in the solid state and in solution through a sextuple DDADA H-bonding motif (K_a = 4•10^4 M^{-1} in $CHCl_3$).[7] ODIN has interesting optical properties, presenting in solution an absorbance maximum around 340 nm and a fluorescent emission around 375 nm, when excited at 325 nm.

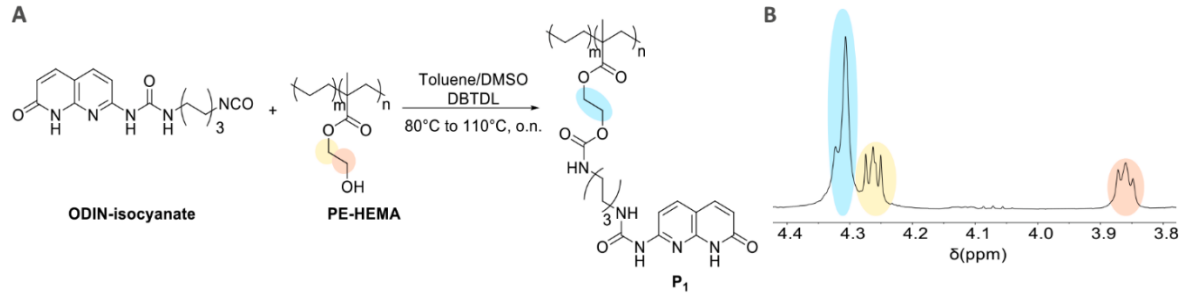

Figure 1. (A) Functionalization of PE-HEMA with ODIN. (B) Selected portion of PE-HEMA-ODIN ^{1}H NMR (80 °C, TCE-d_2, 400 MHz), highlighting the HEMA hydroxyethyl signal region.

The grafting of ODIN onto PE requires the presence of suitable functional groups on the PE. We selected PE-HEMA, a functional polyethylene with pendant hydroxyl groups, since the hydroxyl groups of HEMA allow for easy grafting of the isocyanate functionalized ODIN (Figure 1A). PE-HEMA with a minimal HEMA content of 2.1% molar was chosen, to obtain a polymer as close as possible to pristine PE. The grafting reaction of ODIN onto PE-HEMA was carried out at 110°C in toluene and DMSO for

12 hours, by using dibutyltin dilaurate (DBTDL) as catalyst. Precipitation of the final product **P1** was promoted by the addition of isopropanol to the reaction mixture.

The degree of functionalization in **P1** was investigated by monitoring the intensity of the diagnostic signals of the HEMA methylene protons *via* ^{1}H-NMR (Figures S1-S2). As shown in Figure. 1B, the two unreacted methylene groups of the pristine HEMA are clearly distinguishable at 3.86 and 4.26 ppm (pink and yellow highlighted). The formation of the carbamate bond in **P1** results in a downfield shift of both signals that combined in a single peak around 4.30 ppm (light blue highlighted). From the ratio of these signals (non-functionalized and ODIN-functionalized HEMA) the degree of functionalization was determined in 67% of the OH groups. This functionalization degree was confirmed by elemental analysis by determining the nitrogen content in **P1**, since nitrogen is present only in ODIN. (see experimental section in the ESI). Overall, the ODIN molar content in **P1** is 1.4 mol %.

3.1.2 Preparation of the blends B1, B2 and B3.

Three blends of **P1** and EVOH were prepared in the following weight-to-weight EVOH/**P1** ratio: 7:3, 1:1 and 3:7. Homogeneous solutions of EVOH in DMSO and **P1** in ODCB were mixed at 110°C for three hours as reported in Scheme 1. The blends were recovered by precipitation adding isopropanol to the resulting solution cooled to room temperature.

Using the same conditions, a control batch was prepared by mixing two different solutions of EVOH and unfunctionalized PE-HEMA. As shown in Figure S3A, after addition of isopropanol to the polymer mixture cooled to room temperature, two macroscopically different precipitates were obtained. ATR measurements performed onto the two polymers 1 and 2 (see ESI, Figure S5) revealed that polymer 1 corresponds to PE-HEMA, while polymer 2 is EVOH. As comparison, the picture of blend **B2** is reported in Figure S3B: the resulting precipitate is macroscopically homogeneous.

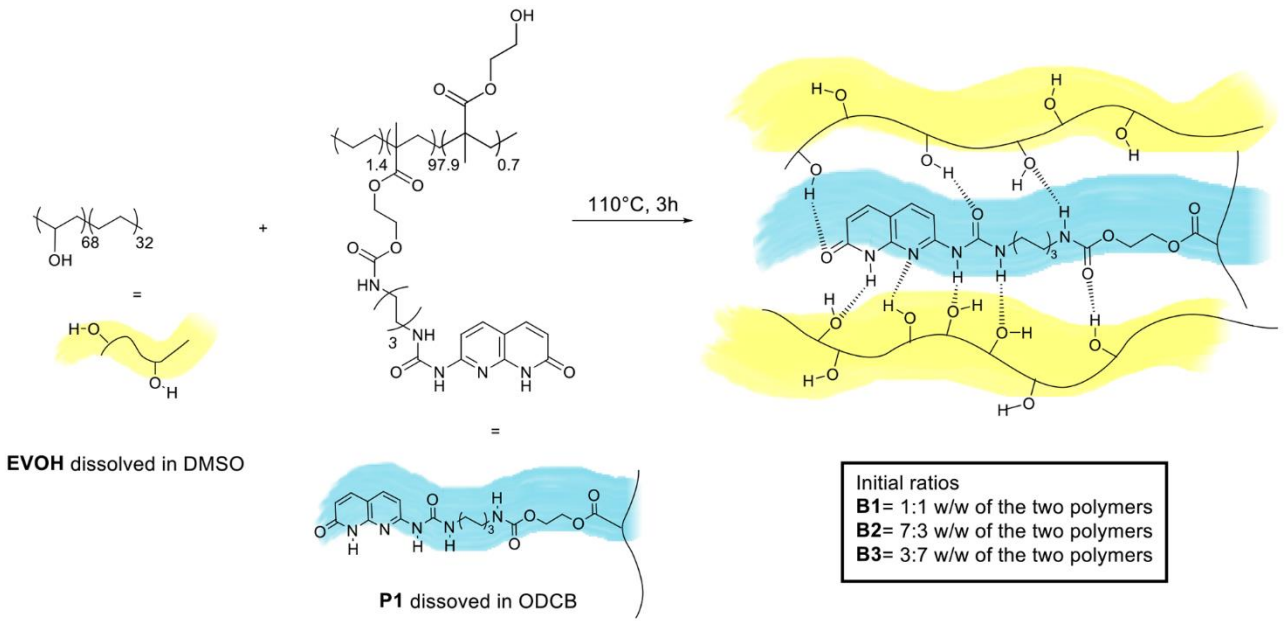

Scheme 1. Blend formation between EVOH and PE-HEMA-ODIN (**P1**).

The presence of a limited amount of ODIN is sufficient to induce the compatibilization of the two polymers by reducing their interfacial energy *via* H-bonding. When mixed together, the ODIN motif can act as multiple H-bond acceptor/donor[17] for the OHs of EVOH, as shown in Scheme 1. The potentially competitive ODIN dimerization is statistically disfavored, since an overwhelming number of OHs surrounds the few ODIN units. This tenet is confirmed by the 2PM measurements (see dedicated section), since the emission spectra of **P1** and EVOH/**P1** are different. The experimental composition of **B1**, **B2** and **B3** can be assessed by determining the nitrogen content in the blends *via* EA, since ODIN is the only component containing nitrogen (Table 1). The blends underwent extensive cycles of drying under vacuum at 60°C to eliminate any trace of solvent, which could jeopardize the EA analyses. The presence of residual DMSO (the highest boiling solvent used) was determined *via* sulfur EA, so the blends were dried until the sulfur content was zero.

Table 1. Theoretical composition of **B1**, **B2** and **B3**, content of nitrogen obtained *via* Elemental Analysis and corresponding experimental composition of the resulting blend.

Blend	**Initial component composition (EVOH:P1 w/w)**	**Nitrogen calculated**	**Nitrogen experimental**	**Experimental blend composition (EVOH:P1 w/w)**
P1	-	-	2.82	-
B1	7:3	0.84	0.85	7:3
B2	1:1	1.41	0.87	7:3
B3	3:7	1.97	1.35	1:1

Table 1 reports the theoretical and experimental nitrogen content in the three blends from which the experimental composition of **B1**, **B2** and **B3** is obtained. EA analyses indicate that an excess of EVOH is always present in the obtained blends. A possible explanation for the bias toward EVOH in the blends is the following: part of the PE-HEMA with a very low HEMA content (2.1% in this case) is pure PE without HEMA. It is reasonable to assume that this fraction remains in solution since not involved in H-bonding with EVOH.

3.1.3 Thermal properties of the blends

The melting temperature T_m of the three blends were determined *via* DSC (Figure S7-S9), while their T_β were evaluated using DMTA (Figure S17). Table 2 resumes these thermal data for **B1**, **B2** and **B3** in comparison to those of the pristine polymers.
The degree of crystallinity (X_C) was calculated according to Equation (1).[19]

$$\boldsymbol{Xc}\ (\%) = \frac{\Delta \boldsymbol{H_f}}{\emptyset \Delta \boldsymbol{H_f^0}}\ \boldsymbol{x}\ \mathbf{100} \qquad (1)$$

Where ΔH_f is the experimental melting enthalpy, ΔH_f^0 is the enthalpy corresponding to 100% crystalline PE or EVOH, and Ø is the weight fraction of **P1** or EVOH in each blend. A substantial decrease of ΔH_f and crystallinity is observed moving from PE-HEMA to **P1**. This is attributed to the bulkiness of ODIN, which hinders crystallization, as already observed.[8] The ODIN dimers form physical cross-links between the PE chains, leading to a rubbery plateau after the melting temperature as shown by DMTA of **P1**. (see Figure S19B). The DSC data of the three blends show a

decrease in the EVOH component T_m as expected upon blending. The presence of a single T_g is diagnostic to assess the compatibilization between two immiscible polymers.[11] In our case, T_g transition inflection point was hardly visible in the DSC curve. For this reason, we decided to monitor the T_β transition, generally equated to T_g, through DMTA. DMTA analyses evidenced the presence of a single T_β value for each blend in Tanδ thermograms, indicative of homogeneous mixing (see Table 2 and Figure S17).

Table 2. Thermal data of EVOH, PE-HEMA **P1**, **B1**, **B2** and **B3** obtained from DSC and DMTA. T_β data of PE- HEMA is referred to literature.[10]

Polymer	T_m[a] (°C)	ΔH_f[a] (J/g)	X_c[a] (%)	T_β[b] (°C)
EVOH	172	76.0	59	67
PE-HEMA	103	98.6	34	10[10]
P1	96	73.3	26	47
B1	98^x, 147^y	16.1^x, 14.5^y	19^x, 16^y	49
B2	97^x, 164^y	34.6^x, 25.6^y	40^x, 29^y	52
B3	96^x, 163^y	38.7^x,11.7^y	27^x, 18^y	44

The superscripts x and y correspond to P1 and EVOH, respectively. [a]Det. *via* the second heating curve of DSC; *Xc* calc. with heat of fusion for 100% crystalline of PE= 286.2 J/g[19] and of EVOH 32mol%= 128.1 J/g.[20] [b]Det. *via* DMTA.

3.1.4Two-photon microscopy of P1 and B1, B2, B3

In 2PM, the sample is excited by the simultaneous absorption of two photons, and the fluorescence generated by two-photon excitation is then detected. Unlike traditional fluorescence microscopy (including confocal microscopy), which exploits one-photon absorption and consequently adopts UV-Vis light sources to excite the fluorophores, 2PM typically uses near infrared (NIR) light sources. The use of NIR light brings to great advantages in terms of light scattering, which is strongly suppressed in NIR compared to UV-Vis light, and reduced photo bleaching. Moreover, since two-photon absorption is a nonlinear optical process, it occurs only when the density of photons is very high, i.e. in a very small volume defined by the focus of the laser (the so-called voxel). Thus, 2PM has an intrinsic three-dimensional resolution and by moving the voxel (or, in other terms, by moving the focus of the laser) within the sample, 3D images are collected. The reduced scattering and the intrinsic volume confinement of the non-linear process also allow for a penetration depth up to 1mm, which cannot be achieved by

traditional fluorescence and confocal microscopy. Hence, taking advantage of the fluorescence of ODIN, 2PM was used to visually assess the distribution of ODIN as monomer/dimer inside the blends.

Fluorescence images of **P1** and polymer blend films were collected with the 2PM setup described in the experimental section. In each sample, the detected signal is assigned to ODIN since both PE-HEMA and EVOH films do not show any detectable emission signal. Figure 2A reports the image of the surface of **P1**, while Figure 2B shows a reconstruction of the first 100 μm. Both images show several fluorescent domains, which are homogeneously distributed on the surface and within the sample. The color of the emitted light is yellow-greenish: the fluorescence signal is detected in all the three adopted detectors (blue, green and red, see Figure S20). The emission spectra collected at the surface and at 50 μm below the surface are superimposable, and are reported in Figure 2C. The very broad emission is attributed to ODIN dimers. In fact, ODIN self-dimerizes in **P1**, due to its strong tendency to form H-bonds.[7]

The random grafting of ODIN into the polymer matrix is probably responsible for the fluorescent domains observed in Figure 2A. The fluorescence images collected from the three polymer blends show a completely different color and morphology with respect to **P1**, as reported in Figures 2D-M. The images acquired on the surface of the films (Figures 2D, 2G and 2L) show an emission signal which is characterized by a more pronounced contribution in the blue channel with respect to **P1** (in Figure S20 the fluorescence signal collected from each detector is reported), and only a few fluorescent yellow-greenish domains which are similar to those observed in **P1**. The more pronounced blue emission is confirmed by the fluorescence spectra acquired on the polymer blends (Figures 2F, 2I and 2N), showing a maximum around 450 nm. This emission is assigned to monomer ODIN forming H- bonds with EVOH and the few green domains observed at the surface could be attributed to some residual emission of ODIN dimers. This result is in line with the spectroscopic characterization of ODIN in solution, reported in reference 8: in $CHCl_3$ a red shift of the emission band was observed with increasing the ODIN concentration, as a consequence of the formation of dimers. The 3D images (Figures 2E, 2H and 2M) confirm that homogeneous distribution of ODIN is achieved for the three samples **B1**, **B2** and **B3** in the bulk. Moreover, for each specimen the emission spectrum collected at 50 μm below the surface is superimposable with the spectrum collected at the surface, a further confirmation that ODIN is homogenously distributed within the samples.

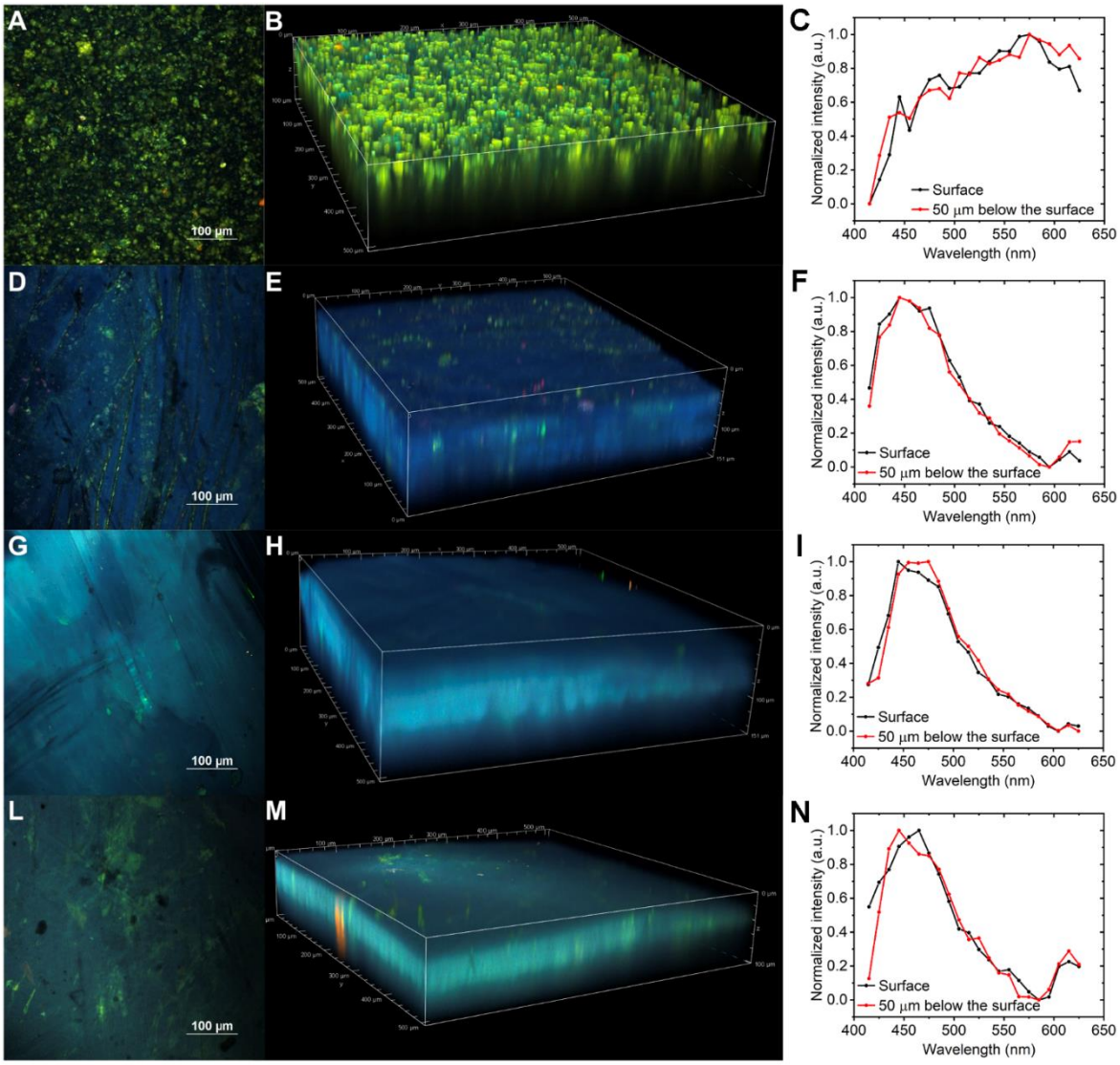

Figure 2. Fluorescence images of the surface of **P1** (A), **B1** (D), **B2** (G) and **B3** (L); 3D reconstruction of Z-stack images of **P1** (B), **B1** (E), **B2** (H) and **B3** (M), all images were collected exciting the sample at 820nm; emission spectra acquired exciting the samples at 820 nm on the surface and 50 µm below it of **P1** (C), B1 (F), **B2** (I) and **B3** (N).

3.1.5 Reprocessability test.

All the samples were reprocessed *via* compression molding at 180°C for 1 min under a pressure of 2 ton m^{-2}. **B2** was selected to monitor the stability of blending after reprocessing. The reprocessability of the blend **B2** was investigated *via* DMTA, DSC and 2PM to assess the tensile and thermal properties preservation as well as the integrity of the blend. **B2** was reprocessed three times and four different specimens were produced by compression molding: one from freshly synthesized (**B2**) and the others after one (**B2-1**), two (**B2-2**) and three (**B2-3**) recycling steps.

The 2PM images acquired on the pristine and the reprocessed blends (Figure 3) show small but significant differences between the specimens both in terms of morphology and fluorescence signal. The contribution of the yellow-greenish emission, that dominates the signal of **P1**, increases at each recycling step, as shown in Figures 3A-D. This trend is confirmed by emission spectra as reported in Figure 3E: at each recycling step, the long wavelength region of emission spectra progressively acquires intensity. Moreover, in **B2-2** and **B2-3** (Figures 3C and 3D), some dark crevice-like features appear, together with yellow-greenish domains.

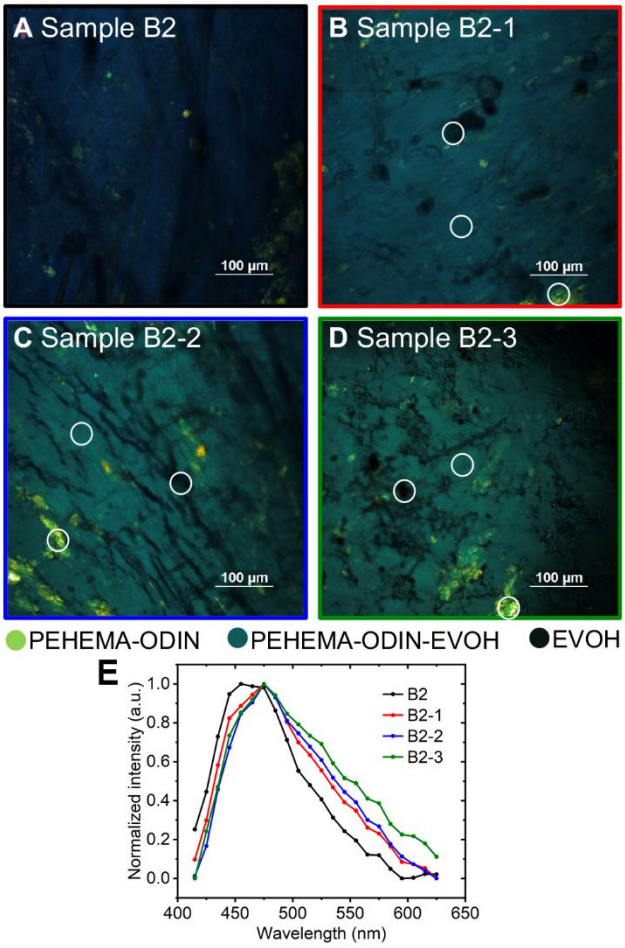

Figure 3. (A) Image acquired at the surface of sample **B2**; (B) image acquired at the surface of sample **B2-1**; (C) image acquired at the surface of sample **B2-2**; (D) image acquired at the surface of sample **B2-3**; (E) emission spectra acquired on the four specimens. All the measurements were performed exciting at 820 nm.

DMTA was used to monitor the T_β[21] of the four specimens (see Figure S18), while enthalpy values were determined using DSC (Figures S8, S13, S14 and S15). As

shown in Table 3, T_β increases moving from **B2** to **B2-3** and the enthalpies of fusion get closer to the values of the individual constituents of the blend.

Table 3. Thermal data of **B2**, **B2-1**, **B2-2**, and **B2-3** obtained from DSC and DMTA.

Polymer	T_m[a] (°C)	ΔH_f[a] (J/g)	X_c[a] (%)	T_β[b] (°C)
B2	97[x], 164[y]	34.6[x], 25.6[y]	40[x], 29[y]	52
B2-1	96[x], 173[y]	30.2[x], 34.9[y]	35[x], 39[y]	46
B2-2	95[x], 167[y]	26.1[x],36.9[y]	30[x], 41[y]	56
B-3	96[x], 164[y]	30.4[x],27.5[y]	35[x], 31[y]	61

The superscript x and y correspond to **P1** and EVOH, respectively. [a]Det. *via* the second heating curve of DSC; X_c calc. according to equation 1 with heat of fusion for 100% crystalline of PE= 286.2 J/g[19] and of EVOH 32mol%= 128.1 J/g[20] [b]Det. *via* DMTA.

These data support the morphological evidence derived from 2PM of the partial but progressive segregation of the two components, triggered by the reprocessing. It is worth noting that the blends were synthesized in a DMSO/ODCB solution, where the presence of DMSO favors the ODIN monomeric form. Instead, at the solid state, during thermal reprocessing, the most stable H-bonding array of ODIN dimers is favored, causing the partial blend segregation.

3.2 Conclusion

The molecular level compatibilization of immiscible polymers has been successfully achieved using ODIN both as compatibilizer and fluorescent probe. The ability of ODIN to act as multiple H-bond donor and acceptor has been exploited to blend EVOH with PE. A limited amount of ODIN (1,4% molar) grafted on PE-HEMA is sufficient to obtain homogenous blends at different polymer compositions.

ODIN florescence allowed introducing 2PM as an innovative tool to investigate the degree of blending at the sub-micrometric level, both on the surface and in the bulk. The compatibilization of the three blends **B1**-**B2**-**B3** has been demonstrated by tracking the fluorescence emission of ODIN. In all cases, ODIN is evenly distributed both on the surface and in the bulk as shown by the 3D images of Figure 2. Yellow-greenish emission is diagnostic of the dimer formation, while blue emission results from the

monomeric form: the dimer is dominant in **P1**, while the monomer in **B1**-**B2**-**B3** (Figure 2).

2PM has also allowed tracking the onset of segregation between the two components upon thermal reprocessing. ODIN emission changes progressively after the triple reprocessing of **B2** blend with concomitant increase of inhomogeneous dimer emission interspersed in fluorescent silent EVOH patches. This last result show that thermal processing can reverse the compatibilization, triggering the reformation of ODIN dimers as the most stable H-bonding array in the solid state. Future work will explore the use of non-dimerizing H-bonds units to form thermally stable blends.

Overall, 2PM can be considered a complementary technique to SAXS/SANS when a suitable chromophore is present in one of the blended polymers.

3.3 Experimental section

Methods

Nuclear magnetic resonance (NMR). NMR spectra were recorded on a Bruker Advance 400 (400 MHz). Chemical shifts are reported in parts per million (ppm). ^{1}H-NMR chemical shifts are given in reference to the residual solvent peak (2.50 ppm for deuterated dimethyl sulfoxide (DMSO-d_6) and 6.00 ppm for deuterated 1,1,2,2-Tetrachloroethane (TCE-d_2). High temperature NMR spectra were recorded at 80°C in TCE-d_2.

Infrared spectroscopy (IR). Infrared absorption spectroscopy analyses were performed with a Perkin Elmer FT-IR Spectrum Two instrument in the mode of Attenuated Total Reflectance (ATR) using powder samples. The background was subtracted from every spectrum recorded.

Elemental Analysis (EA). Elemental analyses were recorded on a CHNS Thermo Fisher FlashSmart. The nitrogen content was determined by means of thermal conductivity (TC) and volumetric analysis.

Differential scanning calorimetry (DSC): Melting temperatures (T_m) and enthalpies of the transition (ΔH_m) were measured by differential scanning calorimetry (DSC) using a DSC6000 from Perkin Elmer. DSC measurements were carried out under nitrogen between 0 and 200 °C at a scan rate of 10 °C min^{-1}. The sample weight was in the range 5-10 mg. The transitions were measured in the second heating curves.

Compression molding. Films of the samples were obtained by compression molding the polymers between Teflon plates, with an appropriate spacer, at 180 °C for 1 min under a pressure of 2 ton m^{-2} (Carver C12, laboratory press).

Dynamic mechanical analysis (DMTA). Rectangular samples suitable for DMTA were cut to dimension of 3 x 5 x 0.5 mm (length x width x thickness). Samples were measured on a TA Instruments *Q800* in tensile mode. The E', E" and Tanδ were monitored while screening the samples during a temperature sweep from -100 °C to 150 °C at 3 °C min^{-1}. An oscillation frequency of 1 Hz with an oscillation amplitude of 10 µm were applied.

Two-photon microscopy (2PM): The polymer specimens were characterized with a Two-Photon Microscope Nikon A1R MP+ Upright supplied with a femtosecond pulsed laser Coherent Chameleon Discovery (~ 100 fs pulse duration with 80 MHz repetition rate, tunable wavelength output 660-1320 nm). To focus the excitation beam and to collect the two-photon excited fluorescence (TPEF) signal, a 25x water dipping objective with numerical aperture (N.A.) 1.1 and working distance 2.0 mm was used. Due to the

characteristics of the samples (thin films) we decided to collect images in air (instead of water). This choice affects the N.A. (which becomes lower), and as a consequence the resolution. In fact, according to the Rayleigh criterion, in multiphoton microscopy the lateral resolution (x-y) is $d = \frac{0.61\lambda}{N.A.}$, while the axial resolution is $z = \frac{2n\lambda}{N.A.^2}$, where λ is the excitation wavelength, n the medium the refractive index, and $N.A.$ the numerical aperture.[22]

TPEF signal was directed by a dichroic mirror to a series of three non-descanned detectors (high sensitivity GaAsP photomultiplier tubes) allowing fast image acquisition. Optical filters preceded the detectors allowing the simultaneous acquisition of three separated channels: blue channel (415-485 nm), green channel (506-593 nm), and red channel (604-679 nm). The operation software of the microscope performed the overlay and the processing of the three channels images. A fourth photomultiplier GaAsP detector, connected to the microscope through an optical fiber and preceded by a dispersive element, was used to record emission spectra of the two-photon excited samples (wavelength range 400-630 nm with a bandwidth of 10 nm).

Z-stack acquisitions were collected with 0.5 μm steps and images with a field of view of 500x500 μm (1024x1024 pixel) and a 2.2 s dwell time. During Z-stack acquisitions, several 2D images of the sample are collected at different depths (in this case one image every 0.5 μm) and then processed by the microscope software to obtain a 3D reconstruction of the sample.

Materials

Unless otherwise specified, chemicals and solvents were purchased from Sigma-Aldrich and used as received. Poly(ethylene-co-(2-hydroxyethyl methacrylate) (PE-HEMA, 2.1% mol of HEMA) was provided by SABIC. Co-polymer Ethylene Vinyl-Alcohol (EVOH, 32 mol% of ethylene) was purchased from EVALTM. The synthetic procedures for ODIN isocyanate 2 and PE-HEMA-ODIN (P1) were adapted from literature[8] (Schemes S1 and S2).

Synthesis.

1-(6-isocyanatohexyl)-3-(7-oxo-7,8-dihydro-1,8-naphthyridin-2-yl)urea **(ODIN-isocyanate)**:

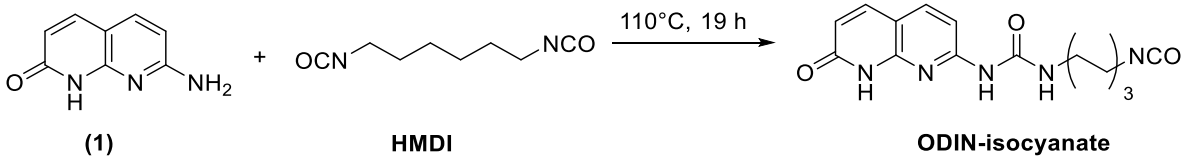

7-Amino-1,8-naphthyridin-2(1H)-one **(1)**[23] (4 g, 0.025 mol) was added to a round-bottom flask and allowed to dry for 1 h under vacuum. The flask was kept under nitrogen atmosphere by three consequent vacuum/nitrogen cycles. Hexamethylene diisocyanate (HMDI, 60 mL, 0.37 mol) was added to the reaction flask. The reaction mixture was heated to 110 °C while stirring. After 19 h, the reaction mixture was cooled to room temperature and quenched with 500 mL of hexane. The obtained precipitate was filtered off to remove the excess of HDI, and the yellow/brown obtained solid was dried in a vacuum oven at 40°C for 2 hrs (71% yield).

^{1}H NMR (400 MHz, DMSO-d_6): δ (ppm) = 1.16-1.47 (m, 4H), 1.56 (m, 4H), 3.21 (q, J= 6.6 Hz), 3.35 (t, J= 6.6 Hz, 2H), 6.35 (dd, J_1= 9.4 Hz, J_2= 1.9 Hz, 1H), 6.85 (d, J= 8.6 Hz, 1H), 7.78 (d, J= 9.4 Hz, 1H), 7.92 (d, J= 8.5 Hz, 1H), 9.01 (t, J= 5.8 Hz, 1H), 9.65 (s, 1H), 12.18 (s, 1H).

IR, ϋ (cm^{-1}): 3390 (N-H stretching), 2926 (C-H stretching), 2938 (C-H stretching), 1660 (C=O stretching), 1594 (N-H bending, urea), 1533 (C-N stretching), 1242 (C-O stretching).

Synthesis of PEHEMA-ODIN (**P1**):

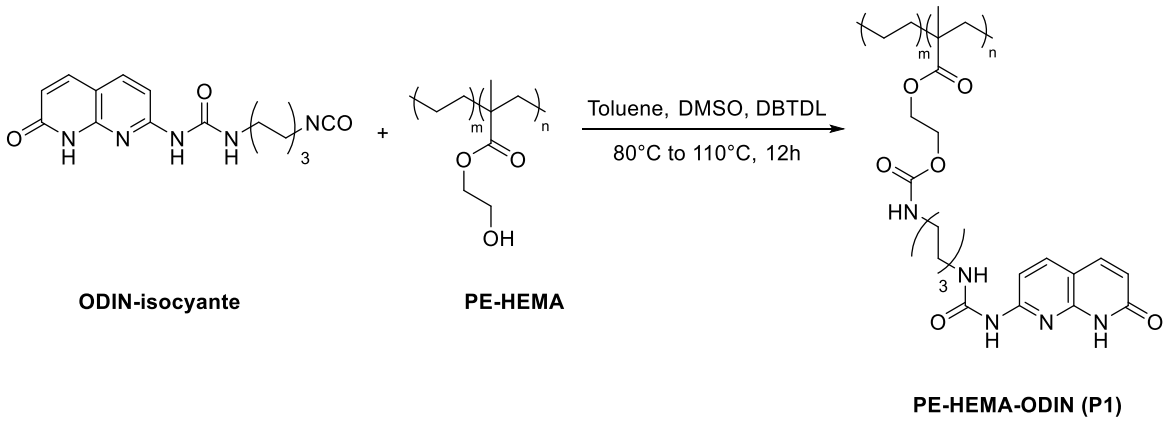

50 mL of dry toluene were inserted into an anhydrous Schlenk equipped with a magnetic stirrer. The solvent was degassed through three cycles of freeze-pump-thaw, then PE-HEMA (1 g) was added under nitrogen and dissolved under stirring at 80 °C for 1 h. Once a clear solution was obtained, ODIN-isocyanate(400 mg) was added under nitrogen as a solid, followed by addition of few drops of DBTDL as catalyst and 5 mL of dry DMSO to promote the dissolution of ODIN-isocyanate. The temperature of the mixture was raised to 110 °C and stirred for 12 hrs. The solution was cooled to room temperature and isopropanol was added to promote the precipitation of the functionalized polymer. The yellow product was then filtered under vacuum, washed with isopropanol, and dried in a vacuum oven ad 40°C for 12 hrs.

^{1}H NMR (400 MHz, TCE-d_2, 80°C): δ(ppm) = 0.85-2.00 (m, PE backbone), 3.24 (m, 2H), 3.40 (s, 2H), 3.86 (t, J=4.8 Hz, 2H), 4.26 (t, J=4.8 Hz, 2H), 4.30 (s, 6H), 6.61-7.89 (m, 4H), 8.23 (s, 1H), 11.09 (s, 1H), 12.71 (s, 1H).

IR, ϋ (cm-1): 3406 (N-H stretching), 2916 (C-H stretching), 2849 (C-H stretching), 1729 (C=O stretching, HEMA), 1660 (C=O stretching, ODIN), 1595 (N-H bending), 1532 (C-N stretching), 1472 (C-H bending), 1234 (C-O stretching, ODIN), 1138 (C-O stretching, HEMA).

Elemental Analysis, the degree of functionalization of PE-HEMA is 1.4 mol% calculated by the content of nitrogen (C 78.57%, H 12.83%, N 2.82%).

*General procedure for the formation of the blends between EVOH and PE-HEMA-ODIN (**P1**).*

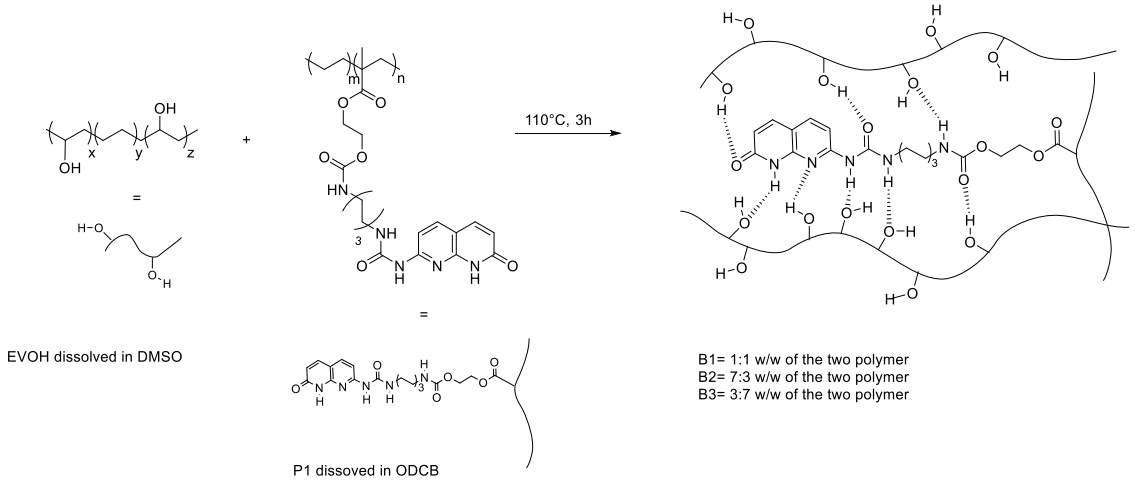

Compound P1 was dissolved in o-dichlorobenzene (ODCB, 1 mg/mL) at 110°C, while EVOH was dissolved in DMSO (25 mg/mL) at the same temperature (Scheme 1). Once the dissolution of both polymers was reached, the solution of EVOH was slowly added to the solution of P1, and the resulting solution was stirred at 110°C for 3 hrs. Subsequently, the solution was cooled to room temperature and 50 mL of isopropanol were added. The obtained precipitate was filtered, washed with isopropanol and dried under vacuum at 60°C for 72 hrs. The blends were characterized by elemental analysis (EA) (see Table 1), dynamic mechanical thermal analysis (DMTA) and differential scanning calorimetry (DSC) (see Table 2 and Figures S7, S8, S9 and S17).

3.4 Supporting information

^{1}H-NMR

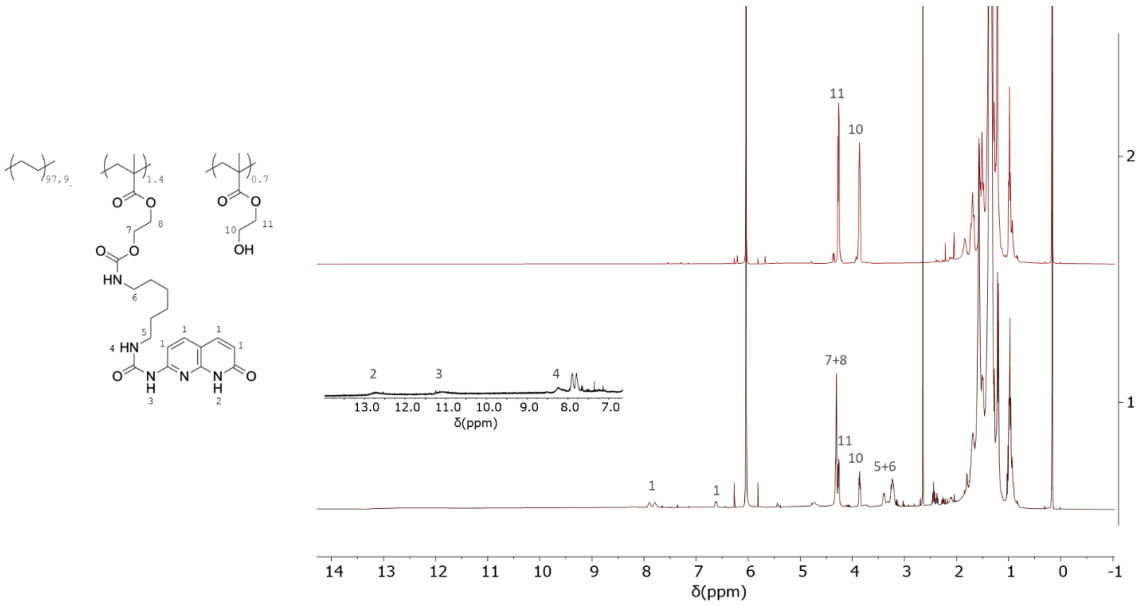

Figure S1. ^{1}H-NMR spectra of **P1** (spectrum below) and PE-HEMA (spectrum above). In the upper part of the figure the magnification (between 6 and 13 ppm) of the spectrum of **P1** is reported to show the signals related to the hydrogen bonding.

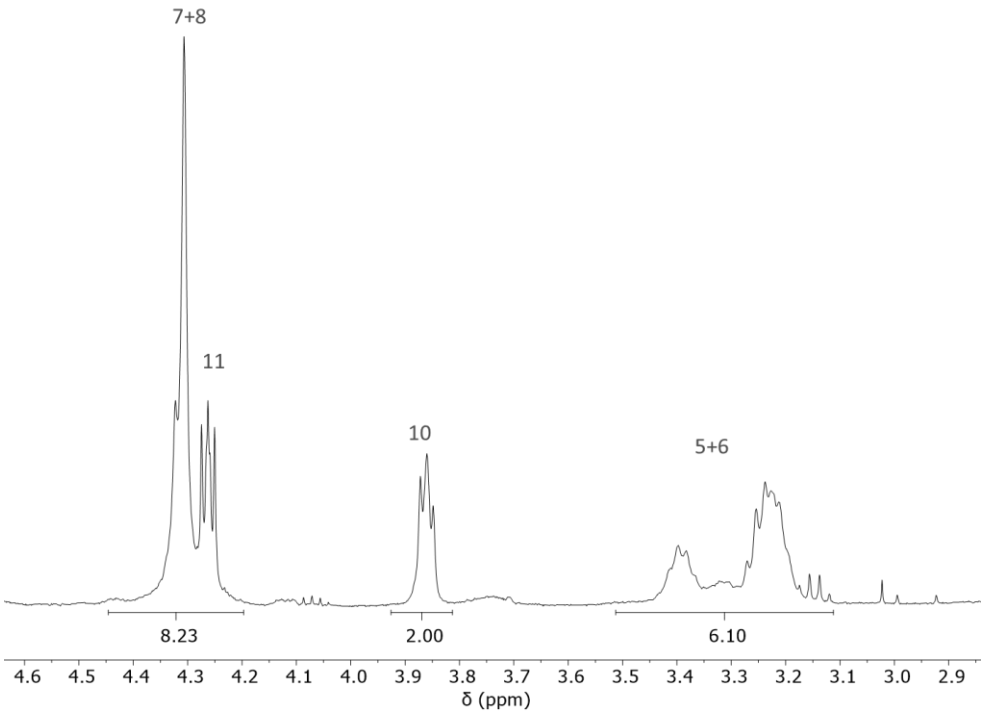

Figure S2. magnification (between 2.9 and 4.6 ppm) of the ^{1}H-NMR spectrum of **P1** is reported.

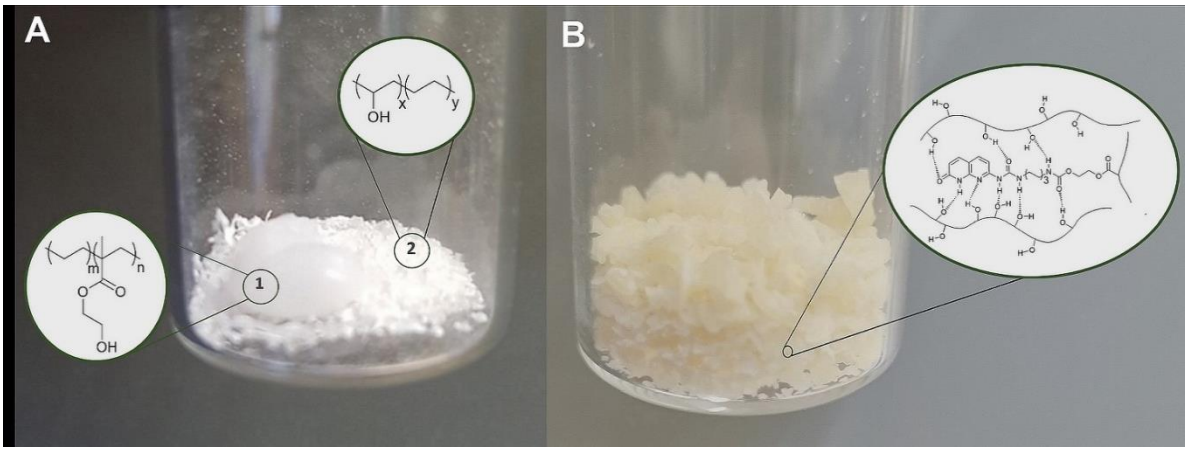

Figure S3. (A) EVOH/PE-HEMA mixture, (B) **B2** blend composed by EVOH/**P1** 1:1 w/w.

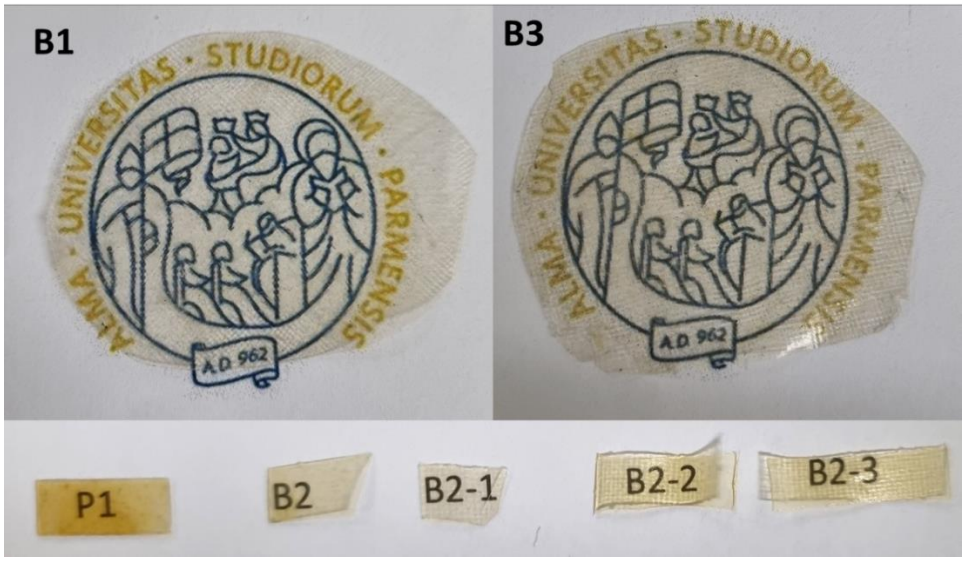

Figure S4. Images providing the transparency of the films obtained by compression molding.

ATR

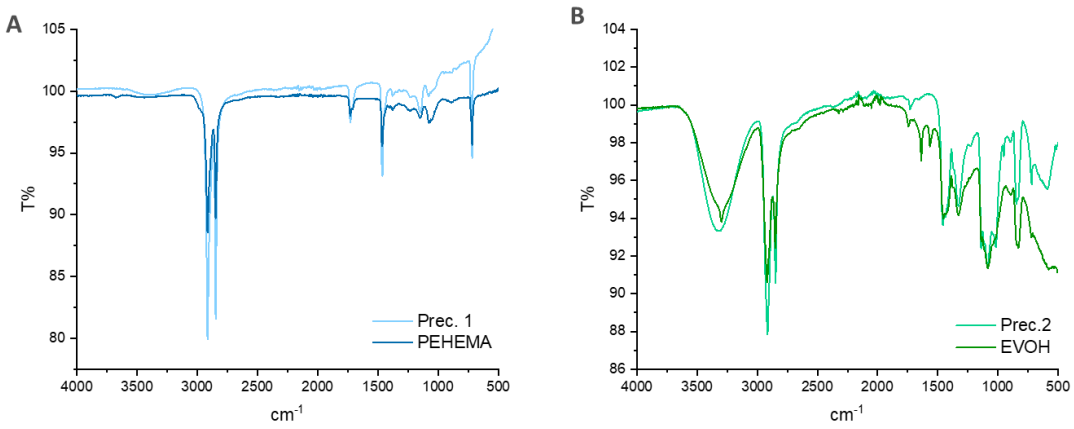

Figure S5. ATR spectra of (A) precipitate 1 and PE-HEMA polymer and (B) precipitate 2 and EVOH polymer.

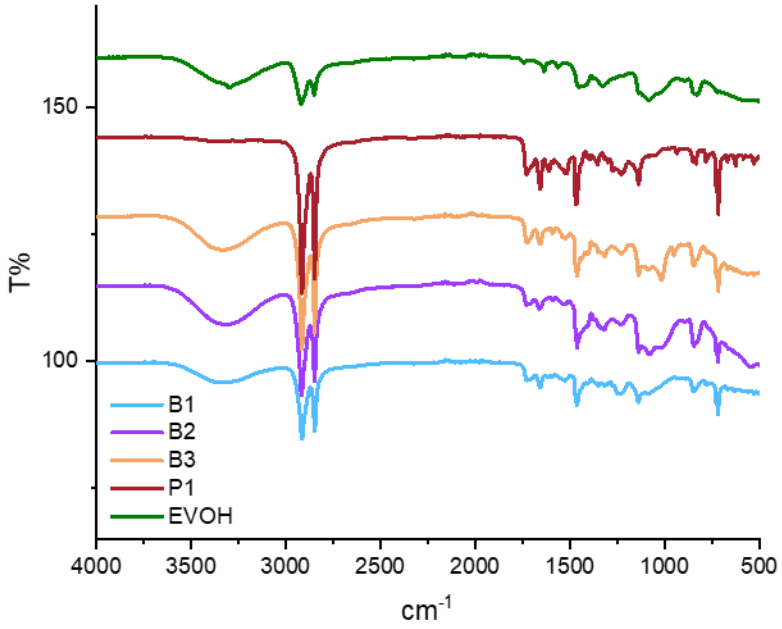

Figure S6. ATR spectra of **B1**, **B2**, **B3**, **P1** and EVOH.

DSC

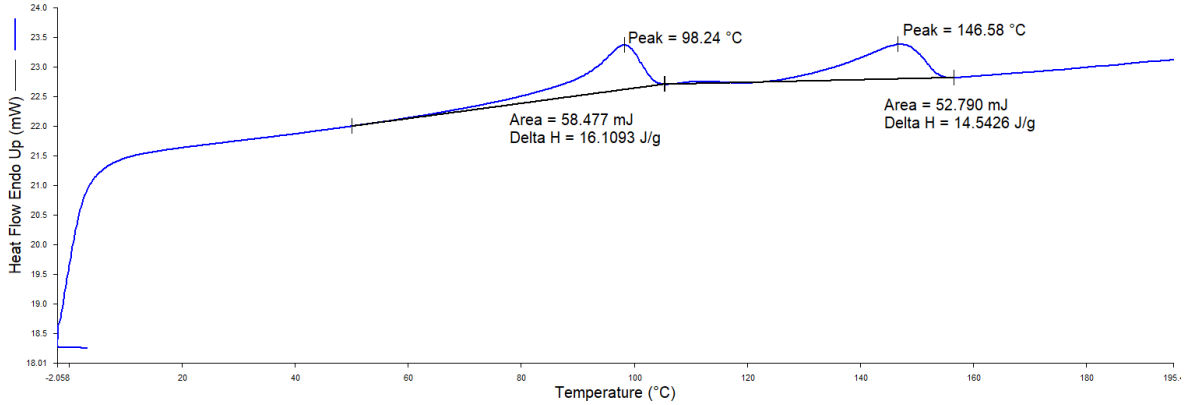

Figure S7. DSC thermographs of **B1**.

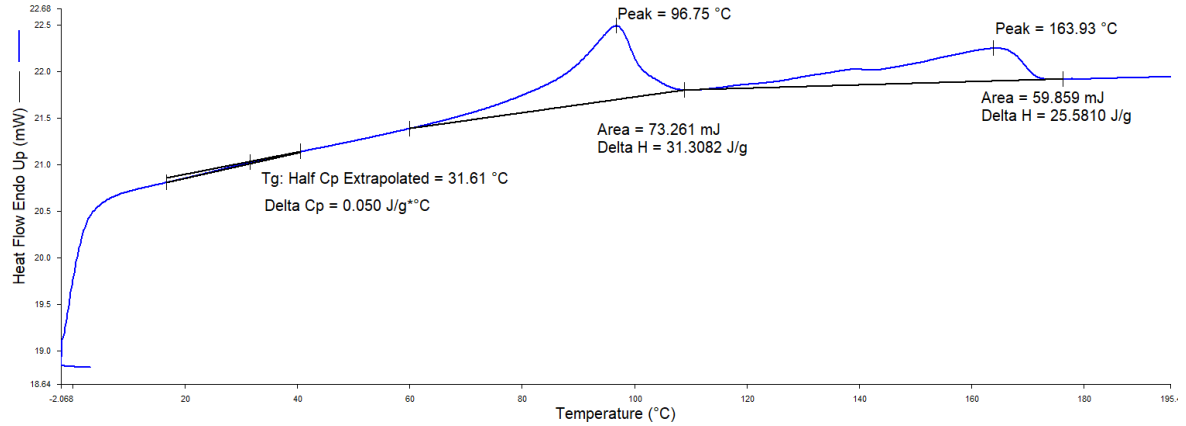

Figure S8. DSC thermographs of **B2**.

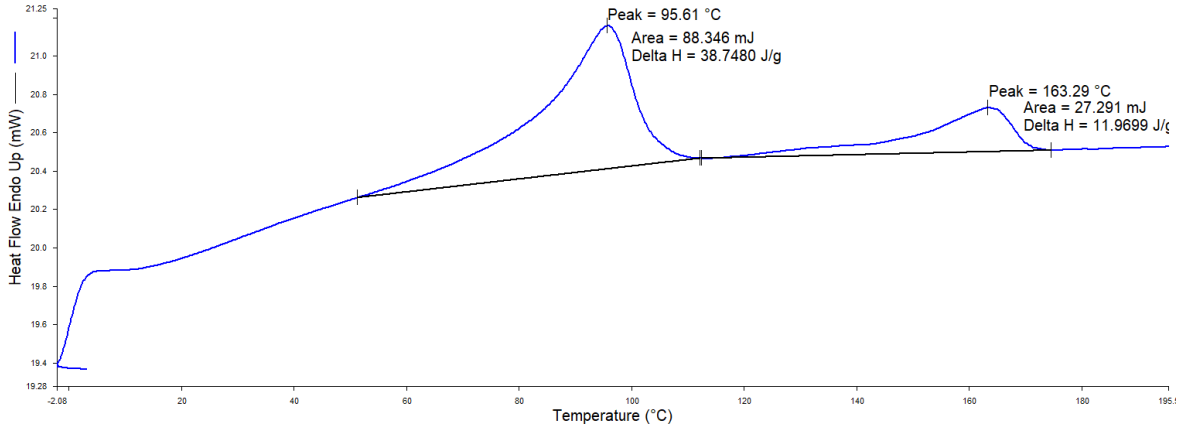

Figure S9. DSC thermographs of **B3**.

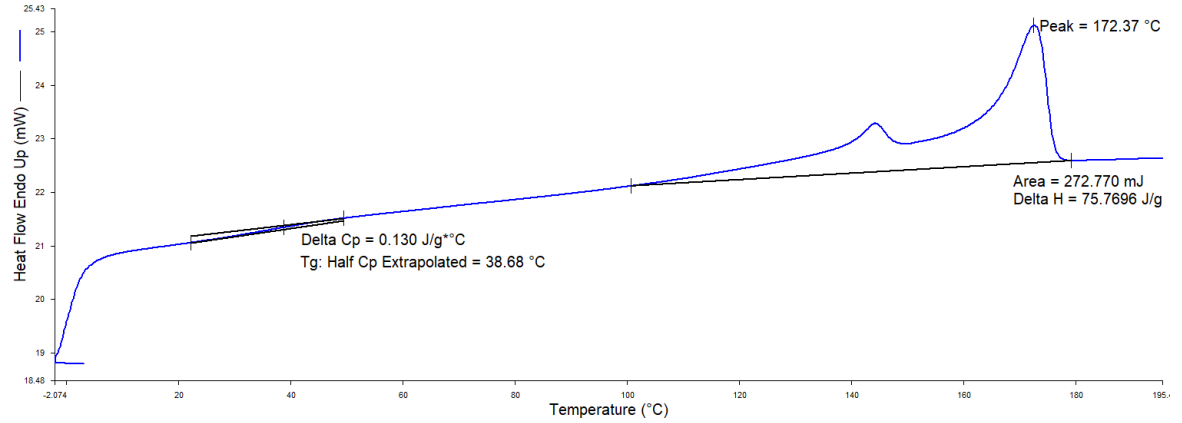

Figure S10. DSC thermographs of EVOH.

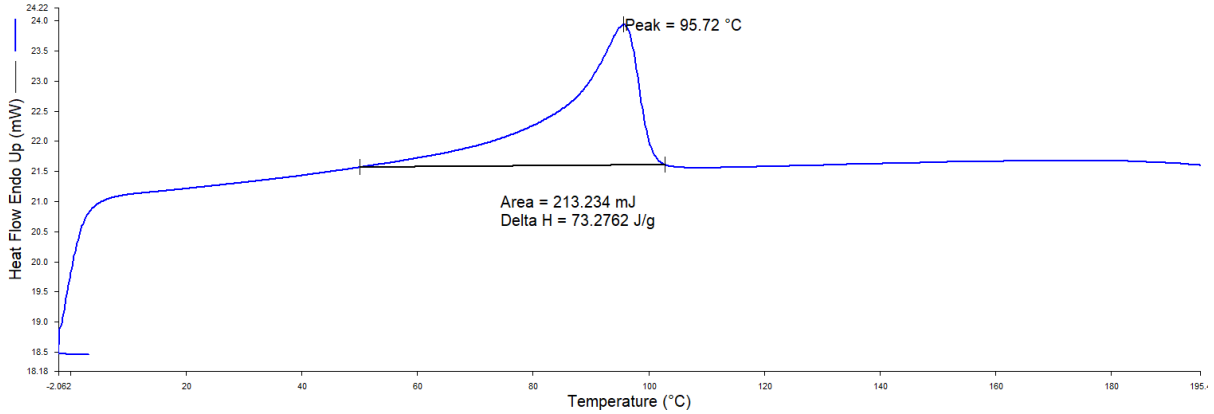

Figure S11. DSC curve of **P1**.

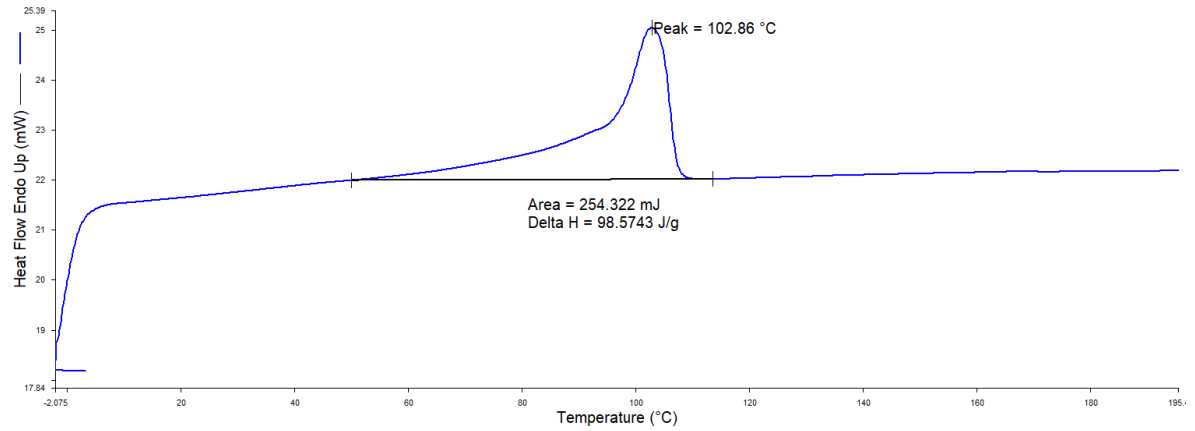

Figure S12. DSC curve of PE-HEMA.

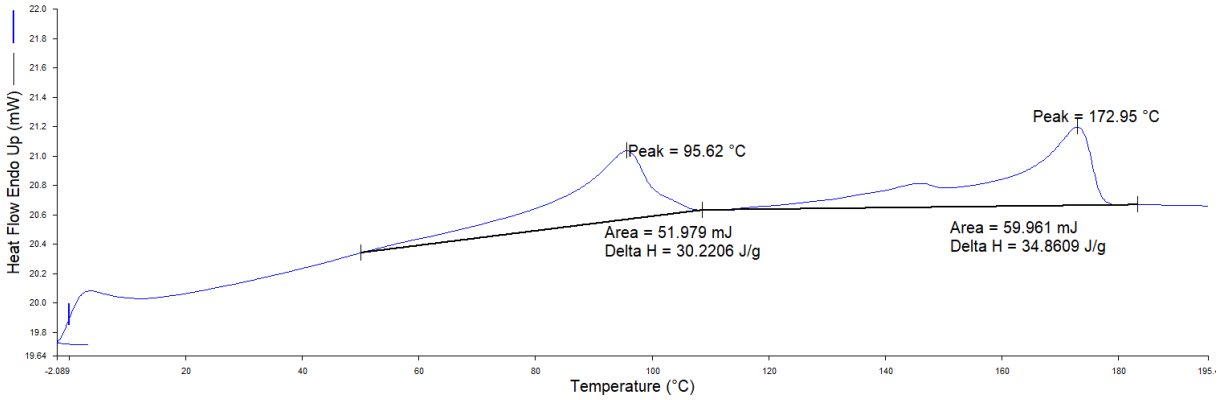

Figure S13. DSC curve of **B2-1**.

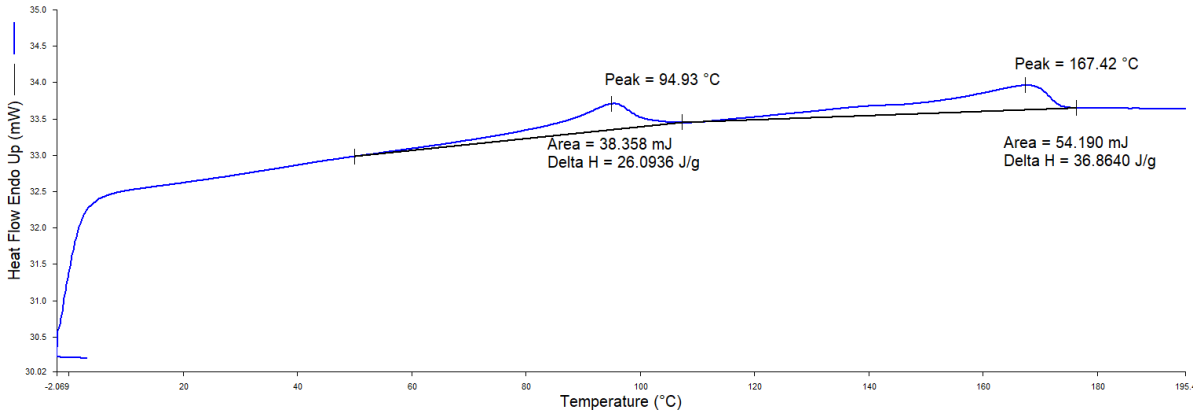

Figure S14. DSC curve of **B2-2**.

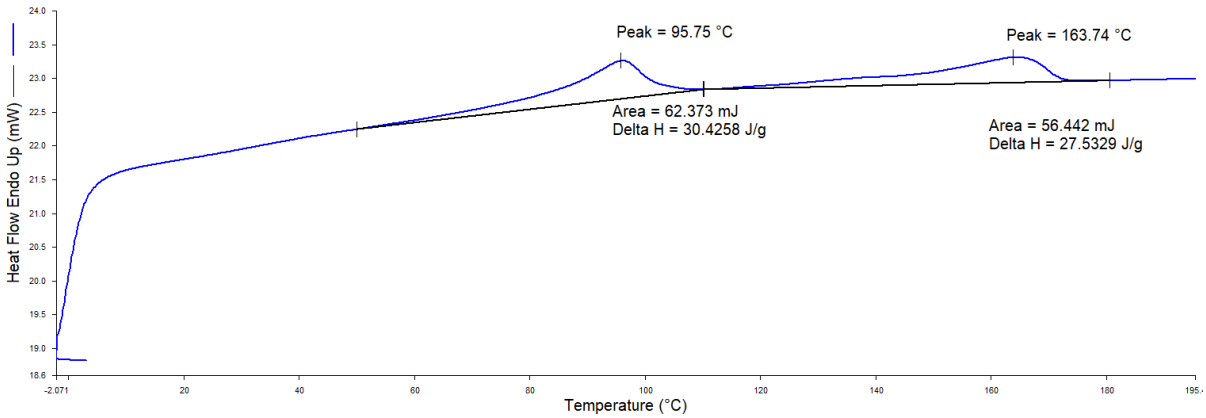

Figure S15. DSC curve of **B2-3**.

DMTA

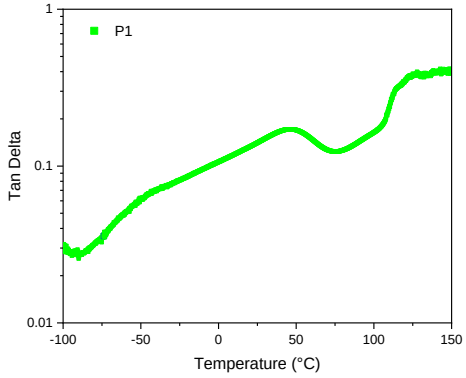

Figure S16. DMTA thermogram of **P1** shows the crosslinking effect of PEHEMA after the melting temperature.

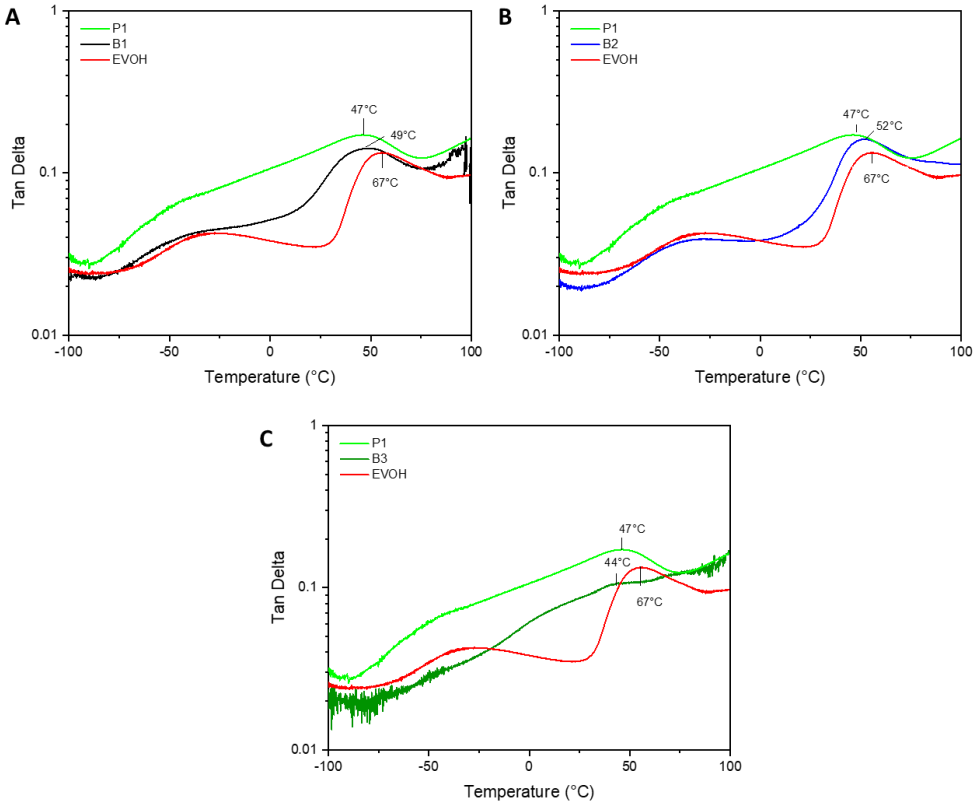

Figure S17. DMTA thermograms of (A) **B1** (black curve), (B) **B2** (blue curve) and (C) **B3** (dark green curve) using **P1** (light green curve) and EVOH (red curve) as reference in each figure to monitor the T_β of the polymer blends.

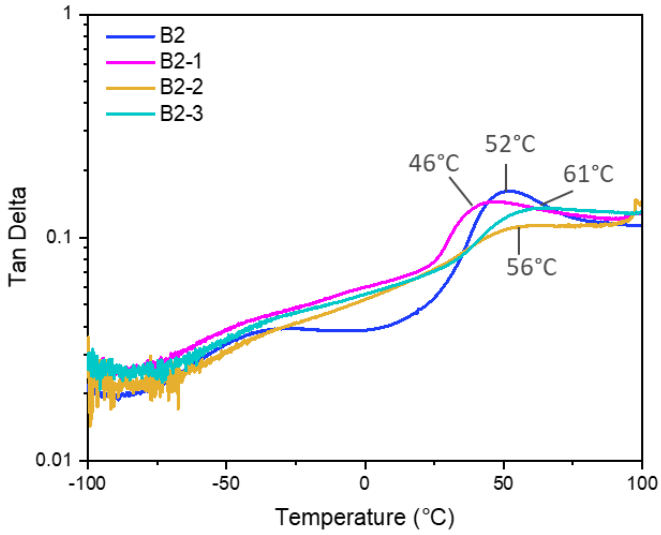

Figure S18. DMTA thermograms of **B2** (blue curve), **B2-1** (pink curve), **B2-2** (ochre curve) and **B2-3** (light blue curve) to monitor the T_β of the polymer blend after reprocessing.

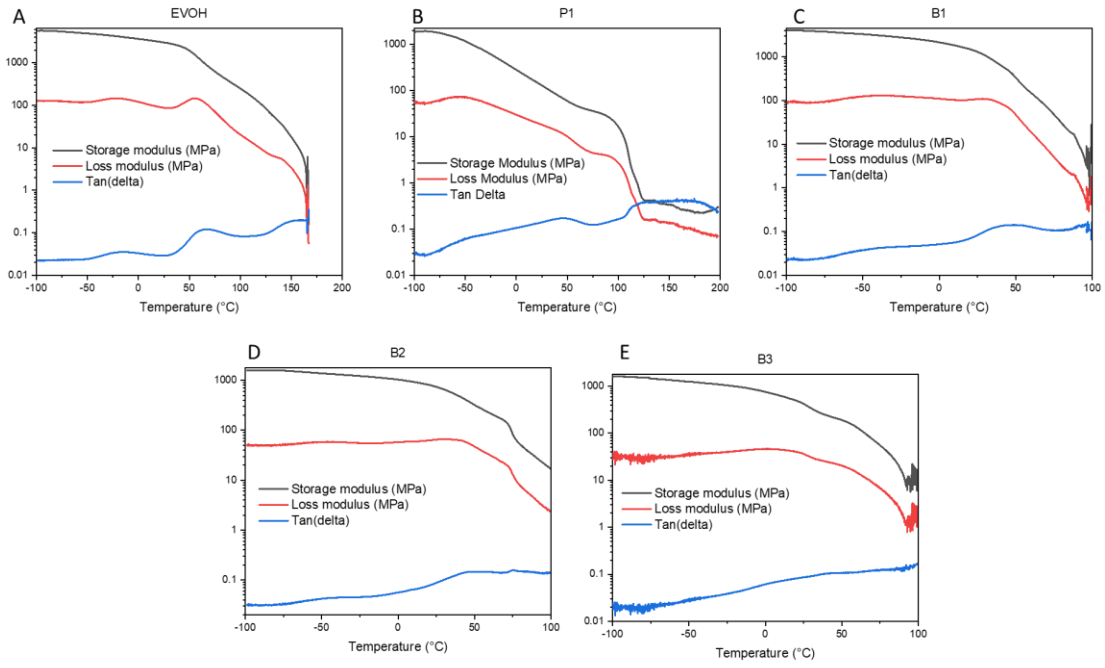

Figure S19. DMTA thermograms of **B2** (blue curve), **B2-1** (pink curve), **B2-2** (ochre curve) and **B2-3** (light blue curve) to monitor the T_β of the polymer blend after reprocessing.

Two-photon microscopy

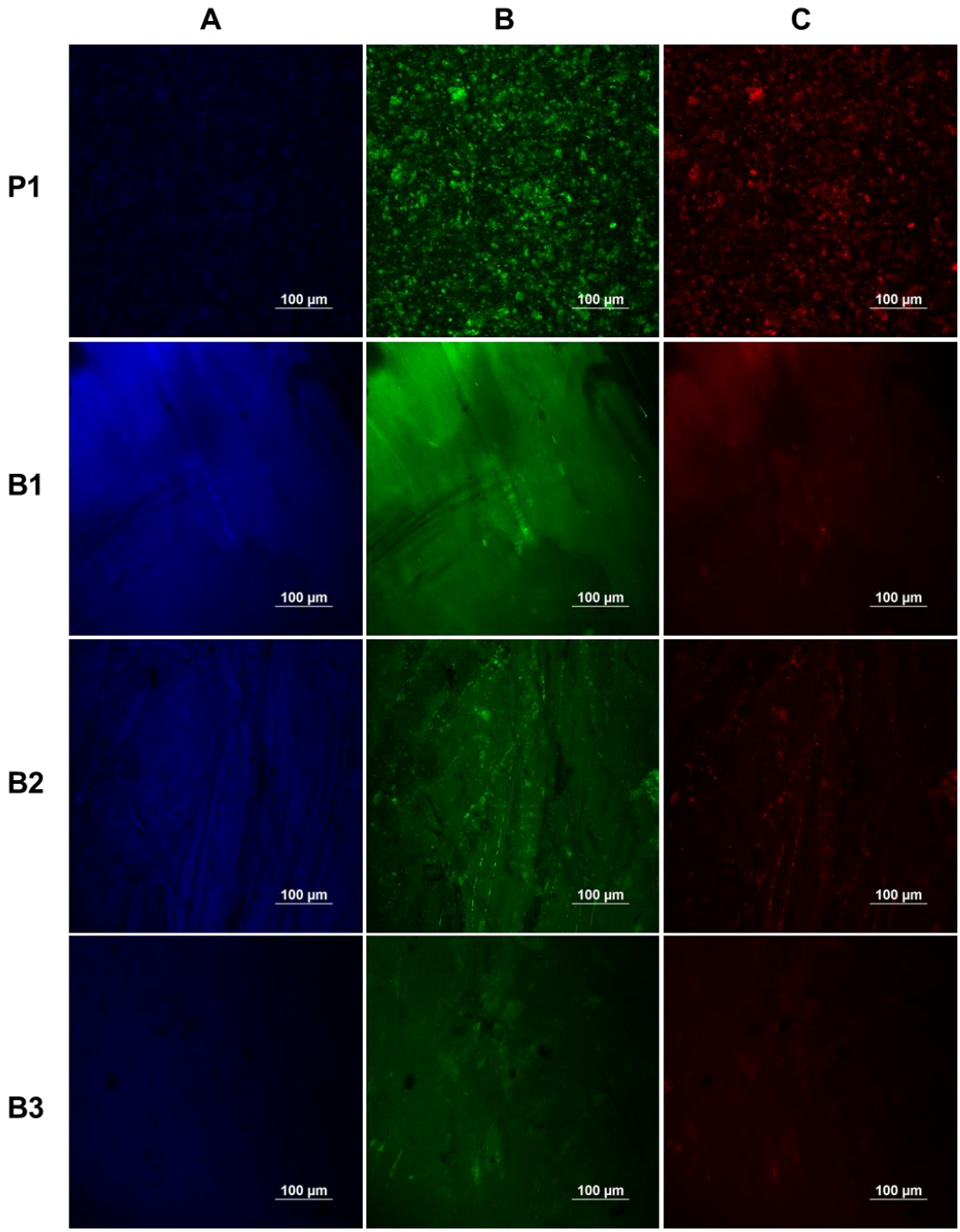

Figure S20. Images acquired on the surface of specimens **P1**, **B1**, **B2** and **B3**. Panels A: blue channel; panels B: green channel; panels C: red channel. All images were collected exciting the samples at 820 nm.

3.5 References

[1] H. Pernot, M. Baumert, F. Court, L. Leibler, *Nat. Mater.* **2002**, *1*, 54.
[2] D. R. Paul, J. W. Barlow, *Polymer Blends* **1980**, *18*, 109.
[3] S.-W. Kuo, *J. Polym. Res.* **2008**, *15*, 459.
[4] T. Park, S. C. Zimmerman, S. A. Nakashima, *J. Am. Chem. Soc.* **2005**, *127*, 6520.
[5] K. F. Feldman, M. J. Kade, T. F. A. de Greef, E. W. Meijer, E. J. Kramer, C. J. Hawker, *Macromolecules* **2008**, *41*, 4694.
[6] P. Song, H. Wang, *Adv. Mater.* **2020**, *32*, 1901244.
[7] J. Tellers, S. Canossa, R. Pinalli, M. Soliman, J. Vachon, E. Dalcanale, *Macromolecules* **2018**, *51*, 7680.
[8] M. Golkaram, L. Boetje, J. Dong, L. E. Aguilar Suarez, C.Fodor, D. Maniar, E. van Ruymbeke, S. Faraji, G. Portale, K. Loos, *ACS Omega* **2019**, *4*, 16481.
[9] L. Brunsveld, B. J. B. Folmer, E. W. Meijer, R. P. Sijbesma, *Chem. Rev.* **2001**, *101*, 4071.
[10] J. Tellers, A. Zych, P. Neuteboom, M. Soliman, J. Vachon, *Eur. Polym. J.* **2020**, *131*, 109721.
[11] M.Aubin, R. E. Prud'homme, *Macromolecules* **1988**, *21*, 2945.
[12] M. Dionisio, L. Ricci, G. Pecchini, D. Masseroni, G. Ruggeri, G. Cristofolini, E. Rampazzo, E. Dalcanale, *Macromolecules* **2014**, *47*, 632.
[13] S. Xie, B. Zhang, F. S. Bates, T. P. Lodge, *Macromolecules* **2021**, *54*, 6990.
[14] C. M. Wolf, L. Guio, S. C. Scheiwiller, R. P. O'Hara, C. K. Luscombe, L. D. Pozzo, *Macromolecules* **2021**, *54*, 2960.
[15] F.Helmchen, W. Denk, *Nat Methods* **2005**, *2*, 932.
[16] H-Y. Tan, M-G. Lin, W-C. Hsiao, S-J. Lin, L-K. Wen, W-L. Chen, C-Y. Dong, T-H. Young, *Optics Express* **2008**, *16*, 3818.
[17] Y. L. A. Rezus, H. J. Bakker, *Proc. Natl. Acad. Sci. USA* **2006**, *103*, 18417.
[18] H. Sutar, P. C. Sahoo, P. S. Sahu, S. Sahoo, R. Murmu, S. Swain, S.C. Mishra, *Mater. sci. and app.* **2018**, *9*, 502.
[19] B. Wunderlich, C. M. Cormier, *J. Polym. Sci.: Polym. Phys.* **1967**, *5*, 987.
[20] S. W. Kim, H. M. Choi, *High Perform. Polym.* **2015**, *27*, 694.
[21] S. Martin, J. F. Vega, M. T. Expósito, A. Flores, J. Martinez-Salazar, *Colloid Polym. Sci.* **2011**, *289*, 257.
[22] M. D. Young, J. J. Field, K. E. Sheetz, R. A. Bartels, J. Squier, *Adv Opt Photonics* **2015**, *7*, 276.
[23] C. A Anderson, P. G. Taylor, M. A. Zeller, S.C Zimmerman, *J. Org. Chem.* **2010**, *75*, 4848.

Chapter 4

Synthesis and characterization of EVOH and PE blends for oxygen barrier monolayer films

Part of this work was carried out in collaboration with Prof. Cristina Sissa (University of Parma), Prof. Matteo Masino University of Parma) and Prof. Claudia Graiff (University of Parma)

Preface

The initial part of the following chapter is referred to the samples synthesized and characterized in Chapter 3.

4. Introduction

4.1 Permeation of gasses through the polymers

The process by which gaseous species permeate across a polymer barrier is susceptible to a variety of factors. The solubility coefficient is dependent on the interaction between the penetrating molecule and the polymer, the condensability of the penetrating molecule, and the cohesive energy density (CED) of the matrix. This means that the size of the penetrating molecule, free volume of the polymer, and rigidity of the polymer chains all affect the diffusion coefficient. The most important factors that influence the permeability of gases into a polymeric matrix are described in the following paragraph.

4.1.1 Free Volume dependence

The dependence of the transport properties of a penetrant in a polymeric matrix is often described using correlations involving the fraction of free volume (FFV) of the polymer used. It consists of the total amount of static voids created by inefficient bundling of chains or transient voids created by thermally induced chain rearrangements. The more numerous and larger these pathways are, the faster the molecules migrate through the polymer. The free volume fraction is defined as:[1]

$$FFV = \frac{V_{SP} - V_0}{V_{SP}} \quad (1)$$

where V_{SP} is the specific bulk volume of the polymer, while V_0 is the volume occupied by the polymer chains. The volume occupied is usually estimated by the Bondi method as $V_0 = 1.3V_w$, where

V_w is the tabulated van der Waals volume of the repeat unit of the polymer.[1],[2] FFV was related to the diffusion coefficient by the Doolittle equation:[3]

$$D = A\, e^{\frac{-B}{FFV}} \qquad (2)$$

where A and B are empirical constants. The higher the FFV, the larger the diffusion. Several attempts have been made to correlate the FFV of polymers with the gas permeability. A linear correlation has been identified between the logarithm of the oxygen permeability coefficient and the inverse of the FFV in different families of amorphous polymers, vitreous polymers, and liquid crystal polymers.

The free volume can be altered by thermal manipulation of the sample. For example, high cooling rates create a high free volume in the glass state and vice versa. A more significant way to alter the free volume is to vary the chemical structure, for example, by adding or removing hanging groups on the main polymer chain. Ito et al.[4] and Muramatsu et al.[5] looked at the relationship between oxygen permeability and free volume hole size in EVOH copolymers. Ito et al.[6]observed that the free volume size of EVOH copolymers increases with the increasing content of ethylene. This increase in free volume size was related to the reduction of hydrogen bonding interactions at higher ethylene contents, allowing polymer chains greater flexibility.[7],[8]

4.1.2 Cohesive Energy Density (CED)

The cohesion energy density (CED), which significantly affects the penetrant permeation, is a measure of the interaction between the polymer chains. The CED of a polymer is equal to the square root of its solubility parameter.[9] Polyethylene (PE), for example, has a low CED due to its flexible chains. The molecular matrix provides low resistance to gas diffusion; therefore, this polymer has a high permeability to oxygen.

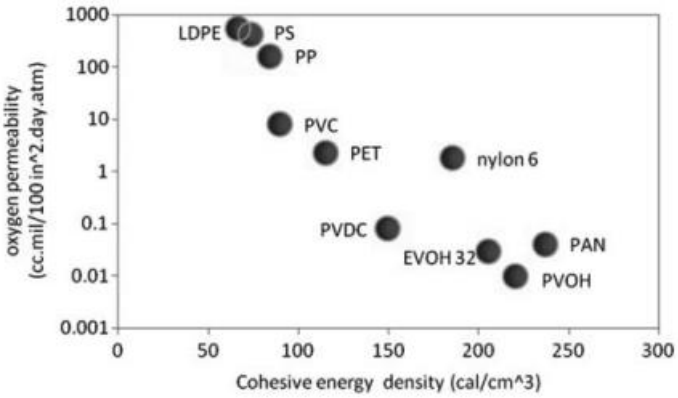

Figure 19. relationship between oxygen barrier and CED of some polymers (measured at 23°C and 0% RH).[10]

4.1.3 Crystallinity and T_g

An increase in the crystallinity of a polymer usually decreases the gas permeability (Table 1).[11] [12]The crystalline sections, which are significantly denser and more organized than the amorphous ones, prevent the absorption of the penetrant and hence decrease the solubility. Additionally, the presence of impermeable crystallites in a polymer matrix acts as a barrier to diffusion, lengthening the path the gas must cross and, in some cases, increasing chain stiffness, which lowers the diffusion coefficient.[13],[14]

Table 1. Effect of Crystallinity on oxygen permeability.

Polymer	Crystallinity (%) and Morphology	Oxygen Permeability (g/100 in 2 days)
EVOH[a]	58	0.71
	68	0.25
	70	0.15
LDPE[b]	50	480
	75	110
PET[b]	10	10
	50	5
PP[b]	Atactic (low crystallinity)	250
	Isotactic (high crystallinity)	150

[a]oxygen permeability measured at 20°C, 100%RH [15]for EVOH with 32% of ethylene. [b]oxygen permeability measured at 23°C, 50%RH.[10]

The glass transition temperature (T_g) is a further factor that influences chain mobility and, as a result, the permeability of a polymer. This occurs because of a considerable increase in the free volume within the polymer during the change from a glassy to a rubbery state.[16] Since the glass transition is a second-order transition, it establishes a discontinuity in the specific volume of the polymer that allows cooperative movements of large chain segments, promoting penetration in low-T_g polymers.[17],[18]The introduction of bulky or polar substituent groups in the polymer chain often increases the rigidity of the chain itself, leading to an increase in the glass transition temperature and packing density of the chains.[19],[20]Bulky side groups, such as aromatic groups, decrease the chain flexibility and increase the T_g and, therefore, reduce the diffusion coefficients of the penetrant.[21] Changes in the polymer's molecular structure frequently affect more than one aspect of permeability, and the overall result can be challenging to predict. For instance, as was already mentioned, adding bulky side groups can stiffen polymer chains, which would lead to a decrease in diffusion coefficients. However, the same modification might also decrease the crystallinity of the polymer and the packing of amorphous chains, both of which should raise the diffusion coefficients.

4.1.4 EVOH as an oxygen barrier in food packaging

Copolymerization of monomer units based on polyvinyl acetate, PVOH, and PE yields EVOH copolymers with an increased gas barrier, processability, and moisture sensitivity.[22] Copolymerization is commonly utilized to provide the ability to customize characteristics to specific requirements. PVOH has excellent gas barrier qualities but is water soluble and difficult to produce. PE, the other constituent, is water resistant yet has one of the lowest gas barrier characteristics. EVOH resins are commercially available in a variety of formulations, the most popular of which include ethylene concentrations ranging from 24 to 48 mol%. Thanks to the optimal combination of the qualities of the constituents, EVOH is one of the polymers most used in the food packaging field. However, its barrier properties are affected by several factors, the most important of which are the effect of the moisture and the ratio between the two comonomers.

4.1.5 Humidity effect

Water absorption may increase, decrease, or have no effect on the permeability of barrier polymers. Hydrophilic barrier polymers, usually, lose their barrier properties as relative humidity

increases. This is because water acts as a plasticizer and increases the free volume of the polymer. EVOH is extremely sensitive to moisture, due to the associations between water molecules and the polar hydroxyl groups in EVOH. [23],[24]Water is easily integrated into the macromolecular structure of the polymer due to its small size.[25]Plasticization causes an increase in the distance between nearby chains in the polymer lowering the energy of polymer-polymer interactions, which may result in the weakening or breaking of hydrogen bonds between polymer chains.[26], [27] Water plasticization influences the glass transition by lowering the T_g of the polymer matrix. According to Soarnol®, for EVOH with 32 mol% ethylene, T_g dropped from 60 °C to 3 °C as RH rose from 0% to 100% confirming that the diluting of the main chain by water results in greater mobility and chain flexibility in the amorphous part of the polymer.[27]

4.1.6 Content of ethylene

The amount of ethylene present in EVOH copolymers is a second element that influences the permeability of the material. Increasing the PE component T_g and T_m decrease, enhancing the material's thermal stability, and reducing its sensitivity to the effects of moisture. However, it also tends to create a permeation behavior tending to that of PE. To reconcile the processing requirements with the requirements of a high gaseous-barrier species, it is necessary to properly examine the ethylene component content before using this material for specific barrier purposes. In particular, an ethylene content below 20 mol% is excessively hygroscopic instead with a content equal to or higher than 50 mol% ethylene the efficiency to provide a high barrier to gases is lost.[28],[29],[30] The right ethylene to satisfy both criteria is considered to be between 25 mol% and 45 mol%.

4.1.7 EVOH in multilayer packaging

EVOH copolymers, in addition to poor moisture resistance, have poor compatibility (adhesion and miscibility) with other polymers, both polar and non-polar, caused by the strong self-interactions of EVOH copolymers. Because of this and because of its moisture sensitivity, EVOH is almost always used in multilayer packaging where it is shielded by water-resistant polymers. PP and PE are the most commonly utilized water-resistant polymers in multilayer films. The normalized water vapor transmission rates of oriented PP and LDPE, measured at 38°C and 90% RH, is between 0.3-0.5 g/100 in 24 h and 1.0-1.5 g/100 in 24 h respectively, compared to 1.4–8.0 g /100 in 24 h for EVOH

copolymers, reported by EVAL Americas. Thin layers of adhesives (usually, copolymers of ethylene, polyesters, acrylic, or polyurethanes) are necessary to attach the layers to prevent delamination.[31]

4.1.8 Polymer blends

Polymer blends are gaining traction in the plastics market. A significant increase in the number of papers, patents, and practical applications for this type of material has been observed since the 1970s. The advantage of blending lies in the possibility of obtaining materials with specific properties by mixing different polymers without the need to study and synthesize new polymers. Simultaneously, the packaging industry has experienced rapid development in recent years, and considerable efforts have been made to develop materials that can provide better performance than traditional polymer commodities. For example, in the field of food packaging, a very important aspect is the possibility of reducing the thickness of containers to achieve a significant reduction in the cost of raw materials as well as the synthesis and transportation of final products. With traditional materials, this reduction in thickness leads to a decrease in barrier properties, resulting in a drop in the shelf life of products due to their high sensitivity to the permeation of gaseous species such as O_2, CO_2, and water vapor. Although attempts at improvement have been made through the implementation of surface treatments or multilayer systems, these solutions are costly and require specific investment in terms of manufacturing equipment. The following chapter discusses the possibility to create polymer blends acting as oxygen barrier, to evaluate the applicability of a monolayer instead of a multilayer as a solution to produce goods with commercial value. Ethylene-co-vinyl alcohol (EVOH) which is already used in the food and pharmaceutical industry for its oxygen barrier property, and polyethylene-co-hydroxyethyl methacrylate (PE-HEMA), which acts as a water barrier, have been utilized.[32] The study included the realization of binary blends, by mixing the components in solution, and the following characterization of the blends, paying particular attention to the oxygen permeability measures. The use of solvents to form the blends was chosen to have at this preliminary stage of the investigation, the highest mixing rate possible of the two polymers, and therefore to get valid results on whether or not the application functions and is feasible.

4.2 Results and Discussion

4.2.1 B1, B2 and B3 as oxygen barrier monolayers

In the previous chapter, the formation and characterization of homogenous blends between EVOH and PE-HEMA have been described. The introduction of hydrogen-bonding crosslinking in the amorphous phase of B1, B2, and B3 may increase the cohesive energy between the chains which could be translated into a reduction of gas permeability. To investigate the effect of the formation of homogenous blends on oxygen permeability, standard measurements (38 °C, 50% RH) were performed according to ASTM D3985 procedure by the group of Prof. Graiff of the University of Parma.

The thickness-corrected oxygen transmission rates of the PE-HEMA, B1, B2, and B3 are illustrated in Table .

Table 2. Thermal data of PE-HEMA, B1, B2 and B3 obtained from DSC and DMTA. Tβ data of PE- HEMA is referred to literature. [33] The Oxygen barrier values are normalized for the thickness of the films.

Polymer	T_m[a] (°C)	X_c[a] (%)	T_β[b] (°C)	Oxygen barrier [cc · mm/ m² · 24h]
PE-HEMA	103	34	10[33]	384.34
B1	98[x], 147[y]	19[x], 16[y]	49	Too permeable
B2	97[x], 164[y]	40[x], 29[y]	52	833.66
B3	96[x], 163[y]	27[x], 18[y]	44	Too permeable

The superscripts x and y correspond to P1 and EVOH, respectively. [a]Det. *via* the second heating curve of DSC; X_c calc. with heat of fusion for 100% crystalline of PE= 286.2 J/g[34] and of EVOH 32mol%= 128.1 J/g.[35] [b]Det. *via* DMTA.

Upon the formation of the blend between EVOH and P1, a loss of the crystallinity generated by the introduction of ODIN is observed, leading to an increase of the oxygen transmission in both three blends with respect to PE-HEMA. Specifically, B1 and B3 result to be completely ineffective as oxygen barrier films, while B2 which has higher crystallinity values, performs somehow better but worse than PE-HEMA. The introduction of ODIN provides a network of hydrogen bonds capable of generating a homogeneous blend between the two polymers; however, this effect is offset by an increase in the free volume and a decrease in crystallinity, making the blends unsuitable for this kind of application.

4.2.2 Synthesis and characterization of new blends of EVOH and PE-HEMA

Being ODIN a bulky molecule whose introduction led to the strong decrease in the crystallinity of the blend, a novel, and smaller molecule has been synthesized and used for the compatibilization of EVOH and PE-HEMA through hydrogen bonds. Phenyl-urea isocyanate **(1)** has been synthesized by reacting aniline with hexamethylene diisocyanate at room temperature under nitrogen atmosphere (Scheme).

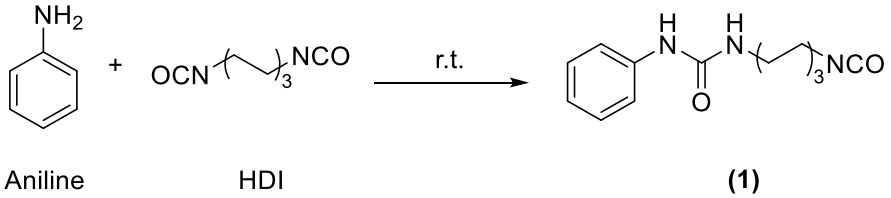

Scheme 1. Synthesis of phenyl urea-isocyanate.

The effects of introducing different content of HEMA into PE were investigated in a study conducted by this research group.[33] A decrease in the PE-HEMA crystallinity has been detected with the increasing content of HEMA, favoring both oxygen and water penetration. For this reason, PE-HEMA with a low content of HEMA (2.1 mol%) was used and grafted with **(1)**.

The synthesis of the grafting reaction is depicted in scheme 2. The reaction was carried out at 100°C in toluene and DMSO, by using dibutyltin dilaurate (DBTDL) as catalyst to promote the reaction. After 12h, at room temperature the promotion of the precipitation of the product was promoted by the addition of isopropanol, and a white polymer was collected after washing with hexane (Scheme).

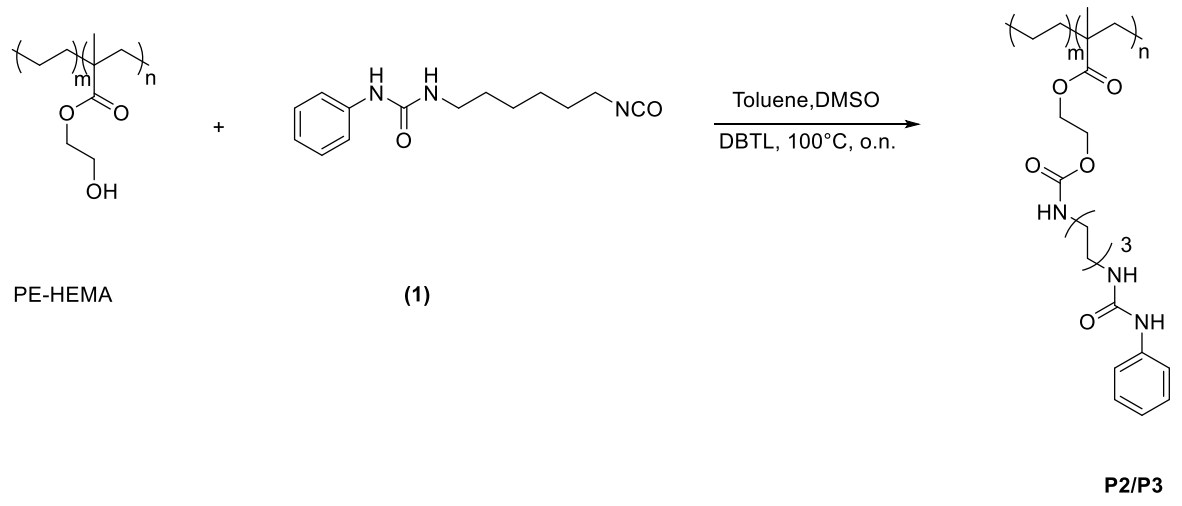

Scheme 2. Synthesis pathway of P2 and P3.

P2 and P3 were obtained by changing the content of **(1)** in the reaction determining different grades of functionalization of HEMA moieties. Table indicates the equivalent (eq.) of **(1)** used, and the corresponding content effectively introduced, determined *via* either NMR or nitrogen elemental analysis (EA). The nitrogen content is diagnostic of the presence of grafted 1.

Table 3. equivalent of **(1)** used in the grafting reaction, content of **(1)** introduced in P2 and P3 calculated *via* ^{1}H-NMR and elemental analysis (EA).

Polymer	eq. of **(1)** in the reaction	Content of **(1)** *via* ^{1}H-NMR (mol%)	Content of **(1)** *via* Nitrogen-EA (mol%)
P2	2.2	52	54
P3	4.4	90	88

The equivalent of **1** is referred to one equivalent of OH groups present in PE-HEMA.

The content of **(1)**, effectively grafted onto PE-HEMA chains, obtained *via* NMR peak integration, matched with the one given by elemental analysis using the nitrogen content for quantification, confirming that no traces of unreacted **(1)** are dispersed into the polymer. ^{1}H-NMR spectra, as already described in chapter 3, revealed the downfield shift of the signals related to the functionalized methylene groups of HEMA (Figure). From the ratio of the unfunctionalized and functionalized HEMA methylene signals is possible to determine the degree of functionalization.

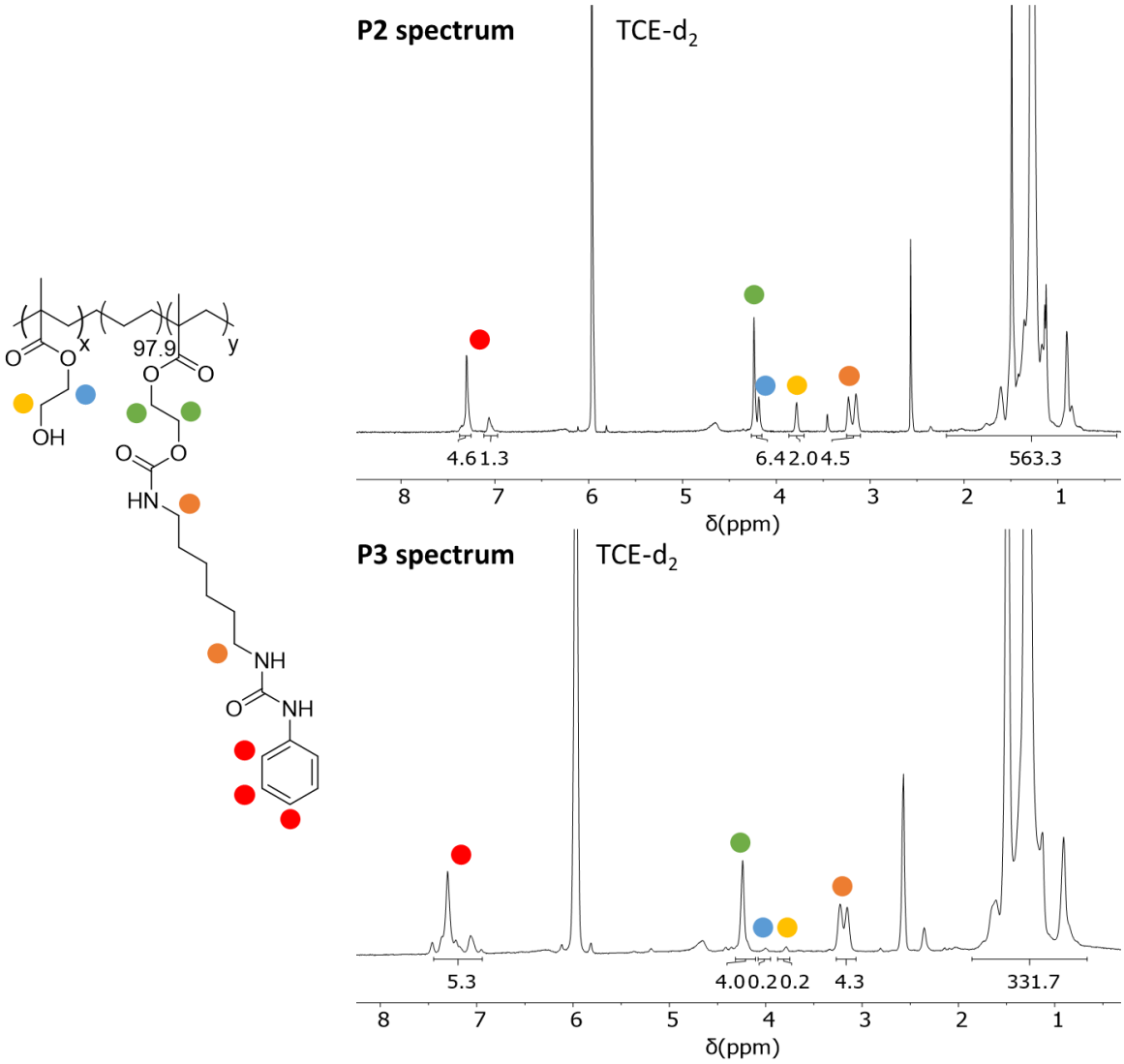

Figure 2. ^{1}H-NMR (TCE-d_2, 80°C, 400 MHz) of P2 (top) and P3 (bottom); for P2 x =1, y = 1.0; for P3 x = 0.1, y = 1.9.

A single blend of P2 with EVOH and another one of P3 and EVOH were prepared by mixing the two polymers with a ratio of 1:1 weight-to-weight. Homogeneous solutions of EVOH in DMSO and **P2** or **P3** in ODCB were mixed at 110°C for three hours. The possible interactions provided by the H-bonds between the polymers, in the resulting blends are reported in Scheme .

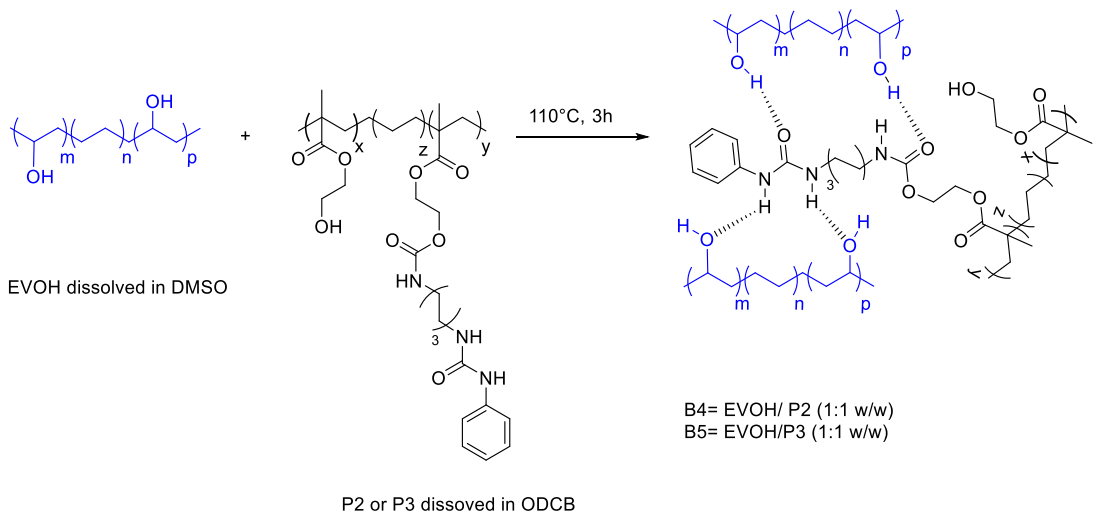

Scheme 3. Formation of the blends B4 and B5 with H-bonding motifs.

Homogenous white precipitates were recovered by adding isopropanol to the solution cooled at room temperature. The two blends obtained, underwent extensive cycles of drying under vacuum at 60°C to eliminate any trace of solvent. The experimental composition of B4 and B5 have been determined by detecting the nitrogen content in the blends *via* EA, since only P2 or P3 contains nitrogen (Table). As with B1, B2, and B3, the new two blends, once formed were insoluble in both DMSO, ODCB, and combinations of these solvents.

Table 4. Initial composition of B4 and B5, content of nitrogen obtained *via* Elemental Analysis and corresponding experimental composition of the resulting blend.

Polymer	Initial component composition (EVOH:P2/P3)	Calculated Nitrogen content (%)	Nitrogen content (%)	Experimental composition (EVOH:P2/P3)
EVOH	-		-	-
P2	-		2.3	-
P3	-		3.1	-
B4	1:1 (w/w)	1.2	0.6	7:3
B5	1:1 (w/w)	1.6	1.3	6:4

The experimental composition of the blends obtained *via* elemental analysis indicates an excess of EVOH, as already noted for B1, B2, and B3. In B5, which is made with the richest phenyl-urea PE-HEMA, the content of P3 capable to interact with EVOH is slightly higher than B4 which brings fewer phenyl-urea moieties.

Table 5. Thermal data of EVOH, P2, P3, B4 and B5 obtained from DSC and DMTA.

Polymer	T_m [a] (°C)	X_c [a] (%)	T_β [b] (°C)
EVOH	172	59	67
P2	95	33	32
P3	97	34	22
B4	103^x,175^y	23^x, 18^y	52
B5	98^x,154^y	20^x, 10^y	44

The superscripts x and y correspond to P2 or P3 and EVOH, respectively. [a]Det. *via* the second heating curve of DSC; *Xc* calc. with heat of fusion for 100% crystalline of PE= 286.2 J/g[34] and of EVOH 32mol%= 128.1 J/g.[35] [b]Det. *via* DMTA.

Table shows the thermal properties of the P2 and P3 and the corresponding blends. The melting temperature and the degree of crystallinity (calculated as in equation 1 in chapter 3) were detected *via* DSC (Figures S1-S4), while the T_β were determined *via* DMTA (Figure). Upon the formation of blends B4 and B5, the degree of crystallinity decreases in comparison with EVOH, P2, and P3. The presence of a single T_g is one of the diagnostic information to assess the compatibilization between two immiscible polymers.[36] The T_g transition is usually detected *via* DSC, but since this transition is not visible for these polymers, the T_β transition detected *via* DMTA is considered. Tanδ thermograms in Figure 3 show the presence of a single T_β for each blend, located in the middle of the T_β of the blend constituents, which is indicative of homogeneous mixing.

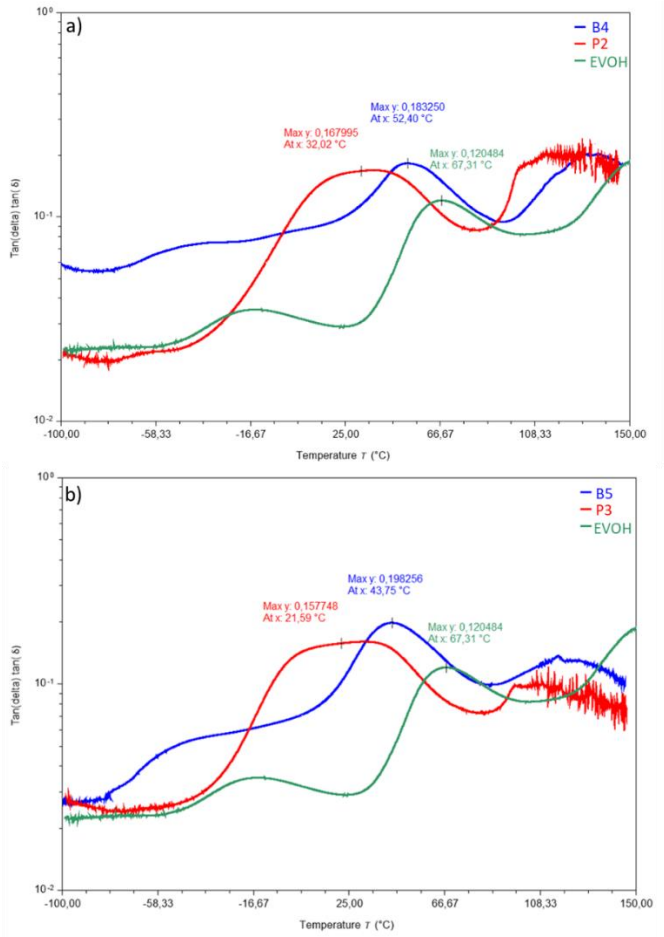

Figure 3. Tanδ curves obtained *via* DMTA of a) B4 (blue line), P2 (red line), EVOH (green line) and b) B5 (blue line), P3 (red line), EVOH (green line).

4.2.3 Morphological study of P2, P3, B4, and B5

In order to study the morphology of the blends, films of each sample were obtained *via* compression molding at 180°C. Samples P2, P3, and the respective blends, B4 and B5, were analyzed by multiphoton microscope to evaluate the distribution of PEHEMA functionalized with phenyl-urea within the material. All samples were analyzed with excitatory radiation at three different wavelengths of 820 nm by the group of Prof. Sissa of the University of Parma.

The images in Figure a,b show the distribution of the chromophore in P2 and P3. A homogeneous emission in the region spectral of green is observed, even if chromophore accumulations can be identified in some areas of the materials (Figure a,b).

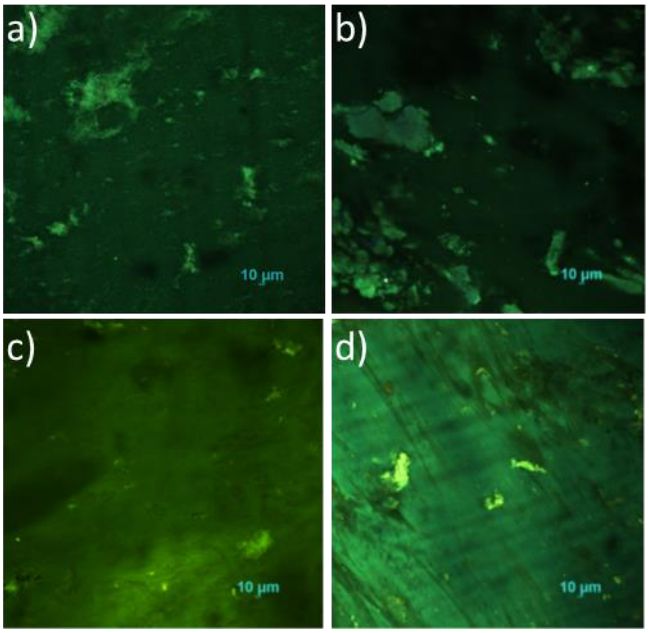

Figure 4. Fluorescence images of the surface of a) P2, b) B4, c) P3, and d) B5 acquired exiting the samples at 820 nm.

The correspondent blends B4 and B5, exhibit a morphology more homogeneous than P2 and P3. Three-dimensional scans were also taken using a wavelength of 820 nm (Figure). P2 and P3 have a homogeneous chromophore distribution within the sample, however, the emission of B4 and B5 is not homogeneous across the entire thickness, but on the surfaces, the emission is more intense compared to the central portion. Images of the blends show that EVOH, is almost present in the inner part of the film, instead, P2 and P3 are placed close to the surfaces. The hydrogen bonds provided by phenyl-urea are insufficient to achieve the creation of a homogeneous blend and hence the compatibilization of the two polymers.

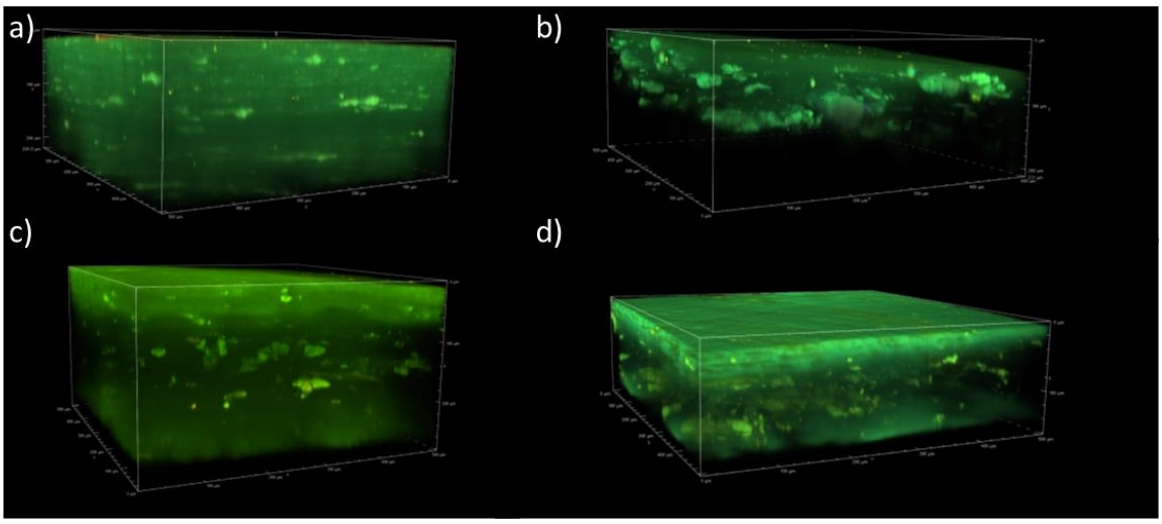

Figure 5. 3D reconstruction of Z-stack images of a) P2 (thickness of 250 µm), b) P3 (thickness of 260 µm), c) B4 (thickness of 210 µm), and d) B5 (thickness of 180 µm). The images were collected exciting the samples at 820 nm.

To better analyze the distribution of the two polymers in the samples, Raman spectroscopy was used thanks to the collaboration with Prof. Masino of the University of Parma. The spectra were acquired at 785 nm to reduce the fluorescence of the samples. The spectra of the blends, acquired at three different points of the surface, are a linear combination of the spectra of the pure components. Thus, preliminary measurements confirm a homogeneous composition on the surface of the blends (Figure).

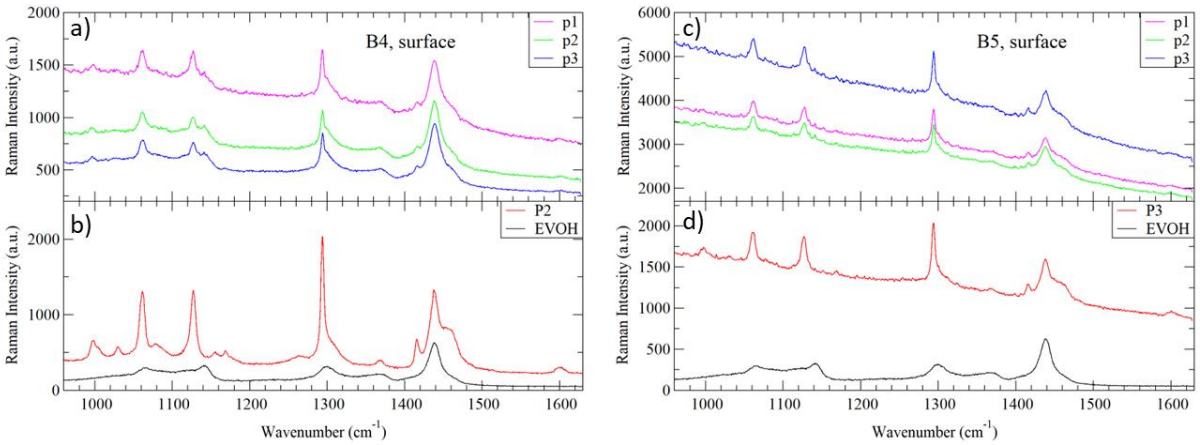

Figure 6. Raman spectra collected at 785 nm of a) surface of B4 in three different points p1, p2, and p3; b) surface of P2 and EVOH; c) surface of B5 in three different points p1, p2, and p3; d) surface of P3 and EVOH.

Classical least-squares (CLS) method was used to identify and quantify from the Raman spectra the content of the two polymers inside the blends. The composition of the blends has been defined by mapping both the surface (xy axes) and thickness (xz axes) at various positions. Figure a depicts the examined part of the surface of B4 and the corresponding content of P2. The darker areas correspond to the regions with the lowest amount of P2, while the light green areas correspond to the regions with the most. The average of these measurements on the surface results in a P2:EVOH composition ratio of 70:30. The similar approach was applied for B5, resulting in an 80:20 P3:EVOH ratio on the surface(Figure b). The visual distribution of the two polymers on the surface of the samples obtained *via* 2PM, is confirmed by Raman spectroscopy both for the homogeneity and for the composition (excess of PE-HEMA).

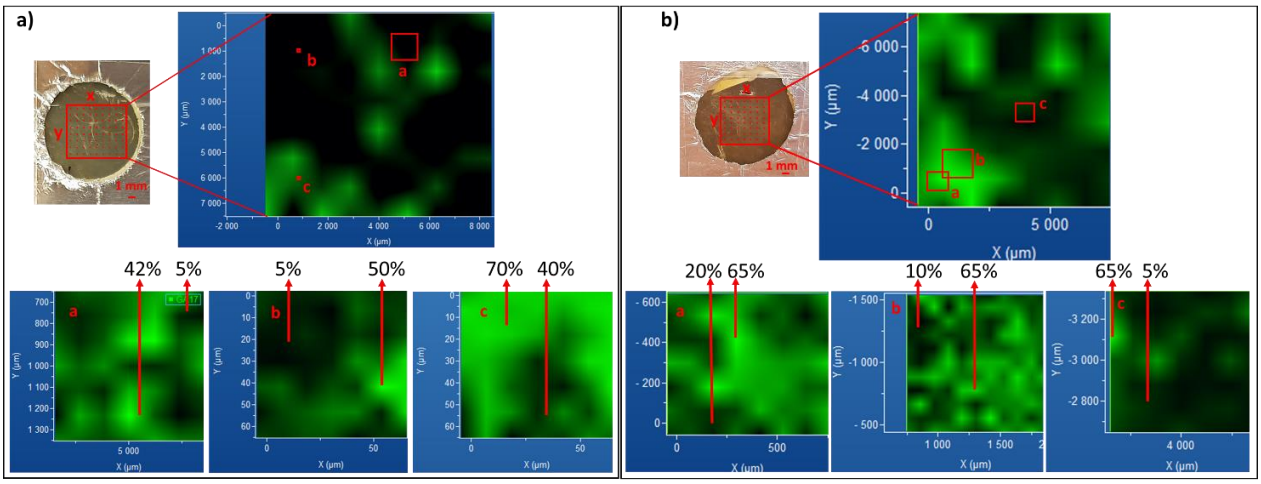

Figure 7. images obtained from the mapping of a) B4, and b) B5. The percentage indicated are referred to the content of a) P2, and b) P3.

Mapping the section of both B4 and B5, two layers with different P2/P3:EVOH ratios are observed. The darker portion, in the inner part of the films, is formed of a P2/P3:EVOH ratio of 5:95 for both the blends, supporting the 2PM findings on the presence of different layers in the films (Figure and Figure S11 for B5). The comparison between the spectra of the surface and the incision area of B4 (see Figure c,d) highlights the difference in composition, revealing that the peaks associated with P2 are no longer visible in the incision spectrum.

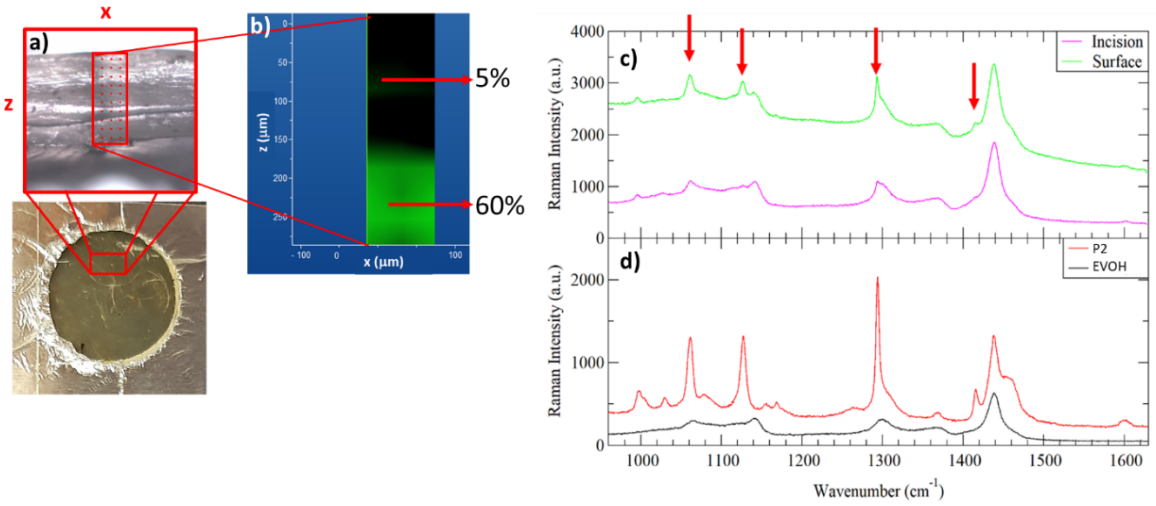

Figure 8. a) microscope image of the incision area xz (top) image of B4 film (below), b) images of the xz mapping of B4, c) comparison of the spectra of the surface (green line) and the bulk (pink line) of B4, d) spectra of reference materials P2 (red line) and EOVH (black line); the percentage are referred to the content of P2.

The compositions obtained from Raman investigations are summarized in the table below (Table).

Table 5. Surface and incision composition of the blends obtained *via* Raman spectroscopy.

Blend	Surface composition (EVOH:P2/P3) [%]	Incision composition (EVOH:P2/P3) [%]
B4	30:70	95:5
B5	20:80	95:5

4.2.4 Barrier properties

The characterization of the barrier properties of the different blends and the functionalized PE-HEMA was carried out by O_2 permeability measurements under conditions of 38 ºC and 50% relative humidity. The results of measurements conducted in oxygen are shown in Table .

Table 6. Thickness of the films and O_2 transmission rate obtained after thickness correction of PE-HEMA, P2, P3, B4, and B5.

Material	Thickness [μm]	O_2 transmission rate thickness correction [cc·mm/(m^2·24h)]
PEHEMA	210	384.35
P2	250	14063.78
B4	210	1639.80
P3	260	382.85
B5	180	294.0

The outcomes of the two functionalized PE-HEMA are rather heterogeneous as regards the data obtained. It is possible to notice how the addition of compound **(1)** can, at 54 mol% of functionalization, favor the drastic increase of the permeability with respect to PE-HEMA, but as regards P3, a functionalization of 88 mol% almost makes the permeability behavior unchanged compared to PE-HEMA. The difference in the performances between P2 and P3 could be explained by considering a larger amount of H-bonding between the phenyl-urea – phenyl-urea moieties, which increases the cohesive energy density (CED) of P3 over P2 and hence decrease permeability. The stronger interaction between the phenyl-urea moieties can be observed considering the rubbery plateau of the storage modulus thermograms (Figure). P3 exhibit a higher rubbery plateau from 100°C to 145°C, specifically at 145°C the modulus of P3 is 2.2 MPa, instead, the modulus of P2 is 0.7 MPa.

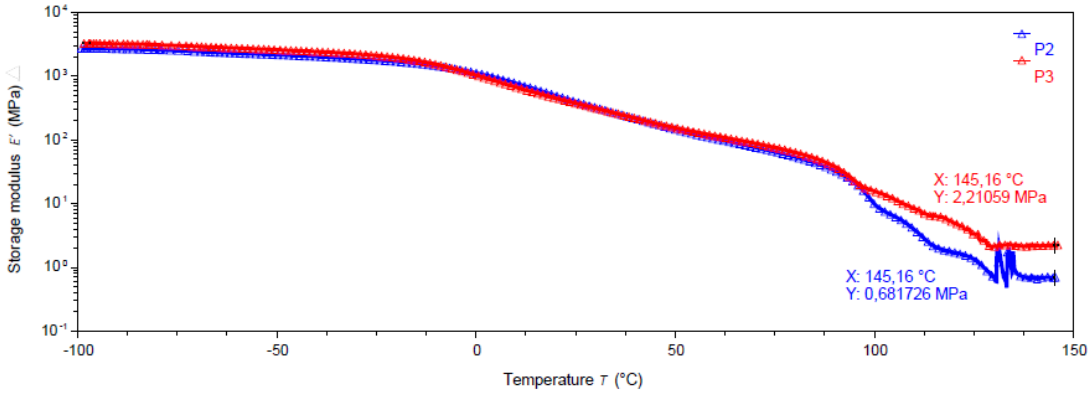

Figure 9. storage modulus thermograms of P2 and P3.

Mixing EVOH with P2 and P3 results in an increased permeability performance with respect to both functionalized PE-HEMA. Although B4 experiments a very important reduction of the diffusion of oxygen through the film compared to P2, its performance is still poor. B5, on the contrary, lowers the oxygen transmission rate with respect to PE-HEMA. The enhanced performance of the blends is most likely due to an uneven distribution of the two components. Because PE-HEMA is largely present on the surface and EVOH is in the core of the films, this should help protect EVOH from humidity and hence increase the barrier properties.

Several attempts have been made to boost the barrier characteristics by adjusting the ratio of P3 and EVOH. Unfortunately, increasing the EVOH, a complete loss of the barrier properties is observed, instead, increasing the percentage of P3 results in a macroscopical segregation of the two polymers, demanding further investigation.

4.3 Conclusions

This research aims to develop polymer blends that can operate as oxygen barriers in order to replace the multilayer films now used in food packaging and to assess the viability of a monolayer. The permeability to the oxygen of several blends of EVOH and PE-HEMA was tested under standard conditions at 38°C and 50% RH. The blends B1, B2, and B3 produced by combining EVOH and PE-HEMA functionalized with ODIN are not capable of acting as oxygen barrier monolayers, because the introduction of a bulky molecule like ODIN generates too much free volume between the polymer chains. As a result, the compatibilization of the two polymers was attempted using phenyl-urea, a smaller molecule that, through the hydrogen bond network, should be able to compatibilize the two polymers while retaining the crystallinity of the blends. Phenyl-urea isocyanate was used to functionalize PE-HEMA, and two different levels of functionalization were obtained: ~50% for P2 and ~90% for P3. The latter has slightly higher barrier characteristics than pristine PE-HEMA, but P2 exhibits a significant loss in performance. Two blends were produced by mixing P2 or P3 with EVOH with a weight ratio of 1:1, the actual composition of the blends was calculated *via* elemental analysis which always reveals an excess of EVOH in the final blend in comparison to the theoretical composition. The actual formation of homogenous blends was investigated through the use of both 2PM and Raman spectroscopy. Both approaches validate the uneven polymer distribution in both blends, B4 and B5, demonstrating the presence of functionalized PE-HEMA on the surfaces of the films while leaving the EVOH in the inner part. The obtained partial segregation of the two polymers mirrors the commercial PE-EVOH-PE triple layer films and appears to improve the barrier properties of the blends: a lower oxygen transmission rate compared to the respective functionalized PE-HEMA, is observed. More research is needed to determine whether changing the ratio of the blend compositions can increase self-segregation and barrier characteristics.

4.4 Experimental section

Methods

Nuclear magnetic resonance. NMR spectra were recorded on a Bruker Advance 400 (400 MHz). Chemical shifts are reported in parts per million (ppm). ^{1}H-NMR chemical shifts are given in reference to the residual solvent peak (2.50 ppm for deuterated dimethyl sulfoxide (DMSO-d_6) and 6.00 ppm for deuterated 1,1,2,2-Tetrachloroethane (TCE-d_2). High-temperature NMR spectra were recorded at 80°C in TCE-d_2.

Infrared spectroscopy (IR). Infrared absorption spectroscopy analyses were performed with a Perkin Elmer FT-IR Spectrum Two instrument in the mode of Attenuated Total Reflectance (ATR) using powder samples. The background was subtracted from every spectrum recorded. The IR spectra were measured also in transmission mode, using a Bruker IFS-66 FT-IR spectrometer coupled to a Hyperion 1000 IR microscope.

Elemental Analysis (EA). Elemental analyses were recorded on a CHNS Thermo Fisher FlashSmart. The nitrogen content was determined using thermal conductivity (TC) and volumetric analysis.

Differential scanning calorimetry (DSC): Melting temperatures (T_m) and enthalpies of the transition (ΔH_m) were measured by differential scanning calorimetry (DSC) using a DSC Q20N V24.11 Build 124 from TA instrument. DSC measurements were carried out under nitrogen between -50°C and 200 °C at a scan rate of 10 °C min^{-1}. The sample weight was in the range of 2-4 mg. The transitions were measured in the second heating curves.

Compression molding. Polymer films and samples for DMTA and microscopy analysis were obtained by following the following protocol: Appropriate molds were filled with the polymer powder, followed by treating the material in a pre-heating step for 5 min at 180 °C, then for 10 min at 180 °C with an applied force of 100 kN and finally cooling at a rate of 15 K min^{-1} until a temperature of 40°C was reached while maintaining the applied force.

Dynamic mechanical analysis (DMTA). Rectangular samples suitable for DMTA were cut to a dimension of 3 x 5 x 0.5 mm (length x width x thickness). Samples were measured on a TA Instruments *Q800* in tensile mode. The E',E" and Tanδ were monitored while screening the samples during a temperature sweep from -100 °C to 150 °C at 3 °C min^{-1}. An oscillation frequency of 1 Hz with an oscillation amplitude of 20 µm was applied.

Two-photon microscopy (2PM): The polymer specimens were characterized with a Two-Photon Microscope Nikon A1R MP+ Upright supplied with a femtosecond pulsed laser Coherent Chameleon Discovery (~ 100 fs pulse duration with 80 MHz repetition rate, tunable wavelength

output 660-1320 nm). To focus the excitation beam and to collect the two-photon excited fluorescence (TPEF) signal, a 25x water dipping objective with a numerical aperture (N.A.) 1.1 and a working distance of 2.0 mm was used. Due to the characteristics of the samples (thin films), we decided to collect images in the air (instead of water). This choice affects the N.A. (which becomes lower) and as a consequence the resolution. In fact, according to the Rayleigh criterion, in multiphoton microscopy the lateral resolution (x-y) is $d = \frac{0.61\lambda}{N.A.}$, while the axial resolution is $z = \frac{2n\lambda}{N.A.^2}$, where λ is the excitation wavelength, n the medium the refractive index, and $N.A.$ the numerical aperture.[37] TPEF signal was directed by a dichroic mirror to a series of three non-descanned detectors (high sensitivity GaAsP photomultiplier tubes) allowing fast image acquisition. Optical filters preceded the detectors allowing the simultaneous acquisition of three separated channels: blue channel (415-485 nm), green channel (506-593 nm), and red channel (604-679 nm). The operation software of the microscope performed the overlay and the processing of the three channels images. A fourth photomultiplier GaAsP detector, connected to the microscope through an optical fiber and preceded by a dispersive element, was used to record emission spectra of the two-photon excited samples (wavelength range 400-630 nm with a bandwidth of 10 nm). Z-stack acquisitions were collected with 0.5 µm steps and images with a field of view of 500x500 µm (1024x1024 pixel) and a 2.2 s dwell time. During Z-stack acquisitions, several 2D images of the sample are collected at different depths (in this case one image every 0.5 µm) and then processed by the microscope software to obtain a 3D reconstruction of the sample.

Raman micro-spectrometer: Raman spectra with 785 nm excitation were recorded with Horiba LabRAM HR Evolution spectrometer equipped with the appropriate edge filter. Spectral resolution was 2 cm^{-1} and objective magnification of 50x was used. Map of the incision of B4 was obtained with the following parameter: 300 µm x 90 µm, 30 points, step 30 µm. Three maps of the surface of B4 were made using for Map a) 700 µm x 700 µm, 49 points, step 100 µm; Map b) 70 µm x 70 µm, 49 points, step 10 µm; Map c) 70 µm x 70 µm, 49 points, step 10 µm. Section map of B5 was obtained with: 80 µm x 110 µm, 88 points, step 10 µm. Three maps of the surface of B5 were made using for Map a) 800 µm x 700 µm, 56 points, step 100 µm; Map b) 1100 µm x 1100 µm, 121 points, step 100 µm; Map c) 700 µm x 700 µm, 49 points, step 100 µm

Measurements of oxygen permeability: The measurements were made with an Extrasolution multiperm instrument 050, the sample surface analyzed is 2.01 cm2. Reference standard: ASTM D 3985. The samples were conditioned in advance in a ventilated oven at 30 ºC for at least 5 hours

before analysis. The following conditions were chosen for the analysis: 38°C and 50% relative humidity.

Materials

Unless otherwise specified, chemicals and solvents were purchased from Sigma-Aldrich and used as received. Poly(ethylene-co-(2-hydroxyethyl methacrylate) (PE-HEMA, 2.1% mol of HEMA) was provided by SABIC. Co-polymer Ethylene Vinyl-Alcohol (EVOH, 32 mol% of ethylene) was purchased from EVALTM.

Synthesis

Synthesis of 1-(6-isocyanatohexyl)-3-phenylurea (**1**).

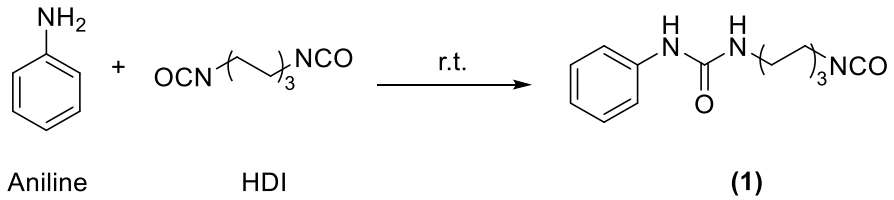

Aniline (1 g, 0.011 mol) was added to a round-bottom flask and kept under nitrogen atmosphere by three consequent vacuum/nitrogen cycles. Hexamethylene diisocyanate, HDI, (20 mL,0.12 mol) was added to the reaction flask. The reaction mixture was maintained at room temperature while stirring. After 4 h, cyclohexane was added to promote the precipitation. The precipitate was filtered off and washed with cyclohexane to remove the excess of HDI, and the white obtained solid was dried in a vacuum oven at 40°C for two hours (75% yield).

^{1}H NMR (600 MHz, DMSO-d6): δ (ppm) = 1.29 (m, 4H), 1.38 (m, 2H), 1.52 (m, 2H), 3.03 (m, 2H), 3.31 (t, J= 6.7 Hz, 2H), 6.05 (t, J= 5.6 Hz, 1H), 6.83 (tt, J_1= 7.4 Hz, J_2= 1.2 Hz, 1H), 7.16 (m, 2H), 7.33 (dd, J_1= 8.7 Hz, J_1= 1.2, 2H), 8.31 (s, 1H).

IR, ϑ (cm^{-1}): 3319 (N-H stretching), 2933 (C-H stretching), 2958 (C-H stretching), 2262 (N=C=O stretching), 1648 (C=O stretching), 1596 (N-H bending, urea), 1551 (C-N stretching).

*Synthesis of PE-HEMA-phenylurea polymer (**P2 and P3**).*

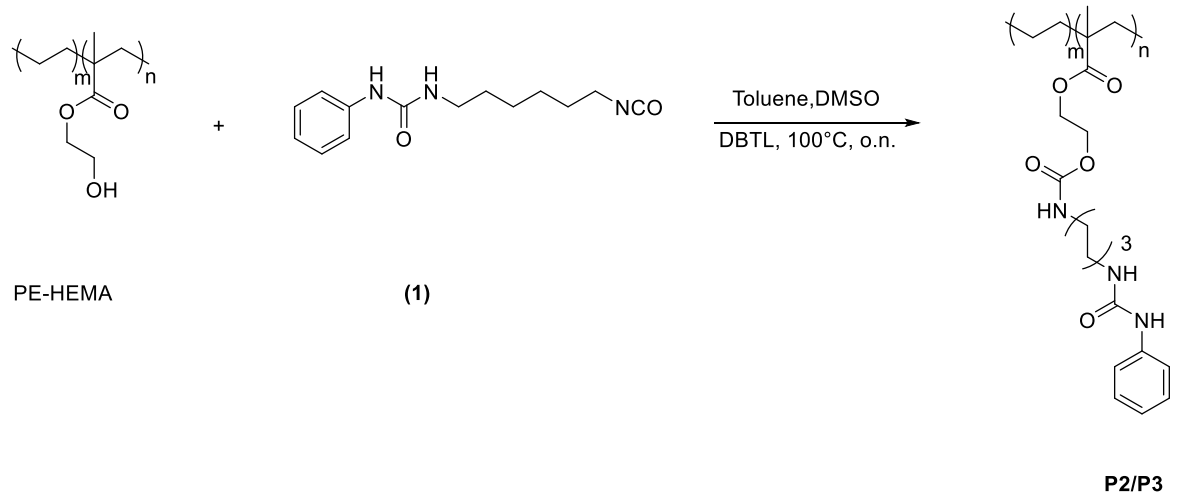

P2

The PE-HEMA *co*-polymer was functionalized according to the following procedure: dry toluene (45 mL) was inlaid in an anhydrous Schenk, and after three cycles of freeze-pump-thaw PE-HEMA (1 g, 1 eq of OH groups) was added and dissolved at 100 °C for 1 h. Compound **1** (200 mg, 2.2 eq. with respect to OH groups of PE-HEMA) was added as a solid, followed by the addition of 1 mL of DBTDL as catalyst and 5 mL of DMSO to promote the dissolution of **1**. After 12h the solution was cooled at room temperature and the formation of a gel is observed. Isopropanol was added to promote the precipitation of the functionalized polymer as a solid. A white product was then filtered under vacuum, washed with isopropanol, and dried in a vacuum oven ad 60°C for 72 h.

^{1}H NMR (400 MHz, TCE-d_2, 80°C): δ(ppm) = 0.5-2.5 (m, PE backbone), 3.11-3.43 (m, 4H), 3.86 (t, J=4.7 Hz, 2H), 4.26 (t, J=4.7 Hz, 2H), 4.31 (bs, 4H), 7.13 (m, 1H) 7.24-7.48 (m, 4H).

IR, ϑ (cm-1): 3321 (O-H, N-H stretching), 2915 (C-H stretching), 2848 (C-H stretching), 1730 (C=O stretching, HEMA), 1563 (C=O stretching, urea), 1462 (C-H bending), 1246 (C-O stretching, ODIN).

Elemental Analysis: From the content of nitrogen given by the elemental analysis the percentage of functionalized HEMA is calculated to be 54 mol%. Since HEMA is the 2.1 mol% of the entire polymer we can easily conclude that the degree of functionalization of PE-HEMA is 1.1 mol%. (C, 79.55%; H, 12.86%; N,2.33%).

P3

The PE-HEMA *co*-polymer was functionalized according to the following procedure: dry toluene (45 mL) was inlaid in an anhydrous Schenk, and after three cycles of freeze-pump-thaw PE-HEMA (1 g, 1 eq of OH groups) was added and dissolved at 100 °C for 1 h. Compound **1** (400 mg, 4.4 eq. with respect to OH groups of PE-HEMA) was added as a solid, followed by the addition of 1 mL of DBTDL as catalyst and 5 mL of DMSO to promote the dissolution of **1**. After 12h the solution was cooled at room temperature and the formation of a gel is observed. Isopropanol was added to promote the precipitation of the functionalized polymer as a solid. A white product was then filtered under vacuum, washed with isopropanol, and dried in a vacuum oven ad 60°C for 72 h.

^{1}H NMR (400 MHz, TCE-d_2, 80°C): δ(ppm) = 0.5-2.5 (m, PE backbone), 3.11-3.33 (m, 4H), 3.79 (bs, 2H), 4.97 (bs, 2H) 4.28 (bs, 4H), 7.13 (m, 1H) 7.24-7.48 (m, 4H).

IR, ϑ (cm-1): 3321 (O-H, N-H stretching), 2915 (C-H stretching), 2848 (C-H stretching), 1729 (C=O stretching, HEMA), 1554 (C=O stretching, urea), 1463 (C-H bending), 1237 (C-O stretching, ODIN).

Elemental Analysis, From the content of nitrogen given by the elemental analysis the percentage of functionalized HEMA is calculated to be 70%. Since HEMA is the 2.1 mol% of the entire polymer we can easily conclude that the degree of functionalization of PE-HEMA is 1.5 mol%. (C, 79%; H, 12.76%; N, 3.08%).

General procedure for the formation of the blends between EVOH and PE-HEMA-phenyl-urea ***(P2/P3)***

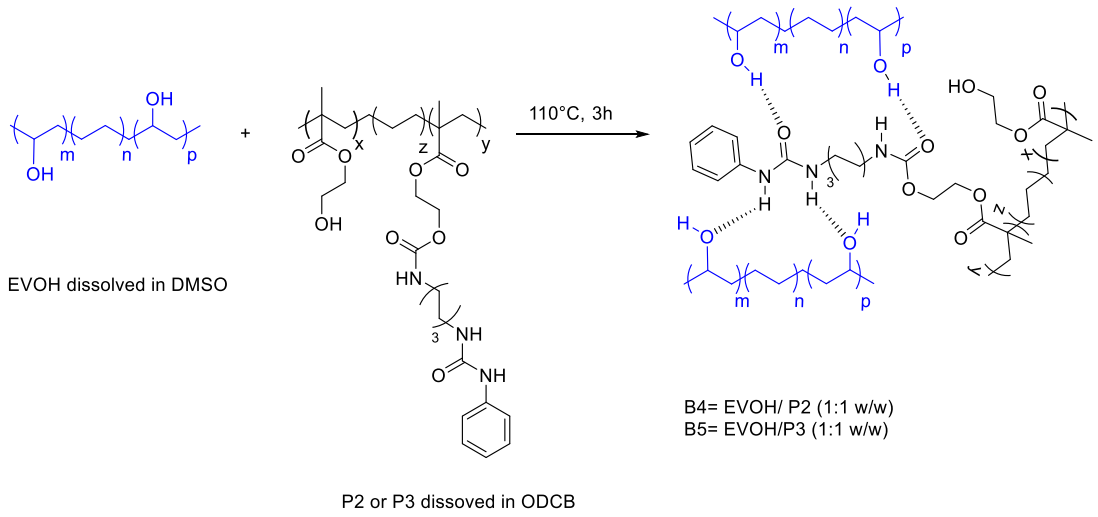

Compound **P2/P3** was dissolved in *o*-dichlorobenzene (8 mg/mL) at 110°C, while EVOH was dissolved in DMSO (50 mg/mL) at the same temperature (Scheme 1). Once the dissolution of both polymers was reached, the solution of EVOH was slowly added to the solution of P1, and the resulting solution was stirred at 110°C for 3 hrs. Subsequently, the solution was cooled to room temperature and 50 mL of isopropanol were added. The obtained precipitate was filtered, washed with isopropanol and dried under vacuum at 60°C for 72 hrs. The blends were characterized by EA and DSC.

4.5 Supporting information

DSC

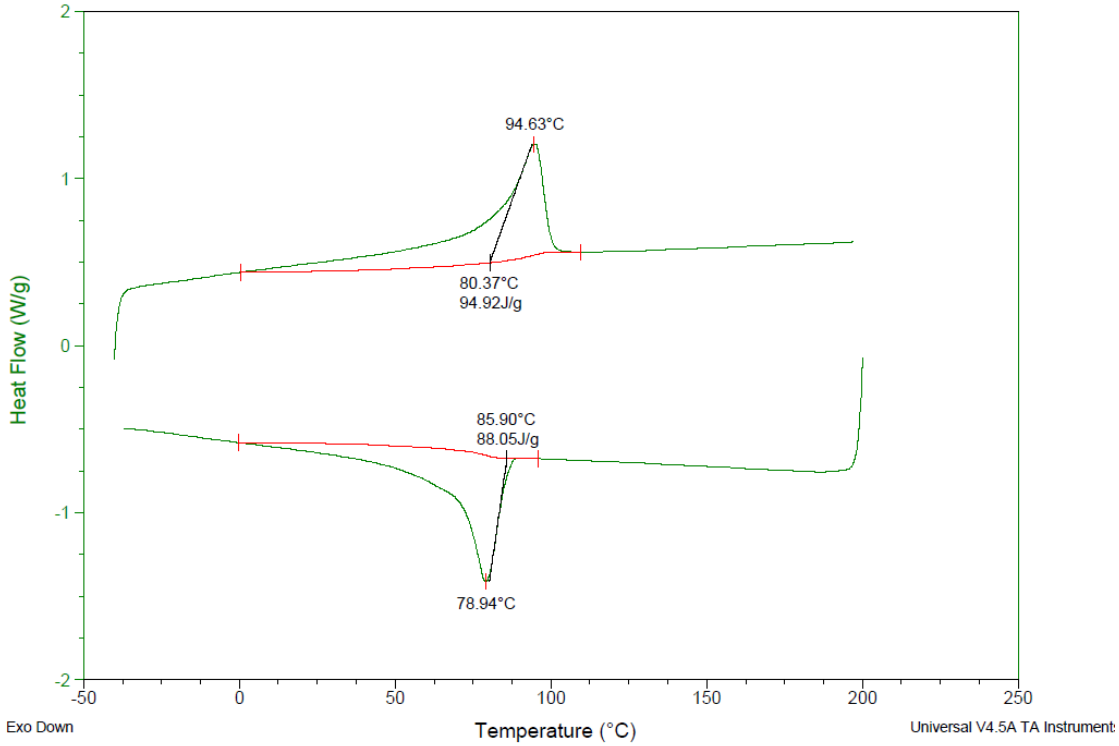

Figure S1. DSC curve of P2.

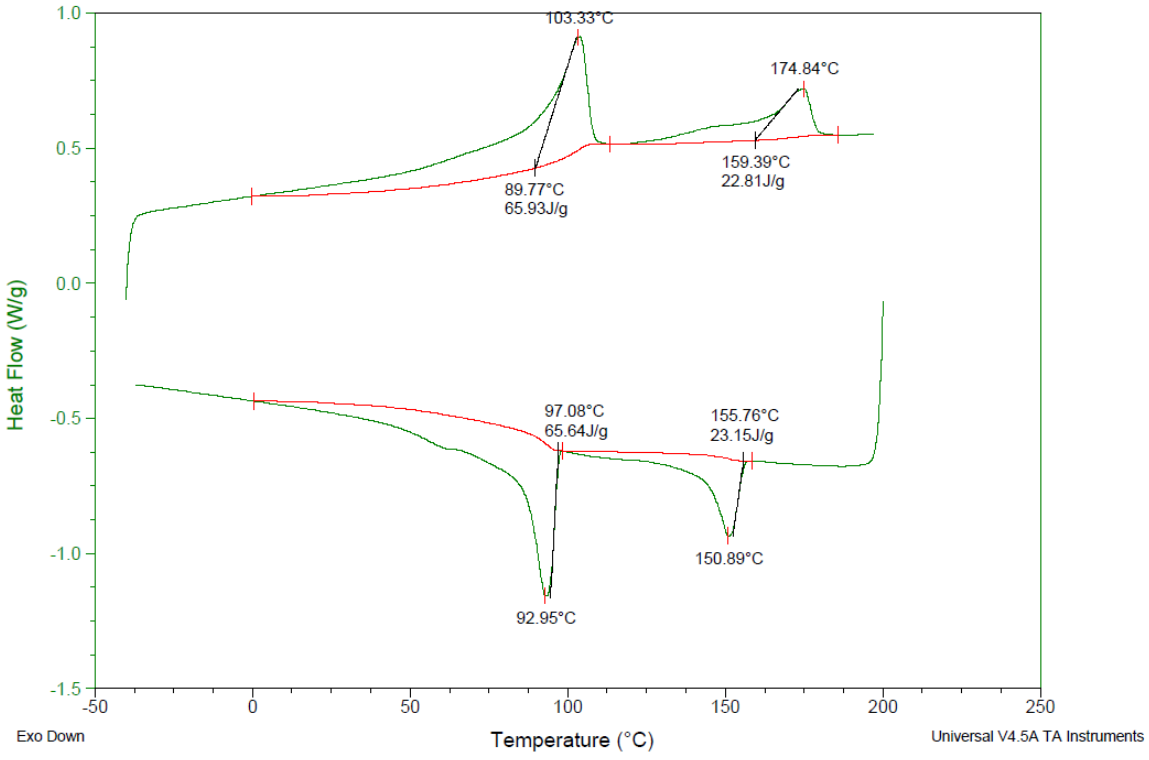

Figure S2. DSC curve of B4.

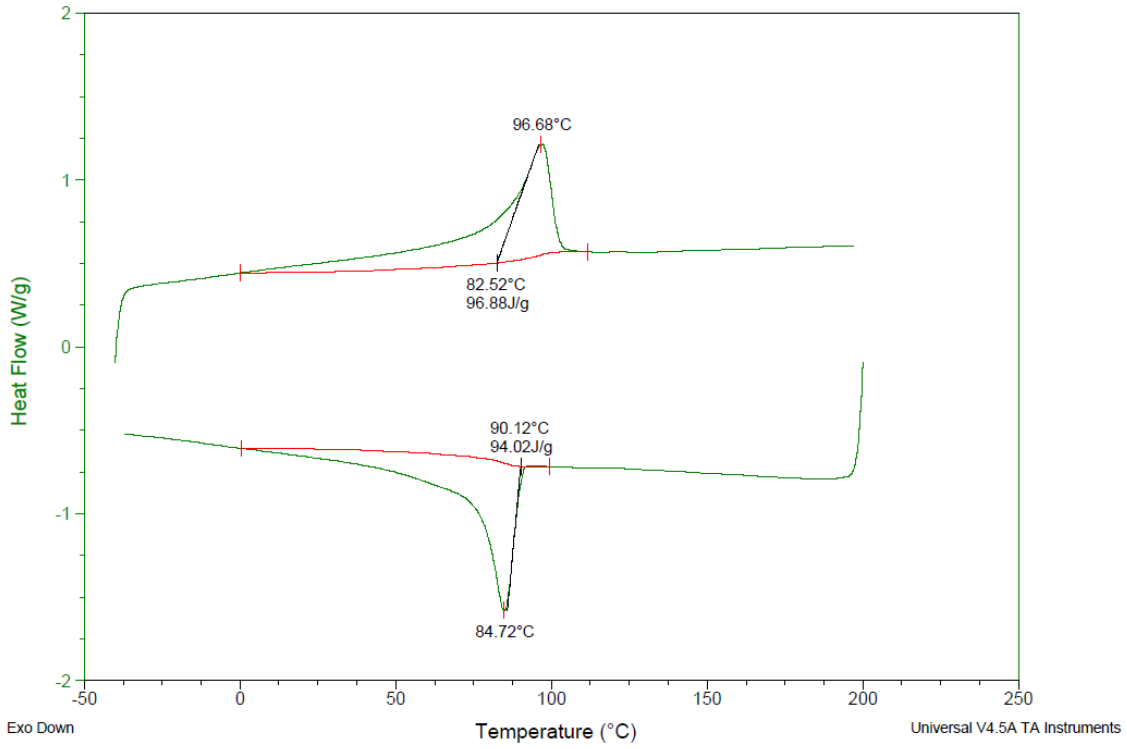

Figure S3. DSC curve of P3.

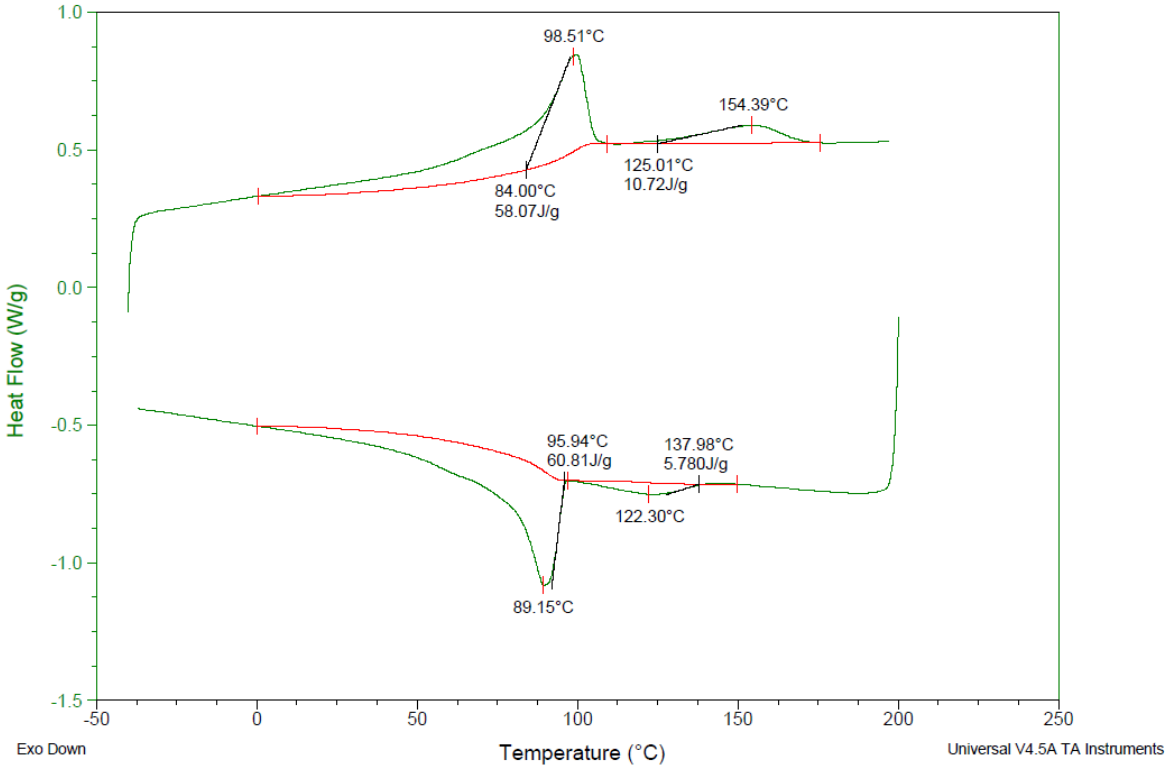

Figure S4. DSC curve of B5

IR spectroscopy

Transmission mode

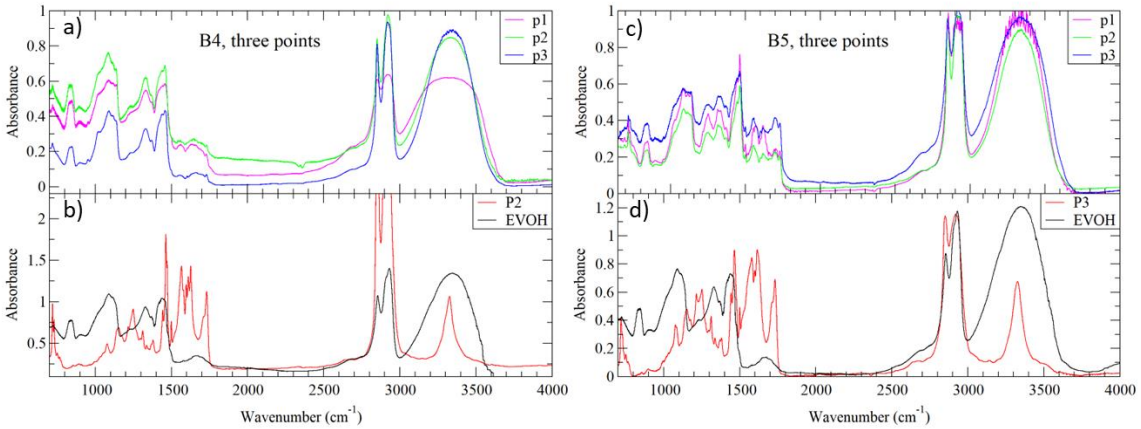

Figure S5. IR spectra of a) surface of B4 in three points, b) surface of P2 and EVOH, c) surface of B5 in three points, and d) surface P3 and EVOH.

Attenuated Total Reflectance - ATR

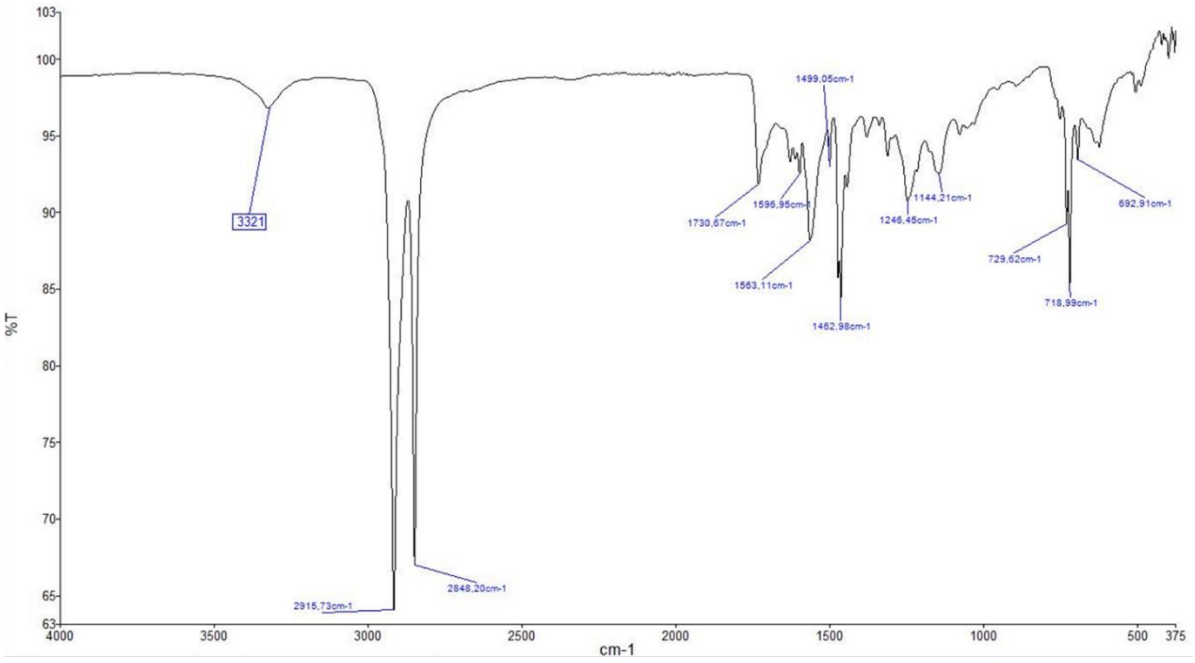

Figure S6. ATR of P2.

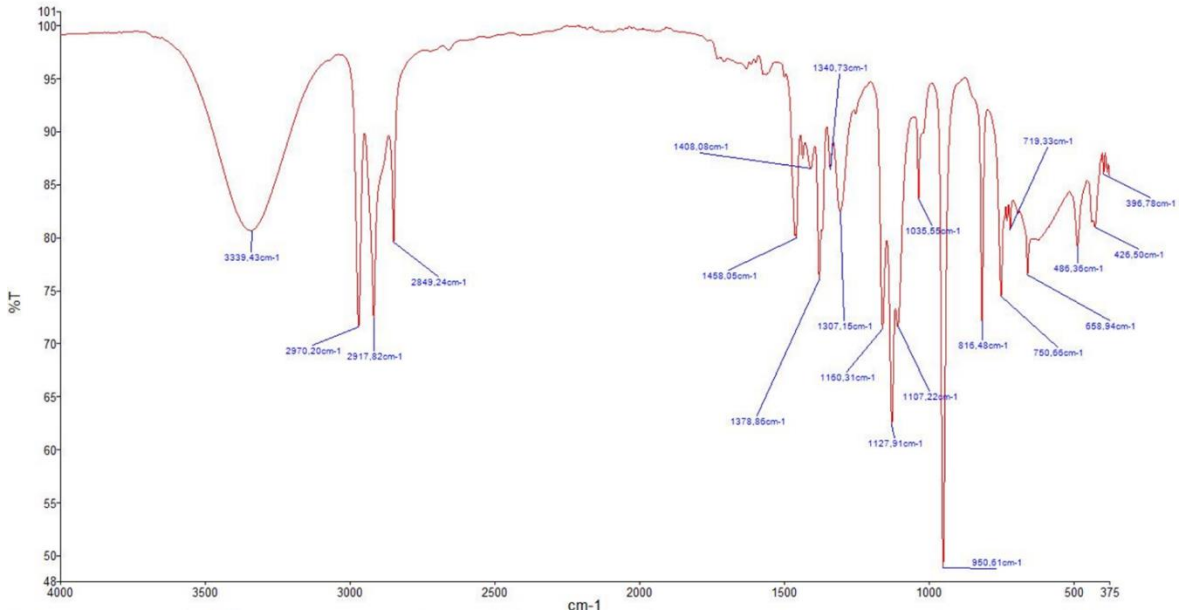

Figure S7. ATR of B4.

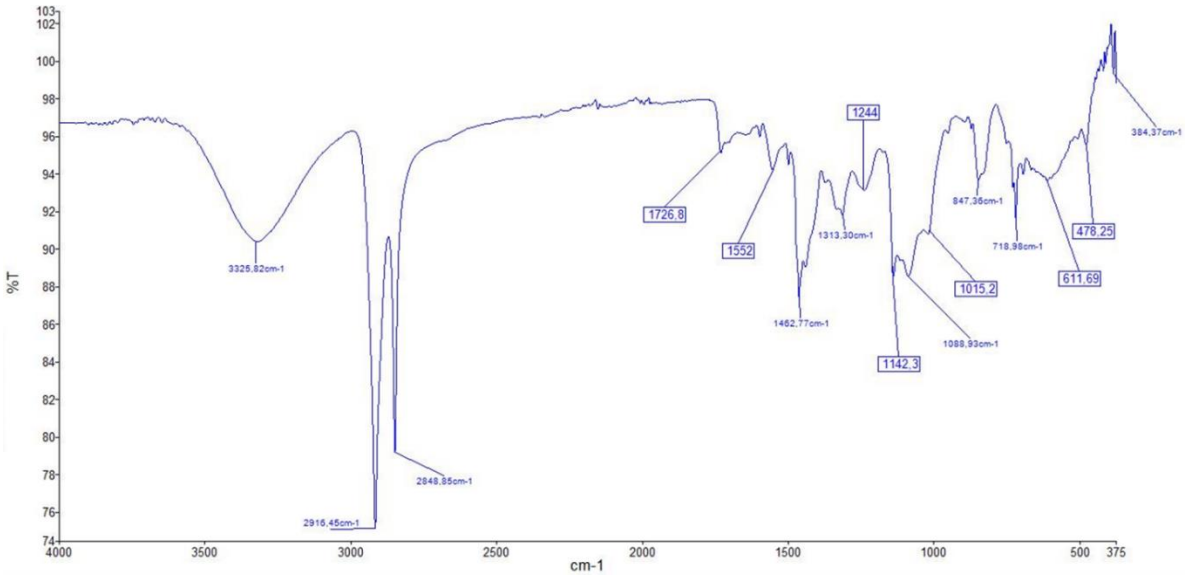

Figure S8. ATR of P3.

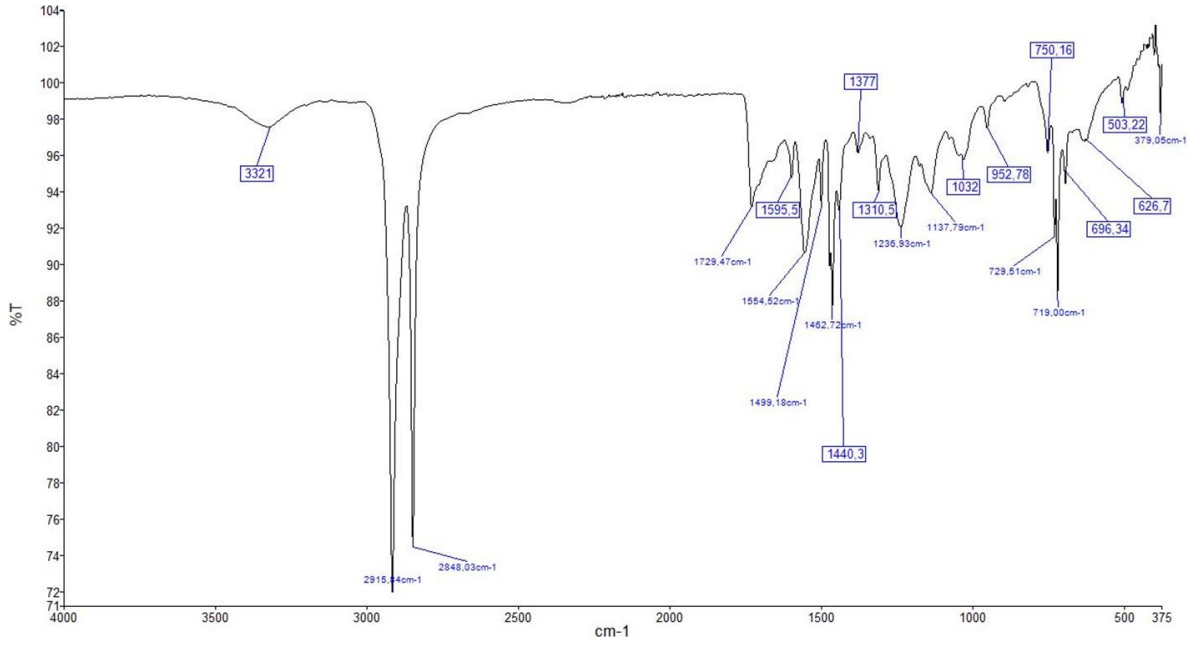

Figure S9. ATR of B5.

2PM

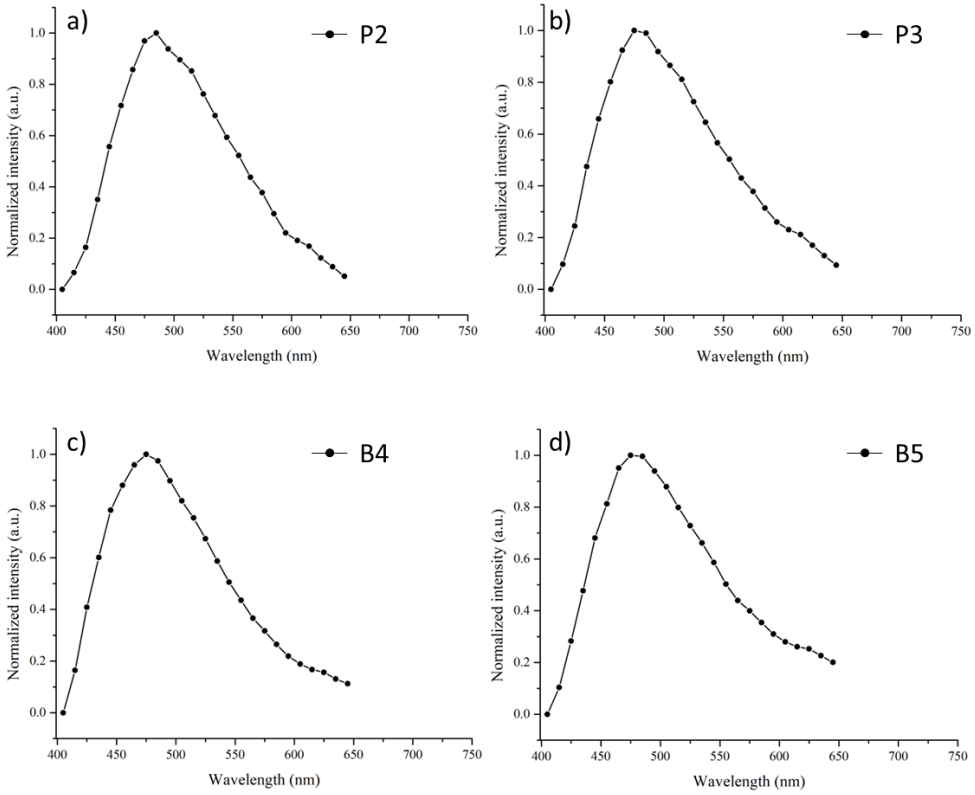

Figure S10. Emission spectra acquired exciting the samples at 820 nm on the surface of a) P2, b), P3, c), B4 and d) B5.

Raman

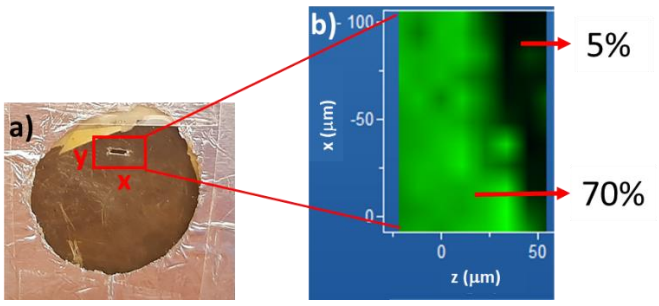

Figure S11. a) image of B5 film; b) images of the xz mapping of B5.

4.6 Reference

[1] A. Bondi, *J. Phys. Chem.* **1964**, *68*, 441.

[2] D. W. van Krevelen, K. te Nijenhuis, *Properties of Polymers: Their Correlation with Chemical Structure: Their Numerical Estimation and Prediction from Additive Group Contributions*, Elsevier, Amsterdam, **2009**.

[3] M. H. Cohen, D. Turnbull, *J. Chem. Phys.* **1959**, *31*, 1164.

[4] K. Ito, L. Hong-ling, Y. Saito, T. Yamamoto, Y. Nishihara, Y. Ujihira, K. Nomura, *JRNC* **2003**, *255*, 437.

[5] M. Muramatsu, M. Okura, K. Kuboyama, T. Ougizawa, T. Yamamoto, Y. Nishihara, Y. Saito, K. Ito, K. Hirata, Y. Kobayashi, *Radiation Physics and Chemistry* **2003**, *68*, 561.

[6] Z. Chen, K. Ito, H. Yanagishita, N. Oshima, R. Suzuki, Y. Kobayashi, *J. Phys. Chem. C* **2011**, *115*, 18055.

[7] H. H. Ketels, Synthesis, characterization and applications of ethylene vinylalcohol copolymers. [Phd Thesis 1 (Research TU/e / Graduation TU/e), Chemical Engineering and Chemistry]. Technische Universiteit Eindhoven, **1989**.

[8] Q. Zhang, W. Lin, Q. Chen, G. Yang, *Macromolecules* **2000**, *33*, 8904.

[9] J.H. Hildebrand, R.L. Scott, *The Solubility of Nonelectrolytes Reinhold*, New York, NY, USA, **1936.**

[10] K. K. Mokwena, J. Tang, *Crit. Rev. Food Sci. Nutr.* **2012**, *52*, 640.

[11] A. S. Michaels, W. R. Vieth, J. A. Barrie, *J. Appl. Phys.* **1963**, *34*, 1.

[12] A. S. Michaels, W. R. Vieth, J. A. Barrie, *J. Appl. Phys.* **1963**, *34*, 13.

[13] J. M. Lagaron, R. Catalá, R. Gavara, *Mater. Sci. Technol.* **2004**, *20*, 1.

[14] W. J. Koros, Ed., *Barrier Polymers and Structures*, ACS Symp. Ser. Am. Chem. Soc., Washington, DC, **1990**.

[15] R. B. Armstrong, *Effects of Polymer Structure on Gas Barrier of Ethylene Vinyl Alcohol (EVOH) and Considerations for Package Development.*, TAPPI Press, **2002**.

[16] S. M. Aharoni, *Polym. Adv. Technol.* **1998**, *9*, 169.

[17] G. Adam, J. H. Gibbs, *J. Chem. Phys.* **1965**, *43*, 139.

[18] H. Eyring, *J. Chem. Phys.***1936**, *4*, 283.

[19] Z. Xu, N. Hadjichristidis, L. J. Fetters, J. W. Mays, *Physical Properties of Polymers*, Springer Berlin Heidelberg, Berlin, Heidelberg, **1995**, 1.

[20] V. P. Privalko, Yu. S. Lipatov, *J. Macromol. Sci., Part B* **1974**, *9*, 551.

[21] T. deV. Naylor, in *Comprehensive Polymer Science and Supplements*, Elsevier, **1989**, 643.

[22] P. L. Robertson, G. Verona, *Aust Econ Hist Rev* **2006**, *46*, 70.

[23] J. M. Lagaron, A. K. Powell, G. Bonner, *Polym. Test.* **2001**, *20*, 569.

[24] S. Aucejo, C. Marco, R. Gavara, *J. Appl. Polym. Sci.* **1999**, *74*, 1201.

[25] C. L. Soles, A. F. Yee, *J. Polym. Sci. B Polym. Phys.* **2000**, *38*, 792.

[26] R. M. Hodge, G. H. Edward, G. P. Simon, *Polymer* **1996**, *37*, 1371.

[27] H. Levine, L. Slade, in *Water Science Reviews 3* (Ed.: F. Franks), Cambridge University Press, **1988**, 79.

[28] Z. Zhang, I. J. Britt, M. A. Tung, *J. Polym. Sci. B Polym. Phys.* **1999**, *37*, 691.

[29] D. Cava, C. Sammon, J. M. Lagaron, *Appl Spectrosc* **2006**, *60*, 1392.

[30] Z. Zhang, I. J. Britt, M. A. Tung, *J. Appl. Polym. Sci.* **2001**, *82*, 1866.

[31] W. A. Jenkins, K. R. Osborn, *Plastic Films: Technology and Packaging Applications*, CRC Press, **1992**.

[32] J. Tellers, S. Canossa, R. Pinalli, M. Soliman, J. Vachon, E. Dalcanale, *Macromolecules* **2018**, *51*, 7680.
[33] J. Tellers, A. Zych, P. Neuteboom, M. Soliman, J. Vachon, *Eur. Polym. J.* **2020**, *131*, 109721.
[34] B. Wunderlich, C. M. Cormier, *J. Polym. Sci. A-2 Polym. Phys.* **1967**, *5*, 987.
[35] S. W. Kim, H. M. Choi, *High Perform. Polym.* **2015**, *27*, 694.
[36] M. Aubin, R. E. Prud'homme, *Macromolecules* **1988**, *21*, 2945.
[37] M. D. Young, J. J. Field, K. E. Sheetz, R. A. Bartels, J. Squier, *Adv. Opt. Photon.* **2015**, *7*, 276.